R-08-32

KBS-3H Design Description 2006

Jorma Autio, Erik Johansson, Annika Hagros
Saanio & Riekkola Oy

Lennart Börgesson, Torbjörn Sandén
Clay Technology AB

Paul-Erik Rönnqvist, Fortum Nuclear Services Ltd

Magnus Eriksson, Vattenfall AB

Jarno Berghäll, Raimo Kotola, Ilpo Parkkinen
Finnmap Oy

December 2008

SKB

KBS-3H Design Description 2006

Jorma Autio, Erik Johansson, Annika Hagros
Saanio & Riekkola Oy

Lennart Börgesson, Torbjörn Sandén
Clay Technology AB

Paul-Erik Rönnqvist, Fortum Nuclear Services Ltd

Magnus Eriksson, Vattenfall AB

Jarno Berghäll, Raimo Kotola, Ilpo Parkkinen
Finnmap Oy

December 2008

Abstract

This document provides the status of the design description of a KBS-3H repository design alternative as of early 2006. The design is in progress and the main objective of this document is to provide a description of the status of the design for the safety assessment. In the KBS-3H design alternative, multiple canisters containing spent fuel are emplaced at about 420 m depth in bedrock in parallel, 100–300 m long, approximately horizontal deposition drifts. In this report, the number of alternative technical design solutions has been reduced from the previous design description. Additionally, the design of some components has been developed further, most significantly that of the compartment plug and bentonite distance blocks. This report also summarizes the most important new research findings and highlights differences with respect to the previous design description. Two different alternative KBS-3H designs, Basic Design (BD) and Drainage, Artificial Watering and air Evacuation (DAWE), which have both been assessed as being technically feasible, are presented together with estimated groundwater inflows, sealing techniques, Olkiluoto-specific layout and estimates of amount of residual materials. Both alternatives have still uncertainties and the design developments to resolve these are in progress. The distance block in the BD alternative is the design component, for which significant uncertainties have been identified concerning buffer behaviour, design requirements and design basis. These critical issues and related uncertainties have significant impact on the final selection of the design, which may differ from the present understanding.

Sammanfattning

Denna rapport beskriver statusen för utformningsbeskrivningen av ett KBS-3H-slutförvars-alternativ vid början av år 2006. Utformningsarbetet är fortgående och avsikten med detta dokument är att beskriva statusen för säkerhetsanalysarbete. I KBS-3H-alternativet placeras ett flertal kapslar med använt kärnbränsle på ca 420 meters djup, i parallella 100–300 meter långa horisontala deponeringshål i berget. Till denna rapport har antalet alternativa utformnings-lösningar reducerats från tidigare beskrivning. Utformningen av vissa komponenter har vidare-utvecklats, exempelvis sektionspluggar och distansblock. Rapporten summerar även viktiga forskningsframsteg och belyser skillnader i relation till tidigare beskrivning.

Två alternativa KBS-3H-utformningar har bedömts tekniskt genomförbara, kallade Basic Design och DAWE (Drainage, Artificial Watering and air Evacuation). De presenteras med uppskattade grundvatteninflöden, tätningsmetoder, Olkiluoto-specifik layout och uppskattade mängder främmande material. Båda alternativen har fortfarande osäkerheter och arbetet med att finna lösningar på dessa är framåtskridande. Distansblocket i Basic Design är den komponent för vilken betydande osäkerheter har identifierats, gällande buffertbeteende, utformningskrav och förutsättningar. Dessa viktiga frågor och relaterade ovissheter har betydande inverkan på det slutliga valet av utformningen, vilken kan avvika från nuvarande kunskap.

Denna rapport finns även tryckt i Posivas rapportserie POSIVA WR 2007-105.

Nyckelord: KBS-3H, Horisontal deponering, Slutförvar, Använt kärnbränsle.

Contents

Foreword

This KBS-3H design work carried out during was managed by Jorma Autio from Saanio & Riekkola Oy. The work was carried out by KBS-3H Design Group in close cooperation with KBS-3H Safety Case subproject.

The KBS-3H Design Group consisted of the following members with the specified field of responsibility and reporting being shown:

- Jorma Autio (KBS-3H design project manager, Saanio & Riekkola Oy) project management, coordination, reporting.
- Lennart Börgesson (Clay Technology AB) activity leader in buffer design.
- Torbjörn Sandén (Clay Technology AB) buffer design.
- Paul-Erik Rönnqvist (Fortum Oy) mechanical engineering, steel design, pipe removal.
- Jarno Berghäll (Finnmap Oy) compartment plug design.
- Raimo Kotola (Finnmap Oy) compartment plug design.
- Ilpo Parkkinen (Finnmap Oy) compartment plug design.
- Erik Johansson (Saanio & Riekkola Oy) lay out design, acitivity leader.
- Annika Hagros (Saanio & Riekkola Oy) evaluation of engineered and other residual materials.
- Magnus Eriksson (Vattenfall AB) groundwater control.
- Nina Sacklén (Saanio & Riekkola Oy) project administration, quality control, secretarial services, report editing.

In addition Timothy Schatz (Saanio & Riekkola Oy) has carried out the language check.

The following persons from KBS-3H Safety Case group, in addition the Safety Case project manager Margit Snellman (Saanio & Riekkola Oy), were following the work and contributed significantly to it: Barbara Pastina (Saanio & Riekkola Oy), Lawrence Johnson (Nagra), Paul Smith (SAM LtD), Peter Gribi (S+R Consult) and Bill Lanyon (Fracture Systems). The Safety Case group also provided the long-term safety requirements (Appendix A) and the List of input parameters (Appendix D).

1   General

This document provides a description of the design of a KBS-3H repository. The design is a work in progress and the main objective of this document is to provide a description of the status of the design for the safety assessment. In the KBS-3H repository design alternative, multiple canisters containing spent fuel are emplaced in parallel, 100–300 m long, approximately horizontal deposition drifts. Posiva and SKB are engaged in a research, development & demonstration (RD&D) programme with the overall aim of developing the KBS-3H as a feasible alternative to KBS-3V, in which single canisters are emplaced in individual vertical boreholes drilled into the floor of horizontal deposition tunnels.

The previous KBS-3H design, which considered two different candidate alternatives, was based on Olkiluoto site data and was presented in the KBS-3H Design Description 2005 report /Autio 2007/. The candidate alternatives included several options for certain design components. Since the Design Description 2005 was reported, the number of alternative technical design solutions was reduced and more information was obtained regarding some of the identified uncertainties. Additionally, the design of some components was developed further, most significantly the steel compartment plug and distance blocks.

Significant progress was made in the KBS-3H design and this document describes the present situation for use as input in the compilation of a Safety Case. The reduction in the number of various design alternatives within the main design should facilitate work on the Safety Case. This report also summarizes the most important new research findings and highlights differences with respect to the design reported in the Design Description 2005. The KBS-3H design is a work in progress and therefore some of the presented aspects are preliminary. The design work will be reported in greater detail by the end of 2007.

2　KBS-3H design alternative and development since Design Description 2005

2.1　General description of the KBS-3H design alternative

The KBS-3H design is a variant of the KBS-3 method and an alternative to the KBS-3V design. The KBS-3H design is based on horizontal emplacement of spent fuel canisters in a drift whereas the KBS-3V design calls for vertical emplacement of the canister in individual deposition holes, see Figures 2-1 and 2-2. Under Posiva's current plans, the repository is to be located at the depth of –420 m below sea level at Olkiluoto. These conditions serve as the basis for the reference design presented in this report. The preliminary design of the KBS-3H repository includes both one-storey and two-storey alternatives as in the case of the KBS-3V repository as well.

In the KBS-3H design, if necessary, drifts sections that are suitable for the emplacement of the spent fuel assemblies are compartimentalised to isolate them from sections that are not suitable due to water inflow. The division into compartments is accomplished through the use of compartment plugs. The canister and buffer are placed in a perforated steel shell and the entire assembly is called "supercontainer" and it is emplaced in the horizontal drift. A distance block of compacted bentonite, a key component in the design, is positioned between each supercontainer to obtain proper thermal spacing and isolation. One of the most important functions of the distance block is to seal the drift section between the supercontainers to prevent flow and advective transport along the drift. The sealing and plugging is assumed to occur when the distance block absorbs water, swells and obtains proper swelling pressure.
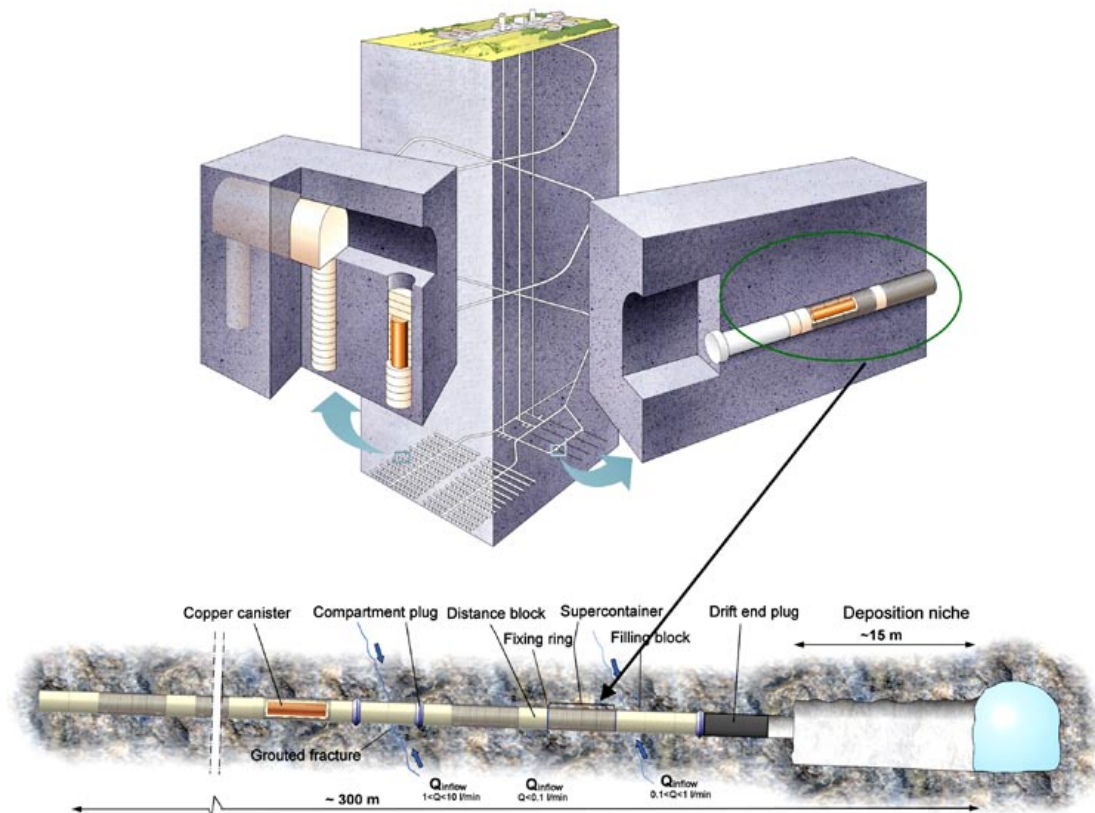
Figure 2-1. *Principles of the KBS-3V (upper left) and KBS-3H (upper right) repository designs and a more detailed illustration of the KBS-3H design (lower).*
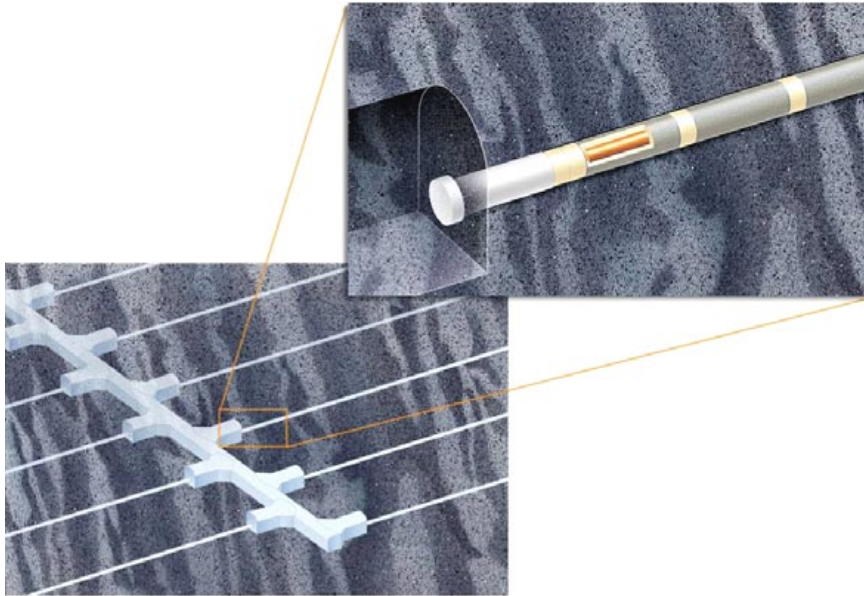
Figure 2-2. *Main tunnel, deposition niches, and deposition drifts /Thorsager and Lindgren 2004/.*
The illustration is based on a preliminary asymmetrical positioning design.

There are two different variations (candidate designs) of the KBS-3H design: 1) Basic Design (BD) and 2) Drainage, Artificial Watering and air Evacuation (DAWE) design. These alternatives are described in Chapters 4 and 5.

2.2   Development of both candidate designs

The continued development of the candidate designs has resulted in several changes, modifications and added detail to the designs presented in 2005. These new developments are summarized below and more fully described later in this report:

- The canister spacing was evaluated and accurately specified. The reasons for the large difference in the degree of rock volume utilization for the KBS-3H versus KBS-3V designs between Posiva and SKB were analyzed.

- The thermo-mechanical behaviour of rock adjacent to KBS-3H deposition drift walls was re-evaluated and the results indicate significant susceptibility to spalling, which then concerns the design.

- The long-term safety requirements with an impact on the design and the effects of the rate of increase in groundwater pressure were evaluated resulting in changes to the design basis.

- The design of the steel compartment plug was established in more detail allowing for more accurate estimates of the engineered materials requirements. Also, the design was modified to withstand loading from both sides of the plug.

- A drift end plug based on the use of a rock kernel as an alternative to the solid concrete plug was introduced. This alternative results in reduced quantities of engineered materials in the plug.

- Drip and spray shields were tested at Äspö and estimates were made of the engineered material quantities.

- The analysis of engineered and other residual materials was performed.

- A new layout, based on the new Olkiluoto bedrock model, was produced.

- The grouting techniques were developed (mainly the Mega-Packer technique) and the amount of residual grouting material in the rock was estimated.

2.3 Development of DAWE (Drainage, Artificial, Watering and air Evacuation) alternative

In the Design Description 2005 several alternative designs for the drainage and watering system were presented. The development of the distance block design resulted in the possibility of using the free flow of any incoming water as a drainage option. This option simplified the design and allowed for the selection of a watering system based on the use of separate pipes for supercontainer positions.

One of the most critical design issues presented in the Design Description 2005 /Autio 2007/ was the potential for cracking of distance blocks. The use of steel nets around the distance blocks was advocated as a solution to this issue; however, it was found to be unacceptable from long-term safety point of view. A subsequent design, forgoing the use of a net, was then developed. This design relied on an increase in the initial water content of the compacted bentonite to reduce cracking potential and increase block stability.

2.4 BD (Basic Design) alternative

Two alternative designs, with regard to the gap between the host rock and distance blocks, were presented in the Design Description 2005:1) a design incorporating a large gap (42.5 mm) filled with bentonite pellets and powder and 2) a design based on a small gap ("tight fit", i.e. 10 mm). The results from buffer testing indicate that the large gap alternative will not fulfil functional requirements and is therefore rejected, which leaves the small gap tight fit design as the only alternative. The pellet filling option in the large gap alternative was tested using uniform pellet size and was found to be quite susceptible to piping and erosion (see Appendix K). Similar results were obtained in SKB's BACLO project. As a consequence, several tight fit alternatives were developed and one was introduced as the reference design.

The drift quality requirements for the use of a tight fit distance blocks are much stricter than previously specified because rock surface unevenness must be taken into account in the gap size. Measures to ensure adequate surface quality were developed.

The emplacement of tight fit distance blocks will also require more time than previous designs and affect operation timetables as such.

3　Design basis

3.1　General

One main objective of the KBS-3H candidate design work is to produce a design that fulfils the functional requirements and technical prerequisites under the specified environmental boundary conditions.

The basis for design is divided into the following categories:

- **Functional requirements** specify how the buffer system must perform.

- **Environmental boundary** conditions describe the properties of the bedrock where the buffer system must perform according to the functional requirements.

- **Technical prerequisites** specify the aspects of the technical design that are fixed and cannot be changed (e.g. the diameter of the deposition drift).

- **Design guidelines** describe the advice, instructions, opinions and proposals offered by experts to be followed in order to fulfil the functional requirements.

The requirements mentioned above, along with other general functional requirements, environmental boundary conditions, technical prerequisites, general design guidelines, and candidate design specific guidelines for developing a repository design were presented earlier by /Autio 2007/. Subsequently, several important changes in the design basis were realized:

a) The long-term safety requirements were revised resulting in some significant new requirements particularly with respect to canister positioning, which affects drift utilization degree.

b) The maximum rate of increase in groundwater pressure was evaluated and increased from 100 kPa/h to a few MPa/h.

c) The supercontainer end plate structure was modified from perforated to solid. It was previously assumed that the supercontainer design is fixed, however it was necessary to alter the end plate structure in order to obtain the required sealing functionality.

d) The operational times depend on the design of distance blocks. The emplacement technique presented earlier by /Autio 2007/ is not valid for "tight distance blocks" in the BD alternative and therefore a new technique was developed. The technique used for emplacement of distance blocks in the DAWE alternative is assumed as fixed and remains as previously described /Autio 2007/.

e) The long-term safety consequences of the interaction between the steel components and the bentonite surrounding the canisters are still under investigation: no quantitative restrictions for the use of steel have been specified so far.

3.2　The long-term safety requirements

The long-term safety requirements are presented in Appendix A and include both qualitative and quantitative requirements for various system components. These requirements are not to be understood as absolute requirements in order to achieve sufficient safety. Rather, if it can be argued that relevant requirements are fulfilled, this indicates that a particular barrier will perform as intended for safety. A summary of the most important requirements with respect to design is presented below.

3.2.1 Canister positioning

The canister positioning criteria is based on groundwater inflow rate. The rate of inflow to the drift during saturation is related to the transmissivity and frequency of rock fractures intersecting the drift, and hence to long-term flow subsequent to saturation.

In terms of the transport barrier provided by the geosphere, a transmissivity of about $3 \times 10^{-9}\,\mathrm{m^2/s}$ provides a transport resistance on the order of 10,000 years per metre, which corresponds to an effective geosphere transport barrier for many safety relevant radionuclides. A roughly equivalent transmissivity value was used to determine the maximum inflow rate into a supercontainer unit volume (supercontainer and distance block of length approximately 10 m) prior to rock sealing of 0.1 litre per minute. This inflow rate is the overall long-term safety criterion for intersecting fracture transmissivity at supercontainer and distance block emplacement locations prior to sealing. This long-term safety criterion is based on conditions existing before possible sealing of rock fractures because the effect of any sealing materials is assumed to be viable over the short-term only.

3.2.2 Buffer, distance block and filling component properties

In the case of the buffer (defined as the compacted bentonite inside the supercontainer and comprising distance blocks), many long-term safety requirements (e.g. stiffness, plasticity, impermeability, swelling pressure) are related to buffer density. There are various mechanisms, such as erosion by transient water flow and differential swelling of bentonite components, whereby some loss or redistribution of buffer mass may occur during the saturation of a KBS-3H repository. Scoping calculations of potential buffer density changes during the early phase of evolution are described in the KBS-3H Process and Evolution Reports /Gribi et al. 2007, Smith et al. 2007/. The magnitude of the resulting changes in density affects whether the buffer can perform its safety functions, which are, a) protection of the canisters, b) limitation of radionuclide releases in the event of canister failure, and c), of specific importance for a KBS-3H repository, hydraulic separation of the supercontainers from one another preventing the formation of preferential pathways for flow and advective transport within the drifts through the corrosion products or altered buffer. The hydraulic conductivity and swelling pressure of the buffer, which contribute to these safety functions, are functions of buffer density. They are, however, also functions of buffer pore water salinity, which will vary over time due to transient changes in groundwater composition. Appendix A presents a discussion of how, in the case of a KBS-3H repository at Olkiluoto provided the saturated buffer density remains in the range of about 1,890 to 2,050 kg/m^3, changes in swelling pressure and hydraulic conductivity caused by salinity variations are expected to be minor; therefore this density range is compatible with the buffer fulfilling its safety functions. A key requirement for filling components (filling blocks, filling material next to compartment plugs and between them) is that they should not undergo volume changes (due, e.g. to swelling or compaction), which could lead to density changes outside the compatible range.

3.3 Groundwater pressure increase rate

The research and development of distance block design in the BD alternative demonstrated the possibility that flow channels ("piping") might form through the distance block adjacent to the rock interface if the distance block design is not adequate /Börgesson et al. 2005/. This phenomenon was specified as a critical issue for resolution and is addressed in current buffer tests. The development of a proper design is apparently very sensitive to inflow rate (Q) from the surrounding rock into the open volume (V, on the order of a few cubic meters) between supercontainer units (i.e. filling time of the open volume), rate of pressure increase, and time until the full hydrostatic pressure is reached after the volume was filled with water (Figure 3-1).
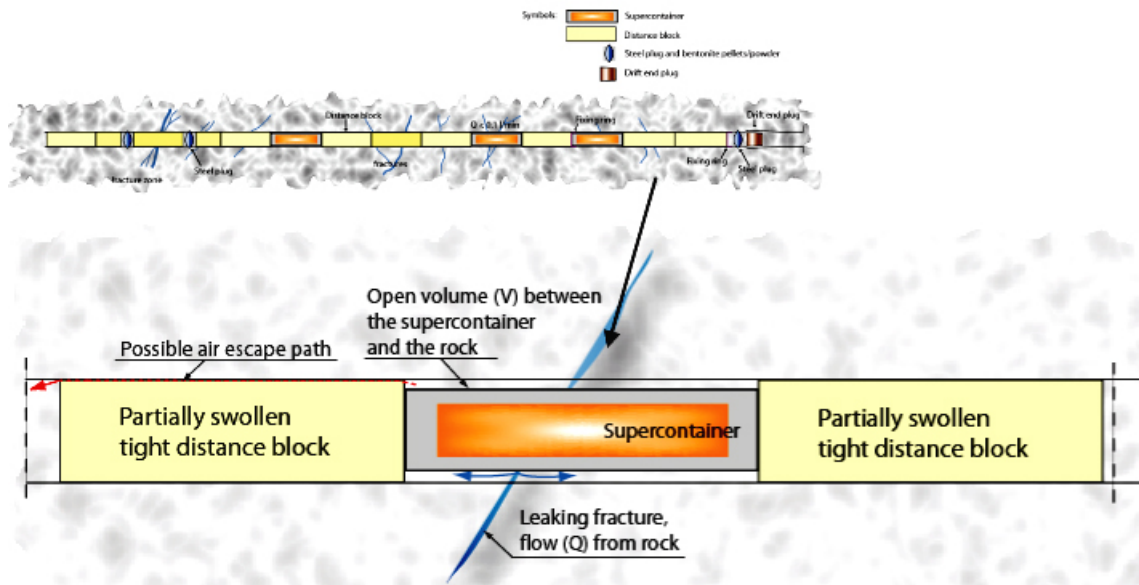
Figure 3-1. *Groundwater inflow into the supercontainer section in the KBS-3H design.*

Appendix B provides assessments of the rate of increase in groundwater pressure in a sealed supercontainer unit. To the extent possible, these estimates were based on Olkiluoto specific hydrological data. The estimates for the pressure increase from initial atmospheric pressure to a full hydrostatic pressure of 4 MPa with time in the supercontainer section were derived from two simplified cases. The first case evaluates a closed supercontainer section allowing for no escape of air, and the second case considers the increase in hydraulic pressure after the escape of air. Input inflows were in the range of 0.1 l/min to 1 l/min.

These estimates were primarily derived for the planning of buffer tests to commence during 2006 and 2007 with the rate of pressure increase being one significant test parameter.

For the closed, airtight supercontainer section scenario (first case), assuming the initial void space to be equal to the open space between the supercontainer and the drift wall, the maximum groundwater pressure build-up rate is 1.6 MPa/h at an inflow of 1 l/min or 0.16 MPa/h at an inflow of 0.1 l/min.

For the scenario concerning hydraulic pressure after the escape of air (second case) the rate of increase is based on the solution to Theis's equation and, assuming radial flow, depends on the storativity to transmissivity ratio S/T, which is assumed to be in the range from 1 to 1,000. In the case of S/T equal to 100, a value relevant for the drifts considering the estimated storativity and possible transmissivities of the fractures, the maximum pressure build-up rate can be as high as 25 MPa/h. At smaller S/T ratios the pressure build-up rate increases and, conversely, at larger S/T ratios value, i.e. lower transmissivities, the pressure build-up rate decreases. Site-specific storativity data is lacking and causing uncertainties in the estimations. Furthermore, the analytical solution does not take into account the changing flow rate, which means that the resulting pressure increase rates are upper limits for a given S/T value.

The rate of pressure increase appears to change during the flooding of supercontainer sections. In the second case the pressure increase is very rapid after the escape of air, whereas in the first case where there is significant amount of trapped gas in the supercontainer section, the pressure increase starts significantly earlier but builds at a slower rate.

The values of pressure increase rates presented above are rough estimates as they are based on simplified cases neglecting many phenomena, e.g. skin effects actually occurring in the drift, which may retard the actual pressure increase. Storativity values themselves are also quite uncertain. Nevertheless, the estimates are considered to give an idea of the possible range of the pressure increase rate.

Using DFN modelling /Lanyon and Marschall 2006/ also estimated the rate of pressure increase. Their results indicate the rate is largely controlled by the geosphere inflow and the assumptions concerning the storage term associated with the supercontainers and distance blocks. In models where no storage is associated with the drift sections, pressure rises very quickly with derivatives of greater than 1 MPa/hr. In the models containing greater storage either due to trapped air or the use of a larger storage term then the highest gradients are only associated with high transmissivity features located in blank or seal sections. Typically pressures rise faster around the distance blocks, as these have been associated with smaller storage terms. The effect of the storage term for a drift section intersecting a 0.1 l/min feature (transmissivity 2.65×10^{-9} m^2/s) is clearly seen in Figure 3-2 where for storage term (CT value) greater than 8×10^{-8} m^3/Pa the pressure derivative is below 100 kPa/hr.
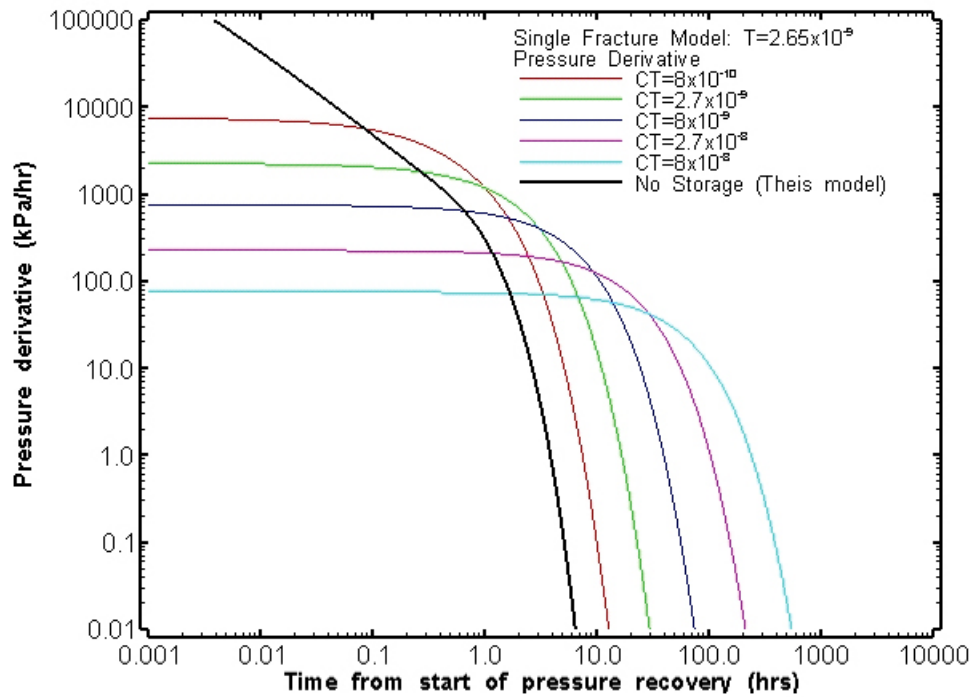
Figure 3-2. *Effect of storage term (CT in m^3/Pa) on pressure derivative (rate of pressure increase in kPa/hr) in a drift section intersecting a leaking fracture (inflow = 0.1 l/min, T = 2.65x10^{-9} m^2/s) using nSights models /Lanyon and Marschall 2006/.*

3.4 Supercontainer unit

3.4.1 Supercontainer and buffer

The engineering drawing of the supercontainer unit (see Figure 3-3) is presented in Appendix C and includes SKB's BWR 1,700 W canister (length = 5,560 mm) in the design. All of the relevant dimensions are tabulated in Appendix D; the diameter of the supercontainer is 1,765 mm, the length of Posiva's BWR 1,700 W canister (reference design) is 5,525 mm, the weight, including feet, is 1,071 kg, and the steel cylinder is 8 mm thick with a perforation of 60%.

The current buffer material used inside the supercontainer is MX-80 sodium bentonite with 10% initial water content. The diameter of the bentonite rings is 1,740 mm and the thickness of the end blocks is 350 mm. The initial dry density is 1,887 kg/m^3 (1,789–1,977 kg/m^3). The density after swelling and saturation is 2,000 kg/m^3 (1,950–2,050 kg/m^3) and the estimated swelling pressure 7–8 MPa. The properties of the buffer end blocks differ slightly from those of the ring blocks (see Appendix D).
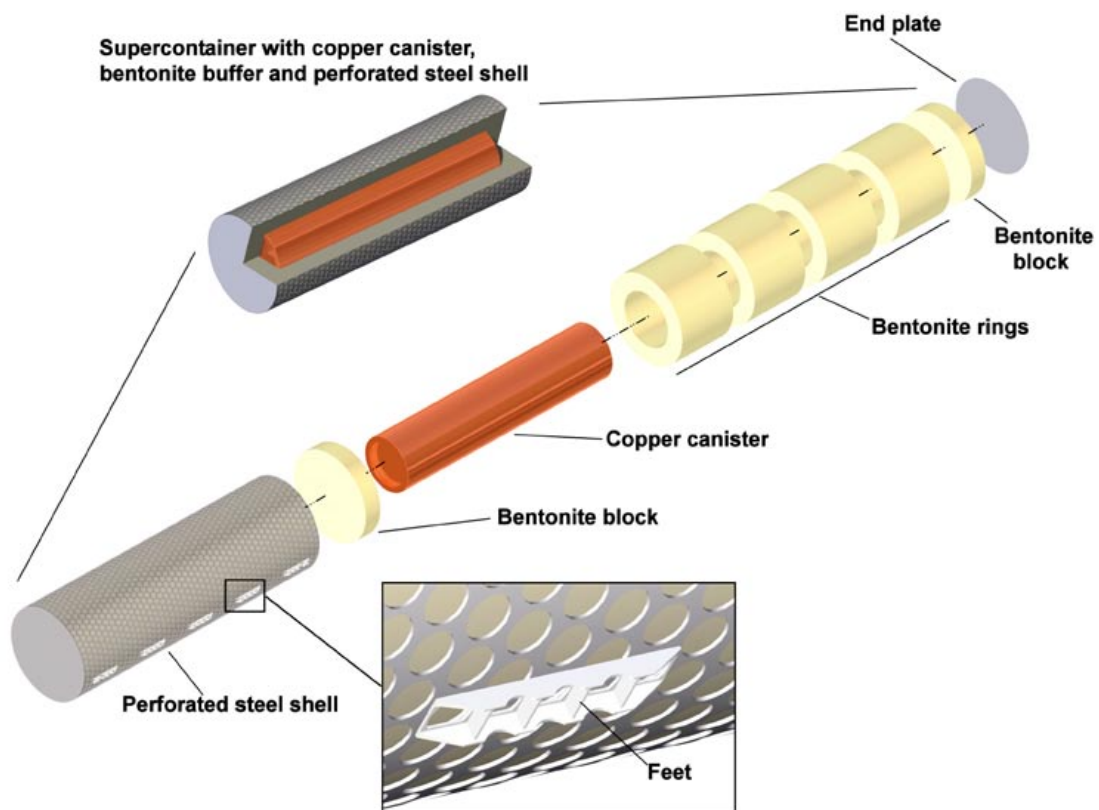
Figure 3-3. *Illustration of the supercontainer unit in the KBS-3H design.*

3.4.2 Modification of supercontainer end plate

The supercontainer end plate was previously specified to the same degree of perforation as the cylinder. This end plate specification was found to be problematic because the use of perforated material results in an increase to the effective gap size between the supercontainer and distance block. The gap size is a critical issue as it is key to ensuring that the hydraulic pressure exerted on the distance blocks can be reasonably and technically managed.

The magnitude and distribution of loads induced by hydraulic pressure on the face of the distance blocks may have an effect on the movement of the distance blocks and the dimensioning of the load-bearing fixing ring in the BD design. The main uncertainty associated with the nature of the loading is whether the load is exerted on a narrow rim on the inner end face, which is not covered by the supercontainer end surface, or whether the hydraulic pressure present at the end closest to the supercontainer is exerted on the entire surface of the distance block. The latter, full-face hydraulic jacking situation is not currently technically manageable. The present estimate suggests that if the width of the gap between the supercontainer and distance block is 7 mm or smaller, swelling bentonite will fill the gap and hydraulic pressure will affect only a narrow rim on the distance block face. Therefore, the reference gap size in the present design is set at 7 mm.

The total gap between the supercontainer buffer and distance block is comprised of any separation between the supercontainer end plate and distance block face resulting from deviations in planarity, the thickness of the any increased distance due to the use of perforated materialgap caused by perforation and also any gap between the supercontainer end plate and buffer inside it, see Figure 3-4.

Present plans call for supercontainer assembly in a vertical position to facilitate a structure without any gap between the buffer blocks. The end plate will be mounted in contact with the uppermost buffer blocks.
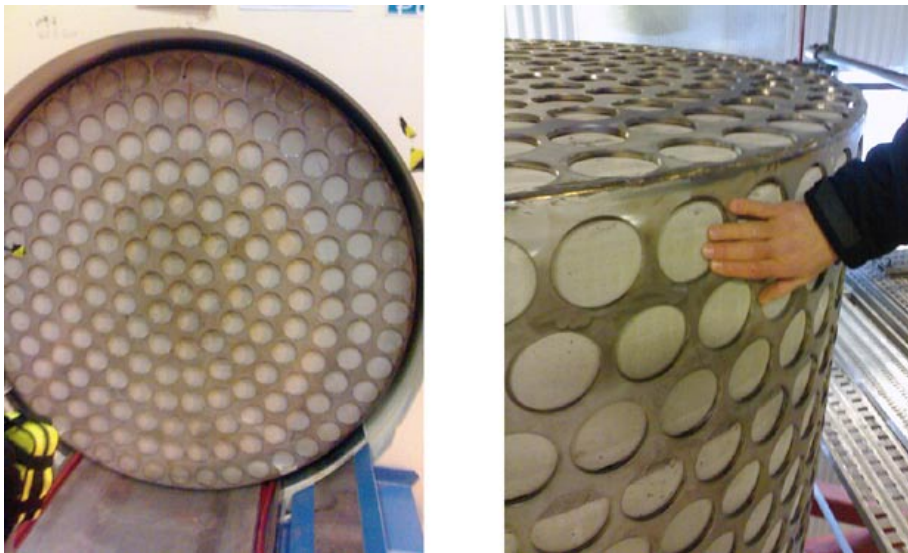
Figure 3-4. The supercontainer end plate as seen during transportation in the demonstration drift at Äspö and in a vertical position during assembly (see hand for scale). The largest allowed gap between distance block and steel supercontainer end plate is assumed to be 7 mm. The total gap between buffer and distance block is composed of gap between the supercontainer end plate and distance block face, perforation in the end plate (increase in open volume in holes) and also gap between supercontainer end plate and buffer inside it, which will be reduced so that buffer will be in contact with supercontainer end plate. Photos by J. Autio.

If the supercontainer end plate is perforated, the effective gap size will be increased by approximately 5 mm. If the assumed acceptable target size of gap is 5 mm, this would results in situation where the supercontainer end plate has to be absolutely planar and there are no gaps allowed between buffer in side the supercontainer and end plate and distance block and end plate. This is practically impossible and therefore the end plates are to be solid plates with as high planarity (straightness) as possible. It is also likely that the perforation will induce several other undesired processes in the behaviour of buffer – supercontainer end plate such as piping and erosion, which can be eliminated by making the end plate solid.

3.5   Drift quality

The present distance block designs in the BD alternative consider gap sizes from 0 to 10 mm between the distance block and drift surface.

The presently defined nominal gap width between the rock surface and supercontainer is 42.5 mm. In the final state, this gap will depend on the geometric tolerances (e.g. straightness and surface roughness) of the drift and the size of the supercontainer. During operation the canister will be lifted and lowered stepwise, and the free gap will be reduced to something closer to 20 mm.

The drift geometry and quality requirements in the deposition drift for demonstration at Äspö are displayed in Figure 3-5. According to specification (see Appendix F), the nominal drift diameter is 1,850 mm with an allowed decrease of 10 mm at a length of 300 m as a consequence of the expected wear and tear in the cutting head of the boring machine. Additionally, stepwise unevenness and roughness were specified with allowances up to 5 mm each.
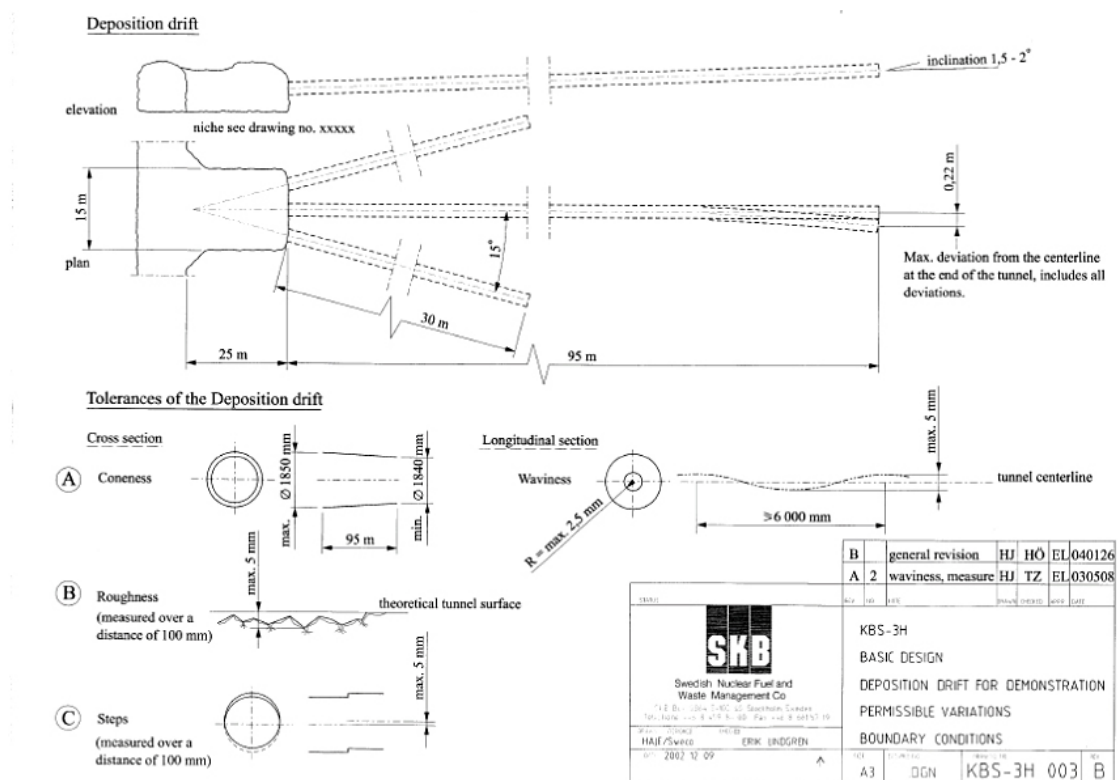
Figure 3-5. *Drift geometry and quality requirements in the deposition drift for demonstration at Äspö Hard Rock Laboratory.*

Further quality requirements in the KBS-3H drift design are as follows:

• The maximum allowed deviation of the floor of the drift from ideal cylindrical shape including all sources of error, is ± 5 mm over the length of the canister (6 m).

• The maximum allowed deviation from the theoretical centre line of the tunnel at the end of the tunnel drift (300 meters) is ± 2 meters in total (note that the deviation requirement in Figure 3-5 differs from that), which includes all horizontal and vertical deviation components.

• The maximum allowed waviness is R = ± 2.5 mm for the pilot hole over the length of the canister (6 m), see Appendix F.

• The maximum allowed roughness is 5 mm over a length of 1 meter.

• The deposition drift must have a positive inclination angle of 1.5–2.0 degrees; the larger inclination is favourable for muck flushing.

The 10 mm reduction in drift diameter due to boring machine wear is the largest diameter variation expected. Additional reduction in effective diameter is caused by waviness and roughness, the maximum allowable deviation being ± 2.5 mm (total 5 mm) in all directions at wavelength of 6 m or more (see Figure 3-5). A stepwise deviation of 5 mm was defined in vertical direction. This would result in a situation where the largest effective diameter reduction in vertical direction at the length of 300 m would be 20 mm, consisting of 10 mm diameter reduction, 5 mm waviness reduction and 5 mm stepwise deviation. The corresponding reduction of diameter in horizontal direction would be 15 mm, assuming that the stepwise deviation is excluded.

The corresponding smallest width of the free gap between supercontainer and rock surface would therefore be 20 mm above the supercontainer, assuming that the feet under the supercontainer keeps the gap below it to a constant 45 mm. The gap on the sides would be reduced to 35 mm. The gap above the canister will become smaller during operation when the canister is lifted 10 mm upwards. The width of the gap at the sides will however remain. The diameter of the supercontainer has a tolerance of ± 5 mm.

It is not possible to use a single standard size of distance block in the BD alternative due to the drift quality specifications outlined previously. If the distance block diameter is defined by the minimum diameter of the drift, a maximum gap distance of 5 mm will result, depending on how the distance blocks are centralized. If a stepwise unevenness of 5 mm is added to that, the gap will be 10 mm wide or more, which is larger than what can be tolerated according to the present understanding system performance. In addition, a sufficient safety margin for the gap dimension is required for robustness, which is not possible with a universal distance block standard.

If the distance block design is based on essentially no effective gap, then surface roughness and stepwise unevenness are not allowed and the distance block must have same diameter as the drift. A difference of 10 mm in diameter will result in gaps between the distance block and drift surface.

Examples of different type of surface unevenness found in the KBS-3H demonstration drifts at Äspö are shown in Figures 3-6 and 3-7.

The issues raised by drift quality can be resolved by adjusting distance block geometry in BD alternative to each specific position or by improving the drift quality or by combination of both. If the distance blocks are modified to each position, an accurate 3D surface model of the drift has to be measured and exact positions of each distance block must be specified, which is in line with present plans. Before installation, the distance blocks must be machined to within millimetre precision.

Figure 3-6. *Some typical types of surface unevenness in deposition drift: rifle type grooves on the drift wall (top) and notches at fracture intersections on the floor (above).*

Figure 3-7. Some typical types of surface unevenness in deposition drift: cavities on the drift roof (top) and rims shaped grooves and a notch (above). Photos by J. Autio.

The drift quality can be improved in order to resolve the gap dimension problem. One alternative is to smooth the surfaces and adjust the drift diameter through treatment of the surface of the holes after excavation. This alternative can be accomplished by using rotary boring type equipment with a finishing cutter head or by use of a novel finishing machine. An illustration of a possible technique is shown in Figure 3-8.

An important aspect of fulfilling the quality requirements is the pilot boring of deposition drifts to produce a pilot hole with the required straightness and waviness. The pilot hole is used to guide the cutting head of the boring machine. Achieving the waviness requirements seems to be more of a challenging task than deviating from the theoretical straight axis and, therefore, development work on the steering of pilot boring is in progress.

SKB - 3H DRIFT POLISHING AND NOTCH PREPARATION MACHINE
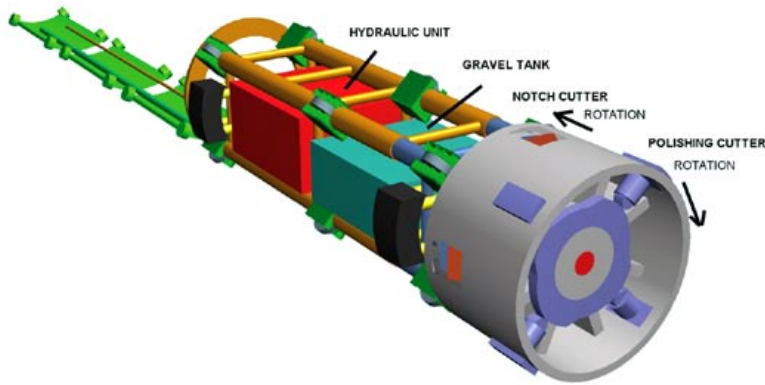
7.6.2006 P-E Rönnqvist

Figure 3-8. *Illustration of a possible machine to be used to smoothen deposition drift surfaces and to produce constant diameter.*

3.6   Olkiluoto bedrock model

The KBS-3H design and analysis of long-term safety is based on Olkiluoto bedrock model 2003 as shown in Figure 3-9 /Vaittinen et al. 2003/. A new bedrock model was recently completed /Paulamäki et al. 2006, Ahokas and Vaittinen 2007/ and was used in the KBS-3H layout adaptation 2007 /Johansson et al. 2007/ as shown in Figure 3-10. The new bedrock model included some changes in the fracture zones and new hydraulic conductivity data for fractures and fracture zones were acquired.
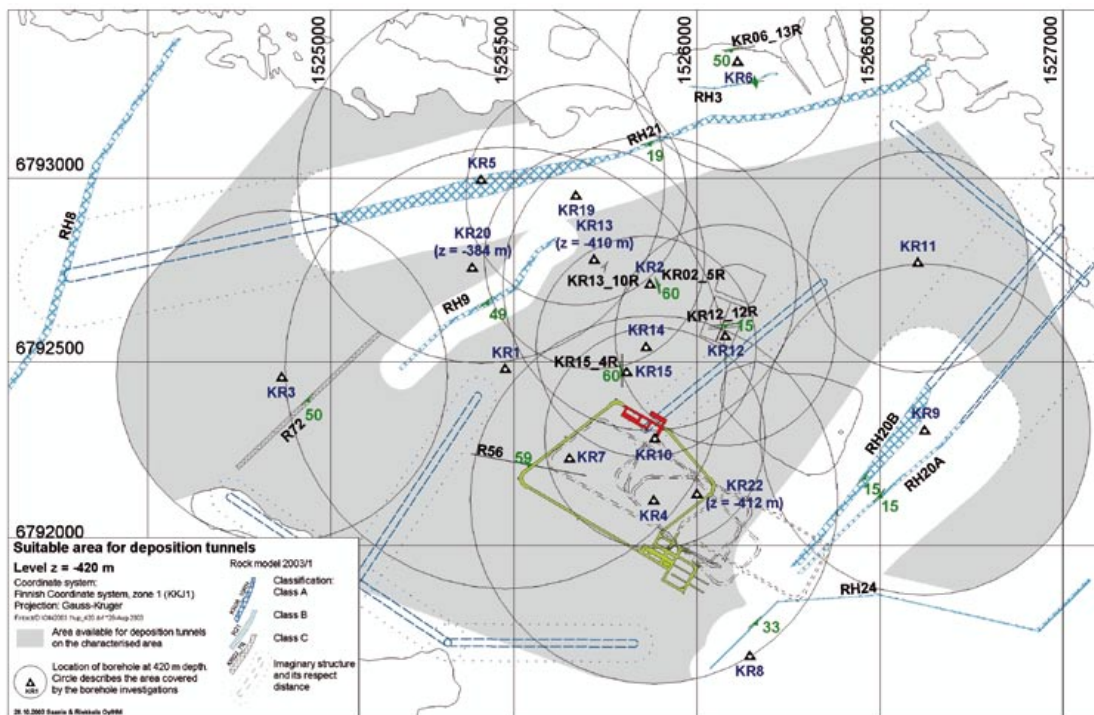
Figure 3-9. *Olkiluoto bedrock model 2003, level –420 m /Vaittinen et al. 2003/.*
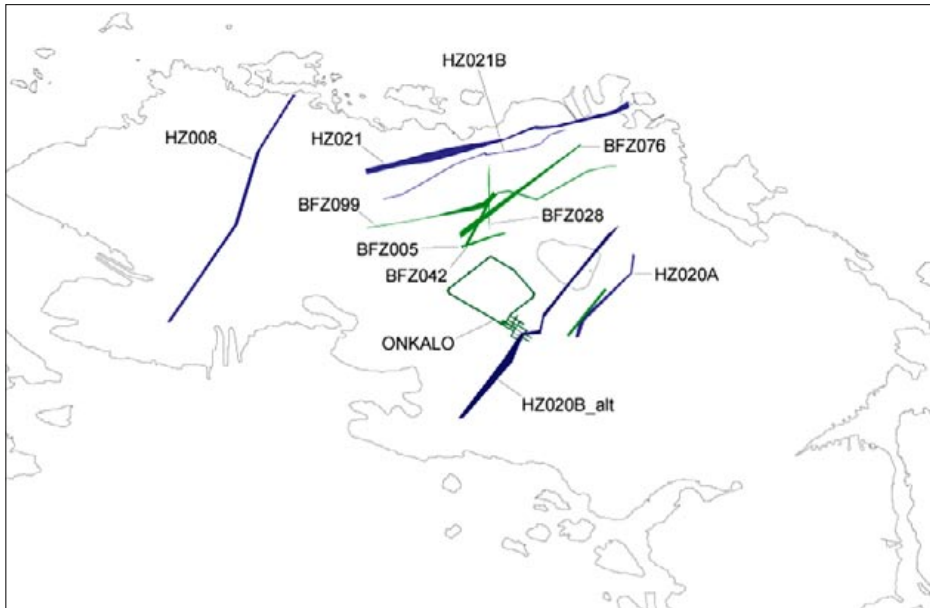
Figure 3-10. *Bedrock model 2006, level –420 m at Olkiluoto showing the layout determining fractures and also the location of ONKALO and the shoreline of Olkiluoto island /Kirkkomäki 2006/. The model is based on /Paulamäki et al. 2006/.*

The development of the new bedrock model has not resulted in any significant changes to the KBS-3H design itself. The direction of deposition drifts, number of compartments, etc has not changed; however the adjustments in fracture zones produced some differences in the appearance of layout. Addtionally, the new bedrock model and new data on hydraulic conductivity enabled a new layout adaptation (see Chapter 7).

3.6.1   Number of compartments and inflows

The hydraulic description of the bedrock at Olkiluoto has been given by /Hellä et al. 2006/ and in Appendix D. The description presented by /Hellä et al. 2006/ is focused on defining the number of fracture intersections in a KBS-3H deposition drift and leakage rates. The number of compartments and several other features were also evaluated by /Lanyon and Marschall 2006/ using the Discrete Fracture Network (DFN) modelling approach.

The present estimate is that, in an average 300 m-long deposition drift, the following features will be encountered /Hellä et al. 2006/, although there may be significant local variations from average conditions:

• There are long "dry" sections without visible leakage.

• The drift is intersected by 1–3 local fracture zones.

• The drift is intersected by approximately three fractures or fracture zones (one per 100 m).

• There are six 5 m long sections (length of supercontainer or distance block) with inflow larger than 0.1 l/min.

• There are four to five 10 m long sections with inflow larger than 0.1 l/min.

The main results with respect to design presented by /Lanyon and Marschall 2006/ are:

• The geometric simulations indicate a consistent layout across all the geosphere model variants and realisations.

• Typically, each 300 m drift is divided into 2 compartments by a single seal.

• Each drift on average contains 23 supercontainers with 3-4 blank sections.

- Total average inflow to the compartments (prior to grouting) within a drift is about 1.5 l/min.

- Average inflow to a single compartment (prior to grouting) is below 1.0 l/min.

- Approximately 18% of drifts exceed the suggested 30 l/min limit without grouting. If grouting can be successfully performed (reduction to 10^{-8} m²/s) the maximum inflow should be reduced to about 15 l/min with less than 1% of drifts exceeding 10 l/min. Inflow estimates are likely to be conservative (see /Lanyon and Marschall 2006/).

3.6.2 Hydraulic characteristics

Hydraulic pressure in neighbouring supercontainer sections during the first years after emplacement

One critical issue in distance block design and related testing is the filling of the open volume by inflowing groundwater and the subsequent rapid development of hydraulic pressure. The filling and pressure development has been evaluated by /Lanyon and Marschall 2006/ and is found to be heterogeneous for the majority of supercontainers not intersecting transmissive fractures. Within these sections no significant pressure rise is predicted within the first years as any water inflow is taken up by the bentonite.

Furthermore, there are indications that only a fraction of the supercontainers may become pressurised during the first year of operation. The result will be a system of neighbouring supercontainers and distance blocks with full hydrostatic pressure on one side of the distance block and none on the other. This situation is graphically represented in Figure 3-11 where filling time and pressure are analysed with respect to inflow and position in a 300 m long deposition drift. Large pressure gradients and forces over the distance blocks are expected. The effect may be different between the DAWE and BD alternatives.

Influence of excavation of adjacent drifts

The excavation of several deposition drifts at the same time may form flowpaths between drifts and also other tunnels, which reduces the hydraulic pressure. The results from DFN-modelling by /Lanyon and Marschall 2006/ suggest that pressure disturbances due to the excavation of adjacent drifts may be large (~ 2 MPa) and rapid. Typically the most transmissive features react most quickly, but drawdown is seen in almost all intervals intersected by transmissive features.
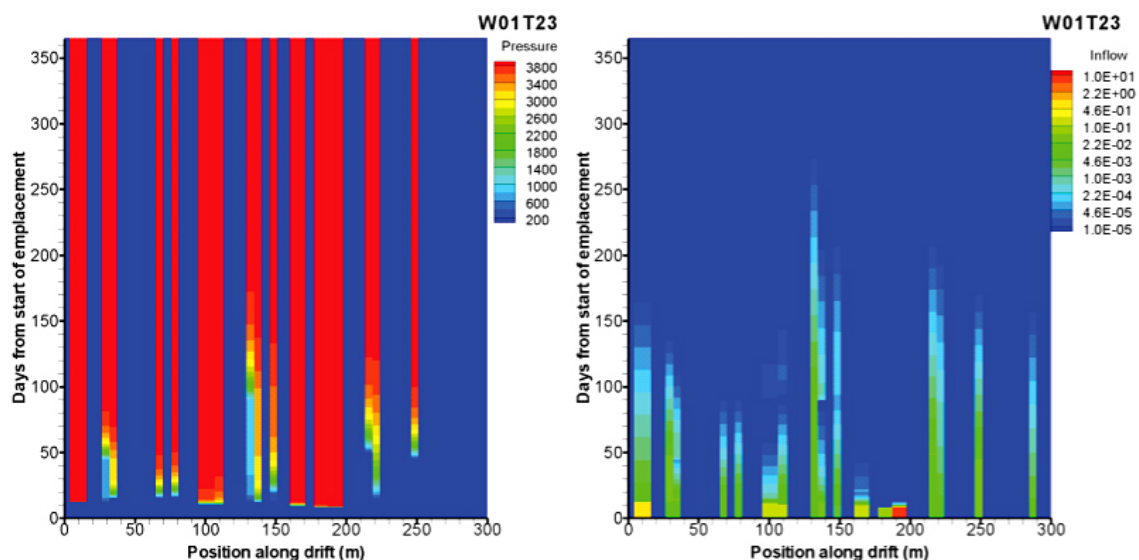
Figure 3-11. *Example of pressure (on left) and inflow (on right) as a function of time and position along a drift /Lanyon and Marschall 2006/. The heterogeneity along a 300 m long drift with respect to pressure is significant.*

Time to fill gap volume

The results from DFN-modelling by /Lanyon and Marschall 2006/ suggest that some of the supercontainer gap volumes will be filled within 10–20 days after the start of emplacement. This situation conforms to the supercontainer positioning criteria requiring inflow less than or equal to 0.1 l/min into an open volume of 1.342 m^3 around the supercontainer and results in a maximum filling time of roughly 10 days.

A filling time of 200 days or more is expected in sections where the transmissivity of features is below 10^{-10} m^2/s. In tight sections with no transmissive fractures, the filling time will clearly be longer.

3.7 Length of distance blocks and canister spacing

3.7.1 Basis of canister spacing

The present canister spacing and length of distance blocks together with the division of Posiva's different fuel canister types are presented in Tables 3-1, 3-2 and 3-3 based on input from Appendix E. The supercontainer is assumed to be 0.725 m longer than the canister (see Appendix C), and contains 0.35 m of buffer on both sides of the canister. The steel cylinder and end plates are 8 mm thick and there is a total gap of 5 mm. The thermal analysis by /Ikonen 2003b/ was performed on the basis of a steel thickness of 10 mm.

Table 3-1. Canister spacing (centre to centre) at Olkiluoto in KBS-3V and KBS-3H repositories at a 25 m deposition drift/tunnel separation and a depth of 420 m. The values for SKB's canister spacing are at 40 m drift/tunnel separation.

Fuel	Spacing KBS-3V [m] *	Spacing KBS-3H [m] **	Difference between 3V and 3H [%]
Posiva BWR 1700 W	11.0	11.0	0.0
Posiva VVER 1370 W	8.6	9.1	5.8
Posiva EPR 1830 W	10.6	10.6	0.0
SKB BWR 1700 W***	6.35	7.30–7.95	15.0–25.2

* /Ikonen 2003a/ for Posiva fuel.

** /Ikonen 2003b/ for Posiva fuel.

*** /Hökmark and Fälth 2003/ for all SKB fuel.

Table 3-2. Canister spacing (centre to centre) and length of distance blocks in KBS-3H repository at a 25 m drift separation in a single level repository at a depth of 420 m at Olkiluoto. SKB values are based on 40 m drift separation.

Fuel	Canister spacing [m]	Canister length [m]	Super container length* [m]	Distance block length [m]**	Distance block length with 5 mm gaps [m]
Posiva BWR 1700 W	**11.0**	4.80	5.53	5.475	5.465
Posiva VVER 1370 W	**9.1**	3.60	4.33	4.775	4.765
Posiva EPR 1830 W	**10.6**	5.25	5.98	4.625	4.615
SKB BWR 1700 W	**7.30–7.95**	4.84	5.56	1.74–2.39	1.73–2.38

* The supercontainer is 0.725 m longer than canister.

** No gaps included, a gap of 5 mm on both sides would reduce the length by 0.01 m.

Table 3-3. Posiva's inventory of 2,840 spent fuel canisters. *

Source of fuel canister	Quantity
Olkiluoto 1 and 2 fuel	1,210
Olkiluoto 3 fuel	930
Loviisa 1 and 2 fuel	700
Total	2,840

* /Pastina and Hellä 2006/

3.7.2 Evaluation of present canister spacing and conclusions

Differences between KBS-3H and KBS-3V design alternatives

The reason for longer canister spacing in KBS-3H when compared to KBS-3V in general originates from the geometry of the canister. The shorter the canister spacing, the larger is the effect on heat distribution when the canister orientation is changed from vertical to horizontal, see Figure 3-12. The larger the drift separation, the shorter the canister spacing. SKB's drift separation is 40 m (compared to Posiva's 25 m), which results in shorter canister spacing and therefore the effect of the orientation of canister becomes more significant.

Differences between Posiva's and SKB's designs

The canister spacing is the same in KBS-3V and KBS-3H alternatives at Olkiluoto in case of BWR and EPR spent fuel. In case of VVER fuel there is a 6% difference, which means that 6% more drift length is needed for the same amount of canisters in KBS-3H repository.

In SKB's design the difference in canister spacing between KBS-3V and KBS-3H is 17–27%, /Hökmark and Fälth 2003/, which differs clearly from Posiva's corresponding value as seen in Table 3-1.
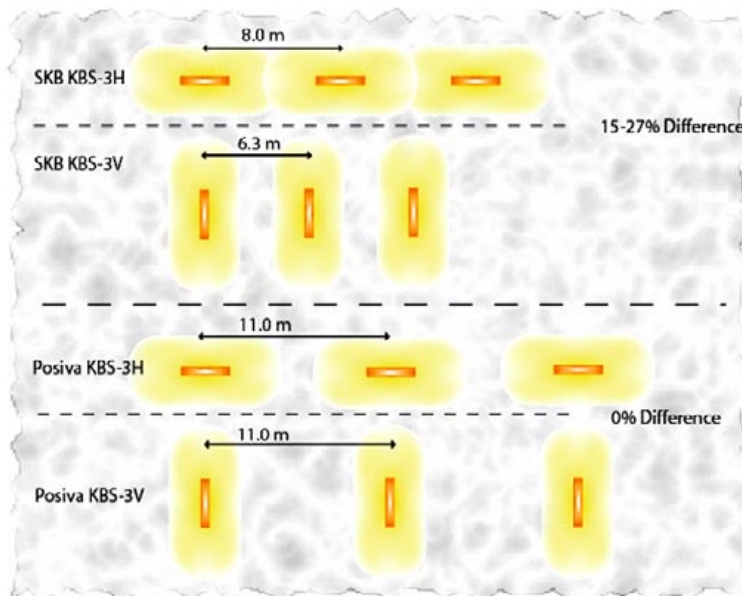
Figure 3-12. Illustration of the effect of canister orientation on spacing in KBS-3V and KBS-3H designs.

In the thermal dimensioning calculations /Hökmark and Fälth 2003, Ikonen 2003ab/ there are some differences due to different site properties, e.g. the thermal conductivity is higher in Swedish candidates sites than in Olkiluoto, as well as the ambient temperature of the repository rock. Furthermore, some of the effects of air gaps around the canister and around the supercontainer are modelled differently. These variations lead to different canister spacings between the different sites.

There are also distinctions between the KBS-3H and KBS-3V repository analyses themselves. The gaps are of different width and in the KBS-3H repository the rock/supercontainer interface is assumed to be air filled whereas in the KBS-3V case the rock/bentonite gap is assumed to be water filled.

Furthermore, in the KBS-3H repository, the interaction between adjacent canisters in the tunnel is the greater the closer the canisters are to one another. Therefore the main reason for the significant difference in Posiva's and SKB's designs originates from the larger 40 m drift separation in SKB's design compared to Posiva's 25 m separation distance, which results in shorter canister spacings and intensifies the effect of canister orientation.

If the rock thermal conductivity is higher (as is the case in SKB site candidates) the canisters can be located closer to each other. The interaction between adjacent canisters is higher in the KBS-3H repository than the KBS-3V. At the Olkiluoto site the rock thermal conductivity is lower and the canister distances are somewhat greater than in SKB sites. The greater distance lowers the interaction of adjacent canisters in the KBS-3H case and the KBS-3H and KBS-3V canister spacings differ less from each other for the Olkiluoto site than in case of SKB's candidate sites.

VVER fuel (Posiva)

If the spacing between canisters is the same (or close to it) for both the KBS-3V and KBS-3H alternatives, there is no significant difference in site-utilization ratio. However, in the case of Loviisa VVER fuel, which is 23% of the total amount, the canister spacing is 17% smaller than in the case of Olkiluoto BWR fuel. The site utilization efficiency is increased slightly from that presented in the previous layout adaptation study, where the spacing has been assumed to be a constant 11 m regardless of the spent fuel type.

Canister spacing

The canister spacing is function of drift separation and it can be optimised with respect to cost and site utilization. Smaller drift separation results in better site utilization and yields a more compact layout. However, as the utilization becomes better, the cost may increase depending on the cost of backfilling and sealing of central tunnels versus the cost of distance blocks.

The shortest distance block is 1.7 m (SKB) and the longest block assembly is 5.5 m (Posiva). The longer block is about 3.2 times longer than the shortest block and it is possible that the longer blocks may function better overall.

It is proposed that the present drift separation and canister spacing be re-evaluated when the functional impacts of canister spacing are resolved, the cost of backfilling and buffer are known, and the importance of site utilization is understood.

4 General design and common design components

4.1 General description of the KBS-3H repository design

The KBS-3H repository design is based on emplacement of spent fuel canisters in the horizontal direction (see Figures 4-1 and 4-2). Deposition drifts start from deposition niches off the main tunnel, and those sections of the drift that are suitable for the emplacement of canisters are called compartments. The design of the deposition niches is considered preliminary and remains a work in progress. Compartment plugs are used to isolate suitable sections of the drift from certain water-bearing fracture zones as substantial water inflow may have detrimental effects on buffer material. Inflow limits are used to determine zone suitability. Inflow limits are also used to establish supercontainer and filling block positions. Filling blocks are placed in positions which are not suitable for supercontainers. Current estimates of inflow limits and their effect on repository design is presented in Table 4-1.

As mentioned previously the supercontainer consists of the canister, the buffer and a perforated steel shell (see Section 3.4). A distance block of compacted bentonite is emplaced between each supercontainer to obtain proper mutual thermal spacing and isolation.

As mentioned previously (Section 3.2.2) one of the most important functions of the distance block is to seal the drift section between the supercontainers to prevent flow and advective transport along the drift. The sealing and plugging is assumed to occur when the distance block absorbs water (saturates), swells and obtains proper swelling pressure.
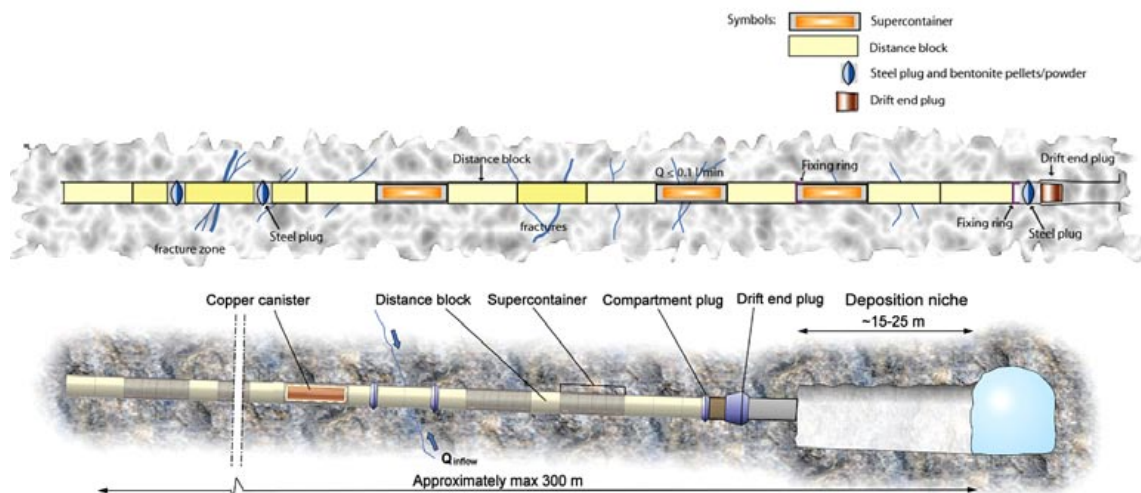
Figure 4-1. *KBS-3H repository design alternative.*

33
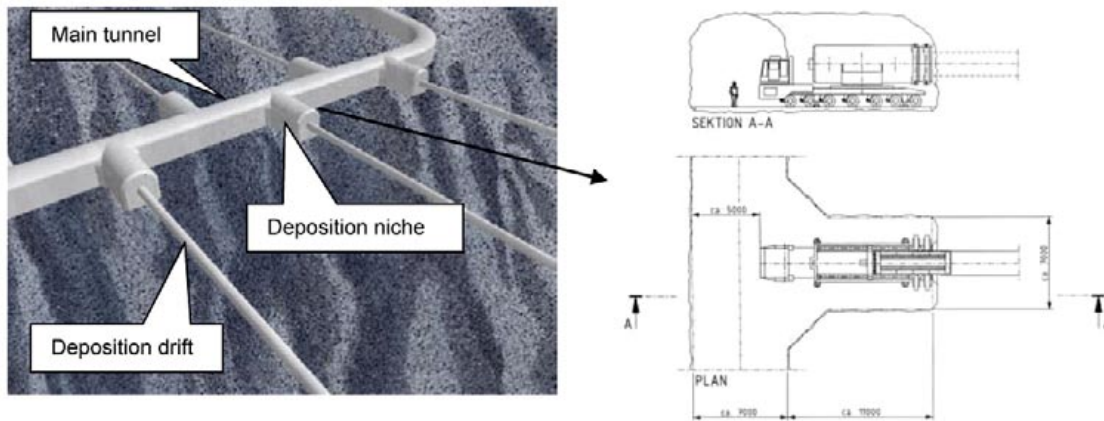
Figure 4-2. *Main tunnel, deposition niches and deposition drifts in the KBS-3H repository design /Thorsager and Lindgren 2004, SKB 2001/.*

Table 4-1. Present estimates for inflow limits based on /Lanyon and Marschall 2006/ and corresponding effect on design.

Inflow (l/min) into a drift section of about 10 m assuming inflow from one fracture	Transmissivity (m²/s) assuming one inflowing fracture [a]	Hydraulic aperture, e, microns	Design action	Reduction in drift utilization degree
Inflow < 0.1	T< 2.65E–9	e < 15	Supercontainer units (one unit is about 10 m).	No effect (a supercontainer can be located into the section).
0.1 ≤ Inflow < 1	2.65E–9 ≤ T< 2.65E–8	15 ≤ e < 32	Filling blocks, estimated length about 10 m.	A bentonite block of 10 m shall be located into the section. One unit reduces the utilization degree by 4%.
1 ≤ Inflow < 10	2.65E–8 ≤T< 2.65E–7 [b]	32 ≤ e < 69	The drift is divided to compartments and the inflow zone is isolated by using compartment plugs. The length of plugged zone is 20–30 m.	A compartment plug unit of 30 m [c] in total shall be located into the section. One compartment plug unit reduces the utilization degree by 11%.

[a] Transmissivity calculated from inflow using Thiem's equation and assuming a constant head of 400 m at a radius of 50 m from the tunnel (radius 0.925 m), see Appendix A.

[b] *If T ≥ 1E–7 m²/s, the section probably belongs to a Class A or B fracture zone and such sections should, therefore, not occur in the bedrock resource where the deposition drifts are located.*

[c] 30 m = stabilization zone 10 m + fracture zone (conductive section) 10 m + stabilization zone 10 m.

As mentioned previously there are two different variations (called candidate designs) of KBS-3H design: a) Basic Design (BD) and b) design based on Drainage, Artificial Watering and air Evacuation (DAWE). BD alternative is based on assumption that the distance blocks will seal the supercontainer units in wet sections stepwise in sequence independently of each other. In DAWE design the drift is filled with water after plugging and sealing the drift compartment and the distance blocks will swell and isolate the supercontainer units simultaneously. These two KBS-3H candidate designs are at the moment being updated to proper level of details based on Olkiluoto bedrock data in order to evaluate the feasibility of the KBS-3H design in 2007.

4.2   Design components common to both alternatives

The components, which are common to both BD and DAWE alternatives, are:

• deposition drift,

• supercontainer,

• buffer material inside supercontainers,

• length of distance blocks,

• compartment plugs,

• drift end plug.

The deposition drift geometry and tolerances were presented in Section 3.5 and Appendix F. The drift design is considered fixed and is identical for both the BD and DAWE alternatives; however it is possible that the requirements for the BD alternative are stricter than for the DAWE.

The supercontainer design was presented in Section 3.4 and is considered fixed with the exception of the modification of end plates from perforated to solid (see Section 3.4.2). The dimensions and properties have been presented in Appendix D and drawing in Appendix C.

The buffer material inside supercontainers has been assumed to be the same in BD and DAWE alternatives. The design parameters have been presented in Appendix D and Section 3.4.1.

The length of distance blocks is the same for BD and DAWE alternatives and fixed for Olkiluoto design and for different type of canisters as discussed in Section 3.8. The nominal length is 5.465 mm based on Posiva BWR 1,700 W type fuel and having 5 mm gaps on both sides of distance block between supercontainers.

4.2.1   Drift end plug

There are in principle three different purposes for the use of plugs: a) sealing and plugging of the drift – designated as a drift end plug, b) isolation of suitable sections and division of the drift into compartments – designated as a compartment plug and c) management of possible operational interruptions – not addressed further in this document.

The drift end plugs are not assigned safety functions, but are designed to be compatible with, and support the safety functions of, the canster, the buffer and the host rock (Appendix A).

All the plugs are in principle temporary structures with respect to long-term function. However the compartment plugs positioned inside the deposition drift end plug are required to function only during the saturation phase, and the drift end plug that seals the drift must maintain its functionality during the period from operation to plugging and sealing the repository.

The plugs can be composed of steel, low-pH concrete, or both. Steel compartment plugs can be installed in relatively short time whereas concrete structures will evidently require a minimum hardening time of two weeks until the structure can be loaded. Steel is favoured over concrete as material because short plugging and sealing time is favourable to the behaviour of buffer under saturation and increases its efficiency. Different design alternatives of concrete drift end plugs have been presented in /Nydahl 2008/ and one type of shotcrete plug alternative has been tested at Äspö.

From the long-term behaviour point of view there are significant differences between plug options as discussed below.

Compartment plug:
- the steel will expand as it corrodes,
- corrosion will produce hydrogen gas,
- after a long period of time the steel converts to impermeable magnetite and other corrosion products,
- the expected lifetime of a steel structure is shorter than that of concrete.

Concrete plug:
- a directly applicable low-pH concrete mixture may not be available today, however it will most likely be available in the near future,
- concrete will dissolve in groundwater after along period of time. The rock aggregate will remain in the position of the former structure and therefore the volume will shrink,
- after concrete dissolving the hydraulic conductivity of the reduced volume will increase,
- the expected lifetime of concrete structure, is longer than that of steel structure.

To satisfy operational and long-term safety requirements an integrated plug with a short-term steel compartment plug and long-term concrete component (as illustrated in Figure 4-3) was selected. The compartment plug enables rapid temporary sealing and isolation from a few weeks to a few months during the early watering of drifts and the concrete plug provides longer term sealing after the concrete hardens, which is estimated to take a few weeks. Based on Olkiluoto data, it is likely that there will be sufficiently dry deposition drifts allowing for the use of concrete-only plugs. In the case of the BD alternative, a concrete-only plug may be able to plug the drift entrance in most cases; however, in the case of the DAWE alternative incorporating artificial watering, the compartment plug is expected in all cases. The use of both steel and concrete plug in series is considered a robust alternative at this phase of design because it functions properly in all situations.

Concrete drift end plug

Conventional low-pH concrete plugs (see Figure 4-4) can be of three different designs:
- friction plug,
- steel reinforced plug positioned in a notch,
- steel reinforces wedge shaped plug positioned in a notch.

Estimated material quantities for these plug alternatives are presented in Table 4-2 and /Nydahl 2008/.
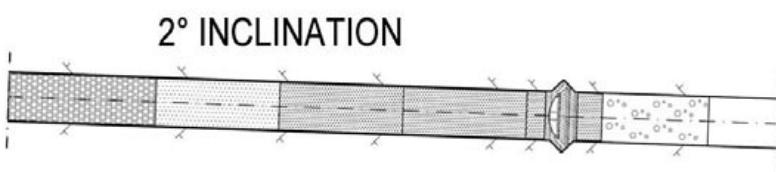
Figure 4-3. The drift end plug arrangement based on a rapidly installed steel compartment plug and a final concrete plug. Extra filling blocks are installed adjacent to plugs to compensate the possible density reduction in future. Note: the picture shows a friction plug, however the reference design is based on steel reinforced concrete plug positioned in a notch.
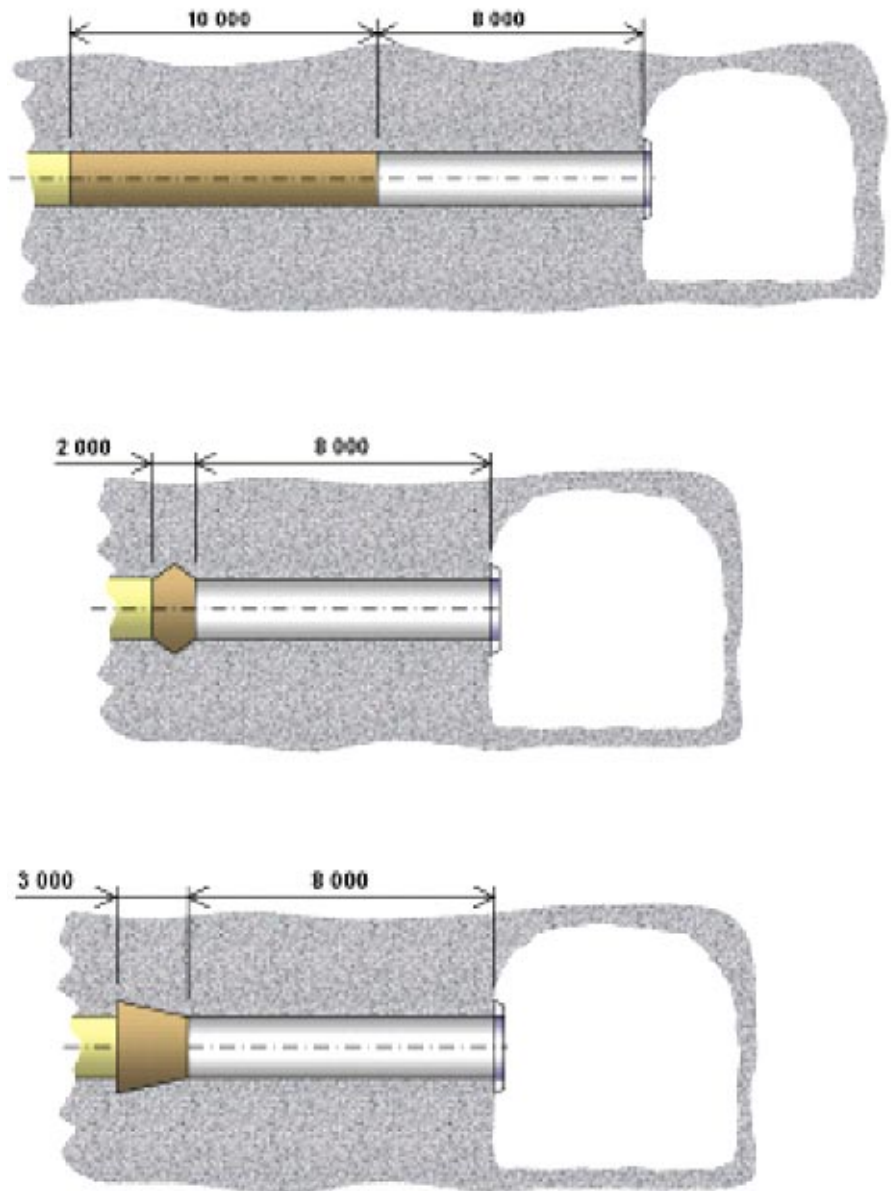
Figure 4-4. *Concrete plug alternatives: Friction plug (top) similar to shotcrete plug, Steel rein-forced plug positioned in a notch (middle) and Steel reinforced plug positioned in a notch (above) /Thorsager and Lindgren 2004/.*

Table 4-2. Material quantities in different plugs. The material quantities are based on /Nydahl 2008/ and have been adjusted from 1.75 m drift diameter to 1.85 m diameter.

Plug type	Friction plug*	Steel reinforced	Steel reinforced wedge shaped	Rock plug
Length, m	11	2	3	2
Concrete, m³	30	8	11	1.2
Steel reinforcement, kg	1,860	860	550	200
Rock	–	–	–	4.5
Cooling and grouting pipes, m	430	123	168	–

* made of concrete or shotcrete.

Cement-grouted rock drift end plug

An alternative plug design based on using a rock kernel is illustrated in Figure 4-5. The kernel is slightly wedge shaped. The amount of concrete in the design is clearly smaller than in other alternatives. Therefore the possible chemical disturbance caused by concrete is smaller than in other alternatives and the potential open void resulting from the long-term dissolution of concrete is also smaller. The design is quite preliminary and has not been tested.

Reference design of drift end plug

The drift end plug reference design (steel reinforced concrete plug positioned in a notch) is shown in Figure 4-6. It was selected on the basis of its technical feasibility and concrete minimization potential. The cement-grouted rock plug is an attractive alternative due to the small quantity of concrete required, but the design is novel and needs to be properly verified. A compartment plug can be positioned adjacent to the concrete plug when necessary for rapid sealing during the hardening of concrete.
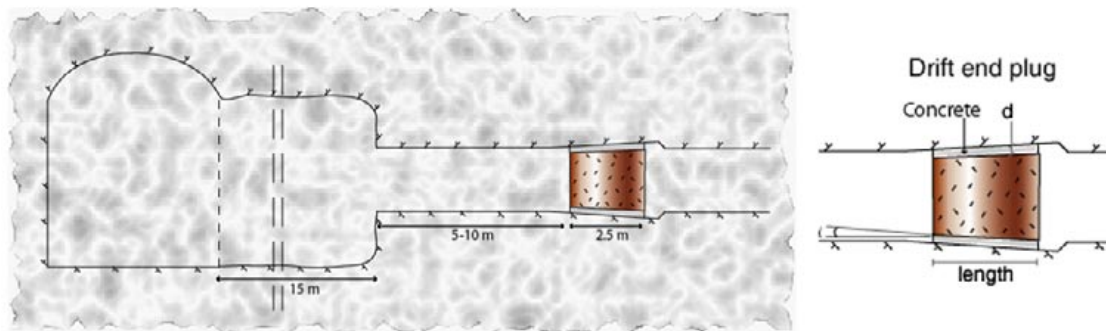
Figure 4-5. *A draft of a rock plug grouted in the drift.*
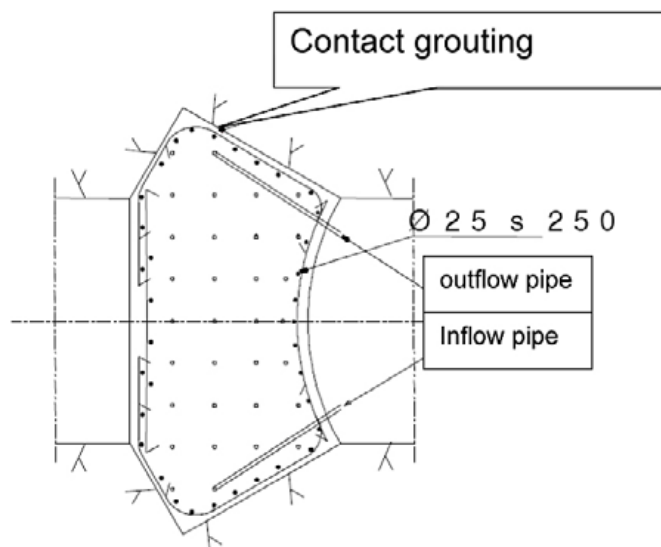
Figure 4-6. *The steel reinforced plug positioned in a notch (see /Nydahl 2008/ for details).*

Low-pH concrete

The concrete plug design is based on the use of low-pH cement. The exact composition of the concrete remains to be developed, but there is reason to believe the design basis will be valid due to several different research and development efforts. For example, the composition of the Low Heat High Performance Concrete (LHHPC) used in the Tunnel Sealing Experiment in Canada at AECL's Underground Research Laboratory URL is presented in Table 4-3 /Martino et al. 2002/.

The composition of the LHHPC is regarded as a potential reference example of possible concrete to be used in the drift end plug because the composition has been specified adequately and it is designed to ensure a very low hydration heat and very good performance in a repository environment.

The LHHPC cement is sulphate-resistant Portland cement (in Canada Type 50) and the silica flour is the filler from grinded quartzite with a very low pozzolanic reactivity. The particle size distribution is 1–100 μm for a silica content of 99.8%, this obtained from US Silica in Illinois in is Sil-Co-Sil 53. The silica fume is product from SKW (Silica Becancour with an average grain diameter of 0.25 μm. The superplasticisers used in the mixture is naphthalene sulfonate, liquid form and the aggregates are of type rounded aggregates, 98% from magmatic rock and some limestone, screened directly at the URL, dried and bagged at the Winnipeg Lafarge plant before the final mix. The gravel particle size is between 4.5 and 12.5 mm and sand is ASTM C33 (9% passing 150 μm sieve) with fineness modulus of 2.66.

4.2.2 Drip and spray shields

The spraying, dripping, and squirting of groundwater (see Figure 4-7) onto buffer material is prevented by placing metal spray shields over inflow points. At single inflow points the shielding can be implemented through the use of stud type nipples. Inflow coming from the roof of the deposition drift will be redirected towards the lower half of the drift.

Table 4-3. Composition of the low-pH concrete called Low-Heat High Performance Concrete (LHHP) used in the Tunnel Sealing Experiment in Canada at AECL's Underground Research Laboratory URL /Martino et al. 2002/.

Constituents (kg/m^3)	
Cement	97.0
Silica fume	97.0
Silica flour	193.8
Sand	894.7
Coarse aggregates	1,039.6
Superplasticisers	10.3
Water	97
Principal properties	
E/C ratio	0.98
Slump (mm)	170
Density (Mg/m^3)	2.424
% mineral addition	80
Compressive strength MPa (28 days)	75
Elastic modulus (MPa)	36,000
Hydraulic conductivity (m/s)	$< 10^{-14}$
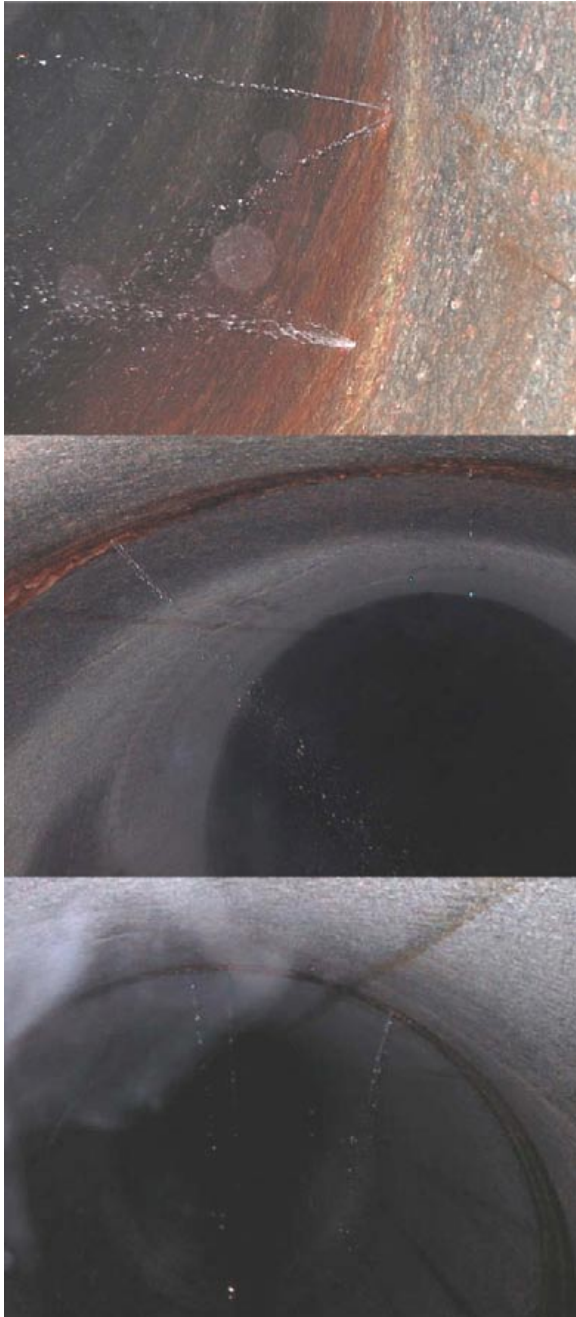
Figure 4-7. *Example of spraying inflow points in the KBS-3H demonstration drift at Äspö*
Photo by J. Autio.

Material alternatives for the shields are copper or steel. Steel is preferred because the structures are thin (in mm range), their number is small, and the steel completely corrodes in a relatively short period of time when compared to the supercontainers. The shields are fastened mechanically with screws into small holes drilled in the rock. Round "penny" type washers are placed in positions of single flow points. The sheets are shaped to follow the rock surface tightly. The drip shields shown in Figure 4-8 were tested in the KBS-3H demonstration drift at Äspö Hard Rock Laboratory (HRL).

The weight of the drip shields that was tested was 220 grams on the average. It is possible that two shields are required in leaking fracture intersections with several inflow points on both sides of drift wall and the mass of shields and attachment bolts is less than or equal to 600 g. The estimated number of shielded sections is 4-5 per drift.

Figure 4-8. *Drip shield attached to the demonstration drift at Äspö (right) and after detachment on the floor (left). Photos by H. Wimelius.*

4.3 Compartment plug

4.3.1 Design

Steel compartment plugs are used to isolate water-leaking fractures or fracture zones, which are unsuitable for deposition of canisters, from more suitable sections of the drift.

A list of design bases as input parameters to be used in the detailed design of steel compartment plug is presented in /Nydahl 2008/. The compartment plugs are not assigned safety functions, but are designed to be compatible with, and support the safety functions of, the canster, the buffer and the host rock (Appendix A).

The design of the steel compartment plug entails installation of a steel collar structure in the rock before the start of deposition operations. The collar is attached to the rock surface and sealed during installation with concrete. This procedure allows the centre part of the plug to be rapidly installed during deposition operations.

The functional purpose of the compartment plug is to isolate "good quality" deposition compartments from "bad quality" water-bearing fracture zones, which may have detrimental effect on the distance blocks and supercontainers during saturation. In general, the design requirements are as follows:

a) Provide an adequate drift seal, which prevents flow through the plug and rock plug interface, to avoid erosion of buffer. The flow should be reduced to the same order of magnitude as the flow through the rock. The plug is positioned in good quality rock sections in the drift.

b) The plug is capable of supporting a full hydrostatic pressure of 5 MPa after installation.

c) Form a confining surface to maintain the supercontainers and other components (e.g. buffer) in position during operation. It is assumed that these forces will be equal to or less than hydrostatic pressure during operation.

The basic design of the compartment plug is the same for the BD and DAWE design alternatives, with the exception perforations for the pipelines found only in the DAWE alternative.

The plug can be used to withstand the groundwater pressure from one or both sides. The plug is composed of one or two caps depending on the direction of the force.

41

The plug consists of a V-shaped groove excavated to the drift, a steel-fastening ring, a collar mounted against the ring, and a cap installed on the collar. The space between the ring and the rock is grouted (see Figures 4-9, 4-10, 4-11, 4-12 and 4-13). The design has been described in Appendix H.

The cap is in the shape of a dome attached to a flange. The shape of the cap has been chosen so that the stress distribution in the cap is as even as possible. The height of the cap is 400 mm.

Construction of a two-sided plug configured with the least possible number of parts, requires a symmetric groove in the rock and a symmetric fastening ring and collar. These components behave similarly in either of the two possible directions of the acting force.

In this construction all, or almost all, of the joints in the steel assembly are sealed by welding. The fastening ring and collar components are welded together, and the collar itself is welded to the fastening ring. The rear side cap, which is installed first, may be fastened with bolts, but the front side cap, under current plans, is fastened and secured by welding.

The final steel weights of the fabricated parts are:

- Fastening ring 400 kg.

- Collar 1,250 kg.

- Cap 440 kg.

The required amount of concrete for casting the space between the ring and rock is approximately 190 litres.

The approximate total steel weight of a one-sided plug without bolts is 2,090 kg. The bolts add ca 20 kg to the weight. The grade of the steel used is general structural steel S355J0.
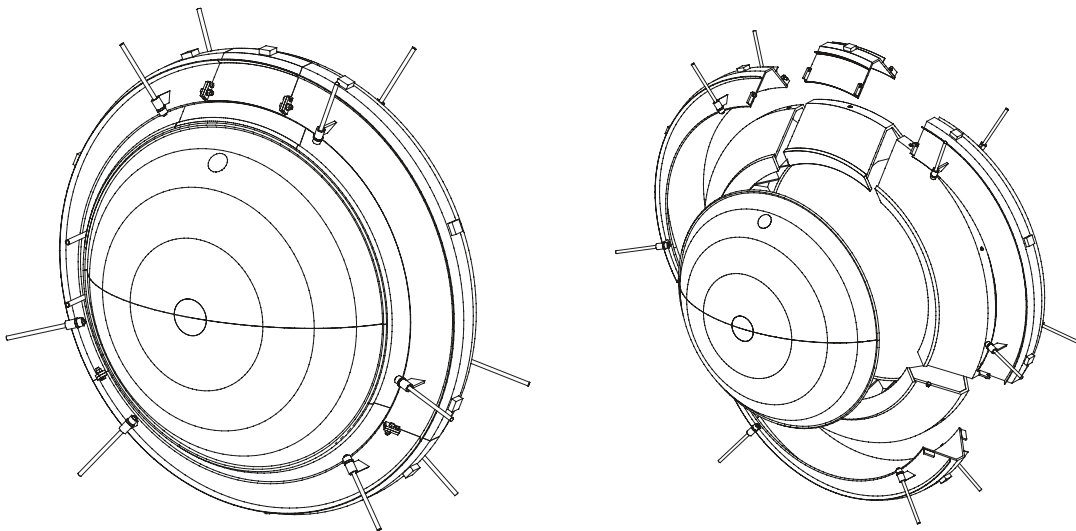
Figure 4-9. *The steel compartment plug as seen from the high-pressure side with a break down to pieces.*
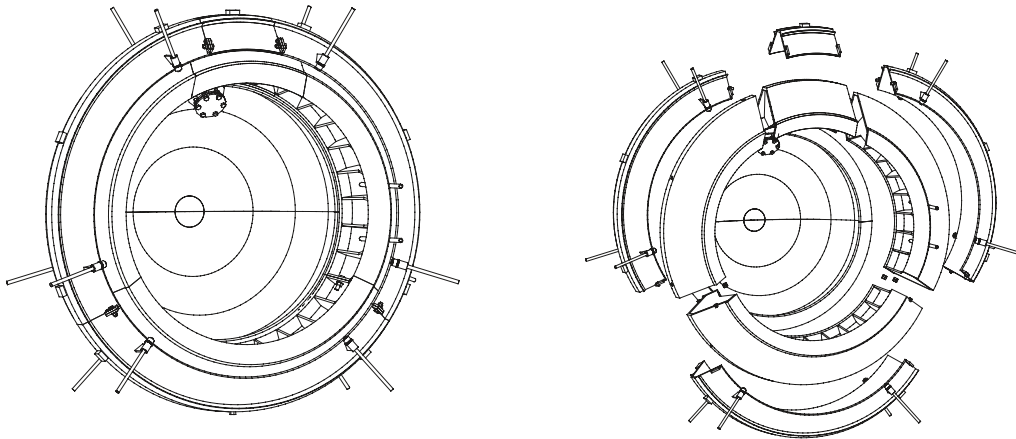
Figure 4-10. *The steel compartment plug as seen from the low-pressure side with a break down to pieces.*
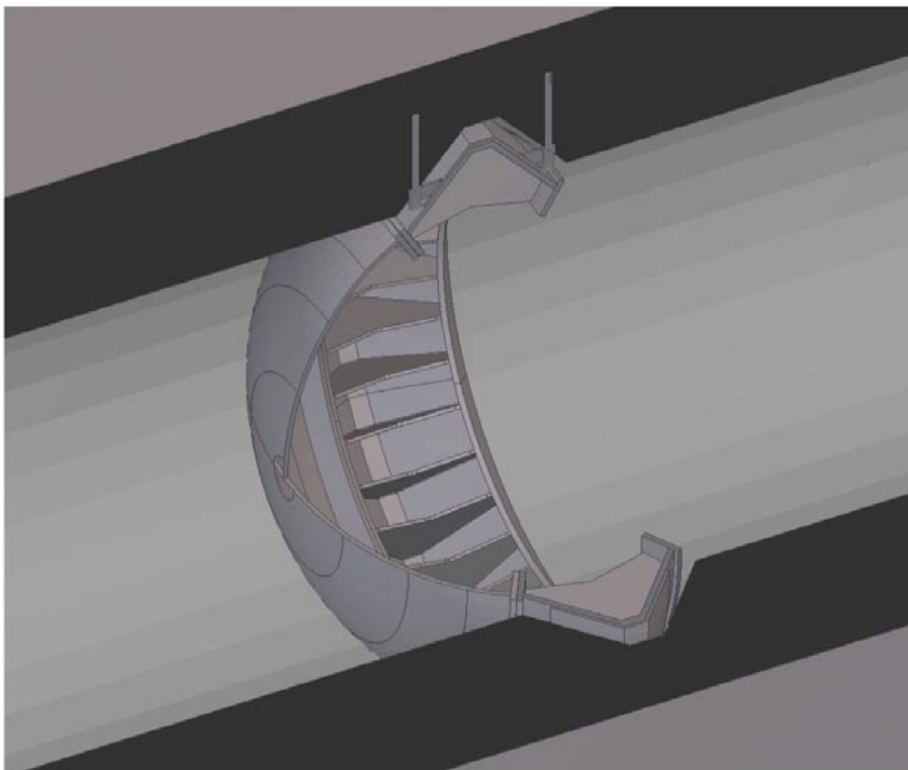
Figure 4-11. *3D image of the steel compartment plug as seen from the high-pressure side.*
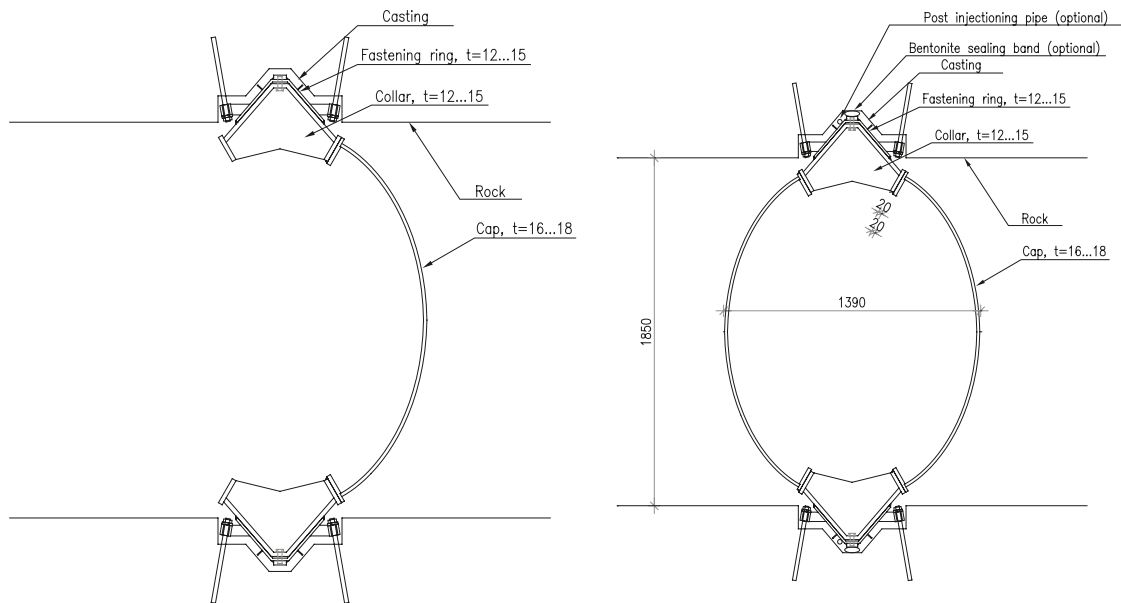
Figure 4-12. *Cross-section of the compartment plug: one-sided with one cap (left) and two sided with two caps (right) dimensioned to withstand pressure from one or both sides respectively.*
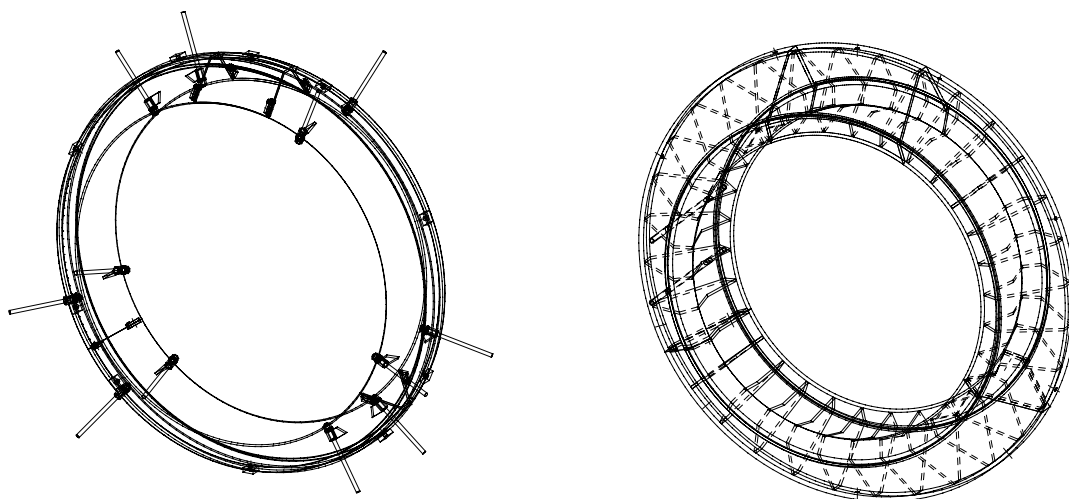
Figure 4-13. *Fastening ring (left) and collar (right). The fastening ring is installed in the drift before operation starts.*

4.3.2 Modeling of plug behaviour

The deformation of the plug under pressure was analysed using the general FEM program Algor. The structure was modelled with either 8- or 6-noded brick elements. Due to symmetry considerations, only a quarter of the plug was modelled. The modelling is fully described in Appendix I.

The basic load acting on the surface of the cap is 5 MPa, which corresponds to the groundwater pressure at 500 meters of depth. The direction of the load is perpendicular to the surface. A load safety factor of $\gamma = 1.35$ and a material safety factor $\gamma = 1.1$, in accord with Eurocode 3, were used (see Table 4-4). The calculation strength of the steel is $f_d = 355$ MPa / $1.1 = 323$ MPa.

Table 4-4. Summary of the design data for modelling of the steel compartment plug.

Design data		Geometry	
Pressure	5 MPa	Diameter of the cap	1,650 mm
Load safety factor	1.35	Height of the cap	400 mm
Material safety factor	1.1	Thickness of the cap	16 mm
Material	Steel S355	Collar main plates thickness	20 mm
Grout elastic modulus	35.5 GPa	Thickness of the grout layer	40 mm
Rock elastic modulus	50 GPa	Thickness of the rock layer	60 mm
Steel elastic modulus	205 GPa		
Poisson's coefficient	0.3 (0.15 grout)		

The load on the dome is defined as a surface load acting perpendicularly to the top surface of the dome. Only one load case, with a pressure load 5 MPa and a load factor 1.35, was considered. The modelled structure includes all of the steel components, the rock surface, and the concrete cast between the rock surface and the steel assembly. The model geometry is shown in Figure 4-14; the different colours correspond to different structural aspects. Contact surfaces were defined between the various structural aspects, allowing for parallel movement between them. The interface between the concrete casting (grey colour) and rock surface is an exception, as adhesion was assumed and a fixed connection defined. Symmetric boundary conditions were applied to the cut planes of the model and a fixed boundary condition was applied to the outer surface of the rock.
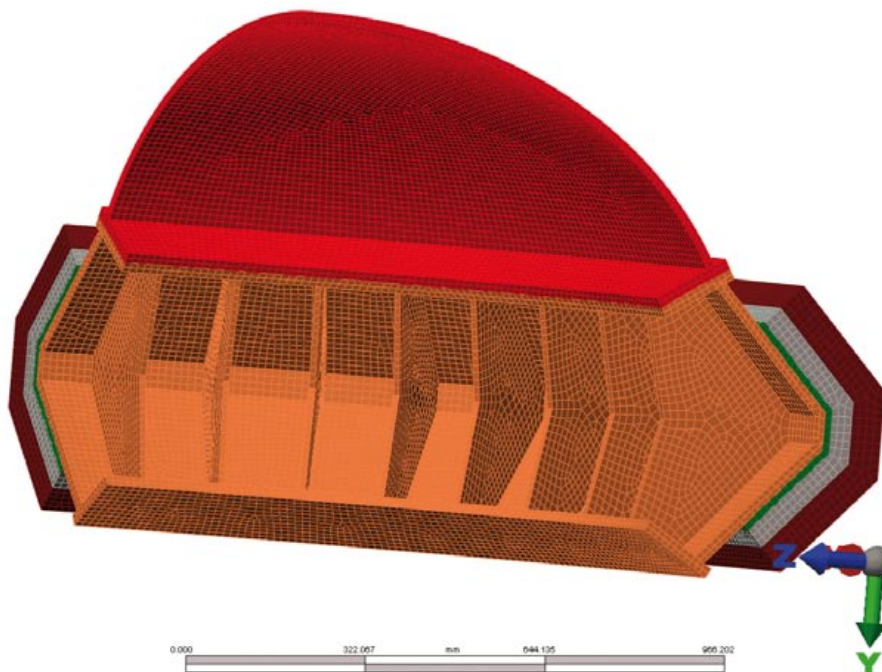
Figure 4-14. *Model geometry of the steel compartment plug.*

The von Mises stress distribution is shown in Figure 4-15 and displacements of the dome in Figure 4-16. As can be seen in Figure 4-15, the highest stresses occur at the centre of the dome. Some stress concentration can be seen at the perimeter of the dome, where there is a fixed boundary condition. The von Mises stresses are below the calculation strength f_d = 323 MPa, and hence the stresses are on an acceptable level. The maximum displacement at the centre of the dome is 1.4 mm with a load factor of 1.35, and thereby the displacement with the nominal load of 5 MPa is ca 1 mm.

The stresses and displacements of other parts of the structure are shown in Figures 4-17 and 4-18. The load factor 1.35 is included in the values. The displacements outside the dome are of a magnitude of tenths of millimetres. Outside the dome, which is covered by the distinct model, highest stresses appear in the stiffening ribs. The stress level (maximum stress 230 MPa) is, however, well below the calculation strength of the steel.

Compression stresses in the concrete cast were also analysed. Stress peaks can be seen at the intersection points of the collar profile and stiffening ribs. The maximum stresses in general are approximately 100 MPa. Stress peaks are somewhat higher, but the area where stresses above 100 MPa occur is negligible. The compression balances out rapidly in the base of the concrete cast. In the rock, at the bottom of the groove, the highest compression stress values are approximately 32 MPa. The stresses are shown in Figure 4-19.

Resistance against snap-through was evaluated with a non-linear Mechanical Event Simulation solver and the load was applied stepwise.

A two-phase approach was used to examine the effect of eventual shape imperfections produced in the manufacturing process (see Appendix I). The results indicated that minor deviations (less than 5 mm) in shape do not cause excessive stresses.
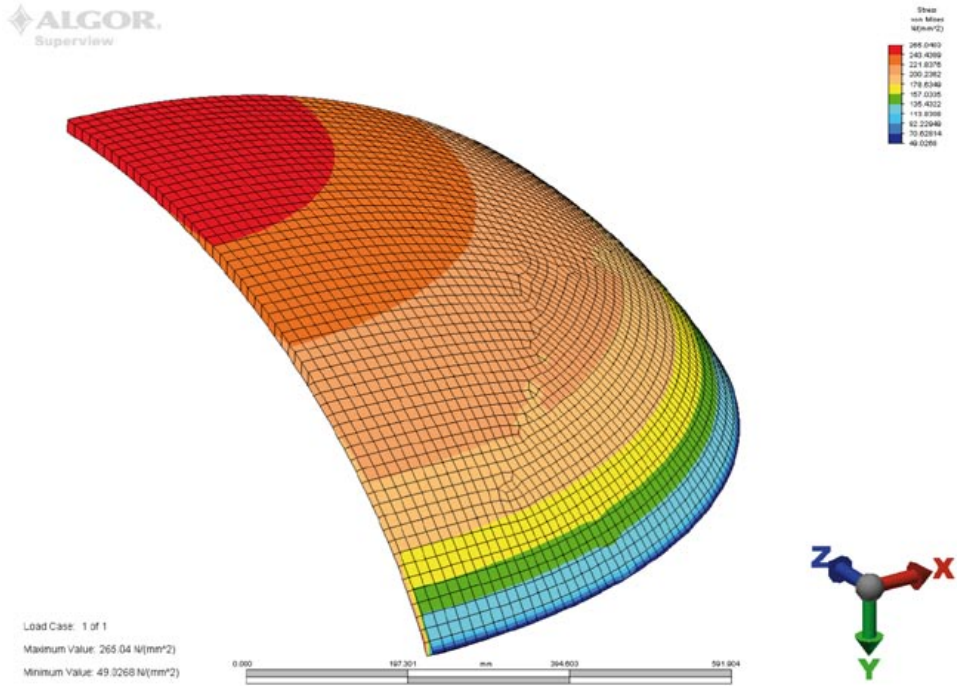
Figure 4-15. The von Mises stress distribution in the steel compartment plug.
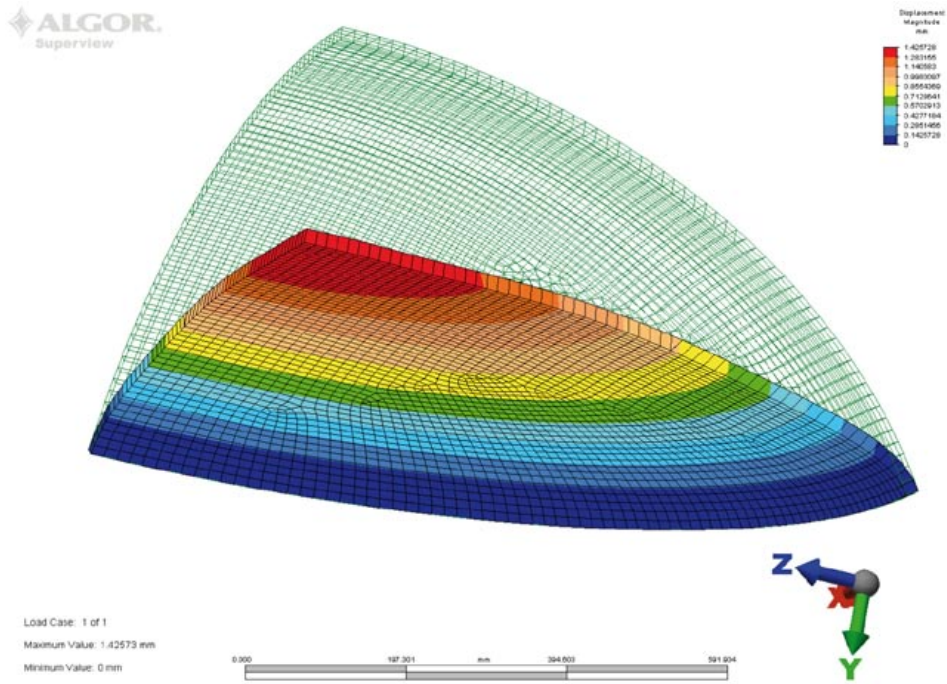
Figure 4-16. *Displacements of the steel compartment plug.*
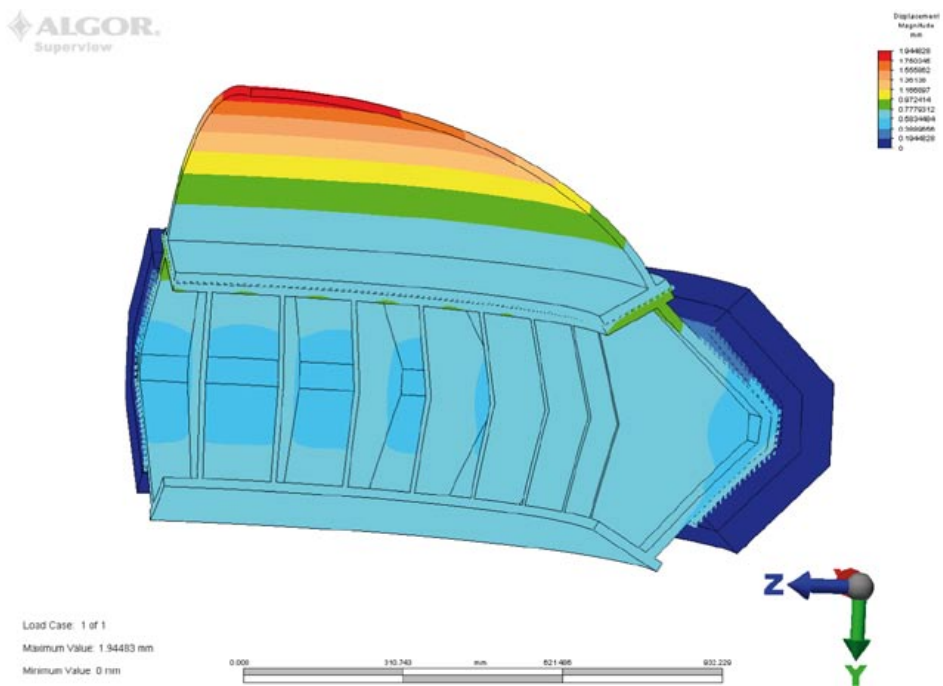
Figure 4-17. *Displacements of the steel compartment plug.*
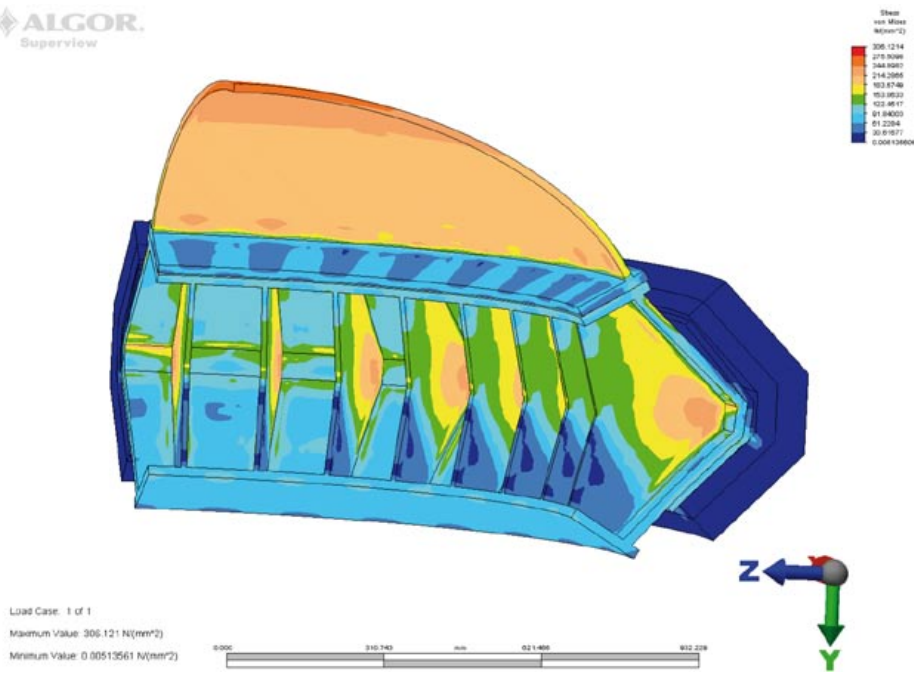
Figure 4-18. *The Von Mises stress in the steel compartment plug.*
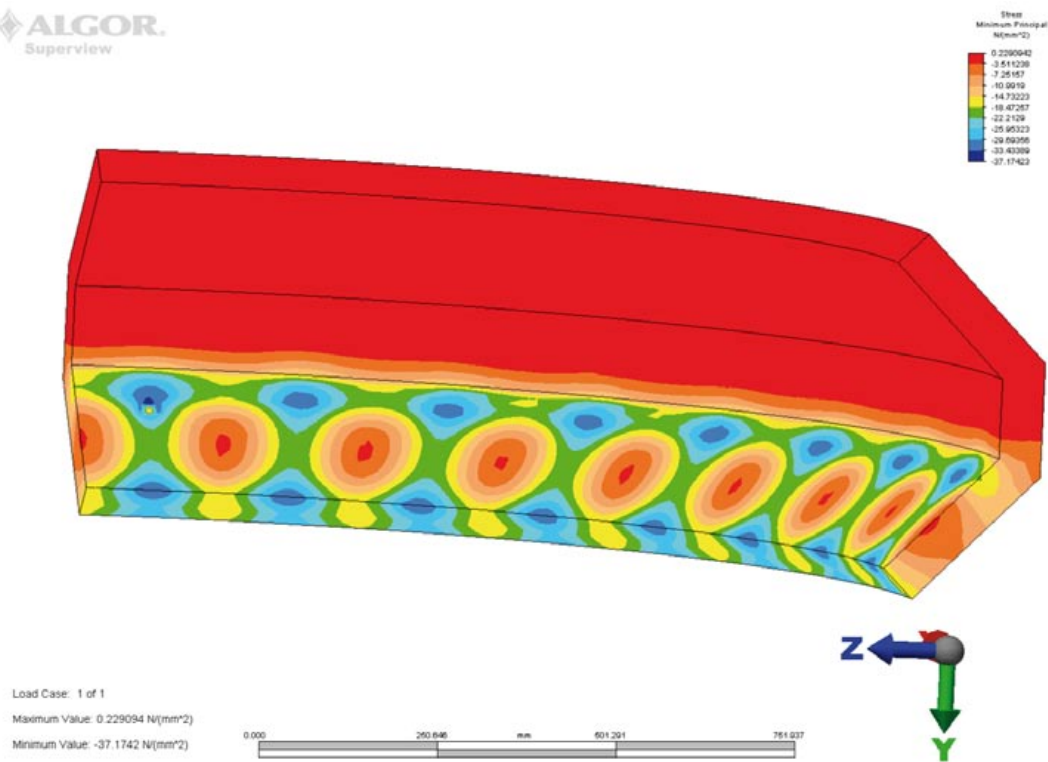
Figure 4-19. *Minimum principal stress in rock at the bottom of the groove.*

5   BD (Basic Design) alternative

5.1   Specification of the functional structure

In the following discussion, it is assumed that the application of proper techniques, which will not be further elaborated, has reduced groundwater inflow. Groundwater control techniques are described in Chapter 9. Additionally, deposition drift, canister, and supercontainer functions are only briefly described here as they are considered as fixed design aspects.

The design is based on the following functional requirements:

- **Prevention of buffer erosion by spray and drip shields.** Direct water flow on buffer surface will cause surface erosion. Spraying, squirting and significant dripping of groundwater on supercontainers and distance blocks is prevented by using shields.

- **Isolation of compartments from water-bearing fracture zones by plugs – compartment formation.** Isolation of deposition compartments from water-bearing fracture zones, which may have detrimental effect on the distance blocks and supercontainer during saturation, will be accomplished through the use of plugs.

- **Sealing of the drift entrance by plugs.** The deposition drift is sealed and plugged after emplacement of canisters. The plug will support hydrostatic pressure in the drift after operation and retain the supercontainers and other components in position. The plug will be exposed to both hydrostatic pressure and swelling pressure from the buffer. The plug is positioned so that flow from the drift into the surrounding open tunnels is small enough to prevent detrimental erosion effects.

- **Interruption of operations by plugs.** The emplacement of supercontainers can be stopped temporarily if the drift is plugged rapidly before the distance blocks start to swell into the open tunnel. Such interruptions are feasible after the plugging of one compartment.

- **Hydraulic isolation of supercontainers by distance blocks.** Hydraulic isolation of successive supercontainer sections from one other during the saturation phase by using distance blocks. In this manner each supercontainer section is saturated by groundwater inflow from bedrock without flow from one supercontainer section to another.

- **Thermal spacing of canisters in the drift by distance blocks.** Adequate thermal spacing between successive canisters is obtained by using a distance block of required length.

- **Prevention of displacement of distance and filling blocks by fixing rings.** Large hydraulic pressure induced forces may cause displacement of distance and filling blocks. The use of fixing ring type supporting structures prevents these situations.

- **Sealing of unsuitable sections by filling blocks.** Positions that are not suitable for emplacement of a supercontainer, because of larger-than-accepted water inflow or other reasons, are packed with filling blocks. The objective of the blocks is to provide extra sealing capacity between neighbouring distance blocks and to reduce the hydraulic pressure induced force exerted on distance blocks adjacent to supercontainer sections.

- **Compensation of local density reductions by filling blocks with extra swelling potential.** Density reductions may be caused by dissolving cement from drift plug or compaction of lower density filling adjacent to compartment plugs.

- **Drainage of major inflows during operation from volume between plugged compartments by permeable low compressibility filling and swelling partially permeable filling.** Sections with significant water leakage, which are not suitable for deposition, are isolated from other sections of the drift by installing two plugs, one on each side of the inflow section. The volume between compartment plugs is backfilled and drained until the second plug is in place.

5.2 Specification of the design components

5.2.1 General

Deposition drift, supercontainer etc design components are kept fixed and are not considered in this context. The Basic Design - Design Components (BD-DC) shown in Figure 5-1 are:

- BD-DC1 Spray and drip shield

- BD-DC2 Distance block

- BD-DC3 Fixing rings to support distance blocks

- BD-DC4 Coupling between supercontainer and distance block

- BD-DC5 Compartment plugs

- BD-DC6 Filling blocks

- BD-DC7 Drift end plug

- BD-DC8 Permeable filling

- BD-DC9 Partially permeable filling.
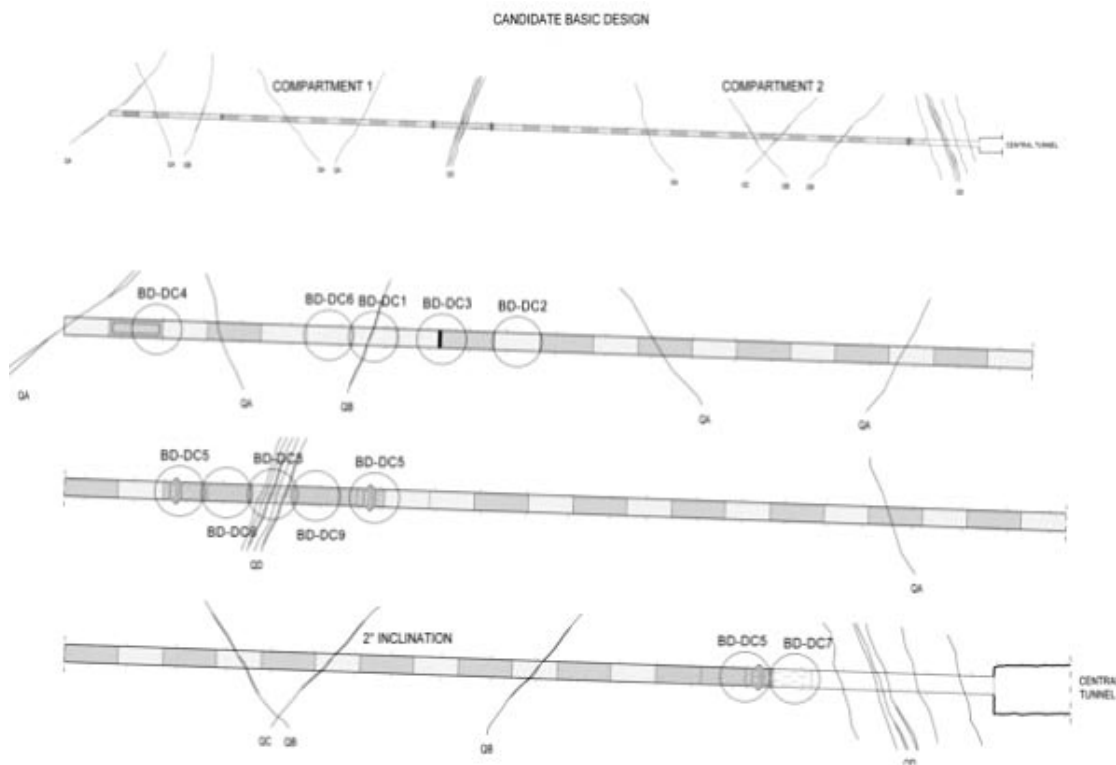
Figure 5-1. *Components of the Basic Design alternative (QA, QB, QC refer to fractures with different inflow rates).*

5.2.2 Distance block

A distance block is positioned between supercontainers. The purpose of the distance block, according to the requirements specified in Appendix A, is to maintain the integrity of the canisters for at least 100,000 years by protecting them from detrimental THMBC (thermo-hydraulic-mechanical-biological-chemical) processes, and to limit and retard the release of any radionuclides from any damaged canisters. The distance blocks also separate the supercontainers hydraulically one from another, thus preventing the possibility of preferential pathways for flow and advective transport within the drifts through the corrosion products or altered buffer. Furthermore, the distance blocks maintain spacing between the canisters along the drifts ensuring that temperatures are maintained at acceptable levels. The distance bocks are required to provide a nearly impermeable, once saturated, tight interface with the drift rock wall within a reasonable time.

Several distance block designs were evaluated and the basis for the selected design is found in Appendix J. The selection was based on experimental observation of sealing ability and also operational aspects such as emplacement technique and time. The preferred reference distance block design is based on using two different components in series; a "tight" block and a "loose" block as shown in Figure 5-2. There is sufficient experimental evidence from previous studies (/Börgesson et al. 2005/, Appendix K) to expect that the sealing ability of the proposed design is adequate. The bentonite used in the distance blocks is MX-80 with an initial water content of 24%, a final saturated density of 1,950–2,050 kg/m^3 and a dry density of 1,481–1,637 kg/m^{-3}.

The first unit is a one-meter long, fixed length "tight" fit block, which is emplaced in contact with the rock surface providing a gap on the order of the surface roughness of a few milli-metres. This component provides for rapid sealing. The overall design is flexible because the length of the "loose" block can be modified to fit different canister spacings. The surface quality of the drift in distance block positions will be improved by mechanical grinding, if necessary, to obtain a constant diameter and a smooth surface to reduce the gap. The "tight" block can be put together in two ways. In both, the block is emplaced in slices and the number of slices is defined by the final required thickness of the block (see Figure 5-3). The number of cylindrical slices, which are composed of smaller blocks, in a 1 m long "tight" distance block is only two. The length of the unit can be adjusted to different canister spacings by adding or subtracting "loose" component blocks, as the "tight" sealing length remains constant.

The "tight" distance block can be composed of three large slightly wedge shaped blocks (see Figure 5-4), which are pushed in place by using the equipment shown in Figure 5-5. As an alternative, the "tight" block can be made of a cylindrical large centre block and a number of small wedge-shaped blocks as shown in Figures 5-6 and 5-7. The longer "loose" block is installed adjacent to the "tight" block by using a different and more efficient technique with a nominal gap of 15 mm. The block is centralized to obtain a constant gap over the whole perimeter by using small, steel feet. An alternative design, which makes use of rock as centralizing material, is also under consideration.
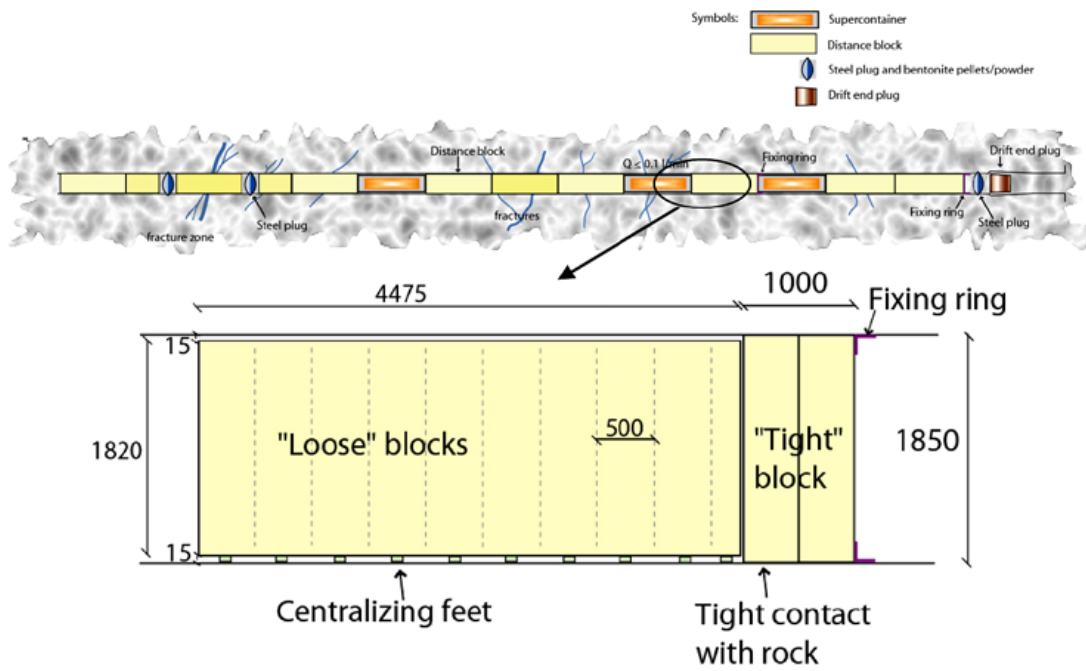
Figure 5-2. *The distance block unit is composed of "tight" and "loose" components in the BD alternative, initial gaps between block and drift surfaces range from 15 mm to a few mm.*
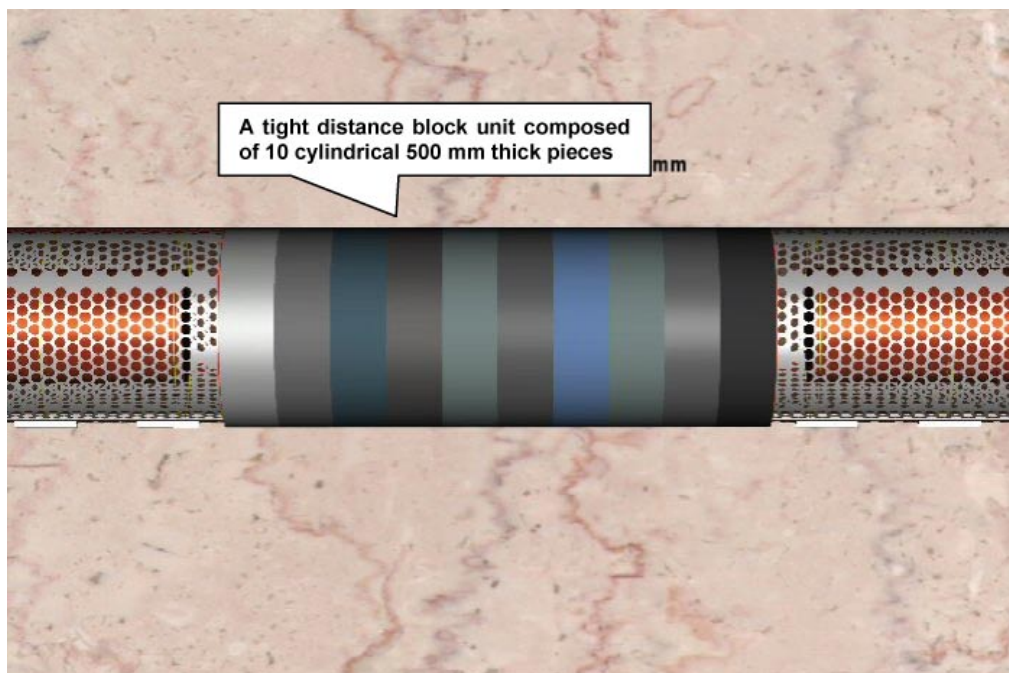
Figure 5-3. *The "tight" component of distance block unit is composed of slices of thickness of approximately 500 mm.*

Tvärsnitt

Ovanifrån
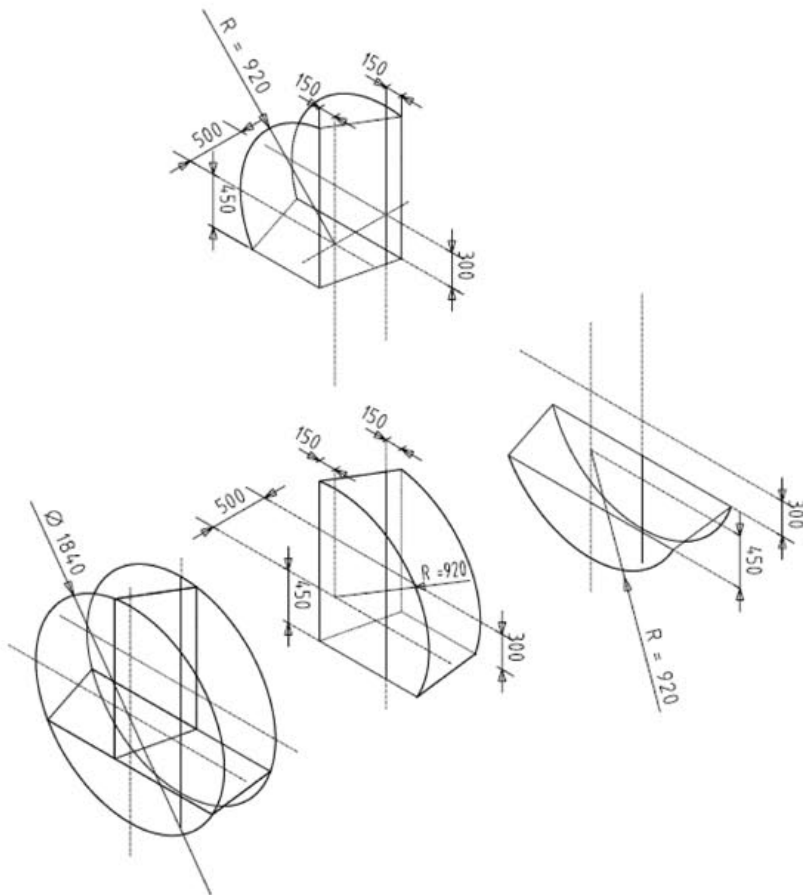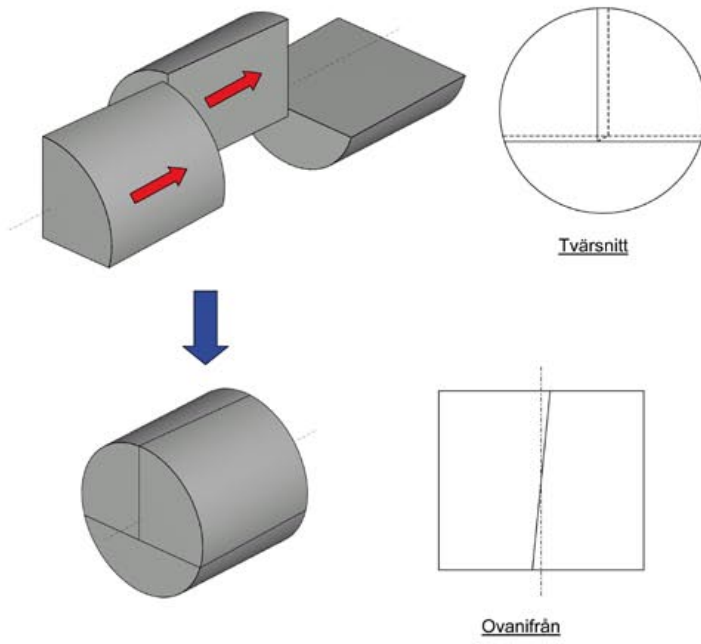
Figure 5-4. *The dimensions of "tight" component of distance block unit based on three pieces in BD alternative.*
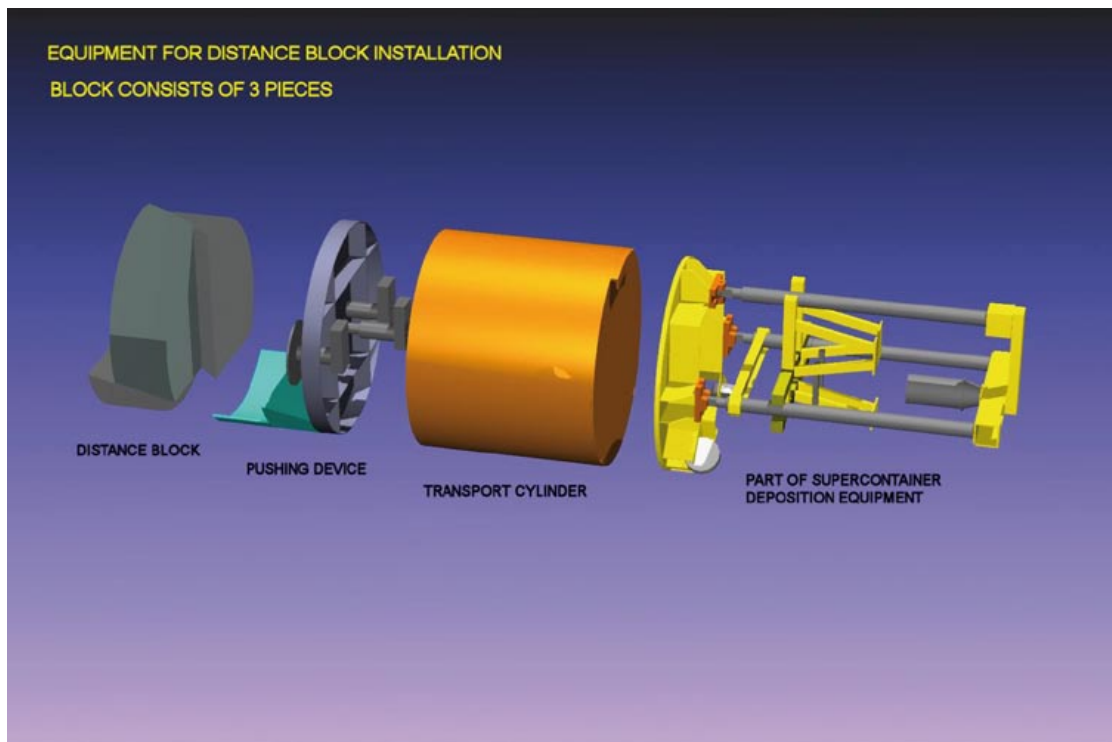
Figure 5-5. The principle of emplacement of "tight" distance block unit based on three pieces.
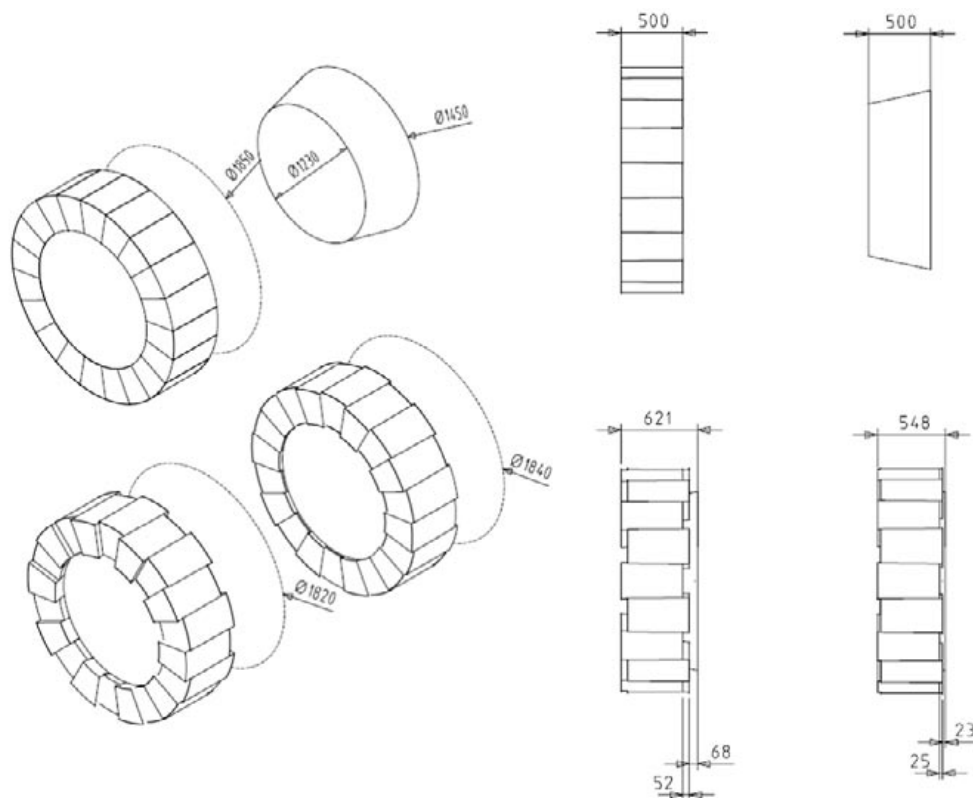
Figure 5-6. The dimensions of the "tight" component of the distance block unit based on a central cylinder and small blocks in the BD alternative.
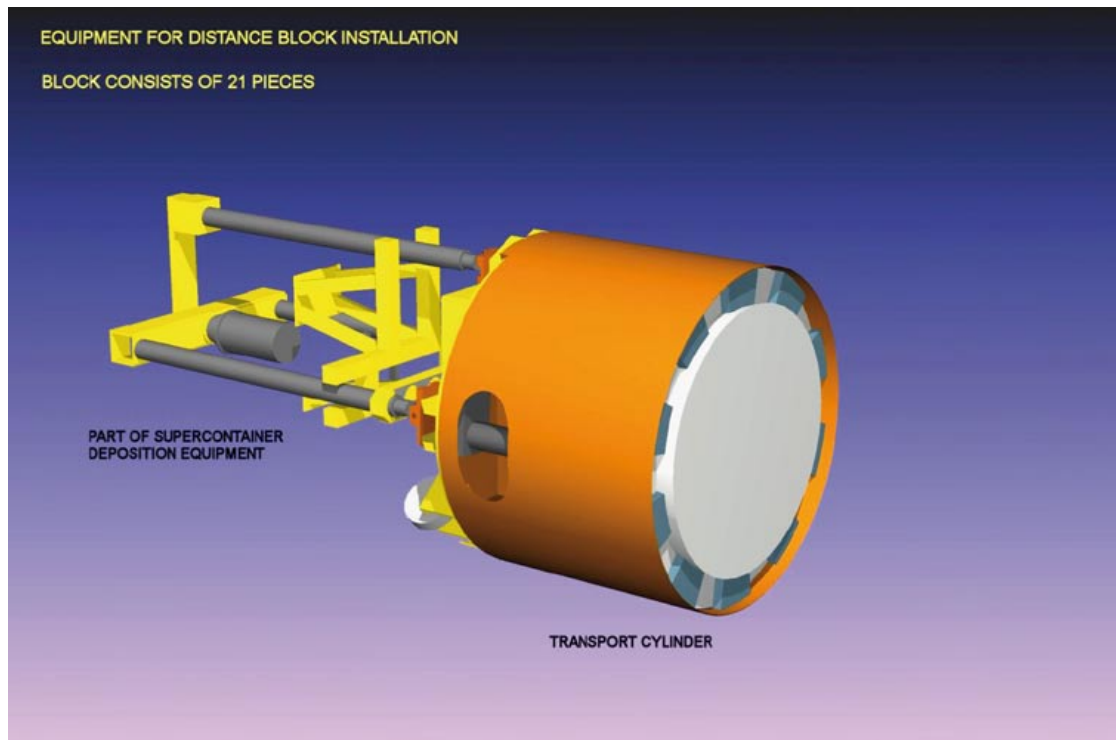
Figure 5-7. *The principle of emplacement of "tight" component of distance block unit based on a centre cylinder and small blocks in BD alternative.*

5.2.3 Fixing rings to support distance blocks

In all probability, there will be supercontainer sections that will stay dry for relatively long periods of time immediately next to sections that will saturate and rapidly obtain full hydrostatic pressure. Saturation times may differ by two orders of magnitude or more from one section to the next. For example, the empty volume in one supercontainer section can fill and the bentonite swell to fill the open gap in 10 days whereas the neighbouring section in tight rock may fill and the buffer swell over 200 days or more.

The distance blocks must maintain their sealing ability between large hydrostatic pressure differences. If there is full hydrostatic pressure on one side of the distance block and no pressure on other side, the resultant force may displace the block (see Figure 5-8). As a result, piping of water flow through the distance block and bentonite erosion may occur.

The displacement of the block is counteracted by the friction of the block against the rock surface and support from the next supercontainer section. Additionally, the use of a supporting structure, which will fix the distance block mechanically in the desired position (Figure 5-9), aids in preventing displacement of distance blocks. This supporting structure will be positioned on one side of the distance block to prevent one-way movement.

Fixing rings are installed in every position where the inflow in the supercontainer unit is larger than 0.01 l/min after sealing. This inflow limit is a rough estimate and needs to be verified.

The fixing ring design is based on the following design requirements:

- The ring shall be constructed in one shift (7 hours).
- The fabrication material is steel, similar to that of the supercontainer.
- The ring is dimensioned to withstand a one-way hydrostatic pressure of 4 MPa exerted on a surface area at the face of a distance block from a drift surface of 10 cm inwards. The surface area in question is 0.55 m^2 yielding a total force of 2.2 MN (220 tonnes). The basis for this estimate is presented in Section 9.4 in /Börgesson et al. 2005/.

- The thickness of the steel in the ring is optimised to obtain corrosion gas generation times similar to those expected from the supercontainer and to prevent the development of any new significant time dependent corrosion processes. The target thickness is on the same order as the thickness of the supercontainer steel, which is 8 mm.

- The ring is composed of smaller size segments, which can be handled and transported inside the drift.

- The ring should fail in a controlled way if the strength is exceeded.

The preliminary design of the fixing ring is shown in Figures 5-9 and 5-10. The ring is based on the following elements:

- Indentation in rock, which is excavated before operation starts.

- A collar attached in the rock surface before operation starts. The collar should be positioned in the required position with a tolerance of 50 mm.

- Rigid fixing ring installed during operation.

The fixing rings are installed using bolts or welds. The weight of the fixing ring is 600 kg if it is made of a 10 mm steel plate. The amount of cement to grout the fixing ring in rock is approximately 15 l, which is equal to about 23 kg of low-pH cement.
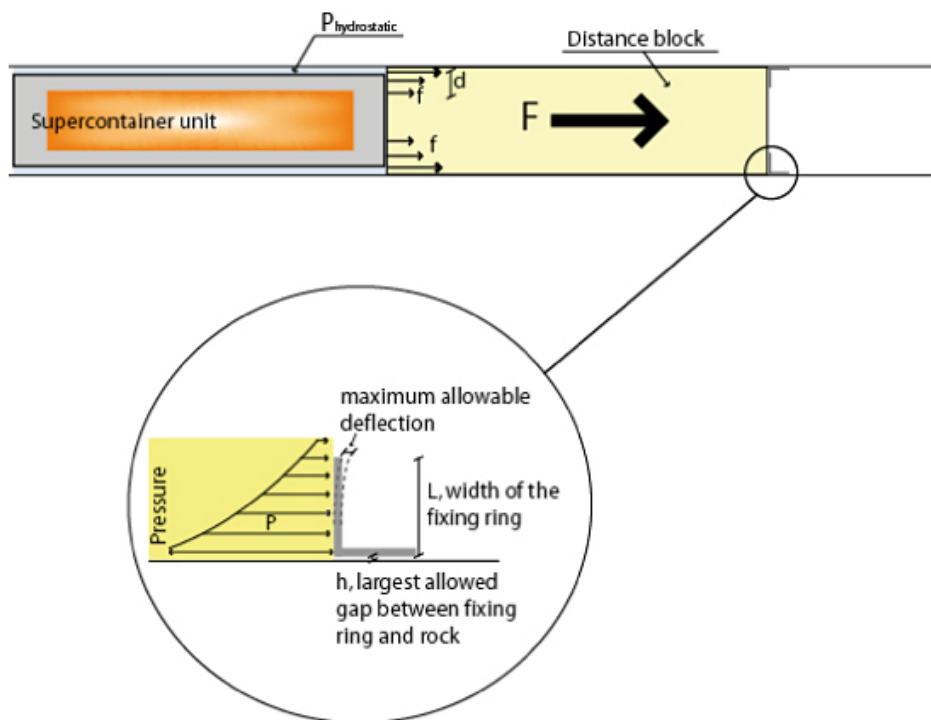
Figure 5-8. *Fixing ring principle and dimensioning parameters.*
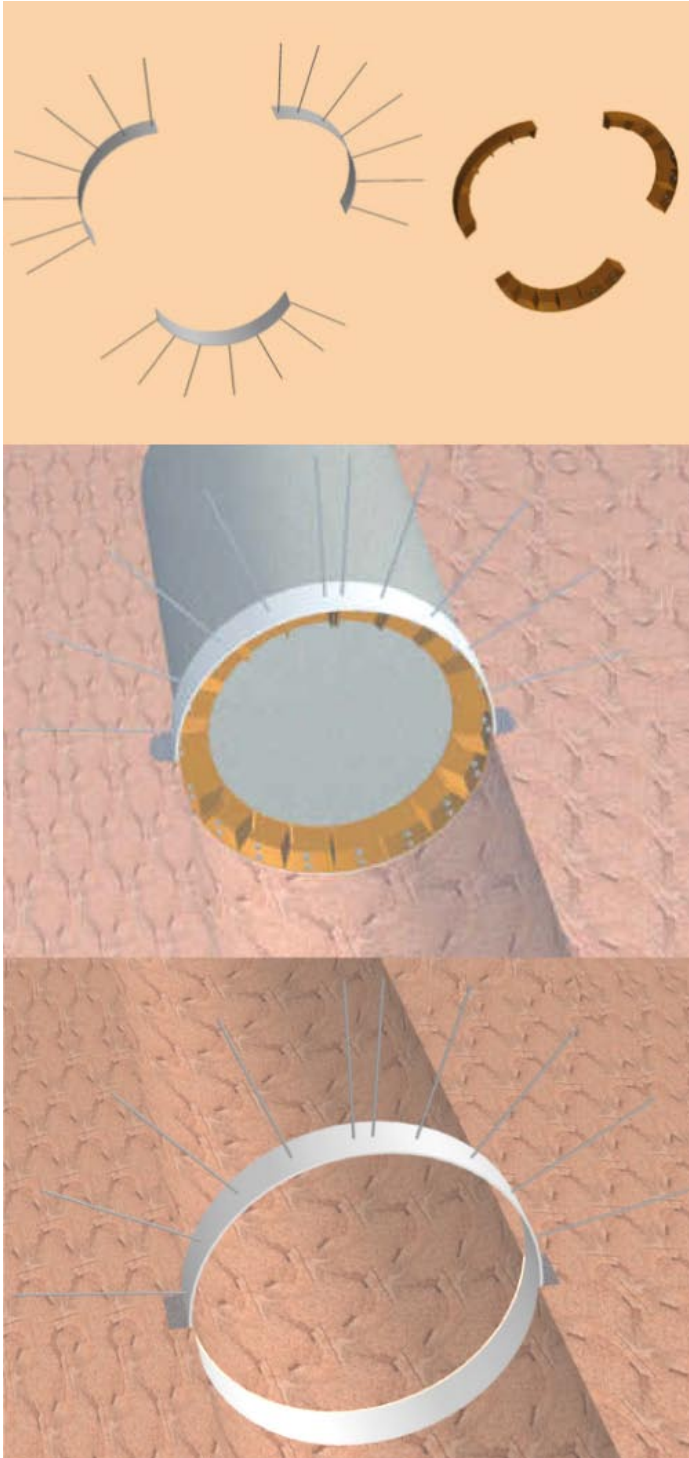
Figure 5-9. *3D visualization of the fixing ring (middle) showing all components (top). The light grey shaded collar (above) is installed before operation starts.*
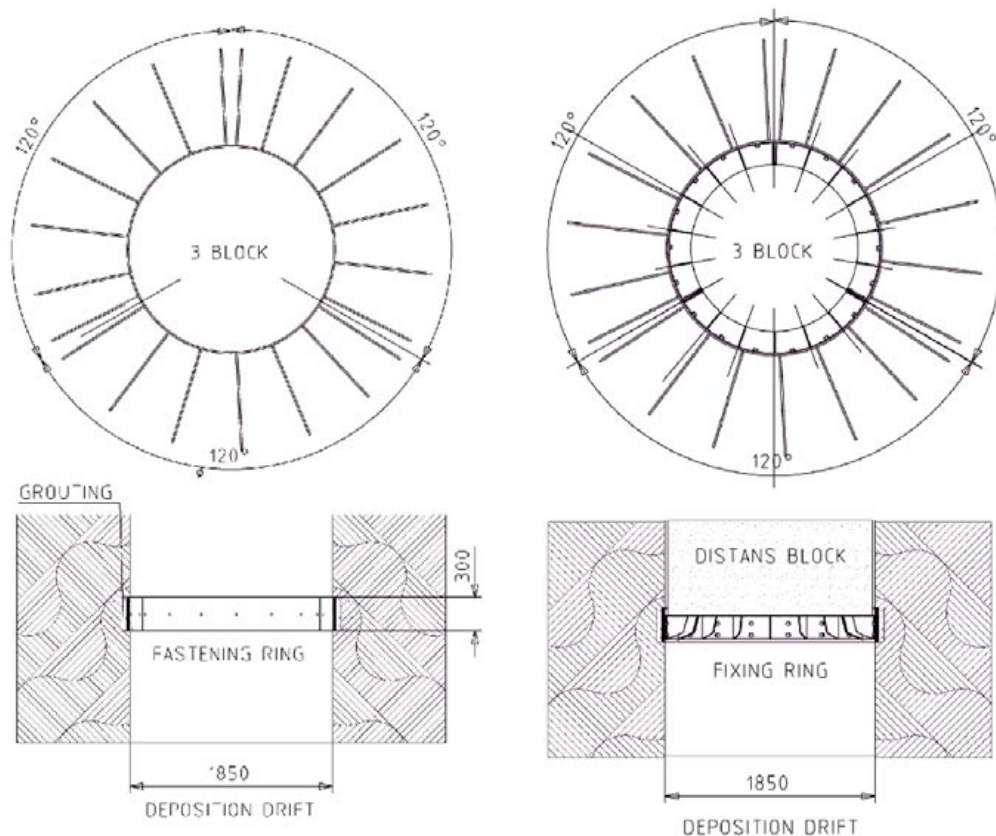
Figure 5-10. *Cross-section of the fastening ring of the fixing ring (left) and the fixing ring (right).*

5.2.4 Contact between supercontainer and distance block

The massive steel fixing rings, intended to minimise the movement of distance blocks when full hydrostatic pressure has been exerted on the whole top surface area, have been assessed as being technically and economically unfeasible. The amount of steel used in the fixing rings can be reduced significantly, and the rings made lighter, if it is assumed that full hydrostatic pressure is not exerted on the entire face of the distance block.

Tests indicate that if the contact (see Figure 5-11) between the distance block and supercontainer is tight (on the order of 7 mm), the pressure is exerted on a limited circular surface area between the rock surface and the outer surface of the supercontainer and about 10 cm radially. The total gap is between the distance block and supercontainer is composed of deviations in planarity between the supercontainer end plate and distance block face, gap increase due to the use of perforated material, and the gap between the supercontainer end plate and internal buffer (see Section 3.4.2).

The contact between supercontainer and distance block is designed to ensure that the distance blocks will be exposed to only partial hydrostatic pressure. The contact may not be a design component in itself, but it is one important part of the distance block design and is therefore regarded as separate component integrated into the distance block design. A good contact may be ensured by e.g. measuring the drift and supercontainer top surface geometry after installation and modifying the first section of distance block to fit in the position tightly.

5.2.5 Critical issues in distance block behaviour

Several significant uncertainties related to the behaviour of distance blocks and buffer material was identified in /Autio 2007/. The most important issues to be resolved were included in an extensive buffer test plan, the latest results of that being presented in Appendix K. These so called critical issues to be resolved in order to produce viable designs were:
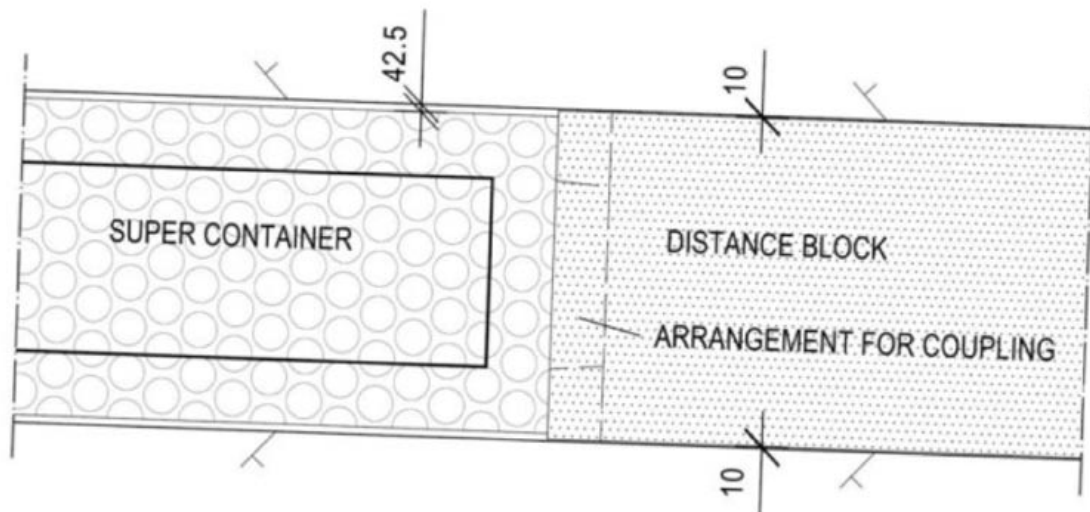
Figure 5-11. *The contact between the distance block and supercontainer can be arranged in several ways all having the same objective to minimize the gap in order to prevent exposure to full hydrostatic pressure on the whole surface area. Note: the gap between rock and block has not been fixed, here it has been assumed to be 10 mm, it is however 15 mm in the reference design.*

1) **Humidity induced swelling.** The process of humidity induced swelling and possible cracking has an effect on the early behaviour of distance blocks before water saturation is achieved. The magnitude of this effect depends on the design alternative(s) selected and is evidently more significant in case of DAWE design.

2) **Erosion of filling blocks and buffer.** The physical erosion of buffer, distance blocks and filling blocks results in transport of bentonite and variation in the buffer density within the emplacement tunnel. Erosion may take place as the result of free–flowing water in the drift between the blocks and the rock, as channelled "piping" type flow or as the result of flow along fractures.

3) **Artificial watering of distance blocks.** The saturation process of distance blocks has significant impact on the sealing ability and piping resistance. The nature of this effect is different in DAWE and BD design. In the case of DAWE design, the effect of artificial watering on saturation and possible later drying and possible shrinkage is an important process and needs to be studied. This redistribution could be caused either by the thermal output of the nearby container or suction-induced water redistribution from the outer perimeter to the drier interior regions of the distance block.

4) **Piping through distance blocks.** In the BD design the distance blocks are supposed to prevent water flow between supercontainer sections. The design of the distance blocks should thus be such that no piping will occur but the influence of the rock hydraulic conditions are strong and more tests are needed to develop a better understanding of how this process works. If piping occurs, transport of bentonite may take place depending on the intensity of the process and this could adversely affect system performance.

5) **Hydraulic pressure on distance block end surface.** The extent and distribution of hydraulic pressure on the inner end face of the distance blocks remains uncertain. The magnitude and distribution of the pressure-induced load on the distance blocks is important since it will affect the movement of these blocks and determine the dimensioning of the fixing rings in the BD design. The main uncertainty is whether the pressure is exerted on a narrow rim on the inner end face which is not covered by the supercontainer end surface or whether it is possible that the pressure is exerted on the whole surface.

5.2.6 Filling components

Filling components are to be used next to plugs as massive sealing elements to compensate for the potential reduction of buffer density caused by the filling of open volume resulting from the dissolution of concrete plugs. Filling components are also used to pack positions that are unsuitable for placement of supercontainers.

The filling components have not been designed in detail. The design principles presented here reflect the present ideas and will be developed further. It is likely that the design of the filling materials between compartment plugs will be modified.

The filling components will inevitably undergo physical and chemical changes over time due to mineral transformations, shrinkage, swelling, erosion, etc. However, it is required that these processes will not involve volume changes that could lead to significant changes in buffer density (mainly distance blocks). Induced density changes should not lead to buffer densities outside the range defined in Appendix A (1,890–2,050 kg/m^3).

The following types of filling units may be used in a drift:

1) Filling adjacent to steel compartment plug

2) Filling between steel compartment plugs

3) Filling blocks in drift positions with water leakages.

Filling adjacent to steel compartment plug

The material used to fill the open volume next to plugs is expected to be composed of MX-80 bentonite pellets. The dry bulk density of the individual pellets is about 1,830 kg/m^3 and the dry bulk density of the emplaced pellets is about 950 kg/m^3. The transition blocks (see Figure 5-12) are similar to the "loose" component of distance blocks.
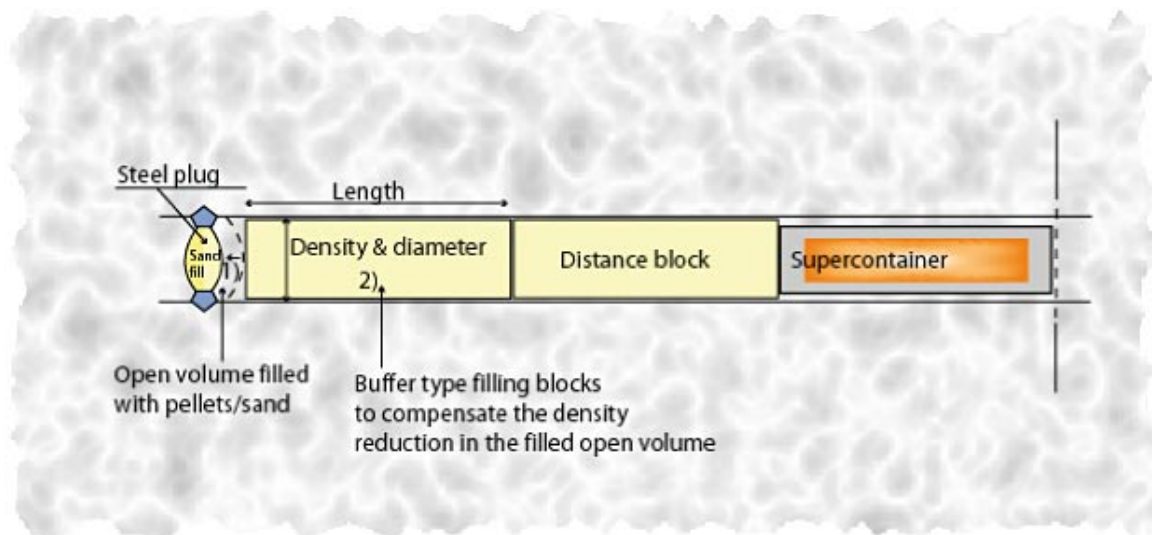
Figure 5-12. *Filling adjacent to compartment plug (1) and transition block (2).*

Filling between steel compartment plugs

The filling material for use between steel compartments plugs has not been completely defined. The filling material is not assigned safety functions, but should be designed to be compatible with, and support the safety functions of, the canister, the buffer and the host rock (Appendix A)

A filling component similar to a distance block is positioned in the "no flow" zone (see Figure 5-13 and 5-14) adjacent to a compartment plug with proper filling. This section will be dry without water flow.

Permeable filling material composed of crushed rock with proper grading for filtering is positioned in the "inflow zone" to drain the inflow section (see Figure 5-14). The objective of grading for filtering is to prevent the penetration and erosion of bentonite.

Additional void space and density reduction can be formed in the drift system by the dissolution of cement from concrete drift plugs, compression of permeable crushed rock filling by swelling buffer, and compression of lower density filling adjacent to compartment plugs. This density reduction should be compensated by additional swelling capacity and density in the filling components.
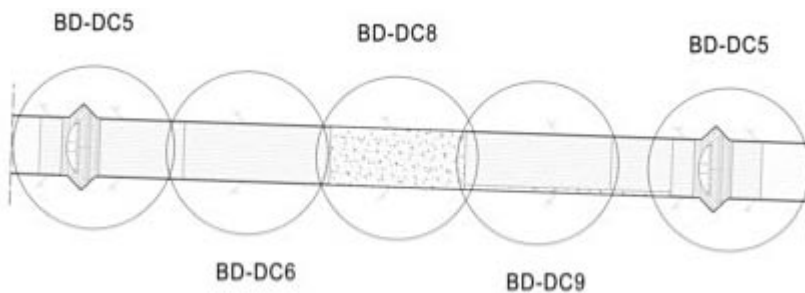
Figure 5-13. Compartment plug system with different filling components. The permeable filling (DC-8) is positioned in the leaking fracture intersection. The leakage is conducted out from the intersection through a partially permeable filling (DC-9). The upstream side of the leakage is filled with an impermeable filling (DC-6), which will have sufficient swelling capacity (with DC-9) to compensate for the possible density reduction caused by the compression of DC-8 when exposed to swelling pressure.
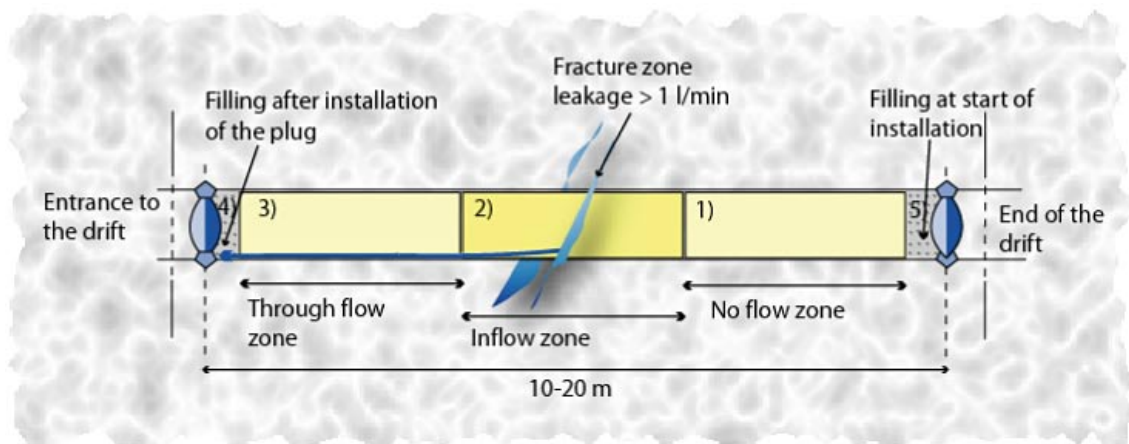
Figure 5-14. Filling between steel compartment plugs.

Filling blocks for use in drift positions with water leakages

Filling blocks (Figure 5-15) similar to distance block units are emplaced in positions where the groundwater inflow is higher than the limit for supercontainer positions (0.1 l/min before sealing of fractures) and lower than the limit for using compartment plugs (1 l/min after sealing). A significant requirement for filling blocks is to maintain the adjoining buffer in place and to prevent significant loss or redistribution of buffer. The limit of 1 l/min for the emplacement of filling blocks is a preliminary value based on the requirement to avoid erosion of the filling blocks by water flowing around the drift through intersecting fractures during saturation. It may be updated in view of future studies and possible design changes.
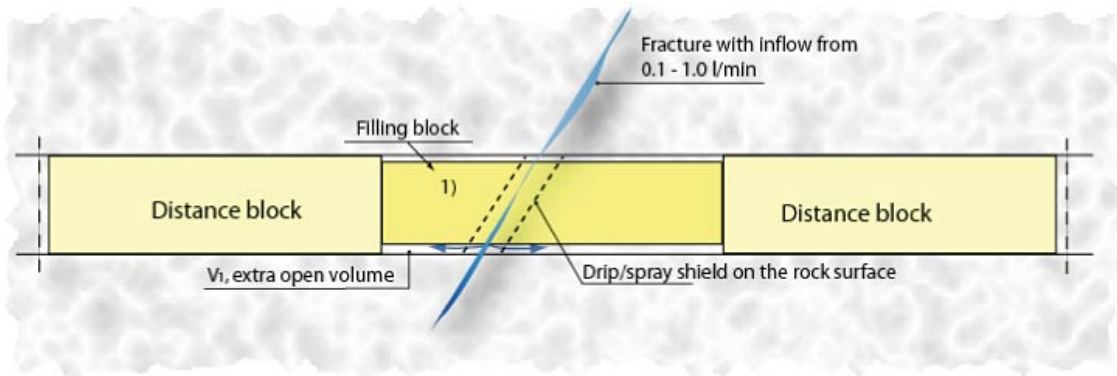
Figure 5-15. *Filling block similar to distance block units are emplaced in positions where water inflow is higher than 0.1 l/min, but less than 1 l/min.*

6 DAWE (Drainage, Artifical Watering and Air Evacuation) alternative

6.1 Specification of the functional structure

In the following discussion, it is assumed that the application of proper techniques, which will not be further elaborated, has reduced groundwater inflow. Groundwater control techniques are described in Chapter 9. Additionally, deposition drift, canister, and supercontainer functions are only briefly described here as they are considered as fixed design aspects. The DAWE design is based on the following functional requrements:

1) **Prevention of buffer erosion by spray and drip shields.** Direct water flow on buffer surface will cause surface erosion. Spraying, squirting and significant dripping of groundwater on supercontainers and distance blocks is prevented by using shields.

2) **Drainage on the bottom of the drift.** The water inflows are drained so that buffer will not be in contact with water. The drift is inclined and therefore water flows naturally towards the entrance of the drift.

3) **The plugged drift is filled with water using artificial watering pipes.** The empty volume in the drift is filled with water to produce even initial wetting of buffer and diminish possible hydraulic pressure differences between supercontainer section, which may cause e.g. piping and detrimental transport of bentonite. All supercontainer sections are filled at the same time prevent axial flow along the drift. As a consequence of filling, bentonite will swell rapidly and seal the drift. The pipes are removed from the drift after watering.

4) **Air and gas is evacuated during filling by using air evacuation pipe.** Large volumes of air and gas are trapped in the drift after plugging. Highly pressurized gas acts as an energy accumulator, which may induce unfavourable flow in the drift and cause operational problems during removal of watering pipes.

5) **Isolation of water-bearing fracture zones by plugs (same as in Basic Design).** Isolation of deposition compartments by using plugs from water-bearing fracture zones, which may have detrimental effect on the distance blocks and supercontainer during saturation.

6) **Sealing of the drift by plugs (same as in Basic Design).** The deposition drift is sealed and plugged after emplacement of canisters.

7) **Interuption of operation using plugs (same as in Basic Design).** The emplacement of supercontainers can be stopped temporarily if the drift is plugged rapidly.

8) **Hydraulic isolation between supercontainers and adequate thermal spacing of canisters is obtained by using distance blocks (same as in Basic Design).** Thermal spacing between successive canisters is obtained by using a distance block of required length.

9) **Sealing and filling of unsuitable sections by filling blocks (same as in Basic Design).** Positions that are not suitable for emplacement of supercontainers, because of larger than accepted water inflow or other reasons, are packed with filling blocks. The objective of the blocks is to provide extra sealing against neighbouring distance blocks and to reduce the hydraulic pressure induced force exerted on distance blocks.

6.2 Specification of the design components

6.2.1 General

Design components considered fixed are not discussed in the context of this chapter. Design components, which are same between the BD and DAWE designs, are described in Section 4.2.

The DAWE Design Components (DAWE-DC) shown in Figure 6-1 are:

- DAWE-DC1 Spray and drip shield.
- DAWE-DC2 Distance block.
- DAWE-DC3 Drainage system of inflowing water.
- DAWE-DC4 Air evacuation system.
- DAWE-DC5 Compartment plugs.
- DAWE-DC6 Filling blocks.
- DAWE-DC7 Artificial watering system.
- DAWE-DC10 Drift end plug.
- DAWE-DC11 Permeable filling.
- DAWE-DC12 Partially permeable filling.

6.2.2 Distance block

A distance block is positioned between the supercontainers. The purpose of the distance block is to provide sufficient thermal spacing between supercontainers and to hydraulically isolate the supercontainers during saturation.

The distance block will swell more rapidly than the buffer in the supercontainer and will prevent the flow of water along the drift.

The initial water content of bentonite in the distance block is 21%. The length of distance block is 5.475 m and the diameter is the same as the supercontainer (1,765 mm). The initial dry density of the distance block is 1,712 kg/m^3 and the final saturated density of the distance block is 2,000 kg/m^3 ranging from 1,950 to 2,050 kg/m^3.
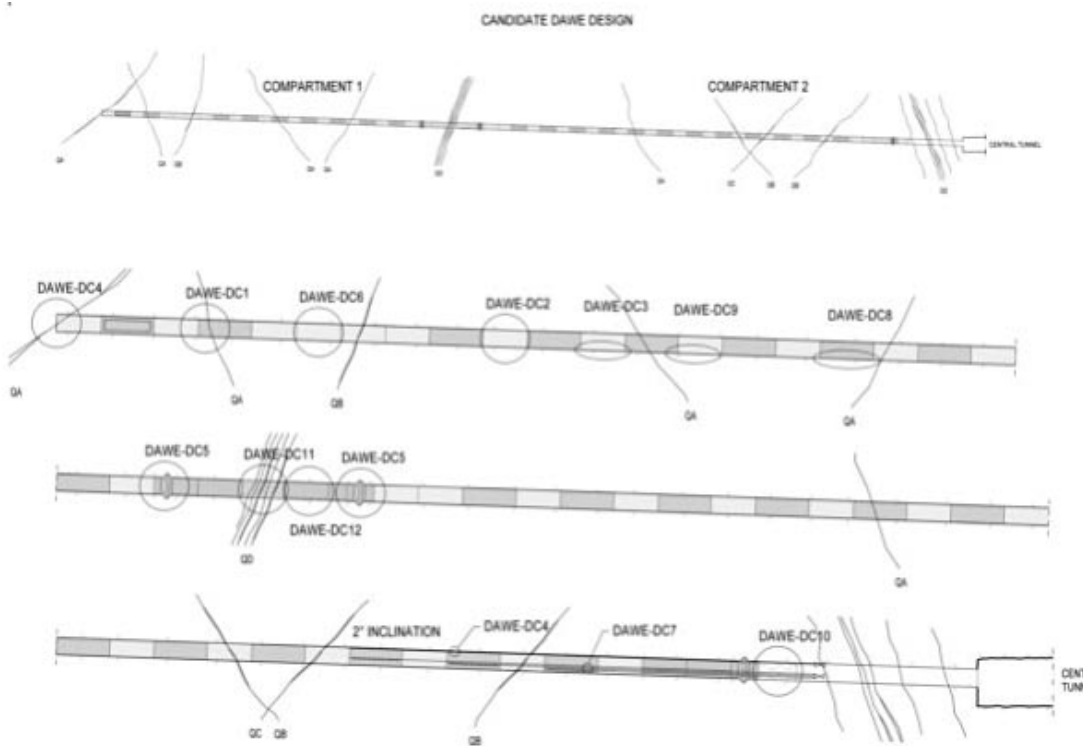
Figure 6-1. The DAWE design in an illustrative vertical section with examples of positions of design components. The identifiers in fractures refer to different types of water leaking fractures. The watering and air evacuation pipes are shown only in the beginning of the drift.

6.2.3 Drainage system of inflowing water

The objective of the drainage system is to remove approximately 10 l/min of water from a 150 m long drift compartment. The drainage system is based on free flow along the drift floor.

6.2.4 Artificial watering system

Sealed drift compartments will be flooded using pipes. The open volume in a supercontainer section is about 1.3 m^3 (42.5 mm gap and 5.56 m length). The open volume in the distance block section of length 5.46 m is 1.3 m^3 (42.5 mm gap). The largest possible total open volume per installation unit is then about 2.6 m^3. It is likely that the final volume will be smaller due to humidity induced swelling of bentonite. In order to artificially fill the total open volume in a 15 supercontainer compartment in 14 hours, a flow rate of 45 l/min is required. This is equal to about 3 l/min per supercontainer section. The open gap between the supercontainers and adjacent rock faces is 20 mm under operation conditions. After operation the gap is 42.5 mm. As a design principle, no pipes will be left in the drift.

The positioning of the pipes on the roof of the drift is preferred over the bottom of the drift in order to avoid possible problems with pipe removal. However, the clearance on the sides of the drifts is clearly larger during operation and, therefore, vulnerability to damage from pipe removal is lessened on the sides of the drifts. Therefore, the preferred position for pipe systems is along the sidewalls (see Figure 6-2). The flooding system is based on the installation of several smaller diameter pipes positioned on the sidewalls of the drift before operation starts. Water is distributed evenly in the supercontainer section through several (10–30) holes to avoid large inflows. If twenty holes are positioned in every supercontainer section, the inflow per hole is 0.13 l/min. Water is not injected in sections where distance blocks are positioned in order to avoid possible erosion.

The pipes are removed after a compartment has been plugged with the steel compartment plug and filled with water. A collar seal system is required in order to remove the pipe or pipes without loss of softened bentonite from the plugged drift. The collar system may be based on similar principle as collar systems used in underwater drilling. Another alternative is to pressurize the drift during the removal period. This procedure would require a pressure of 0.3–0.5 bar at maximum (difference in hydraulic head between the ends of the drift) and will not prevent the leakage of groundwater at higher pressure. Bentonite mud can be pumped into the drift if necessary to fill the open volume left by the pipes during removal.

Steel or copper are the preferred pipe material because it will not introduce any new material in the drift and will corrode in case it is left in the drift as a consequence of deviation in operation.
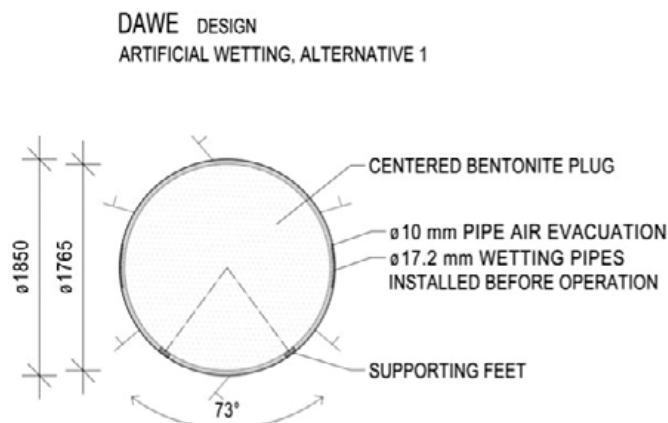
Figure 6-2. *The artificial watering and air evacuation pipes in the DAWE design based on the use of several small 17 mm diameter pipes on the sides of the drift.*

One 17.2 mm diameter, type DN 10 17.2x1.25 steel pipe of is required for every supercontainer section. The capacity is 30 l/min and tensile strength 800 kp/cm^2. The weight is 0.5 kg/m and the weight of water 0.17 kg/m. The pulling strength of the pipe is 500.8 kp with cross sectional area of 0.626 cm^2, which corresponds to removal of 747 m long pipe with friction coefficient of 1.

Installing pipes on both sidewalls, for redundancy purposes, doubles the number of pipes. The air evacuation pipes are installed on top of the watering pipes. If a deposition vehicle were to collide with one set of pipes and render them non-functional, the redundant set on the opposite wall can be used. The number of pipes installed on each wall is about 15 (see Figures 6-1 and 6-2). The pipes are attached on the sidewalls of the drift in U-shaped brackets of weight about 50 g/piece with spacing of 5 m so that they can be pulled out separately. One collar seal is installed in the steel compartment plug for every pipe. The water is distributed through several small holes in the pipes to supercontainer cells.

6.2.5 Air evacuation system

In order to facilitate air removal during artificial drift flooding, a pipe is installed on the tops or sides of the drifts before operation (see Figure 6-2). The end of the pipe is placed in the highest point at the far end of the drift, where air is trapped due to the slight inclination of the drift upwards. The pipe is equipped with a filter to eliminate possible plugging.

Air is evacuated from the drift through a 10 mm-diameter pipe. Two pipes are installed for redundancy. The pipes are dimensioned to allow the same outflow of air as inflow of water (45 l/min). Steel or copper is the preferred pipe material as they will not introduce any new material in the drift. The pipes are removed after a compartment has been plugged with the steel compartment plug and filled with water. A collar seal system is required to remove the pipe without loss of softened bentonite from the plugged drift.

One copper pipe of diameter 12 mm is required for one compartment. The tensile strength is 200 kp/cm^2 (equal to approximately 20 MPa) The weight is 0.31 kg/m and the weight of water 0.08 kg/m totalling 0.318 kg/m. The pulling strength of the pipe (20 MPa) with cross sectional area of 0.35 cm^2 equal to 70 kp (700 kN) which corresponds to removal of 220 m long pipe with friction coefficient of 1. A steel pipe of 12 mm diameter would weight 0.27 kg/m and allow larger pulling force for removal. The pipes are attached to the sidewalls of the drift in U-shaped brackets, weighing about 50 g each, over spacings of 5 m so that they can be pulled out separately.

6.2.6 Plugs

The specification of compartment and drift end plugs are similar to that in Basic Design presented in Section 4.2. The only difference to BD alternative is that the plugs are equipped with lead-through, valves and collar seals for possible drainage, watering and air evacuation pipes.

6.2.7 Filling blocks

Filling blocks, as described for the BD design in Chapter 5, Section 2.5, similar to distance blocks are used next to plugs as massive sealing elements and to fill positions, which are unsuitable for placement of supercontainers.

The filling blocks should seal the section of drift where they are positioned and should resist erosion. The present design is based on using distance blocks as filling blocks, however the properties of the blocks may be developed in the future in several ways, e.g. the resistance for erosion can be increased, swelling potential decreased and hydraulic conductivity increased.

7 Layout

The first major work on KBS-3H layout adaptation to the Olkiluoto site was carried out in 2002 /Johansson et al. 2002/. An update of the KBS-3H layout adaptation was made in early 2006 /see Johansson et al. 2007/ and a new layout based on the present Olkiluoto bedrock model (cf. Figure 7-1) has been made recently by /Johansson et al. 2007/. The new layout is shown in Figure 7-2 and the main results of the work are summarised here. After the 2006 layout was established, some significant changes with regard to the input data occured, which justified the new layout design. The main differences with respect to the last layout work in early 2006 are the following:

- the consideration of the new Olkiluoto site model /Paulamäki et al. 2006, Ahokas and Vaittinen 2007/,
- the principle of not using imaginary fracture zones,
- the revised respect distances to fracture zones,
- results from a DFN modelling study /Lanyon and Marschall 2006/,
- an update of the canister spacings (different spacings for different canister types),
- respect distances to investigation boreholes.

The new layout is based mainly on the aforementioned new models for Olkiluoto, respect distances, other design premises, distribution of water inflow, and design specifications.
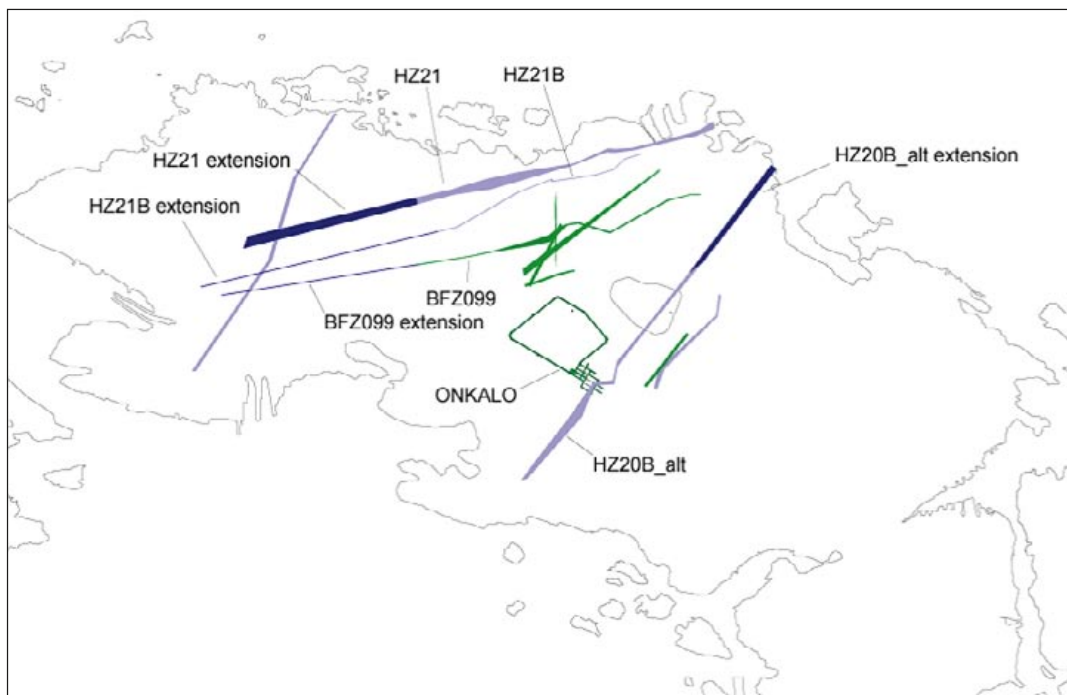
Figure 7-1. *The layout-determining fracture zones at the level –420 m at Olkiluoto showing the extensions of certain fracture zones /Kirkkomäki 2006/ which were considered in this work. HZ indicates major hydraulically conductive fracture zones. Features shown in green are not considered to be layout-determining, as they are allowed to intersect the deposition drifts, although they will require a respect distance to canister positions.*
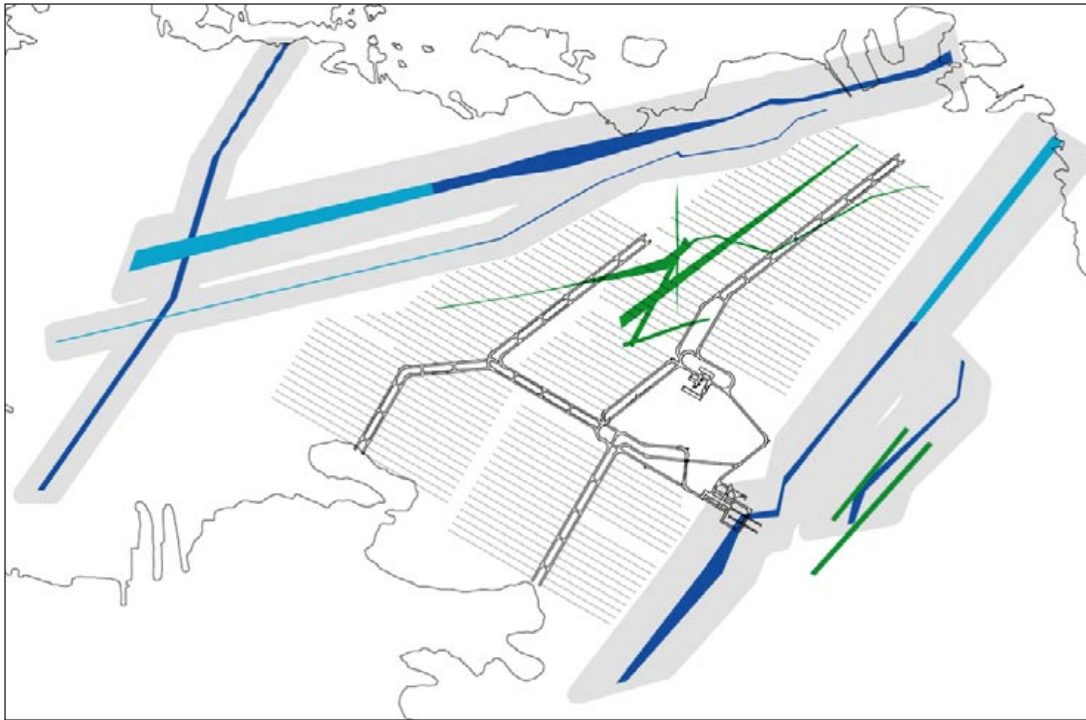
Figure 7-2. *The KBS-3H layout of /Johansson et al. 2007/ with canister drift orientation of 120°, level –420 m at Olkiluoto. Grey areas indicate the respect distances to the layout-determining fracture zones (shown in blue). Features shown in green are allowed to intersect the deposition drifts.*

The total amount of spent fuel assumed in this work is based on an estimate of the quantities produced by the five nuclear reactors in operation or under construction in Finland. The number of canisters and other technical input data used in this work are presented in Table 7-2. Canister lengths, canister spacing and other details related to Posiva's three canister types are given below in Table 7-2. Otherwise the design bases used in this work are the same as those assumed in 2002 /Johansson et al. 2002/ and in the previous design in early 2006.

The input data shown in Tables 7-1 and 7-2 were used to adapt the KBS-3H layout to the Olkiluoto site at the 420 m depth level. The resulting layout, which is comparable to the KBS-3V layout /Kirkkomäki 2006/, is shown in Figure 7-2. There are 171 deposition drifts, the average deposition drift length is 272 m and the total deposition drift length is some 46,400 m. Additionally, there are 3,779 canister locations, which corresponds to the required number (see below).

Approximately 17% of the available bedrock resource in the deposition area is estimated to be unusable due to hydraulic properties and an additional 1% is unusable due to minor (dry) fracture zones. In addition, some 2% is estimated to be unusable due to potentially long (dry) fractures. There may also be other reasons that prevent the use of particular drift sections for disposal (for example, weathered and altered sections), but, as most of such sections are assumed to be located mainly in or near the intersections of fracture zones or drift sections where $T > 2.65·10^{-9}$ m²/s, their effect on the drift utilisation is rather small. However, the percentages related to minor fracture zones and potentially long fractures (1% and 2%, respectively) should be increased, because the actual effect of such sections on the required drift lengths is likely to be greater than 1 and 2 percent. This greater effect arises because the supercontainer will often have to be moved by several metres to avoid an unusable section, no matter how narrow the section. Therefore, it was assumed in the KBS-3H layout adaptation that a total of 25% of the host rock is unusable for disposal within the actual bedrock resource at Olkiluoto. This assumption requires an increase in the total drift length of $25/(100–25) ≈ 33\%$ in the drift sections where supercontainers can be emplaced. In the layout adaptation, this can be taken into account by increasing the number of canister locations by 33%, i.e. from 2,840 to some 3,780.

Table 7-1. Technical input data for the KBS-3H layout adaptation at Olkiluoto.

Parameter	Value/criterion
Number of canisters	2,840
Repository alternative	KBS-3H, one layer, no side tunnels – other parts than length of central tunnels, deposition drifts and related niches are similar to present KBS-3V design
Fracture zone model	Layout model /Ahokas and Vaittinen 2007/ with minor modifications; no imaginary fracture zones
Depth level	420 m (400–420 m)*
Spacing between deposition drifts	25 m
Length of deposition drift	100–300 m
Orientation of deposition drift	120 ± 10° (parallel to main principal stress)**
Filling block length (blank zone)	10 m
Compartment plug unit length	30 m
Other space requirements	First canister 25 m from the central tunnel

* For drainage purposes, the deposition drifts are not exactly horizontal; deepest point is 420 m and uppermost point 400 m. The level 420 m is used in the report.

** As assumed in the report by /Malmlund and Johansson 2002/ and supported by /Posiva 2005/.

Table 7-2. Details on Posiva's three canister types and their positioning in a KBS-3H repository.

Parameter/Canister	BWR 1,700 W	VVER 1,370 W	EPR 1,830 W
Canister length [m]	4.8	3.6	5.25
Canister spacing (centre to centre distance) [m]*	11.0	9.1	10.6
upercontainer length [m]	5.53	4.33	5.98
Distance block length [m]	5.475	4.775	4.625
Distance block length with 5 mm gaps [m]	5.465	4.765	4.615

* Based on /Ikonen 2003b/.

The previous layout model from 2006 is presented in Figure 7-3 for comparison and the corresponding bedrock model was presented in Chapter 3 in Figure 3-10. The differences between the old and new layout are quite limited.

According to the latest layout, the repository can be built in one layer at a depth of 420 m at the Olkiluoto site. However, the KBS-3H layout utilises most of the area between the HZ20 and HZ21 major fracture zones. The KBS-3V layout, on the other hand, allows some area to be left unused /Kirkkomäki 2006/. Accordingly, the KBS-3H design requires a larger area than the KBS-3V design. This requirement is mainly due to the occupation of long sections of the drift by compartment plugs (30 m) and bentonite blocks in the blank zones (10 m), which reduces the usability of the host rock and results in a larger total length of KBS-3H deposition drifts as opposed to the total length of the KBS-3V deposition tunnels. In the KBS-3V design, positioning of the deposition holes is very flexible, and narrow zones with moderate transmissivity usually have only a minor effect on the locations of the canisters.
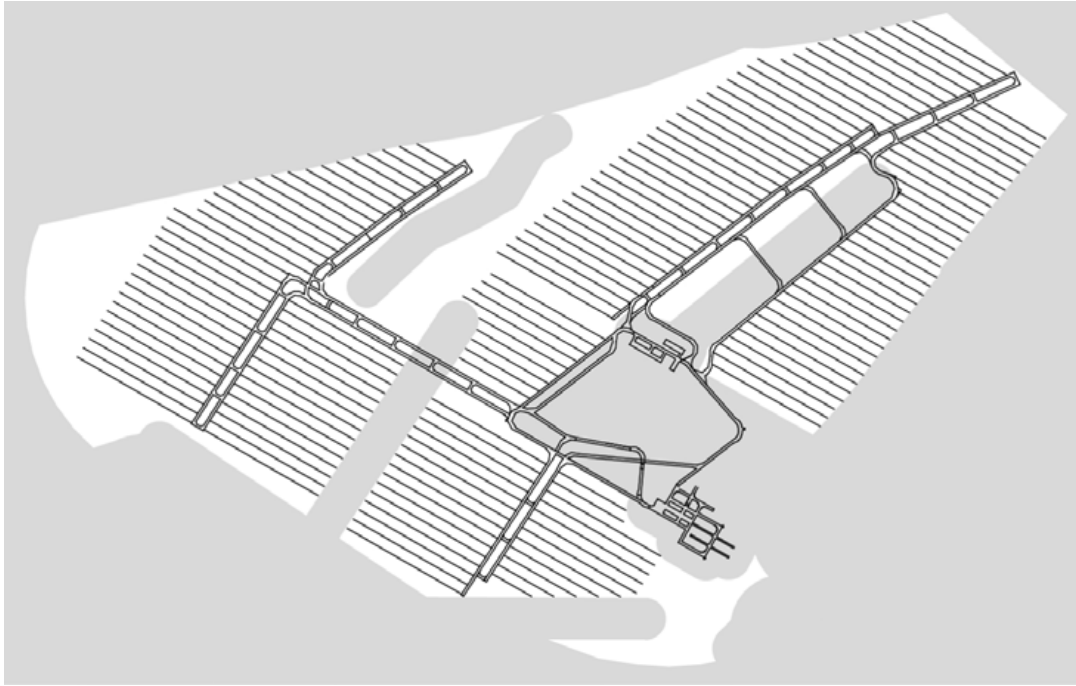
Figure 7-3. *Previous KBS-3H layout adaptation to the Olkiluoto site, depth level 420 m. White areas indicate the usable bedrock resource.*

8 Evaluation of the mechanical behavior and spalling of KBS-3H deposition drifts at Olkiluoto

8.1 General

Thermo-Mechanical (TM) analyses of a KBS-3H deposition drift at Olkiluoto were recently made available /Lönnqvist and Hökmark 2007/. The conclusions drawn here with respect to spalling are based on that study.

TM analyses was performed because previous work on the early evolution of KBS-3H deposition drifts indicated that drift sections located in very dry rock can remain dry for long periods of time /Smith et al. 2007/. These periods (lasting for hundreds of years or longer) are much longer than the time of thermal peak loading in the near-field rock (50–60 years). Therefore, it is unlikely that the bentonite in these dry drift sections will be in a saturated state and exert full swelling pressure on the rock surface during thermal peak loading. The swelling pressure would normally support and stabilise the rock by compensating for the increased stresses caused by thermal loading from the fuel canisters. Where such swelling does not exist, it is possible that rock failure may occur in the form of spalling (see Figure 8-1).

For purposes of the current discussion, spalling is defined as the breaking of a rock surface into splinters, chips or fragments. In addition to spalling, the reactivation of existing fractures, which was also evaluated by /Lönnqvist and Hökmark 2007/, may produce such effects as well. However, this latter phenomenon is not addressed here. The occurrence of spalling depends significantly on *in situ* rock stresses and rock strength and is, therefore, site-specific. This study has been carried out based on Olkiluoto-specific data.

The results indicate that there will almost certainly be thermal spalling after a few years of heating in dry, unsupported tunnels. The results are discussed further below from the design perspective.

Figure 8-1. Spalling at Äspö on the vertical surface of a full-scale deposition hole in the APSE experiment /Andersson and Eng 2005/.

8.2 Stresses after heating and effect on spalling

The measured strength values of Olkiluoto rocks for the TM-3D-analyses are presented mainly in /Posiva 2006a/. These values represent the minimum strength assuming unfavourable loading direction with respect to the foliation:

- The peak compressive strength of rock is 108–122 MPa.

- The crack damage stress is 103–110 MPa.

- The crack initiation stress is 52–59 MPa.

Spalling begins at roughly crack initiation stress levels. This threshold is usually taken to be 55% of compressive peak strength. Spalling in KBS-3V deposition holes was studied in the APSE experiment at Äspö HRL /Andersson and Eng 2005/. The present assumption holds that the spalling strength of APSE rock is about 55% of its uniaxial compressive strength /SKB 2006/.

Based on the reference layout for a KBS-3H repository at Olkiluoto where the deposition drifts are aligned with the major *in situ* rock stress, TM analyses indicated that little or no spalling would occur prior to the emplacement of spent fuel /Lönnqvist and Hökmark 2007/. According to TM modelling of the base case or case A (with upper limit *in situ* stress magnitudes in the presented range), the tangential stress after excavation is about 35 MPa at the roof and floor sections (see Figure 8-2). During the heating phase, the largest tangential stress (110 MPa) occurs after 50 years. Corresponding values for case E (with lower limit *in situ* stress magnitudes in the presented range) are about 19 MPa after excavation and 95 MPa after heating. It should be noted that even in the absence of *in situ* stresses the thermal stress alone would be ~ 75 MPa.
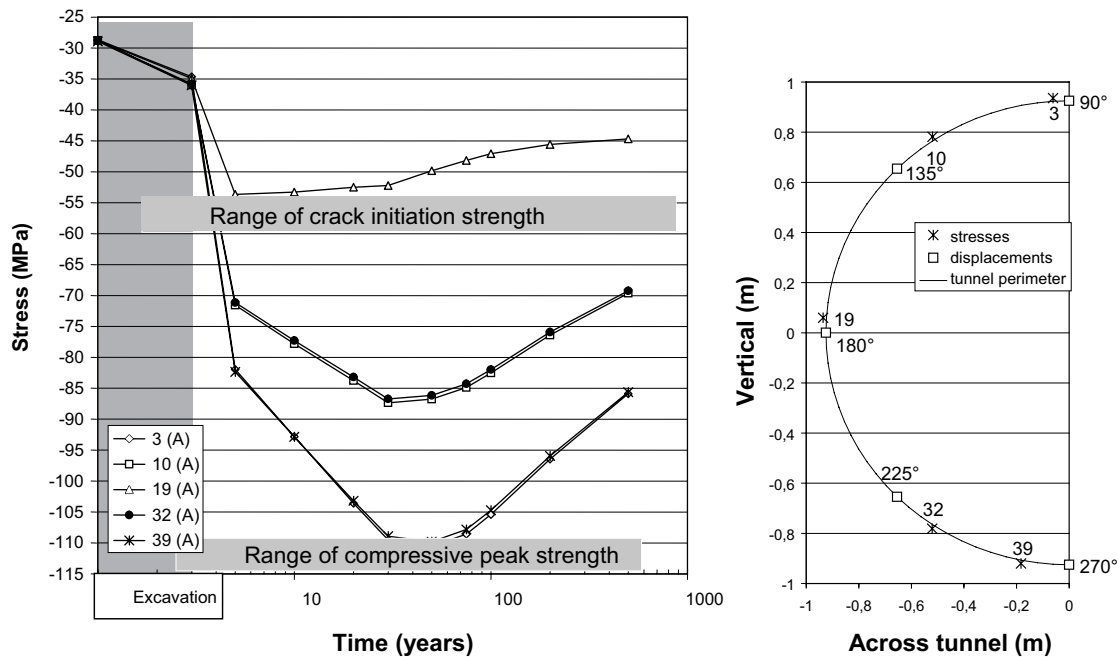
Figure 8-2. *Major principal stresses during the heating phase in the middle of a supercontainer. Grey shaded area represents non-thermal phase with fictitious time (primary equilibrium and excavation from /Lönnqvist and Hökmark 2007/).*

The tangential stresses are below the spalling threshold after excavation and spalling should be unlikely after excavation if the tunnels are sub-parallel to the major stress. However, if the tunnels were to be oriented perpendicularly to the major stress (a highly unlikely scenario), spalling is almost certain to occur, see case G in Figure 8-3.

During the heating period, tangential stresses are clearly over the spalling threshold level and will be at the level of highest compressive strength in the base case and close to it in the lower *in situ* stress case. Tangential stresses are highest adjacent to the rock surface in the middle of the supercontainer. Stresses were only 7% smaller adjacent to the rock surface in the midpoint between canisters than in the middle of a supercontainer.

Considerable thermally-induced spalling will occur in tighter drift sections in which supporting pressure from buffer swelling is not developed within a few years of the emplacement of spent fuel. This outcome is expected irrespective of how tunnels are orientated in relation to the *in situ* stresses.

Similar conclusions have been reached in the case a KBS-3V repository at the sites currently considered in the Swedish programme /SKB 2006/. The view in SR-Can is that the properties of the potential host rocks are such that no rock spalling will occur in the deposition holes prior to canister deposition and, even if it were to occur, detached rock fragments could be removed and filled with bentonite /Hökmark et al. 2006/. On the other hand, following waste emplacement, there will almost certainly be some thermally induced spalling on a timescale of years to centuries at any of the sites. Spalling is most likely in dry deposition holes where the development of some bentonite swelling pressure at the interface with the rock is slow /Hökmark et al. 2006/.

It can be concluded that spalling is not likely to occur in the deposition drifts after excavation in the absence of heating. Spalling will take place in a few years after emplacement of canisters due to the thermal load if there is no bentonite swelling pressure in support of the rock surface. Spalling will continue over 50 years or more until the thermal stresses start to decrease.
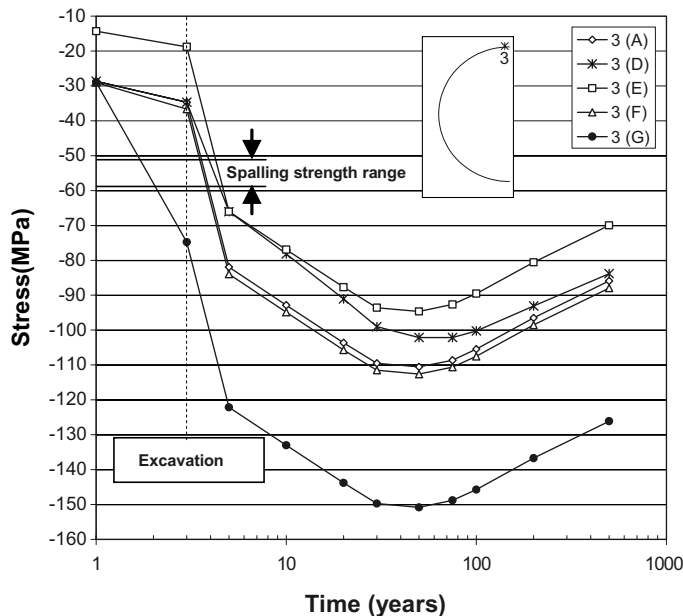
Figure 8-3. Largest principal stress on the tunnel perimeter in the middle of a supercontainer. Grey-shaded areas represent pre-thermal stresses (i.e., in situ stresses and stresses due to excavation). First thermal stress analysis after 5 years (from /Lönnqvist and Hökmark 2007/).

8.3　Uncertainties in the modelling

Uncertainties in the applicability of TM modelling to the KBS-3H repository are discussed in /Lönnqvist and Hökmark 2007/. The conclusions are that it is unlikely that any uncertainties connected to the modelling approach would significantly affect the final results.

Uncertainties in the TM modelling input data were addressed by using both the upper and lower limits of the presented stress range and the results indicated that in both cases the threshold level for spalling is exceeded during the heating period.

In the base case, the orientation of the drift is sub-parallel to the largest *in situ* stress. This orientation is the most favourable with regard to spalling. Other orientations were found to be more susceptible to spalling. The depth of the deposition drifts was assumed to be 400 m. An increase in depth results in increased susceptibility to spalling.

The spalling strength in Olkiluoto rock has not been measured or analysed. It was assumed that the spalling strength corresponds to the crack initiation strength measured in the laboratory; however, a comparison of results from *in situ* and laboratory tests /Martin 2005/ indicated that the spalling strength is 56% of the uniaxial compressive strength (UCS) in Lac du Bonnet Granite and Äspö Diorite and 65% in Granodiorite at the Canadian URL. The corresponding ratios between crack initiation strength (i.e. onset of damage) and UCS are 44% and 52%, respectively. It is possible the crack initiation strength may underestimate the spalling strength by about 20% and therefore it is important to distinguish between these two parameters.

In general, there seems to be a sufficient understanding of the threshold level required for initiation of spalling, but site-specific properties and spalling processes are not known well enough to reliably estimate the extent of failure.

8.4　Swelling pressure required to eliminate spalling

The swelling pressure required to eliminate spalling was addressed in the APSE experiment at Äspö HRL /Andersson and Eng 2005/. Experience suggests that thermal spalling could be completely avoided if a small resisting force (pressure) were to be exerted on the deposition hole wall. It is possible that pressures on the order of 150 to 200 kPa would be sufficient /SKB 2006, Posiva 2006b/.

This range is a rough, rock specific estimate based limited experimental results. The overall process is not yet fully understood and more supporting evidence is needed.

8.5　Swelling pressure of buffer in dry deposition drifts

There are clear indications from the Lasgit experiment at Äspö (see Figures 8-4 and 8-5) that artificially wetted buffer will swell and exert pressure on the rock surface. The results from three laboratory tests with limited amounts of water indicate that the axial swelling pressure against the confining surface is on the order of 100 kPa notwithstanding the appearance of large open cracks on the top surface of the buffer material. The degree of saturation was close to 100% and the maximum swelling pressure at full saturation with freely available water was estimated to be about 10 MPa.

The results indicate that buffer, which has been artificially wetted by filling the gaps between buffer blocks and the gap at the rock/buffer interface with water in dry tight drift sections, may dry out and crack. Such a process might be expected to result in a loss of swelling pressure, but the results indicate the buffer exerted a continuos swelling pressure on the rock surface.

Figure 8-4. *Sample of compacted bentonite after opening and removal from test set-up used in the Lasgit experiment. Note shrinkage cracking on the surface. The sample diameter is about 50 mm (from Clay Technology AB).*
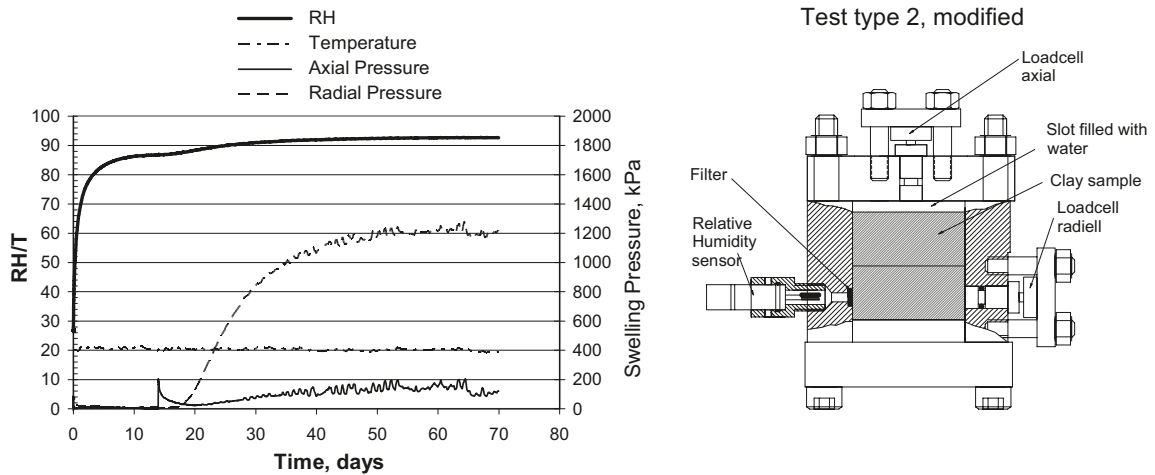
Figure 8-5. *Test set-up used in Lasgit experiment (right) and generation of swelling pressure and radial pressure during experiment (left). Note that the axial swelling pressure has been 100–200 kPa at the end corresponding to situation shown in Figure 8-4 (from Clay Technology AB).*

The results are based on three laboratory tests with small samples and no heating. The observed cracking may be influenced by the stress release caused by opening of the test chamber. The indications are clear although the number of samples has been limited. Therefore more experimental representative evidence is needed to estimate the swelling pressure in dry tight drift sections.

The results from Buffer Container Experiment (BCE) at URL were reviewed with respect to buffer shrinkage in more detail. The results indicate that the buffer in KBS-3H drift might under some conditions provide some swelling pressure in dry drift conditions. The results indicated that the transport of moisture by thermal gradient might have a significant impact on the behaviour of buffer and contact at the rock/buffer interface.

8.6 Effect of spalling in different cases

Supercontainer positions

The gap between the supercontainer and the rock surface is 42.5 mm. Because of the heat from the canister and the effect of the perforated steel supercontainer, which moderates the swelling of buffer inside the supercontainer when compared to neighbouring distance blocks, the expected swelling of the buffer is slower and the supporting force to the rock surface is smaller than in case of the distance blocks.

Distance blocks in DAWE-alternative

The gap between distance blocks and rock surface is 42.5 mm, the same as between the supercontainer and rock surface. Because of the size of the gap it is uncertain if any swelling pressure will be exerted on the rock surface in dry drifts sections over timescales relevant to thermal spalling.

Distance blocks in BD-design alternative

The gap between the distance blocks and rock surface in the BD alternative is from a few millimetres to 15 mm in present preliminary designs. The design remains in progress and the gap size should be considered merely indicative. At any rate, the gap will be smaller than in the DAWE alternative. More rapid development of swelling pressure at the rock surface should be possible for the BD alternative than for either the supercontainers or the DAWE-distance blocks.

The best case – spalling only in dry supercontainer positions

If spalling occurs in tight drift sections, it could be limited by engineering actions to supercontainer locations only (see Figure 8-6). This case could likely be the situation in the BD-design alternative with a small (few millimetres) initial gap between the rock surface and buffer.

The worst case – spalling in all dry supercontainer and distance block positions

The worst case would be that spalling occurs in all dry supercontainer and distance block sections (Figure 8-7). This case is most likely to occur in the DAWE alternative where the gap between the rock surface and distance blocks is the largest and swelling pressure development is the slowest.
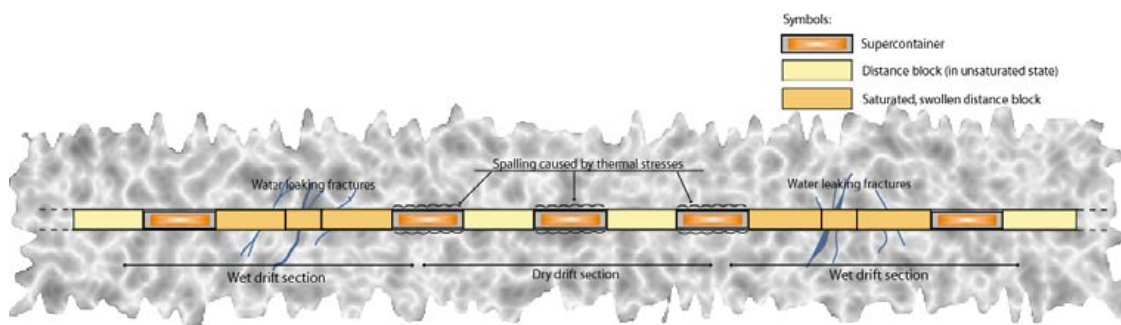
Figure 8-6. *Case where spalling occurs only at supercontainer locations in tight drift sections between water-bearing fractures.*
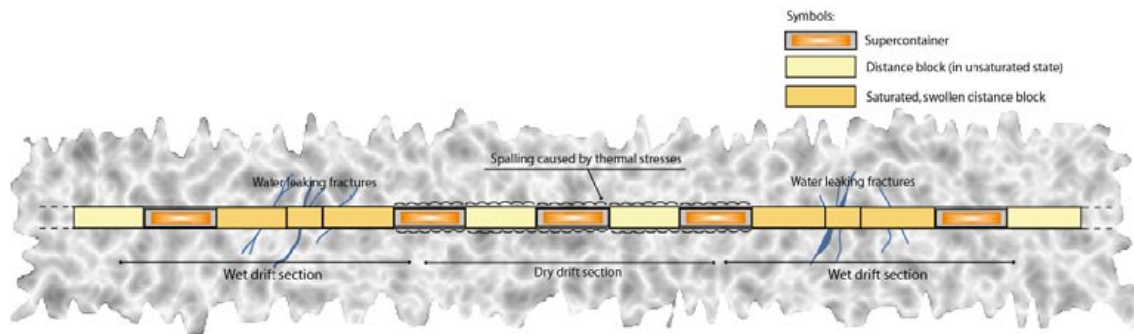
Figure 8-7. *Case where spalling occurs in the entire dry drift section between water-bearing fractures.*

8.7 Conclusions

Spalling (over limited areas) will occur as a result of thermal loading from the fuel canisters if the buffer material exerts no counteractive swelling pressure on the affected rock surface. In the worst-case scenario, spalling will occur along an entire dry drift section. In the best-case scenario, spalling will occur at supercontainer locations only. Regardless, of the development of swelling pressure at the rock surface is uncertain.

Spalling is not likely to occur after excavation. The detrimental effects of possible sparse spalling may be remedied by several engineering actions.

Spalling is both site and design dependent. It depends on the rock strength, state of stress, and the existence and length of dry sections. The results of the TM modelling are based on Olkiluoto data and the situation at other sites could be different.

In the event the buffer exerts some swelling pressure on the rock surface, there are significant uncertainties related to occurrence of spalling:

- the magnitude of the swelling pressure needed to eliminate spalling is uncertain,
- the swelling pressure of bentonite buffer in dry drift sections in unknown,
- the frequency and length of dry drift sections is not fully known.

The supercontainer sections are evidently most susceptible to spalling in dry drift sections. The distance blocks with a large gap in DAWE alternative are susceptible to spalling as well.

The BD alternative with a "tight fit" distance block (small gap) is most likely not susceptible to spalling, however, further demonstration is required.

8.8 Design factors to mitigate spalling

There are several means by which the buffer design can be modified to favourably affect swelling pressure to mitigate spalling; however the eventual swelling pressure values remain uncertain. Some of the design parameters include:

- initial buffer density,
- initial buffer water content,
- gap size at the rock/buffer interface,
- other gap sizes,
- use of artificial water filling of gaps,
- use of pellets in gaps.

Increasing the initial buffer water content from 10 to 20% and reducing the gap size between the distance blocks and the rock surface as in the Basic Design has a significant beneficial impact, which could be incorporated in the present design. The gap size in DAWE design is larger as a design principle and cannot be incorporated into the design without significant changes.

An alternative design based on a small gap between the rock surface and buffer could be developed if, e.g. the principle of using a supercontainer with a 42.5 mm gap is abandoned and the buffer is instead installed based on "tight" fit constraints prior to canister emplacement.

Pellets can be installed in the gap between the buffer and rock surface to mitigate the effect of thermal spalling. If the gap is small and long the installation of pellets in a robust manner is difficult. Pellet filling of the gap at the time of deposition could provide a small swelling pressure on the order of 150–200 kPa.

To minimize the risk of spalling in KBS-3H deposition drifts, the orientation of the drift axis should be parallel with the main principal stress.

A repository depth of 500 m is less favourable than 400 m due to higher *in situ* stresses, which increases susceptibility to spalling. The use of a shallower repository would be beneficial from this standpoint.

9 Groundwater control

9.1 General

The impact of water inflows may ultimately determine the feasibility of the KBS-3H repository design. Groundwater inflows into the deposition drift from intersecting water conductive fractures may cause, among other concerns, erosion and transport of buffer. Such inflow can be prevented through the use of special filling components; however, this approach generally results in a reduction to the degree of drift utilization without fully resolving the problem. The overall objective of groundwater control is to reduce the inflows further by using existing sealing principles and materials. The applicability of existing grouting techniques is limited by the preliminary requirement that holes drilled in a fan outside the drift perimeter must not compromise the safety function of the buffer or rock. Descriptions of grouting techniques and calculations of inflow with holes outside the drift are used to obtain a conservative estimate with respect to largest quantity of residual grouting material.

According to present understanding the natural (i.e. without grouting) inflow (see Sections 3.2 and 4.1) of 0.1 l/min is acceptable for the supercontainer unit, as a proven distance block design exists, which will function properly under this condition. If the inflow is larger, but remains in the range from 0.1 to 1 l/min after grouting, a special type of buffer filling block, with an average length of 10 m, can be used. Naturally the use of such blocks would result in a reduction of the utilization degree of the drift. In positions where inflow rates after the implementation of groundwater control measures are larger yet (in the range from 1 to 4 l/min or greater), the deposition drift is divided into compartments and the fracture zones with large inflows are isolated through the use of compartment plugs. Every set of compartment plugs requires a certain length of the drift (from 15 to 30 m), which cannot, of course, be used for the emplacement of canisters.

The KBS-3H deposition drifts can be oriented on the basis of several factors such as rock stress and groundwater inflow. It would be beneficial to be able to limit the number of independent grouting locations and to avoid singular small fractures. From the grouting perspective it is more favourable to choose an orientation that gives a few but somewhat more leaking location than a sparse leakage from several small fractures. This issue will be evaluated further in later design phases.

9.2 Short description of grouting methods

9.2.1 Introduction

- Three different methods are used for grouting a KBS-3H deposition drift in different phases:
- Pre-grouting with different number of grouting holes to represent grouting in investigations holes, pilot hole, inside the drift and adjacent to the drift
- Traditional post-grouting with singular bore-holes
- Grouting using Mega-Packer.

An evaluation of the sealing efficiency of these techniques is described further below.

9.2.2 Pre-grouting methods

Pre-grouting in investigation and pilot holes

This method is based on using investigation holes (one or several) or the pilot hole to seal water-bearing fractures. The investigation boreholes are likely drilled using a Diamond Head drill to have good control of the borehole direction. Grouting in pilot holes is similar to investigation holes; however, the equipment has to be adapted to the larger diameter of the pilot hole, which is typically 10–35 cm.

The effectiveness of grouting by using pilot holes is hampered by the fact that the grout must penetrate a distance of about one metre from the hole, which is in the centre of the deposition drift, into the rock before it actually seals the rock adjacent to the drift surface. Therefore the technique is probably only beneficial in sealing larger aperture fractures where reasonable penetration beyond one metre can be expected.

If additional investigation holes not centred in the drift are used, the effectiveness of grouting may be improved. In this case the grout must penetrate a shorter distance before it actually seals the rock adjacent to the drift surface.

Pre-grouting in the drift

Using several boreholes inside the perimetre of the drift during excavation allows for pre-grouting.

The number of holes that can be drilled inside the perimetre of the drift increases the risk of intersecting open parts of the fractures and actually improves the filling and sealing of these features compared to one or a few long investigation holes in the drift. The use of this method requires good characterization of the fracture zones to be grouted e.g. by using pilot or investigation hole data. The excavation of the drift has to be stopped during the grouting and the boring equipment has to be removed from the drift, which limits the systematic use of this technique along the whole drift.

9.2.3 Post-grouting by using Mega-Packer

Post-grouting is carried out by using the Mega-Packer technique (also called Large borehole Injection Device – LID). This technique is based on long-term safety requirements, which does not allow boring of holes extending outside the drift perimeter. This technique is being developed for use in KBS-3H deposition drifts and the device is being designed and manufactured for testing in the Demonstration drift at Äspö HRL in 2007.

Mega-Packer consists of a large tube, with only slightly smaller dimensions than the drift, sealed on both ends with packer material, see Figures 9-1 and 9-2. The void between the tube and the rock is filled with grout and the pressure is increased with the expected result that the grout penetrates into the conductive fractures and seals them. A test of a LID was performed at Stripa for sealing vertical pits /Börgesson et al. 1991/.
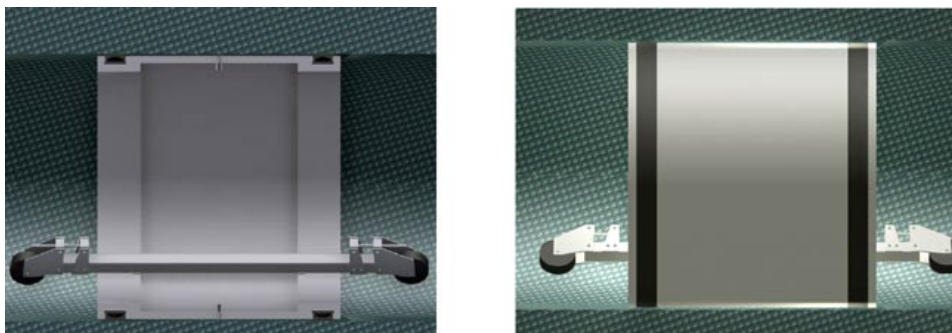
Figure 9-1. *Mega-Packer grouting device, side view and cross section parallel to the drift.*
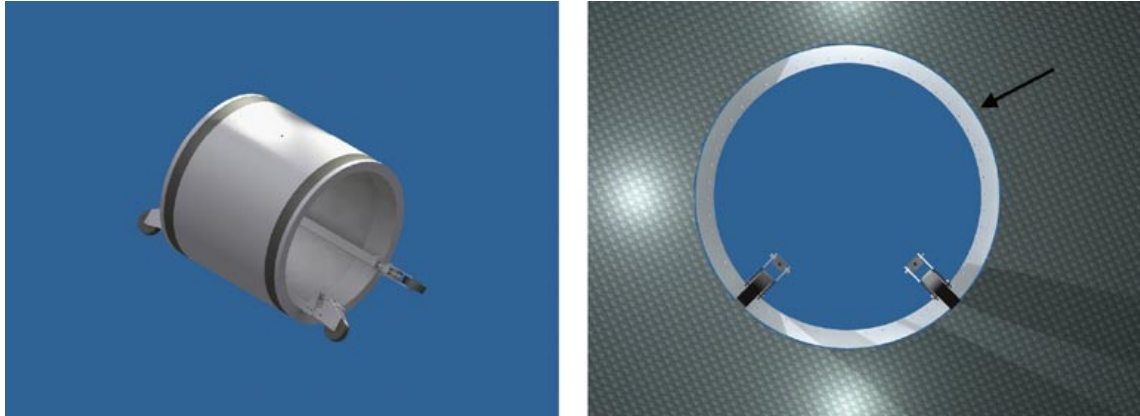
Figure 9-2. Mega-Packer grouting device, 3D view and cross section perpendicular to the drift. The gap between the rock and Mega-Packer is filled with grout, which is forced into the rock fractures by high pressure.

9.3 Hydrogeological conditions

The hydrogeological situation is relevant for the study of groundwater control, both for analysing the probability of inflow and as well for determining suitable grouting methods. For such a study the occurrence, frequency and orientation of water-bearing fractures at a depth of 300 to 700 m is of interest. Flow logs obtained from field investigations provide the basic input and the detection limit is 10^{-9} m²/s. The data mainly originates from /Hellä et al. 2006, Lanyon and Marschall 2006/.

Table 9-1 presents transmissivity distribution data from /Hellä et al. 2006/. Based on this data, a low fracture frequency is expected. Fractures with an inflow rate larger than 4 l/min are found, on average, every 250 m /Hellä et al. 2006/. The transmissivity distribution can be fairly well represented by a power-law distribution and the fracture frequency can be well described by a Poisson distribution.

Based on the results of the transmissivity measurement estimates of distribution functions describing the transmissivity and frequency of fractures can be made:

- 20% of measured 100 m interval lack transmissive fractures.
- 90% of measured 5 m intervals have transmissivities less than 0.1 l/m (equiv. drift inflow).
- 85% of measured 10 m intervals have transmissivities less than 0.1 l/m (equiv. drift inflow).

Table 9-1. Ttransmissivity distribution of fractures in the Olkiluoto bedrock after /Hellä et al. 2006/.

Transmissivity T (m²/s) / distance to the zone (m)	within local zones d = 0 m	Margin of the local zone 0 m < d < 35 m	Outside local zones d > 35 m	Sum	fractures/m
T > 10^{-7} m²/s	11	5	0	16	0.004
10^{-8} m²/s < T < 10^{-7} m²/s	17	12	7	36	0.01
T < 10^{-8} m²/s	29	45	49	123	0.03
Sum	57	62	56	175	0.04
sample length (appr.)	180	1,520	2,350	4,050	
Fractures/m	0.32	0.04	0.02	0.04	

The data includes uncertainties, which have been discussed by /Hellä et al. 2006, Lanyon and Marschall 2006/, e.g:

- Biased data due to the subvertical orientation of the boreholeswith respect to horizontal orientation of deposition drifts.

- Isotropy in hydraulic properties, but evidence of strong heterogeneity.

- Size of transmissive features is generally unknown.

- Channeling and skin-effects are not taken into consideration.

9.4 Calculations

9.4.1 Method of approach

This section discusses the groundwater control program and the estimated amount of grouting material needed and the effects of different orientations of the drifts. Certain calculations (see I and II below) are used to provide insight into the control program and the amount of material required:

I) Groundwater control was assessed in terms of relative measure of the sealing. Different sealing methods can be compared on this basis. /Eriksson 2002/ performed such calculations using a finite difference code. The calculations are probabilistic but are evaluated based on the average calculated value as base for the groundwater study.

The sealing effectiveness (θ), expressed in percent, is calculated as:

$$\theta = \frac{Q_1 - Q_2}{Q_1} \cdot 100 \qquad (9\text{-}1)$$

where Q_1 indicates the calculated inflow before grouting and Q_2 the calculated inflow after grouting.

For fractures of different hydraulic aperture, a certain theoretical inflow is possible. This inflow can be calculated on the basis of transmissivity (T):

$$Q = \frac{2\pi \cdot T \cdot H}{\ln(2H / r_t) + \xi} \qquad (9\text{-}2)$$

where H is the groundwater head, r_t the radius of the tunnel and ς the skin value /Rhén et al. 1997/. Using this equation the inflow in fractures with different transmisivity intervals can be evaluated. For example, the largest transmissivity presented by /Hellä et al. 2006/ is $6.3 \cdot 10^{-7}$ m^2/s. This fracture would result in an inflow of around 33 l/min if no skin effect is assumed and the hydraulic head is 420 m. To reduce the inflow to less than 0.1 l/min would then require a sealing effect of 99.7%. If a first grouting application limited the inflow by only 90%, a second, third, or fourth application or alternative method might be required to achieve the desired sealing effect.

The groundwater control evaluation procedure is as follows:

- For all methods, calculate the best possible expected sealing effectiveness in each fracture.

- Based on these sealing effectiveness, calculate expected the inflow rates after grouting in different geological situations.

- Estimate the value of the grouting method on the basis of a groundwater control program.

II) Calculations concerning the amount of grouting material needed are made based on a semi-continuum fracture model and a statistical description of the geohydrogeological situation (see Section 9.4.3). In the calculations the fracture planes are modelled as plan-parallel discs with apertures based on their transmissivity values according to Equation 9-3.

$$T = \frac{b^3 \cdot \rho g}{12 \cdot \mu_w}$$
(9-3)

Where T is the transmissivity in m^2/s, b the hydraulic aperture in m, ρ the water density in kg/m^3, g the gravitation in m/s^2 and μ_w the water viscosity in Ns/m^2.

The grout spread model used to evaluate the sealing efficincy is based on the description in /Gustafson and Stille 2005/, modified to a numerical model as presented in /Eriksson 2005/. The calculations are performed assuming Silica Sol as the grouting material.

The results of the calculations provide insight on how to fulfil the requirements needed to achieve the desired sealing effectiveness. The volume is calculated based on the distribution of transmissivity and on the assumption that the fractures can be represented by discs, which are completely filled with grout to a maximum of 15 m. It is also assumed that the depth of grout spread is directly correlated to the size of the aperture. As a result, larger fractures consume a majority of the grout. Additionally, the grouting technique is considered to be efficient so that only the necessary grout volumes are used.

9.4.2 Grouting material

Silica Sol is the grouting material assumed to be used. This choice is due to the expected transmissivity distribution. Only a small portion of the fractures is estimated to have hydraulic apertures larger than around 50 µm. Even if larger physical apertures are expected, the ability to effectively seal these fractures with cementitious grouts is limited and not fully understood.

It is assumed in the evaluation that the material behaves as a suspension, i.e., there is a minimum and a critical aperture that the materal can penetrate /Eriksson 2002/. Furthermore the Silica Sol was assumed to behave like water with respect to penetrability, i.e., in its ability to penetrate into any opening. These assumptions are considered to be conservative. The properties of Silica Sol used in the calculations are specified below:

- Yield value   0.1   Pa
- Viscosity [Pas]   0.005   Pas
- b_{min} 10   µm
- $b_{critical}$ 20   µm
- Density   1,200   kg/m^3
- Bleed   0   %.

9.4.3 Hydrogeological condition – scenarious for evaluation

The hydrogeological conditions used in the calculations for groundwater control were fixed in order to limit the number of calculations. Two scenarios are presented: Scenario 1, representing a situation with a singular fracture of small hydraulic aperture, is considered to be the most likely, and Scenario 2, which represents a situation with several fractures with one having a larger hydraulic aperture and the rest have smaller hydraulic apertures.

Scenario 1

This scenario involves one singular fracture with a small hydraulic aperture of 20 µm, which, theoretically, corresponds to an inflow of 0.4 l/min using Equation 9-2 with no skin factor. The fracture is modelled with an aperture variation of 20%, which is less than that used in the channel model in the DFN study by /Lanyon and Marschall 2006/. Although aperture variation can be large, the chosen value as such should not interfere with the discussion and relative comparison between different grouting methods. This last point is not discussed further in this report.

Scenario 2

In Scenario 2, four fractures are modelled with hydraulic apertures of 10, 20, 30 and 90 μm, which, theoretically, corresponds to a situation with a considerable inflow of 35 l/min using Equation 9-2 with no skin factor. These fractures are also modelled with a 20% variation in aperture.

Other bases for estimation

For the estimation of amount of material a stochastic approach is used and the geohydrological scenarios are modelled based on statistics. The transmissivity distribution and fracture frequency distribution is described in /Hellä et al. 2006/. The transmissivity distribution is presented with an average value of –8.8 in Log (T) and with a standard deviation in log (T) of 0.8. The corresponding data for the frequency of the fractures are 19.67 m and 32.47 m. A simulation was made based on these statistics. A number of 300 m long drifts were simulated giving a distribution of possible fracture arrangements for the deposition drifts. Based on this an estimation of grout take was made. The premises for this is that no grout should spread further away than 15 m and that 1 m penetration should be obtained in fractures with an aperture of 50 μm. Even smaller fractures could contain grout but the main amount of grout is to be found in the larger fractures.

9.4.4 Grouting technique

The grouting technique can greatly influence the obtained results (see /Eriksson 2002/ for a more detail). For the purposes of the calculations, the following was presumed:

- Grouting through the investigation hole is based on one grouting hole.

- Grouting in a fan inside the drift perimetre is based on using 8 grouting holes.

- Grouting in boreholes outside the drift is based on using 12 holes.

- The stop criteria used is described with a flow criterion and a maximum grouting time. In all three pre-grouting methods and in the concept of traditional post-grouting the grouting can theoretically continue until a flow of 0.1 l/min is obtained. In reality the grouting is stopped after 20 minutes maximum due to the curing of the grout.

- The pressures used are 1 MPa over the hydraulic pressure in pre-grouting and 0.5 MPa in traditional post-grouting.

- In grouting using Mega-Packer a grouting pressure of 2 MPa over the hydraulic pressure is used.

9.4.5 Grouting requirements

Grouting requirements are precise concerning overall section inflow and point flow. However, in the context of a groundwater control plan, it can be valuable to consider grouting during different stages of drift excavation, which may slightly alter or yield altogether different requirements.

Concerning the overall targets there are two requirements:

- Limit the inflow to less than 1 l/min, which allows use of the deposition drift.

- Limit the inflow to less than 0.1 l/min, which allows for canister emplacement.

9.4.6 Calculated results for the groundwater control study

Pre-grouting

The calculated, median sealing effectiveness is based on 10 simulations in each fracture and makes use of the following conditions:

Method A) Grouting with a single borehole yielded the following result:
Scenario 1: No sealing effect
Scenario 2: 64%

Method B) Grouting with 8 boreholes inside the drift yielded the following result:
Scenario 1: 2% sealing effect
Scenario 2: 99.5% Sealing effect

Method C) Grouting with 12 boreholes outside the drift yielded the following result:
Scenario 1: 5 % sealing effect
Scenario 2: 99.6 %

Traditional post-grouting

Based on the calculations, no effect due to traditional post-grouting in the smaller fractures is expected. There are, however, some alterations in the technical performance that might be favourable if post-grouting is undertaken. That is, some application of post-grouting technique might allow for inflows even less than 0.1 l/min. Such an application would require special pumps and other equipment.

Post-grouting using Mega-Packer

Scenario 1: 61% sealing effect

Scenario 2: 99.8% sealing effect

9.4.7 Calculated results on amount of grouting material

Figure 9-3 displays the resultant grout take over a simulation of 1,000 drifts.
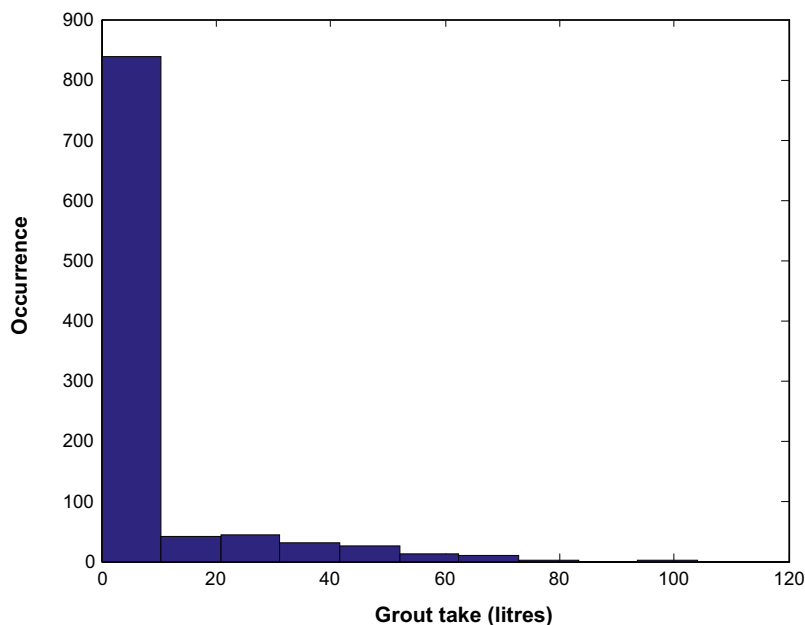
Figure 9-3. *Simulated result of grout takes for 1,000,300 m long KBS-3H drifts.*

9.5   Plan for groundwater control

The groundwater control program is based on using different stages of grouting to limit the inflow and to fulfil the requirements, i.e., facilitate storing. The results of the calculations are used to frame a discussion on a program for groundwater control. The calculated results should only be used as guidance and for the comparison of different methods as the input parameters are subject to considerable uncertainty.

Program for sealing

- Step 1) Investigation hole
  - Evaluate if the position of the drift is suitable from a groundwater control or safety aspect.
  - If a grouting situation with one or a few fractures with a hydraulic aperture larger than around 50 μm (more than around 10 l/min) grouting is meaningfull from the investigation hole: expected effect 50–60%.
  - Investigate the fracture/-s for a later pre- or post-grouting.

- Step 2) Some distance before the leakage area excavation is stopped and 4 investigation holes are drilled in the contour of the drift.

- Step 3) If the grouting scenario contains several fractures make pre-grouting from inside the drift. If the grouting scenario contains only a discrete fracture of limited aperture no pre-grouting is meaningful: expected effect > 99%.

- Step 4) After excavation, Mega-Packer is used for post-grouting of the leaking area: expected effect 50–100%.

9.6   Quantity of grouting material in the rock

All estimations of grout take are associated with considerable uncertainties. In situations discussed here, the largest simulated volume is approximately 100 litres. In the majority of cases (85%), less than 20 litres of grout was estimated. Considering that fractures are not planar discs and rarely show a fully 2D grout spread pattern, 100 litres should be regarded as a fairly conservative estimate. However, the porosity of the rock mass is often found to be larger than the hydraulic porosity and may be a reason to increase the grout volume. According to /Zimmerman et al. 1991/ and /Barton and Quadros 1997/, values of porosity can be several times higher than the hydraulic aperture state. Taking these observations into account, a rough estimate of 500 litres may be in order.

All of the different pre-grouting techniques use boreholes. When pre-grouting in boreholes inside the drift, all grouting material inside the drift perimetre is removed by rock excavation and no holes filled with grouting material remain.

10   Engineered and other residual materials

10.1   Whole repository

The quantities of engineered and other residual materials in a KBS-3H repository have been evaluated in /Hagros 2007a/. This chapter summarizes the main findings of the evaluation.

Regarding the layout of the repository, the results of the latest KBS-3H layout adaptation work at Olkiluoto /Johansson et al. 2007/ are used. Accordingly, the repository is assumed to be constructed in one layer at the depth of 400–420 m in the central part of the Olkiluoto island. The main difference to a KBS-3V repository is that instead of deposition tunnels and vertical deposition holes, there are horizontal deposition drifts. Based on the layout by /Johansson et al. 2007/, the dimensions of the deposition drifts are assumed to be the following:

- The total number of deposition drifts is 171.

- Total length is 46,432 m.

- Cross-sectional area is some 2.69 m^2, except for the deposition niche, the first 15 m, which is a horseshoe-shaped tunnel with the following properties: width 8.5 m, height 6.65 m and cross-sectional area of 50 m^2 (these values are only preliminary).

- Accordingly, the total volume of the deposition drifts is estimated to be 246,166 m^3. This is 61% smaller than the total volume of KBS-3V deposition tunnels and holes.

The dimensions of the central tunnels are also clearly different in KBS-3H and KBS-3V due to the larger total central tunnel length in KBS-3H. Based on the layout by /Johansson et al. 2007/, the dimensions of the KBS-3H central tunnels are assumed to be the following:

- The total length of central tunnels (at –420 m level, excluding ONKALO) is 8,399 m. This is 23% larger than the total length of central tunnels in KBS-3V.

- The total volume of the central tunnels is, accordingly, 309,644 m^3. The concurrent central tunnel concept /Malmlund et al. 2004/ is used, so the given lengths and volumes include both tubes of the double central tunnel as well as the connecting tunnels between them.

The dimensions of all other parts of the KBS-3H repository are the same as in KBS-3V /Hagros 2007b/. Accordingly, the total volume of the ONKALO is 362,039 m^3. The dimensions of the individual parts of ONKALO have not been updated and they are based on /Hjerpe 2004/.

The total volume of the repository (incl. ONKALO) is 1,016,290 m^3 and the total volume of the actual repository is, therefore, 654,251 m^3. The actual repository includes the deposition drifts, the central tunnels at the –420 m level and a total of 98,441 m^3 of other openings.

All volumes presented here are theoretical volumes, whereas the actual excavated volumes are probably slightly (some 10%) larger due to over break. The theoretical volumes will be used, because the difference is minor with respect to other uncertainties involved in the work, and because the data on the excavations carried out so far are also based on theoretical volumes. However, since the excavated volume is very significant for the estimation of the quantities of the tunnel backfill materials, the volumes (except for those of the deposition drifts) will be multiplied by 1.1 when the backfill materials are considered.

When the quantities of the residual materials have been calculated, three different reference deposition drifts have been assumed for the three different canister types (OL1-2, OL3 and LO1-2), based on the new KBS-3H layout /Johansson et al. 2007/. Each reference drift is assumed to be 300 m long and include one compartment plug, which takes up 30 m of the drift length. The number of canisters in one drift varies because different canister types have different thermal canister spacing, and these affect the actual canister spacing. The number of canisters per drift used in the calculations is 18. The rock mass properties are assumed to be similar in all three reference drifts. The details of the three reference drifts are given in Table 10-1. When estimating the total quantities of the materials in the drift end plugs, the real number of deposition drifts (171 in total) has been assumed.

Table 10-1. Compositions of reference deposition drifts (with average properties) for the three different canister types (based on /Johansson et al. 2007/).

Parameter/Canister type	OL1-2	OL3	LO1-2
Total length of drift	300 m	300 m	300 m
Unusable section in the beginning of the drift	25 m	25 m	25 m
Thermal canister spacing	11.0	10.6 m	9.1 m
Number of canisters in drift	17.5	18.2	21.2
Actual canister spacing*	15.7 m	15.1 m	13.0 m
Number / Total length of compartment plugs	1/30 m	1/30 m	1/30 m
Total length of blank zones	52 m	52 m	52 m

* The actual canister spacing is larger than the thermal canister spacing due to sections with unsuitable rock mass conditions. These sections are assumed to make up 25% of the rock mass at Olkiluoto outside major fracture zones and they will have compartments plugs or blank zones (see /Johansson et al. 2007/). The percentage is higher in the KBS-3H alternative than in the KBS-3V in order to take account of the space requirements of the KBS-3H components (compartment plugs and blank zones) that will be used even when the unusable sections are rather narrow.

10.1.1 Quantities per origin of materials

The estimated quantities of residual materials that remain in the repository (incl. ONKALO) after closure are presented in Figure 10-1 and Table 10-2 for the BD design alternative and Table 10-3 for the DAWE alternative. In addition to the remaining quantities, the tables also show the estimated total quantities of materials introduced into the repository, presented separately for their most relevant chemical components. Similarly to the approach used by /Hagros 2007b/, the following components of the materials are not considered here:

- water (H_2O),
- oxygen (O_2),
- nitrogen gas (N_2),
- carbon dioxide (CO_2),
- carbon monoxide (CO),
- rock minerals,
- some other substances which are considered to be of minor relevance for the long-term safety of the repository or which could not be calculated due to a lack of data.

As water is not taken into account, all values presented in the following tables refer to the quantities of the dry materials.
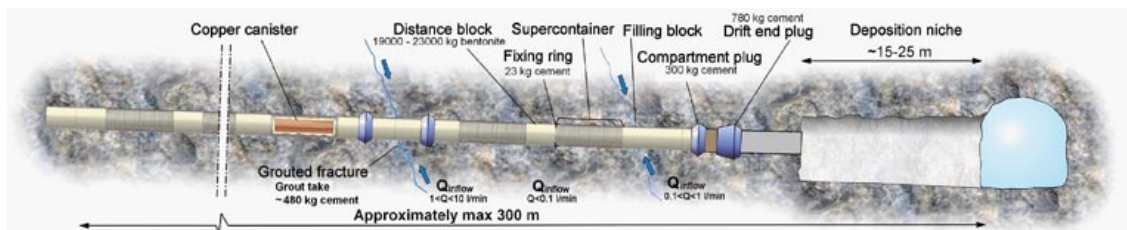
Figure 10-1. *Key components containing engineered and residual materials in BD alternative and estimated quantities of cement. Note that in case of DAWE alternative fixing rings are not needed.*

Table 10-2. Estimated total quantities of residual materials in a KBS-3H repository (BD design alternative), listed by origin (Table 2 in /Hagros 2007a/). Table continues on the next pages.

Origin of the residual materials	Chemical components considered	Total introduced quantity [kg]	Removal efficiency [%]	Remaining quantity [kg]
1 Steel cylinders in supercontainers incl. feet	Steel	3,000,000	0	3,000,00
2 Compartment plugs	Steel	640,000	0	640,000
	Cement	92,000	0	92,000
	Silica (SiO_2)	6,100	0	6,100
	Organic materials	40,000	0	40,000
	Chloride	0.1	0	0.1
	Pyrite	14,000	0	14,000
	Gypsum	140,000	0	140,000
	Carbonates (calcite + siderite)	100,000	0	100,000
3 Drift end plugs				
3.1 LHHP plug alternative	Cement	180,000	0	180,000
	Silica (SiO_2)	400,000	0	400,000
	Organic materials	14,000	0	14,000
	Steel	510,000	0	510,000
	Chloride	0.07	0	0.07
3.2 Rock cylinder alternative	Cement	380,000	0	380,000
	Silica (SiO_2)	20,000	0	20,000
	Organic materials	140	0	140
	Steel	360,000	0	360,000
	Chloride	0.4	0	0.4
4 Spray and drip shields	Steel	500	0	500
5 Fixing rings	Steel	410,000	0	410,000
	Cement	16,000	0	16,000
	Silica (SiO_2)	1,000	0	1,000
	Organic materials	6	0	6
	Chloride	0.02	0	0.02
6 Impurities in bentonite buffer	Organic carbon	89,000	0	89,000
	Pyrite	31,000	0	31,000
	Gypsum	310,000	0	310,000
	Carbonates (calcite + siderite)	220,000	0	220,000
7 Impurities in distance blocks	Organic carbon	120,000	0	120,000
	Pyrite	42,000	0	42,000
	Gypsum	420,000	0	420,000
	Carbonates (calcite + siderite)	300,000	0	300,000
8 Impurities in blank zones (bentonite blocks)	Organic carbon	67,000	0	67,000
	Pyrite	23,000	0	23,000
	Gypsum	230,000	0	230,000
	Carbonates (calcite + siderite)	170,000	0	170,000
9 *Impurities in backfill material*				
9a Backfill alternative a (bentonite/crushed rock)	Organic carbon	1,200,000	0	1,200,000
	Pyrite	410,000	0	410,000
	Gypsum	4,100,000	0	4,100,000
	Carbonates (calcite + siderite)	2,900,000	0	2,900,000
9b Backfill alternative b (Friedland clay)	Organic carbon	10,000,000	0	10,000,000
	Pyrite	11,000,000	0	11,000,000
	Gypsum	14,000,000	0	14,000,000
	Carbonates (calcite + siderite)	100,000	0	100,000
10 Explosives	Nitrogen oxides (NO_x)[1]	1,600	99	16
11 Blasting caps and cords	Aluminium	1,700	90	170
	Plastic	1,800	90	180
12 Support bolts	Steel	220,000	0	220,000
	Zinc	4,200	0	4,200
	Cement	86,000	0	86,000
13 Anchor bolts	Steel	50,000	40	30,000
	Cement	6,300	0	6,300

Origin of the residual materials	Chemical components considered	Total introduced quantity [kg]	Removal efficiency [%]	Remaining quantity [kg]
14 Shotcrete				
14A Shotcrete alternative A	Cement	6,900,000	95	350,000
	Aluminium	21,000	95	1,000
	Organic materials	49,000	95	2,400
	Silica (SiO_2)	280,000	95	14,000
	Iron (Fe(III))	4,900	95	200
	Chloride	300	95	17
14B Shotcrete alternative B	Cement	5,100,000	95	260,000
	Aluminium	15,000	95	800
	Organic materials	36,000	95	1,800
	Silica (SiO_2)	2,200,000	95	110,000
	Iron (Fe(III))	3,600	95	180
	Chloride	300	95	13
15 Grouting materials				
15.1 Grouting alternative 1	Cement	780,000	20	620,000
	Organic materials	7,800	20	6,200
	Silica (SiO_2)	78,000	20	62,000
	Chloride	800	20	600
	Nitrate	1,000	20	800
15.2 Grouting alternative 2	Cement	590,000	20	480,000
	Organic materials	10,000	20	8,200
	Silica (SiO_2)	130,000	20	110,000
	Chloride	600	20	500
	Nitrate	900	20	700
15.3 Grouting alternative 3	Cement	420,000	20	340,000
	Organic materials	5,000	20	4,000
	Silica (SiO_2)	230,000	20	190,000
	Chloride	5,700	20	4,600
	Nitrate	800	20	600
16 Floors	Cement	5,200,000	98	100,000
	Steel	710,000	99	7,100
17 Miscellaneous constructions	Cement	4,500,000	98	89,000
	Steel	1,000,000	98	20,000
	Aluminium	100,000	98	2,000
	Zinc	6,800	98	140
18 Drainage pipes	Steel	5,800	95	300
	Polyethylene (PE)	3,500	95	180
	Polystyrene (EPS)	1,400	95	70
19 Wear to tyres	Rubber	160,000	90	16,000
20 Exhaust fumes from diesel engines	Nitrogen oxide	1,400,000	99	14,000
	Soot and ash	82,000	93	5,800
21 Diesel oil	Hydrocarbons	210,000	95	11,000
22 Battery acid	Sulphuric acid	3,200	90	300
23 Hydraulic and lubricating oils	Hydrocarbons	47,000	90	4,700
24 Degreasing agents and detergents	Hydrocarbons + other organic materials	70,000	95	3,600
25 Hard metals and metal fragments	Steel	520,000	98	10,000
	Tungsten and cobalt	2,800	99	30
26 Paints	Hydrocarbons	5,500	0	5,500
27 Urine	Carbamide	1,100,000	95	55,000
28 Miscellaneous human waste	Organic materials	700,000	98	14,000
29 Impurities in ventilation air	Organic materials	10,000,000	99	100,000

[1] this is valid for the gas phase, but if soluble nitrogen compouns are formed their removal efficiency is likely much lower.

Table 10-3. Estimated total quantities of residual materials in a KBS-3H repository (DAWE design alternative), listed by origin (Table 3 in /Hagros 2007a/). Table continues on the next pages.

Origin of the residual materials	Chemical components considered	Total introduced quantity [kg]	Removal efficiency [%]	Remaining quantity [kg]
1 Steel cylinders in supercontainers	Steel	3,000,000	0	3,000,000
2 Compartment plugs	Steel	640,000	0	640,000
	Cement	92,000	0	92,000
	SiO_2	6,100	0	6,100
	Organic materials	40,000	0	40,000
	Chloride	0.1	0	0.1
	Pyrite	14,000	0	14,000
	Gypsum	140,000	0	140,000
	Carbonates (calcite + siderite)	100,000	0	100,000
3 Drift end plugs				
3.1 LHHP plug alternative	Cement	180,000	0	180,000
	SiO_2	400,000	0	400,000
	Organic materials	14,000	0	14,000
	Steel	510,000	0	510,000
	Chloride	0.07	0	0.07
3.2 Rock cylinder alternative	Cement	380,000	0	380,000
	SiO_2	20,000	0	20,000
	Organic materials	140	0	140
	Steel	360,000	0	360,000
	Chloride	0.4	0	0.4
4 Spray and drip shields	Steel	500	0	500
5 Drainage, watering and air evacuation systems (only pipe props are considered)	Steel	500	0	500
6 Impurities in bentonite buffer	Organic carbon	89,000	0	89,000
	Pyrite	31,000	0	31,000
	Gypsum	310,000	0	310,000
	Carbonates (calcite + siderite)	220,000	0	220,000
7 Impurities and feet of distance blocks	Organic carbon	120,000	0	120,000
	Pyrite	40,000	0	40,000
	Gypsum	400,000	0	400,000
	Carbonates (calcite + siderite)	290,000	0	290,000
	Steel	39,000	0	39,000
8 Impurities in blank zones (bentonite blocks)	Organic carbon	67,000	0	67,000
	Pyrite	23,000	0	23,000
	Gypsum	230,000	0	230,000
	Carbonates (calcite + siderite)	170,000	0	170,000
9 *Impurities in backfill material*				
9a Backfill alternative a (bentonite/crushed rock)	Organic carbon	1,200,000	0	1,200,000
	Pyrite	410,000	0	410,000
	Gypsum	4,100,000	0	4,100,000
	Carbonates (calcite + siderite)	2,900,000	0	2,900,000
9b Backfill alternative b (Friedland clay)	Organic carbon	10,000,000	0	10,000,000
	Pyrite	11,000,000	0	11,000,000
	Gypsum	14,000,000	0	14,000,000
	Carbonates (calcite + siderite)	100,000	0	100,000
10 Explosives	Nitrogen oxides (NO_x)[1]	1,600	99	16
11 Blasting caps and cords	Aluminium	1,700	90	170
	Plastic	1,800	90	180
12 Support bolts	Steel	220,000	0	220,000
	Zinc	4,200	0	4,200
	Cement	86,000	0	86,000

Origin of the residual materials	Chemical components considered	Total introduced quantity [kg]	Removal efficiency [%]	Remaining quantity [kg]
13 Anchor bolts	Steel	50,000	40	30,000
	Cement	6,300	0	6,300
14 Shotcrete				
14A Shotcrete alternative A	Cement	6,900,000	95	350,000
	Aluminium	21,000	95	1,000
	Organic materials	49,000	95	2,400
	Silica (SiO_2)	280,000	95	14,000
	Iron (Fe(III))	4,900	95	200
	Chloride	300	95	17
14B Shotcrete alternative B	Cement	5,100,000	95	260,000
	Aluminium	15,000	95	800
	Organic materials	36,000	95	1,800
	Silica (SiO_2)	2,200,000	95	110,000
	Iron (Fe(III))	3,600	95	180
	Chloride	300	95	13
15 Grouting materials				
15.1 Grouting alternative 1	Cement	780,000	20	620,000
	Organic materials	7,800	20	6,200
	Silica (SiO_2)	78,000	20	62,000
	Chloride	800	20	600
	Nitrate	1,000	20	800
15.2 Grouting alternative 2	Cement	590,000	20	480,000
	Organic materials	10,000	20	8,200
	Silica (SiO_2)	130,000	20	110,000
	Chloride	600	20	500
	Nitrate	900	20	700
15.3 Grouting alternative 3	Cement	420,000	20	340,000
	Organic materials	5,000	20	4,000
	Silica (SiO_2)	230,000	20	190,000
	Chloride	5,700	20	4,600
	Nitrate	800	20	600
16 Floors	Cement	5,200,000	98	100,000
	Steel	710,000	99	7,100
17 Miscellaneous constructions	Cement	4,500,000	98	89,000
	Steel	1,000,000	98	20,000
	Aluminium	100,000	98	2,000
	Zinc	6,800	98	140
18 Drainage pipes	Steel	5,800	95	300
	Polyethylene (PE)	3,500	95	180
	Polystyrene (EPS)	1,400	95	70
19 Wear to tyres	Rubber	160,000	90	16,000
20 Exhaust fumes from diesel engines	Nitrogen oxide	1,400,000	99	14,000
	Soot and ash	82,000	93	5,800
21 Diesel oil	Hydrocarbons	210,000	95	11,000
22 Battery acid	Sulphuric acid	3,200	90	300
23 Hydraulic and lubricating oils	Hydrocarbons	47,000	90	4,700
24 Degreasing agents and detergents	Hydrocarbons + other organic materials	70,000	95	3,600
25 Hard metals and metal fragments	Steel	520,000	98	10,000
	Tungsten and cobalt	2,800	99	30
26 Paints	Hydrocarbons	5,500	0	5,500
27 Urine	Carbamide	1,100,000	95	55,000
28 Miscellaneous human waste	Organic materials	700,000	98	14,000
29 Impurities in ventilation air	Organic materials	10,000,000	99	100,000

[1] this is valid for the gas phase, but if soluble nitrogen compouns are formed their removal efficiency is likely much lower.

The design alternatives listed in the tables are the following:

Rock support alternatives are the following: shotcrete with ordinary cement (A) and low-pH cement (B). Grouting alternatives are: ordinary cement (1), low-pH cement (2), and colloidal silica (3). The backfill alternatives are: a mixture of crushed rock and bentonite MX-80 (a) or Friedland clay (b).

For example, design alternative "A1a" means that the selected support alternative is A (shotcrete with ordinary cement), the grouting alternative is 1 (100% ordinary cement) and the backfill alternative is "a" (mixture of crushed rock and bentonite).

10.1.2 Total quantities in the BD design alternative

Total quantities of chemical components are presented in Tables 10-4 to 10-10 for the BD design alternative over different combinations of tunnel support, grouting, backfill and drift end plug alternatives. Low-pH grouting materials and support materials are the recommended materials for the deposition drift. For comparison also combinations of other materials have been presented.

- Table 10-4 features design alternative A1a[1] with an LHHP plug. Ordinary cement is assumed for use in both shotcreting (support alternative A) and grouting (grouting alternative 1). The backfill plan is based on bentonite/crushed rock mixture (backfill alternative a).

- In Table 10-5, other alternatives are the same as in Table 10-4, but the drift end plug is of the rock cylinder type.

- In Table 10-6, other alternatives are the same as in Table 10-4, but the backfill strategy is based on Friedland clay (backfill alternative b).

- In Table 10-7, low-pH cement is assumed for use in both shotcreting and grouting (shotcreting alternative B and grouting alternative 2). The backfill plan is based on a bentonite/crushed rock mixture (backfill alternative a) and the drift end plug is of the rock cylinder type.

- Table 10-8 is similar to Table 10-7, except that grouting is based on the use of silica grouts (grouting alternative 3).

- In Table 10-9, low-pH cement is assumed for use in both shotcreting and grouting (shotcreting alternative B and grouting alternative 2). The backfill plan is based on a bentonite/crushed rock mixture (backfill alternative a) and the drift end plug is a LHHP plug.

- In Table 10-10 low-pH cement is assumed for use in both shotcreting and grouting (shotcreting alternative B and grouting alternative 3). The backfill plan is based on a bentonite/crushed rock mixture (backfill alternative a) and the drift end plug is a LHHP plug.

In these Tables the results are categorised according to their chemical nature. Note that depending on the availability of data, some components have been considered in more detail than others and the categories are, therefore, not necessarily mutually exclusive. For example, the iron (Fe(III)) estimates only take shotcrete into account as a source (some shotcrete additives contain Fe_2O_3) but, clearly, other materials and categorised components contain iron as well. Most notably, iron is a major constituent of steel (metallic iron) but it can also be found as Fe(II) in pyrite and siderite, which occur as impurities in bentonite. Iron is also a constituent of cement, but the chemical constituents of cement were not individually quantified in the tables either.

By using Table 10-2 it is possible to calculate the total material quantities for any combination of alternatives. Only five combinations are presented here for the BD alternative, but the total number of possible combinations is 24.

---

[1] Design alternative "A1a" signifies that the selected support alternative is A (shotcrete with ordinary cement), the grouting alternative is 1 (100% ordinary cement) and the backfill alternative is a (mixture of crushed rock and bentonite). The groutings and shotcretings assumed in these alternatives for the ONKALO are explained in /Hagros 2007b/.

Table 10-4. Estimated total quantities of chemical components, sorted by remaining quantity, from residual materials in a KBS-3H repository (including ONKALO), based on design alternatives BD and A1a (= support alternative A, grouting alternative 1, backfill alternative a) with an LHHP plug (Table 4 in /Hagros 2007a/).

Chemical components	Origin (reference to Table 10-2)	Total introduced quantity [kg]	Removal efficiency [%]	Remaining quantity [kg]
Gypsum	2, 6, 7, 8, 9a	5,200,000	0	5,200,000
Steel	1, 2, 3.1, 4, 5, 12, 13, 16, 17, 18, 25	7,100,000	32	4,800,000
Carbonates (calcite + siderite)	2, 6, 7, 8, 9a	3,700,000	0	3,700,000
Cement	2, 3.1, 5, 12, 13, 14A, 15.1, 16, 17	18,000,000	91	1,500,000
Organic materials (incl. organic carbon and hydrocarbons)	2, 3.1, 5, 6, 7, 8, 9a, 14A, 15.1., 21, 23, 24, 26, 28, 29	13,000,000	87	1,700,000
Pyrite	2, 6, 7, 8, 9a	520,000	0	520,000
Silica (SiO2)	2, 3.1, 5, 14A, 15.1	760,000	37	480,000
Carbamide	27	1,100,000	95	55,000
Rubber	19	160,000	90	16,000
Nitrogen oxides (NOx)	10, 20	1,400,000	99	14,000
Soot and ash	20	82,000	93	5,800
Zinc	12, 17	11,000	61	4,300
Aluminium	11, 14A, 17	120,000	97	3,200
Nitrate	15.1	1,000	20	800
Chloride	2, 3.1, 5, 14A, 15.1	1,100	43	600
Sulphuric acid	22	3,200	90	300
Iron (Fe(III))	14A	4,900	95	200
Plastic	11	1,800	90	180
Polyethylene (PE)	18	3,500	95	180
Polystyrene (EPS)	18	1,400	95	70
Tungsten and cobalt	25	2,800	99	30

Table 10-5. Estimated total quantities of chemical components from residual materials in a KBS-3H repository (including ONKALO), based on design alternatives BD and A1a (= support alternative A, grouting alternative 1, backfill alternative a) with a rock cylinder plug (Table 5 in /Hagros 2007a/).

Chemical components	Origin (reference to Table 10-2)	Total introduced quantity [kg]	Removal efficiency [%]	Remaining quantity [kg]
Gypsum	2, 6, 7, 8, 9a	5,200,000	0	5,200,000
Steel	1, 2, 3.2, 4, 5, 12, 13, 16, 17, 18, 25	6,900,000	32	4,700,000
Carbonates (calcite + siderite)	2, 6, 7, 8, 9a	3,700,000	0	3,700,000
Cement	2, 3.2, 5, 12, 13, 14A, 15.1, 16, 17	18,000,000	90	1,700,000
Organic materials (incl. organic carbon and hydrocarbons)	2, 3.2, 5, 6, 7, 8, 9a, 14A, 15.1., 21, 23, 24, 26, 28, 29	13,000,000	87	1,600,000
Pyrite	2, 6, 7, 8, 9a	520,000	0	520,000
Silica (SiO2)	2, 3.2, 5, 14A, 15.1	390,000	72	110,000
Carbamide	27	1,100,000	95	55,000
Rubber	19	160,000	90	16,000
Nitrogen oxides (NOx)	10, 20	1,400,000	99	14,000
Soot and ash	20	82,000	93	5,800
Zinc	12, 17	11,000	61	4,300
Aluminium	11, 14A, 17	120,000	97	3,200
Nitrate	15.1	1,000	20	800
Chloride	2, 3.2, 5, 14A, 15.1	1,100	43	600
Sulphuric acid	22	3,200	90	300
Iron (Fe(III))	14A	4,900	95	200
Plastic	11	1,800	90	180
Polyethylene (PE)	18	3,500	95	180
Polystyrene (EPS)	18	1,400	95	70
Tungsten and cobalt	25	2,800	99	30

Table 10-6. Estimated total quantities of chemical components from residual materials in a KBS-3H repository (including ONKALO), based on design alternatives BD and A1b (= support alternative A, grouting alternative 1, backfill alternative b) with an LHHP plug (Table 6 in /Hagros 2007a/).

Chemical components	Origin (reference to Table 10-2)	Total introduced quantity [kg]	Removal efficiency [%]	Remaining quantity [kg]
Gypsum	2, 6, 7, 8, 9b	15,000,000	0	15,000,000
Steel	1, 2, 3.1, 4, 5, 12, 13, 16, 17, 18, 25	7,100,000	32	4,800,000
Carbonates (calcite + siderite)	2, 6, 7, 8, 9b	880,000	0	880,000
Cement	2, 3.1, 5, 12, 13, 14A, 15.1, 16, 17	18,000,000	91	1,500,000
Organic materials (incl. organic carbon and hydrocarbons)	2, 3.1, 5, 6, 7, 8, 9b, 14A, 15.1., 21, 23, 24, 26, 28, 29	22,000,000	51	11,000,000
Pyrite	2, 6, 7, 8, 9b	11,000,000	0	11,000,000
Silica (SiO2)	2, 3.1, 5, 14A, 15.1	760,000	37	480,000
Carbamide	27	1,100,000	95	55,000
Rubber	19	160,000	90	16,000
Nitrogen oxides (NOx)	10, 20	1,400,000	99	14,000
Soot and ash	20	82,000	93	5,800
Zinc	12, 17	11,000	61	4,300
Aluminium	11, 14A, 17	120,000	97	3,200
Nitrate	15.1	1,000	20	800
Chloride	2, 3.1, 5, 14A, 15.1	1,100	43	600
Sulphuric acid	22	3,200	90	300
Iron (Fe(III))	14A	4,900	95	200
Plastic	11	1,800	90	180
Polyethylene (PE)	18	4,000	95	180
Polystyrene (EPS)	18	1,400	95	70
Tungsten and cobalt	25	2,800	99	30

Table 10-7. Estimated total quantities of chemical components from residual materials in a KBS-3H repository (including ONKALO), based on design alternatives BD and B2a (= support alternative B, grouting alternative 2, backfill alternative a) with a rock cylinder plug (Table 7 in /Hagros 2007a/.

Chemical components	Origin (reference to Table 10-2)	Total introduced quantity [kg]	Removal efficiency [%]	Remaining quantity [kg]
Gypsum	2, 6, 7, 8, 9a	5,200,000	0	5,200,000
Steel	1, 2, 3.2, 4, 5, 12, 13, 16, 17, 18, 25	6,900,000	32	4,700,000
Carbonates (calcite + siderite)	2, 6, 7, 8, 9a	3,700,000	0	3,700,000
Cement	2, 3.2, 5, 12, 13, 14B, 15.2, 16, 17	16,000,000	91	1,500,000
Organic materials (incl. organic carbon and hydrocarbons)	2, 3.2, 5, 6, 7, 8, 9a, 14B, 15.2., 21, 23, 24, 26, 28, 29	13,000,000	87	1,600,000
Pyrite	2, 6, 7, 8, 9a	520,000	0	520,000
Silica (SiO2)	2, 3.2, 5, 14B, 15.2	2,400,000	90	250,000
Carbamide	27	1,100,000	95	55,000
Rubber	19	160,000	90	16,000
Nitrogen oxides (NOx)	10, 20	1,400,000	99	14,000
Soot and ash	20	82,000	93	5,800
Zinc	12, 17	11,000	61	4,300
Aluminium	11, 14B, 17	120,000	97	3,000
Nitrate	15.2	900	20	700
Chloride	2, 3.2, 5, 14B, 15.2	900	43	500
Sulphuric acid	22	3,200	90	300
Iron (Fe(III))	14A	3,600	95	180
Plastic	11	1,800	90	180
Polyethylene (PE)	18	4,000	95	180
Polystyrene (EPS)	18	1,400	95	70
Tungsten and cobalt	25	2,800	99	30

Table 10-8. Estimated total quantities of chemical components from residual materials in a KBS-3H repository (including ONKALO), based on design alternatives BD and B3a (= support alternative B, grouting alternative 3, backfill alternative a) with a rock cylinder plug (Table 8 in /Hagros 2007a/).

Chemical components	Origin (reference to Table 10-2)	Total introduced quantity [kg]	Removal efficiency [%]	Remaining quantity [kg]
Gypsum	2, 6, 7, 8, 9a	5,200,000	0	5,200,000
Steel	1, 2, 3.2, 4, 5, 12, 13, 16, 17, 18, 25	6,900,000	32	4,700,000
Carbonates (calcite + siderite)	2, 6, 7, 8, 9a	3,700,000	0	3,700,000
Cement	2, 3.2, 5, 12, 13, 14B, 15.3, 16, 17	16,000,000	91	1,400,000
Organic materials (incl. organic carbon and hydrocarbons)	2, 3.2, 5, 6, 7, 8, 9a, 14B, 15.3., 21, 23, 24, 26, 28, 29	13,000,000	87	1,600,000
Pyrite	2, 6, 7, 8, 9a	520,000	0	520,000
Silica (SiO2)	2, 3.2, 5, 14B, 15.3	2,500,000	87	330,000
Carbamide	27	1,100,000	95	55,000
Rubber	19	160,000	90	16,000
Nitrogen oxides (NOx)	10, 20	1,400,000	99	14,000
Soot and ash	20	82,000	93	5,800
Zinc	12, 17	11,000	61	4,300
Aluminium	11, 14B, 17	120,000	97	3,000
Nitrate	15.3	800	20	600
Chloride	2, 3.2, 5, 14B, 15.3	6,000	23	4,600
Sulphuric acid	22	3,200	90	300
Iron (Fe(III))	14A	3,600	95	180
Plastic	11	1,800	90	180
Polyethylene (PE)	18	4,000	95	180
Polystyrene (EPS)	18	1,400	95	70
Tungsten and cobalt	25	2,800	99	30

Table 10-9. Estimated total quantities of chemical components from residual materials in a KBS-3H repository (including ONKALO), based on design alternatives BD and B2a (= support alternative B, grouting alternative 2, backfill alternative a) with a LHHP plug (Table 9 in /Hagros 2007a/).

Chemical components	Origin (reference to Table 10-2)	Total introduced quantity [kg]	Removal efficiency [%]	Remaining quantity [kg]
Gypsum	2, 6, 7, 8, 9a	5,200,000	0	5,200,000
Steel	1, 2, 3.1, 4, 5, 12, 13, 16, 17, 18, 25	6,900,000	32	4,550,000
Carbonates (calcite + siderite)	2, 6, 7, 8, 9a	3,700,000	0	3,700,000
Organic materials (incl. organic carbon and hydrocarbons)	2, 3.1, 5, 6, 7, 8, 9a, 14B, 15.2., 21, 23, 24, 26, 28, 29	13,000,000	87	1,614,000
Cement	2, 3.1, 5, 12, 13, 14B, 15.2, 16, 17	16,000,000	91	1,300,000
Pyrite	2, 6, 7, 8, 9a	520,000	0	520,000
Silica (SiO2)	2, 3.1, 5, 14B, 15.2	2,400,000	90	630,000
Carbamide	27	1,100,000	95	55,000
Rubber	19	160,000	90	16,000
Nitrogen oxides (NOx)	10, 20	1,400,000	99	14,000
Soot and ash	20	82,000	93	5,800
Zinc	12, 17	11,000	61	4,300
Aluminium	11, 14B, 17	120,000	97	3,000
Nitrate	15.2	900	20	700
Chloride	2, 3.1, 5, 14B, 15.2	900	43	500
Sulphuric acid	22	3,200	90	300
Iron (Fe(III))	14A	3,600	95	180
Plastic	11	1,800	90	180
Polyethylene (PE)	18	4,000	95	180
Polystyrene (EPS)	18	1,400	95	70
Tungsten and cobalt	25	2,800	99	30

Table 10-10. Estimated total quantities of chemical components from residual materials in a KBS-3H repository (including ONKALO), based on design alternatives BD and B3a (= support alternative B, grouting alternative 3, backfill alternative a) with a LHHP plug (Table 10 in /Hagros 2007a/).

Chemical components	Origin (reference to Table 10-2	Total introduced quantity [kg]	Removal efficiency [%]	Remaining quantity [kg]
Gypsum	2, 6, 7, 8, 9a	5,200,000	0	5,200,000
Steel	1, 2, 3.1, 4, 5, 12, 13, 16, 17, 18, 25	6,900,000	32	4,550,000
Carbonates (calcite + siderite)	2, 6, 7, 8, 9a	3,700,000	0	3,700,000
Organic materials (incl. organic carbon and hydrocarbons)	2, 3.1, 5, 6, 7, 8, 9a, 14B, 15.3., 21, 23, 24, 26, 28, 29	13,000,000	87	1,614,000
Cement	2, 3.1, 5, 12, 13, 14B, 15.3, 16, 17	16,000,000	91	1,200,000
Pyrite	2, 6, 7, 8, 9a	520,000	0	520,000
Silica (SiO2)	2, 3.1, 5, 14B, 15.3	2,500,000	87	710,000
Carbamide	27	1,100,000	95	55,000
Rubber	19	160,000	90	16,000
Nitrogen oxides (NOx)	10, 20	1,400,000	99	14,000
Soot and ash	20	82,000	93	5,800
Zinc	12, 17	11,000	61	4,300
Aluminium	11, 14B, 17	120,000	97	3,000
Nitrate	15.3	800	20	600
Chloride	2, 3.1, 5, 14B, 15.3	6,000	23	4,600
Sulphuric acid	22	3,200	90	300
Iron (Fe(III))	14A	3,600	95	180
Plastic	11	1,800	90	180
Polyethylene (PE)	18	4,000	95	180
Polystyrene (EPS)	18	1,400	95	70
Tungsten and cobalt	25	2,800	99	30

10.1.3 Total quantities in the DAWE design alternative

The total quantities of chemical components are presented in Tables 10-11 – 10-13 for the DAWE design alternative for two combinations of tunnel support, grouting, backfill and drift end plug alternatives. Low-pH grouting materials and support materials are the recommended materials for the deposition drift. For comparison, also combinations of other materials have been presented.

- Table 10-11 is similar to Table 10-4 in Section 10.1.2 except that DAWE is assumed instead of BD. The design alternative is A1a (ordinary cement in shotcreting and grouting and a bentonite/crushed rock backfill) and an LHHP plug is assumed to be used.

- In Table 10-12, low-pH cement is assumed to be used in both shotcreting and grouting (shotcreting alternative B and grouting alternative 2). The backfill plan is based on bentonite/ crushed rock mixture (backfill alternative a) and the drift end plug is of the rock cylinder type. It is otherwise similar to Table 10-7 in Section 10.1.2 except that DAWE is assumed instead of BD.

- In Table 10-13, low-pH cement is assumed to be used in both shotcreting and grouting (shotcreting alternative B and grouting alternative 2). The backfill plan is based on bentonite/ crushed rock mixture (backfill alternative a) and an LHHP plug is assumed to be used. It is otherwise similar to Table 10-9 in Section 10.1.2 except that DAWE is assumed instead of BD.

By using Table 10-3, it is possible to calculate the total material quantities for any combination of alternatives. Only three combinations are presented here for the DAWE alternative, but the total number of possible combinations is 24.

Table 10-11. Estimated total quantities of chemical components from residual materials in a KBS-3H repository (including ONKALO), based on design alternatives DAWE and A1a (= support alternative A, grouting alternative 1, backfill alternative a) with a LHHP plug (Table 11 in /Hagros 2007a/).

Chemical components	Origin (reference to Table 10-3)	Total introduced quantity [kg]	Removal efficiency [%]	Remaining quantity [kg]
Gypsum	2, 6, 7, 8, 9a	5,200,000	0	5,200,000
Steel	1, 2, 3.1, 4, 5, 7, 12, 13, 16, 17, 18, 25	6,700,000	33	4,500,000
Carbonates (calcite + siderite)	2, 6, 7, 8, 9a	3,700,000	0	3,700,000
Organic materials (incl. organic carbon and hydrocarbons)	2, 3.1, 6, 7, 8, 9a, 14A, 15.1, 21, 23, 24, 26, 28, 29	13,000,000	87	1,700,000
Cement	2, 3.1, 12, 13, 14A, 15.1, 16, 17	18,000,000	91	1,500,000
Pyrite	2, 6, 7, 8, 9a	520,000	0	520,000
Silica (SiO2)	2, 3.1, 14A, 15.1	760,000	37	480,000
Carbamide	27	1,100,000	95	55,000
Rubber	19	160,000	90	16,000
Nitrogen oxides (NOx)	10, 20	1,400,000	99	14,000
Soot and ash	20	82,000	93	5,800
Zinc	12, 17	11,000	61	4,300
Aluminium	11, 14A, 17	120,000	97	3,200
Nitrate	15.1	1,000	20	800
Chloride	2, 3.1, 14A, 15.1	1,100	43	600
Sulphuric acid	22	3,200	90	300
Iron (Fe(III))	14A	4,900	95	200
Plastic	11	1,800	90	180
Polyethylene (PE)	18	3,500	95	180
Polystyrene (EPS)	18	1,400	95	70
Tungsten and cobalt	25	2,800	99	30

Table 10-12. Estimated total quantities of chemical components from residual materials in a KBS-3H repository (including ONKALO), based on design alternatives DAWE and B2a (= support alternative B, grouting alternative 2, backfill alternative a) with a rock cylinder plug (Table 12 in /Hagros 2007a/).

Chemical components	Origin (reference to Table 10-3)	Total introduced quantity [kg]	Removal efficiency [%]	Remaining quantity [kg]
Gypsum	2, 6, 7, 8, 9a	5,200,000	0	5,200,000
Steel	1, 2, 3.2, 4, 5, 7, 12, 13, 16, 17, 18, 25	6,500,000	34	4,300,000
Carbonates (calcite + siderite)	2, 6, 7, 8, 9a	3,700,000	0	3,700,000
Organic materials (incl. organic carbon and hydrocarbons)	2, 3.2, 6, 7, 8, 9a, 14B, 15.2, 21, 23, 24, 26, 28, 29	13,000,000	87	1,600,000
Cement	2, 3.2, 12, 13, 14B, 15.2, 16, 17	16,000,000	91	1,500,000
Pyrite	2, 6, 7, 8, 9a	520,000	0	520,000
Silica (SiO2)	2, 3.2, 14B, 15.2	2,400,000	90	250,000
Carbamide	27	1,100,000	95	55,000
Rubber	19	160,000	90	16,000
Nitrogen oxides (NOx)	10, 20	1,400,000	99	14,000
Soot and ash	20	82,000	93	5,800
Zinc	12, 17	11,000	61	4,300
Aluminium	11, 14A, 17	120,000	97	3,000
Nitrate	15.2	900	20	700
Chloride	2, 3.2, 14B, 15.2	900	43	500
Sulphuric acid	22	3,200	90	300
Iron (Fe(III))	14B	3,600	95	180
Plastic	11	1,800	90	180
Polyethylene (PE)	18	3,500	95	180
Polystyrene (EPS)	18	1,400	95	70
Tungsten and cobalt	25	2,800	99	30

Table 10-13. Estimated total quantities of chemical components from residual materials in a KBS-3H repository (including ONKALO), based on design alternatives DAWE and B2a (= support alternative B, grouting alternative 2, backfill alternative a) with a LHHP plug (Table 13 in /Hagros 2007a/).

Chemical components	Origin (reference to Table 10-3)	Total introduced quantity [kg]	Removal efficiency [%]	Remaining quantity [kg]
Gypsum	2, 6, 7, 8, 9a	5,200,000	0	5,200,000
Steel	1, 2, 3.1, 4, 5, 7, 12, 13, 16, 17, 18, 25	6,500,000	34	4,150,000
Carbonates (calcite + siderite)	2, 6, 7, 8, 9a	3,700,000	0	3,700,000
Organic materials (incl. organic carbon and hydrocarbons)	2, 3.1, 6, 7, 8, 9a, 14B, 15.2, 21, 23, 24, 26, 28, 29	13,000,000	87	1,614,000
Cement	2, 3.1, 12, 13, 14B, 15.2, 16, 17	16,000,000	91	1,300,000
Pyrite	2, 6, 7, 8, 9a	520,000	0	520,000
Silica (SiO2)	2, 3.1, 14B, 15.2	2,400,000	90	630,000
Carbamide	27	1,100,000	95	55,000
Rubber	19	160,000	90	16,000
Nitrogen oxides (NOx)	10, 20	1,400,000	99	14,000
Soot and ash	20	82,000	93	5,800
Zinc	12, 17	11,000	61	4,300
Aluminium	11, 14A, 17	120,000	97	3,000
Nitrate	15.2	900	20	700
Chloride	2, 3.1, 14B, 15.2	900	43	500
Sulphuric acid	22	3,200	90	300
Iron (Fe(III))	14B	3,600	95	180
Plastic	11	1,800	90	180
Polyethylene (PE)	18	3,500	95	180
Polystyrene (EPS)	18	1,400	95	70
Tungsten and cobalt	25	2,800	99	30

10.2 Results for the canister near-field

10.2.1 Results for the BD design alternative

Estimates for quantities of residual materials in a single deposition drift of BD type are presented in Table 10-14 and Table 10-15. The analysed deposition drift in Table 10-16 is based on design alternative B2a, i.e., it incorporates low-pH cement for both shotcreting and grouting purposes and a bentonite/crushed rock mixture as a backfill alternative. A rock cylinder type drift end plug is assumed as well. The analysed deposition drift in Table 10-15 is otherwise similar to Table 10-14 except that the end plug is a LHHP plug.

Table 10-16 presents similar estimates for one deposition location, i.e. an 11 m section of the identical drift.

Table 10-14. Estimated total quantities of residual materials in one 300 m long deposition drift, based on design alternatives BD and B2a (= support alternative B, grouting alternative 2, backfill alternative a) with a rock cylinder plug (Table 14 in /Hagros 2007a/).

Chemical components	Origin (reference to Table 10-2)	Total introduced quantity [kg]	Removal efficiency [%]	Remaining quantity [kg]
Gypsum	2, 6, 7, 8, 9a	10,000	0	10,000
Steel	1, 2, 3.2, 4, 5, 12, 13, 16, 17, 18, 25	31,000	9	28,000
Carbonates (calcite + siderite)	2, 6, 7, 8, 9a	7,500	0	7,500
Organic materials (incl. organic carbon and hydrocarbons)	2, 3.2, 5, 6, 7, 8, 9a, 14B, 15.2, 21, 23, 24, 26, 28, 29	5,000	40	3,000
Cement	2, 3.2, 5, 12, 13, 14B, 15.2, 16, 17	15,000	74	3,800
Pyrite	2, 6, 7, 8, 9a	1,000	0	1,000
Silica (SiO2)	2, 3.2, 5, 14B, 15.2	5,500	88	700
Carbamide	27	200	95	10
Rubber	19	6	90	0.6
Nitrogen oxides (NOx)	10, 20	30	99	0.3
Soot and ash	20	2	93	0.1
Zinc	12, 17	5	0	5
Aluminium	11, 14B, 17	20	95	1
Chloride	2, 3.2, 5, 14B, 15.2	0.8	49	0.4
Sulphuric acid	22	0.1	90	0.01
Iron (Fe(III))	14A	5	95	0.2
Plastic	11	1	90	0.1
Polyethylene (PE)	18	3	95	0.1
Polystyrene (EPS)	18	1	95	0.05
Tungsten and cobalt	25	4	99	0.04

Table 10-15. Estimated total quantities of residual materials in one 300 m long deposition drift, based on design alternatives BD and B2a (= support alternative B, grouting alternative 2, backfill alternative a) with a LHHP plug (Table 15 in /Hagros 2007a/).

Chemical components	Origin (reference to Table 10-2)	Total introduced quantity [kg]	Removal efficiency [%]	Remaining quantity [kg]
Gypsum	2, 6, 7, 8, 9a	10,000	0	10,000
Steel	1, 2, 3.1, 4, 5, 12, 13, 16, 17, 18, 25	31,000	9	28,860
Carbonates (calcite + siderite)	2, 6, 7, 8, 9a	7,500	0	7,500
Organic materials (incl. organic carbon and hydrocarbons)	2, 3.1, 5, 6, 7, 8, 9a, 14B, 15.2, 21, 23, 24, 26, 28, 29	5,000	40	3,080
Cement	2, 3.1, 5, 12, 13, 14B, 15.2, 16, 17	15,000	74	2,680
Pyrite	2, 6, 7, 8, 9a	1,000	0	1,000
Silica (SiO2)	2, 3.2, 5, 14B, 15.2	5,500	88	2,880
Carbamide	27	200	95	10
Rubber	19	6	90	0.6
Nitrogen oxides (NOx)	10, 20	30	99	0.3
Soot and ash	20	2	93	0.1
Zinc	12, 17	5	0	5
Aluminium	11, 14B, 17	20	95	1
Chloride	2, 3.1, 5, 14B, 15.2	0.8	49	0.4
Sulphuric acid	22	0.1	90	0.01
Iron (Fe(III))	14A	5	95	0.2
Plastic	11	1	90	0.1
Polyethylene (PE)	18	3	95	0.1
Polystyrene (EPS)	18	1	95	0.05
Tungsten and cobalt	25	4	99	0.04

Table 10-16. Estimated total quantities of residual materials in one deposition location (an 11 m section of a deposition drift), based on design alternative BD and grouting alternative 2 (Table 16 in /Hagros 2007a/).

Chemical components	Origin (reference to Table 10-2)	Total introduced quantity [kg]	Removal efficiency [%]	Remaining quantity [kg]
Gypsum	6, 7	300	0	300
Steel	1	1,100	0	1,100
Carbonates (calcite + siderite)	6, 7	200	0	200
Organic materials (incl. organic carbon and hydrocarbons)	6, 7, 15.2, 26, 28, 29	100	31	80
Cement	15.2	0.7	20	0.6
Pyrite	6, 7	30	0	30
Silica (SiO2)	15.2	11	20	9
Carbamide	27	3	95	0.1
Chloride	15.2	0.02	20	0.01

The deposition drift of interest in Tables 10-14 and 10-15 is 300 m long and intended for OL1-2 canisters. The quantities of materials per excavated cubic metre (or per metre of tunnel) are considered to be average values for all deposition drifts. It was assumed here that the drift contains 18 canisters, i.e. 18 supercontainers and 18 distance blocks, as well as one compartment plug and blank zones (filled with bentonite) totaling 47 m in length. The deposition niche is also included.

The 11 m long deposition location considered in Table 10-16 includes one supercontainer (with an OL1/OL2 canister) and one distance block. Materials related to the drift end plug, the compartment plug and the blank zones are not taken into account.

Although design alternative B2a includes shotcrete alternative B, any associated materials have no effect on the results shown in Tables 10-14 and 10-15, as shotcrete will not be used in the small-diameter sections of the deposition drifts. Similarly, the backfill alternative has no effect on the displayed results either.

10.2.2 Results for the DAWE design alternative

Tables 10-17, 10-18 and 10-19 present results similar to those in Tables 10-14 – 10-16 with the exception that the DAWE design alternative is considered instead of the BD alternative. The discussion regarding the deposition drift and drift section found in the previous Section 10.2.1 is relevant here as well.

Table 10-17. Estimated total quantities of residual materials in one 300 m long deposition drift, based on design alternatives DAWE and B2a (= support alternative B, grouting alternative 2, backfill alternative a) with a rock cylinder plug (Table 17 in /Hagros 2007a/).

Chemical components	Origin (reference to Table 10-3)	Total introduced quantity [kg]	Removal efficiency [%]	Remaining quantity [kg]
Gypsum	2, 6, 7, 8, 9a	10,000	0	10,000
Steel	1, 2, 3.2, 4, 5, 7, 12, 13, 16, 17, 18, 25	28,000	9	26,000
Carbonates (calcite + siderite)	2, 6, 7, 8, 9a	7,400	0	7,400
Organic materials (incl. organic carbon and hydrocarbons)	2, 3.2, 6, 7, 8, 9a, 14B, 15.2, 21, 23, 24, 26, 28, 29	5,000	40	3,000
Cement	2, 3.2, 12, 13, 14B, 15.2, 16, 17	14,000	74	3,700
Pyrite	2, 6, 7, 8, 9a	1,000	0	1,000
Silica (SiO2)	2, 3.2, 14B, 15.2	5,500	88	700
Carbamide	27	200	95	10
Rubber	19	6	90	0.6
Nitrogen oxides (NOx)	10, 20	30	99	0.3
Soot and ash	20	2	93	0.1
Zinc	12, 17	5	0	5
Aluminium	11, 14B, 17	20	95	1
Chloride	2, 3.2, 14B, 15.2	0.8	49	0.40
Sulphuric acid	22	0.1	90	0.01
Iron (Fe(III))	14A	5	95	0.2
Plastic	11	1	90	0.1
Polyethylene (PE)	18	3	95	0.1
Polystyrene (EPS)	18	1	95	0.05
Tungsten and cobalt	25	4	99	0.04

Table 10-18. Estimated total quantities of residual materials in one 300 m long deposition drift, based on design alternatives DAWE and B2a (= support alternative B, grouting alternative 2, backfill alternative a) with a LHHP plug (Table 18 in /Hagros 2007a/).

Chemical components	Origin (reference to Table 10-3)	Total introduced quantity [kg]	Removal efficiency [%]	Remaining quantity [kg]
Gypsum	2, 6, 7, 8, 9a	10,000	0	10,000
Steel	1, 2, 3.1, 4, 5, 7, 12, 13, 16, 17, 18, 25	28,000	9	26,860
Carbonates (calcite + siderite)	2, 6, 7, 8, 9a	7,400	0	7,400
Organic materials (incl. organic carbon and hydrocarbons)	2, 3.1, 6, 7, 8, 9a, 14B, 15.2, 21, 23, 24, 26, 28, 29	5,000	40	3,080
Cement	2, 3.2, 12, 13, 14B, 15.2, 16, 17	14,000	74	2,580
Pyrite	2, 6, 7, 8, 9a	1,000	0	1,000
Silica (SiO2)	2, 3.2, 14B, 15.2	5,500	88	2,880
Carbamide	27	200	95	10
Rubber	19	6	90	0.6
Nitrogen oxides (NOx)	10, 20	30	99	0.3
Soot and ash	20	2	93	0.1
Zinc	12, 17	5	0	5
Aluminium	11, 14B, 17	20	95	1
Chloride	2, 3.2, 14B, 15.2	0.8	49	0.4
Sulphuric acid	22	0.1	90	0.01
Iron (Fe(III))	14A	5	95	0.2
Plastic	11	1	90	0.1
Polyethylene (PE)	18	3	95	0.1
Polystyrene (EPS)	18	1	95	0.05
Tungsten and cobalt	25	4	99	0.04

Table 10-19. Estimated total quantities of residual materials in one deposition location (an 11 m section of a deposition drift), based on design alternative DAWE and grouting alternative 2 (Table 19 in /Hagros 2007a/).

Chemical components	Origin (reference to Table 10-3)	Total introduced quantity [kg]	Removal efficiency [%]	Remaining quantity [kg]
Gypsum	6, 7	300	0	300
Steel	1, 7	1,100	0	1,100
Carbonates (calcite + siderite)	6, 7	190	0	190
Organic materials (incl. organic carbon and hydrocarbons)	6, 7, 15.2, 26, 28, 29	110	32	80
Cement	15.2	0.7	20	0.6
Pyrite	6, 7	30	0	30
Silica (SiO2)	15.2	11	20	9
Carbamide	27	3	95	0.1
Chloride	15.2	0.02	20	0.01

10.3   Differences between BD and DAWE

The selected KBS-3H design alternative – either Basic Design or DAWE design – may affect the quantities of several materials and such differences can be discerned by comparing, e.g. Tables 10-4 and 10-11. Such differences must be related to the materials in distance blocks, fixing rings or the DAWE pipe system, as all other components are assumed to be identical for both design alternatives.

A comparison between the rounded-off values shown in Tables 10-4 and 10-11 indicates that the main difference between the BD and DAWE design alternatives is related to the quantity of steel, the remaining quantity of which is slightly smaller in DAWE than in BD, the difference being less than 10%. This difference is mainly ascribed to the lack of fixing rings in the DAWE alternative. As the DAWE drainage, watering and air evacuation systems can be essentially removed, they will have negligible effect on the remaining quantity of steel in the repository. The effect of the steel feet in the DAWE distance blocks is also minor and the smaller size of the DAWE distance blocks has a negligible effect on the total quantities of the bentonite impurities as well.

10.4   Comparison with a KBS-3V repository

Both disposal design alternatives – KBS-3H and KBS-3V – include components and materials that are not included in the other alternative. The KBS-3H repository assumed in this work includes the following components and materials that are not present in a KBS-3V repository:

• steel cylinders in the supercontainers,

• compartment plugs,

• spray and drip shields,

• fixing rings (BD only),

• drainage, watering and air evacuation systems (DAWE only),

• distance blocks,

• bentonite blocks in blank zones.

The KBS-3V repository assumed by /Hagros 2007b/ includes the following components and materials that are not present in a KBS-3H repository:

• concrete bottom plates in the deposition holes,

• steel mesh in the deposition tunnels.

In addition, the composition of the drift end plugs (KBS-3H) and concrete plugs (KBS-3V) are different in the two design alternatives. Also, the quantity of bentonite in the KBS-3H supercontainers is 37% smaller than the quantity of the bentonite buffer in KBS-3V. Furthermore, the quantities of several other materials in the deposition drifts are smaller in KBS-3H due to the fact that the small-diameter parts of the deposition drifts are not excavated by drill and blast, they do not have any rock support or conventional installations, they probably require less grouting due to smaller cross-sectional area and they do not have any tunnel backfill material.

Table 10-20 shows a comparison between the remaining quantities of all residual materials considered in this work and in the KBS-3V report by /Hagros 2007b/. The table assumes the B2a design alternative (shotcreting and grouting mainly with low-pH cement, bentonite/crushed rock mixture as tunnel backfill) in both alternatives and the BD design alternative with a rock plug with respect to the KBS-3H specific options. Most of the total material quantities are nearly the same (± 5%) or smaller in KBS-3H, the difference being typically –20%, at most –100% (with respect to copper, which is present in the KBS-3V concrete plugs). The following materials have, however, more than 5% larger remaining quantity in KBS-3H than in KBS-3V:

- steel: some 210% larger quantity in KBS-3H than in KBS-3V, mainly due to the steel cylinders in supercontainers but also due to comaprtment plugs and fixing rings,

- iron (Fe(III)): some 30 % larger quantity in KBS-3H, due to higher consumption of shotcrete as the total central tunnel length is larger in KBS-3H and also the deposition niches are assumed to have shotcrete,

- polyethylene and polystyrene: some 20% larger quantity in KBS-3H, due to the higher consumption of drainage pipes related to shotcrete,

- nitrogen oxides, rubber and soot and ash: slightly larger quantity in KBS-3H, due to larger total length of central tunnels.

Table 10-20. Estimated remaining quantities of chemical components, included in the residual materials, in a KBS-3H and KBS-3V repository (based on /Hagros 2007b/). The design alternative is B2a (= support alternative B, grouting alternative 2, backfill alternative a) in both repository alternatives. The KBS-3H repository is based on the design alternative BD with a rock cylinder plug (Table 20 in /Hagros 2007a/).

Chemical components KBS-3H [kg]	Remaining quantity in KBS-3V [kg]	Remaining quantity in KBS-3V [kg]	Relative difference (KBS-3H compared with KBS-3V)
Gypsum	5,200,000	6,500,000	–19%
Steel	4,700,000	1,500,000	+210%
Carbonates (calcite + siderite)	3,700,000	4,600,000	–19%
Organic materials (incl. organic carbon and hydrocarbons)	1,600,000	2,000,000	–19%
Cement	1,500,000	5,800,000	–74%
Pyrite	520,000	650,000	–19%
Silica (SiO2)	250,000	270,000	–7%
Carbamide	55,000	55,000	0%
Rubber	16,000	15,000	+6%
Nitrogen oxides (NOx)	14,000	13,000	+7%
Soot and ash	5,800	5,400	+7%
Zinc	4,300	140,000	–97%
Aluminium	3,000	2,800	+4%
Nitrate	700	700	+2%
Chloride	500	500	0%
Sulphuric acid	300	300	+6%
Iron (Fe(III))	180	140	+33%
Plastic	180	300	–31%
Polyethylene (PE)	180	140	+23%
Polystyrene (EPS)	70	60	+23%
Tungsten and cobalt	30	40	–25%
Copper	0	12,000	–100%

In all, it can be concluded that the KBS-3H disposal alternative is a better alternative if the total quantities of the remaining materials need to be minimised. The total quantity of all materials listed in Table 10-20 is some 20% smaller in KBS-3H than in KBS-3V. The smaller quantities in KBS-3H are mainly due to the fact that the deposition drifts are much smaller than the KBS-3V deposition tunnels and they are not constructed and furnished in the same way as the KBS-3V deposition tunnels. In particular, the lack of KBS-3V type concrete plugs causes a major reduction in the total quantity of cement in a KBS-3H repository. The KBS-3H drift end plugs contain a significantly smaller quantity of cement than the KBS-3V concrete plugs. This applies to both the rock cylinder plug and the LHHP plug. If cement is not taken into account, the total quantity of materials listed in Table 10-20 is nearly the same for both alternatives.

A significant uncertainty as to the total quantities is caused by the unknown composition of some materials and the possible changes of design, as the KBS-3H design is being further developed and a new design will be published in the near future. The exact composition of any material is not yet completely defined (e.g., the bolt types and grouting recipes may change in the future, and steel may be partly replaced by titanium, nickel or copper), but the largest uncertainties are associated with the following materials:

- There appears to be a great uncertainty regarding the composition of MX-80 bentonite, which is probably due to the fact that the bentonite is not completely homogeneous. Also it is by no means certain that the bentonite to be used in the repository will be of the MX-80 type.

- The crushed rock used in the tunnel backfill material is not assumed to include any significant impurities (residual materials), but this is probably far from the truth. It was not possible to consider such impurities in this work, because it is not known, whether the crushed rock to be used as tunnel backfill is originated from the construction of the repository or from some other source and because factors such as the average time of storage (which affects the accumulation of organic and air-borne impurities) and the cleaning process were also unknown.

- The various KBS-3H specific components such as drift end plugs and distance blocks are still being designed and their composition may be different from that presented in this report. The results concerning especially the BD alternative may include significant uncertainties and should be regarded merely as indicative.

- There is also still a great uncertainty with respect to the removal efficiency of many of the residual materials of importance for long-term safety, such as organic compounds and the soluble nitrogen compounds from the explosives used.

11   Summary and conclusions

Two different alternative KBS-3H designs, BD and DAWE have been presented based on present understanding. Both alternatives have still uncertainties and the design developments to resolve these are in progress. Therefore it is likely that there will be more advanced design available later.

The report has not covered all issues and design aspects consistently, but merely presents the status of development and improvements occurred after the reporting of the previous design phase made in 2005 /Autio 2007/ and presents the preliminary design to be used in the KBS-3H safety assessment. Therefore information on several issues such as e.g. operation timetables and deviations can be found in /Autio 2007/.

In the BD alternative the distance block is the design component, which is associated with significant uncertainties with respect to buffer behaviour, design requirements and design basis. The most important buffer related uncertainties are: 1) Humidity induced swelling, 2) Erosion of filling blocks and buffer, 3) Artificial watering of distance blocks, 4) Piping through distance blocks and 5) Hydraulic pressure on distance block end surface. The most important uncertainties in DAWE alternative are related to evolution of buffer after watering, especially swelling characteristic, humidity induced cracking and erosion. These uncertainties have significant impact on the final selection of the distance block alternative, which may differ from the one reference design presented in this document, and affect the inflow criteria for positioning the buffer and filling components. These uncertainties therefore have an impact also on the quantities of residual materials in drift and rock, as well as on the lay-out adaptation.

Groundwater inflows reduce the utilization degree of KBS-3H deposition drifts (number of canisters that can be emplaced in one drift), e.g. by increasing the number of compartment plugs and filling components and impair conditions during operation. A new groundwater control strategy based on post-grouting by using a Mega-Packer device is presented and may improve the utilization degree significantly, however it is still under development and there are several uncertainties related to the sealing efficiency to be solved by full-scale testing.

Some of the design components such as steel compartment plugs and fixing rings are novel and developed only for KBS-3H alternative. Therefore these need to be tested to prove the viability of designs and identify the need for possible further development.

It should be noted that although BD and DAWE alternatives have been presented as two different preliminary design alternatives, it is likely that these can be used in combination, so that BD could be used in drifts with low inflows and DAWE is drifts with more inflows. However further design development is evaluate to define the effect of different inflow parameters on function of buffer components.

References

Ahokas H, Vaittinen T, 2007. Modelling of hydro-zones for the layout planning and numerical flow model 2006. Working Report 2007-01. Posiva Oy, Olkiluoto, Finland.

Andersson C, Eng A, 2005. Äspö Pillar Stability Experiment. Final experimental design, monitoring results and observations. SKB R-05-02, Svensk Kärnbränslehantering AB, Sweden.

Autio J, 2007. KBS-3H Design Description 2005. Working Report 2007-11 and SKB R-08-29. Posiva Oy, Olkiluoto, Finland and Svensk Kärnbränslehantering AB, Sweden.

Barton N, Quadros E F, 1997. Joint Aperture and Roughness in the Prediction of Flow and Groutability of Rock Masses. Int. J. Rock Mech, and Min. Sci. 34:3–4, Paper No 252.

Börgesson L, Pusch R, Fredrikson A, Hökmark H, Karnland O, Sandén T, 1991. Final report of the rock sealing project – Sealing of the near-field rock around deposition holes by use of bentonite grouts. Stripa Project 91-34. Svensk Kärnbränslehantering AB, Sweden.

Börgesson L, Sandén T, Fälth B, Åkesson M, Lindgren E, 2005. Studies of buffer behaviour in KBS-3H concept. Work during 2002–2004. SKB R-05-50. Svensk Kärnbränslehantering AB, Sweden.

Eriksson M, 2002. Prediction of grout spread and sealing effect – A probabilistic approach. Ph D Thesis. Division of Soil and Rock Mechanics, Royal Institute of Technology, Stockholm.

Eriksson M, 2005. KBS-3H Study of post grouting using Large borehole Injection Device – a theoretical evaluation and design specification. TU-05-06. Svensk Kärnbränslehantering AB, Sweden.

Gribi P, Johnson L, Suter D, Smith P, Pastina B, Snellman M, 2007. Safety assessment for a KBS-3H spent nuclear fuel repository at Olkiluoto - Process Report. Posiva 2007-09 and SKB R-08-36. Posiva Oy, Olkiluoto, Finland and Svensk Kärnbränslehantering AB, Sweden.

Gustafson G, Stille H, 2005. Stop criteria for cement grouting. Felsbau, Vol. 23, No. 3 pp. 62–68.

Hagros A, 2007a. Estimated quantities of residual materials in a KBS-3H repository at Olkiluoto. Posiva Working Report 2007-104 and SKB R-08-33. Posiva Oy, Olkiluoto, Finland and Svensk Kärnbränslehantering AB, Sweden.

Hagros A, 2007b. Foreign materials in the repository − Update of estimated quantities. Working Report 2007-17. Posiva Oy, Olkiluoto, Finland.

Hellä P, Ahokas H, Palmén J, Tammisto E, 2006. Analysis of geohydrological data for design of KBS-3H repository layout. Posiva Working Report 2006-16 and SKB R-08-27. Posiva Oy, Olkiluoto, Finland and Svensk Kärnbränslehantering AB, Sweden.

Hjerpe T, 2004. Engineering and stray materials in the repository for nuclear waste: Estimation of quantities after backfilling. Working Report 2003-72. Posiva Oy, Olkiluoto, Finland.

Hökmark H, Fälth B, 2003. Thermal dimensioning of the deep repository. Influence of canister spacing, canister power, rock thermal properties and near field design on the maximum canister surface temperature. Technical SKB TR-03-09. Svensk Kärnbränslehantering AB, Sweden.

Hökmark H, Fälth B, Wallroth T, 2006. T-H-M couplings in rock. Overview of results of importance to the SR-Can safety assessment. SKB R-06-88. Svensk Kärnbränslehantering AB, Sweden.

Ikonen K, 2003a. Thermal analyses of spent nuclear fuel repository. Posiva 2003-04. Posiva Oy, Olkiluoto, Finland.

Ikonen K, 2003b. Thermal analyses of KBS-3H type repository. Posiva 2003-11, Posiva Oy, Olkiluoto, Finland.

Johansson E, Äikäs K, Autio J, Hagros A, Malmlund H, Rautakorpi J, Sievänen U, Wanne T, Anttila P, Raiko H, 2002. Preliminary KBS-3H layout adaptation for the Olkiluoto site: Analysis of rock factors affecting the orientation of a KBS-3H deposition hole. Working Report 2002-57. Posiva Oy, Olkiluoto, Finland.

Johansson E, Hagros A, Autio J, Kirkkomäki T, 2007. KBS-3H layout adaptation 2007 for the Olkiluoto site. Posiva Working Report 2007-77 and SKB R-08-31. Posiva Oy, Olkiluoto, Finland and Svensk Kärnbränslehantering AB, Sweden.

Kirkkomäki T, 2006. Design and stepwise implementation of the final repository. Working Report 2006-92. Posiva Oy, Olkiluoto, Finland (in Finnish with an English summary).

Lanyon GW, Marschall P, 2006. Discrete fracture network modelling of a KBS-3H repository at Olkiluoto. POSIVA 2006-06 and SKB R-08-26. Posiva Oy, Olkiluoto, Finland and Svensk Kärnbränslehantering AB, Sweden.

Lönnqvist M, Hökmark H, 2007. Thermo-mechanical analyses of a KBS-3H deposition drift at Olkiluoto site. Posiva Working Report 2007-66 and SKB R-08-30. Posiva Oy, Olkiluoto, Finland and Svensk Kärnbränslehantering AB, Sweden.

Malmlund H, Johansson E, 2002. Rock stress measurements at Posiva sites. Working Report 2002-47. Posiva Oy, Olkiluoto, Finland.

Malmlund H, Äikäs K, Hagros A, 2004. Layout adaptation examples for a KBS-3V repository at Olkiluoto. Working Repot 2003-68. Posiva Oy, Olkiluoto, Finland.

Martin D, 2005. Preliminary assessment of potential underground stability (wedge and spalling) at Forsmark, Simpevarp and Laxemar sites. SKB R-05-71. Svensk Kärnbränslehantering AB, Sweden.

Martino J B, Chandler N A, Read R S, Baker C, 2002. Response of the tunnel sealing experiment concrete bulkhead to pressurization. Report No: 06819-REP-01200-10085-R00. Ontario Power Generation, Toronto, Canada.

Nydahl L E, 2008. KBS-3H Betongpluggar för drifttätning av horisontella deponeringshål – Utredning av olika alternativ. SKB R-08-41 (in preparation). Svensk Kärnbränslehantering AB, Sweden.

Pastina B, Hellä P, 2006. Expected evolution of a spent fuel repository at Olkiluoto. Posiva 2006-05. Posiva Oy, Olkiluoto, Finland.

Paulamäki S, Paananen M, Gehör S, Kärki A, Front K, Aaltonen I, Ahokas T, Kemppainen K, Mattila J, Wikström L, 2006. Geological model of the Olkiluoto site area: Version 0. Working Report 2006-37. Posiva Oy, Olkiluoto, Finland.

Posiva Oy, 2005. Olkiluoto Site Description 2004. Posiva 2005-03. Posiva Oy, Olkiluoto, Finland.

Posiva Oy, 2006a. Olkiluoto Site Description 2006. Posiva 2007-03. Posiva Oy, Olkiluoto, Finland.

Posiva Oy, 2006b. TKS-2006. Nuclear Waste Management of the Olkiluoto and Loviisa Power Plants: programme for Research, Development and Technical Design for 2007–2009. Posiva Oy, Olkiluoto, Finland.

Rhén I, Gustafson G, Stanfors R, Wikberg P, 1997. Äspö HRL – Geoscientific evaluation 1997/5. Models based on site characterization 1986–1995. Technical SKB TR-97-06. SSvensk Kärnbränslehantering AB, Sweden.

SKB, 2001. Forsknings-, utvecklings- och demonstrationsprogram för ett KBS-3-förvar med horisontell deponering. SKB R-01-55. Svensk Kärnbränslehantering AB, Sweden.

SKB, 2006. Long-term safety for KBS-3 repositories at Forsmark and Laxemar – a first evaluation – Main report of the SR-Can project. Technical SKB TR-06-09. Svensk Kärnbränslehantering AB, Sweden.

Smith P A, Johnson LH, Snellman M, Pastina B, Gribi P, 2007. Safety assessment for a KBS-3H spent nuclear fuel repository at Olkiluoto - Evolution report. Posiva 2007-08 and SKB R-08-37. Posiva Oy, Olkiluoto, Svensk Kärnbränslehantering AB, Sweden.

Thorsager P, Lindgren E, 2004. Summary report of work done during Basic Design. SKB R-04-42. Svensk Kärnbränslehantering AB, Sweden.

Vaittinen T, Ahokas H, Heikkinen E, Hellä P, Nummela J, Saksa P, Tammisto E, Paulamäki S, Paananen M, Front K, Kärki K, 2003. Bedrock model of the Olkiluoto site, version 2003/1. Working Report 2003-43. Posiva Oy, Olkiluoto, Finland.

Zimmerman R W, Kumar S, Bodvarsson G S, 1991. Lubrication Theory Analyses of the Permeability of Rough-walled Fractures, Int. J. Rock Mech, and Min. Sci. and Geomech Abstr. Vol. 28, No. 4, pp 325–331.

Long-term safety requirements for KBS-3H system components

A.1 Safety functions in the KBS-3H design alternative

The canister, the buffer (i.e. the bentonite material originally inside the supercontainers, together with the distance blocks) and the host rock are the main KBS-3H system components that together ensure isolation of the spent fuel and containment of radionuclides according to the safety concept shown in Figure A-1. Other system components, including the filling blocks, the compartment and drift end plugs, the steel supercontainers, fixing rings and other structural materials, have not been assigned safety functions. They are, however, designed to be compatible with, and support the safety functions of, the canister, the buffer and the host rock.

The main long-term safety function of the canisters is to ensure a prolonged period of complete containment of the spent fuel as in the KBS-3V alternative. As long as its copper shell is not breached, a canister will provide complete containment of radionuclides, and the spent fuel will interact with the environment only by means of heat generation and low level gamma and neutron radiation penetrating through the canister walls.

Long-term safety functions of the buffer are (a), protection of the canisters, and (b), limitation and retardation of radionuclide releases in the event of canister failure. These safety functions are also common to the KBS-3V and KBS-3H alternatives. The current KBS-3H design includes the use of steel components external to the canisters that will corrode over time and give rise to potentially porous or fractured corrosion products. These may interact chemically with adjacent bentonite and the slow formation of an altered zone with perturbed mass-transport properties at the bentonite / rock interface at supercontainer locations cannot be excluded. A final safety function of the KBS-3H buffer (or, more specifically, the distance blocks) is, therefore, (c), to separate the supercontainers hydraulically one from another, thus preventing the possibility of preferential pathways for flow and advective transport within the drifts through the corrosion products or altered buffer.
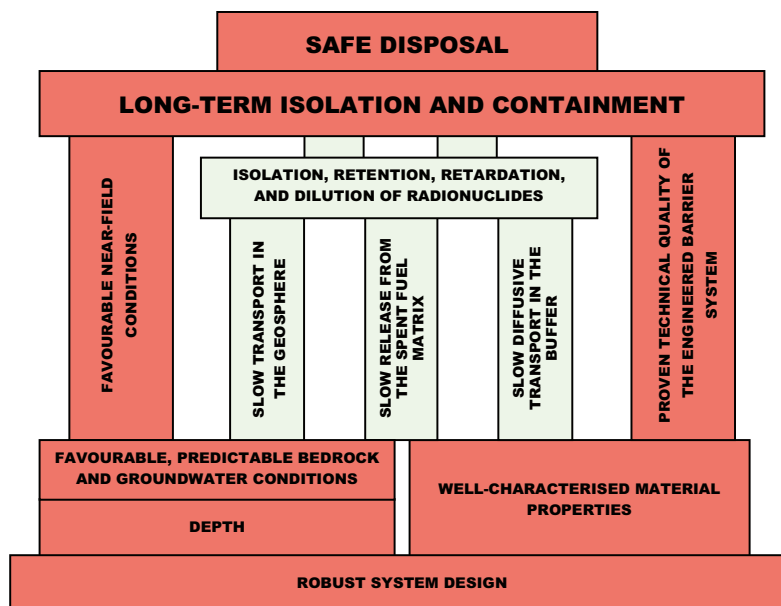

Figure A-1. Outline of the safety concept for a KBS-3 type repository for spent fuel in crystalline bedrock. Red pillars link characteristics of the disposal system to other characteristics on which they primarily depend. Green boxes and pillars indicate secondary characteristics and dependencies (after /Posiva 2006/).

The safety functions of the host rock are again the same as for the KBS-3V alternative. They are (a), to isolate the spent fuel from the biosphere and normal human habitat, (b), to limit and retard inflow to and release of harmful substances[2] from the repository, and (c), to provide favourable and predictable mechanical, geochemical and hydrogeological conditions for the engineered barriers, protecting them from potentially detrimental processes taking place above and near the ground surface.

A.2   Design requirements to support the safety functions

A.2.1   Design requirements related to mutual compatibility of the system components

A requirement common to all engineered system components, including not only the canister and the buffer, but also the filling blocks, the compartment and drift end plugs, the steel supercontainers shells and other structural materials, is that they should be mutually compatible. Although all components will inevitably undergo physical and chemical changes over time (e.g. due to chemical alteration or corrosion, saturation, swelling), none should evolve in such a way as to significantly undermine either the long-term safety functions or the design functions of the others. Thus:

- no component should contain any chemical constituents that lead to significant negative effects on the performance of the others;

- no component should generate gases at rates that could lead to a build-up of potentially damaging gas pressure (taking into account the gas permeability of the other components);

- no component should give rise to mechanical stresses that could lead to significant damage to the canisters or host rock; and

- no component should undergo volume changes (due, e.g. to swelling, compaction, corrosion or alteration) that could lead to significant changes in density of the adjacent buffer.

The degree to which the current reference design meets these requirements is discussed in the KBS-3H Evolution Report /Smith et al. 2007a/, including the significance of interactions of iron and cement[3] with the buffer and (in the case of cement) the host rock, the issue of gas generation and pressurisation, the potential of swelling pressure and gas pressure to damage the rock, and the stability of the canister under isostatic loading.

Scoping calculations of potential buffer density changes during the early phase of evolution are described in the KBS-3H Process and Evolution Reports /Gribi et al. 2007, Smith et al. 2007a/. The range of densities compatible with the buffer fulfilling its safety functions taking into account the evolution of groundwater and buffer porewater salinity (1,890 to 2,050 kg/m³) is discussed in Appendix A.5.

The following sections describe design requirements over and above the general requirement of mutual compatibility, which are intended to support the safety functions, and indicate how they are met in the current design.

A.2.2   Design requirements to support the safety function of the canister

The requirements on the canister are common for KBS-3V and KBS-3H. The canisters have a design lifetime of at least 100,000 years. This means that the canisters are designed to maintain their integrity taking into account the processes and events that are considered likely to take place in the repository over a design basis period of 100,000 years. It does not exclude the possibility that canister integrity will be retained significantly beyond the design basis period, nor that

---

[2]   Including the chemically toxic components of spent fuel.

[3]   No quantitative limits on the maximum amounts of such materials have been set - rather, in view of potentially adverse effects, amounts are kept as low as reasonably achievable.

(less likely) extreme conditions will give rise to earlier canister failures, and these possibilities must be considered in the safety assessment. The terminology is similar to that used in the reactor safety area: a design basis is defined to reflect the most likely conditions for the system but the safety assessment must address less likely situations as well.

In order to achieve its design lifetime, canisters are required to have:

1. a low probability of occurrence of initial penetrating defects;

2. corrosion resistance; and

3. mechanical strength.

The probability of occurrence of initial penetrating defects is still under investigation. In the current design, corrosion resistance is provided by the copper canister shell, and mechanical strength primarily by the cast iron insert.

The minimum design lifetime also implies a number of design requirements on repository layout (avoidance of fractures that may undergo shear movements that could damage the canisters – see Section 2.2.7 of the KBS-3H Evolution Report, /Smith et al. 2007a/ and the buffer.

If the copper shell is breached, then a canister is considered to have failed, even though it may continue to offer some resistance to the ingress of water and the release of radionuclides for a significant period thereafter.

A.2.3   Design requirements to support the safety functions of the buffer

The first safety function of the buffer (a, Section A.1) is to protect the canisters from external processes that could compromise their safety function of the complete containment of the spent fuel. Corresponding design requirements on the buffer are that it should be:

- sufficiently plastic (or ductile) to protect the canister from small rock movements, including shear displacements smaller than 10 cm at canister locations (the issue of potential larger shear movements caused by large earthquakes is discussed in Section 7.4.5 of the KBS-3H Evolution Report, /Smith et al. 2007a/);

- sufficiently stiff to support the weight of the canisters and maintain their central vertical positions in the drift in the long term;

- dense enough that microbes are metabolically barely active in the buffer and thus do not give rise to unfavourable chemical conditions at the canister surface; and

- sufficiently impermeable, once saturated, that the movement of water is insignificant and diffusion is the dominant transport mechanism for corrosive agents present in the groundwater that may reduce the lifetime of the canisters.

A further safety function of the buffer (b, Section A.1) is to limit and retard the release of any radionuclides from the canisters, should any be damaged. This implies design requirements that the buffer be:

- again impermeable enough, once saturated, that the movement of water is insignificant and diffusion is the dominant radionuclide transport mechanism;

and have:

- a sufficiently fine pore structure such that microbes and colloids are immobile (filtered) and microbe- or colloid-facilitated radionuclide transport will not occur.

It also implies a self-healing capability of the buffer, which means that any potential advective pathways for flow and transport that may arise, for example, as a result of piping and erosion, sudden rock movements or the release of gas formed in a damaged canister are rapidly closed.

These safety functions are common to KBS-3V and KBS-3H. In addition, for the KBS-3H design the final safety function of the buffer (c, Section A.1) is to separate the supercontainers hydraulically one from another. This implies the design requirement that the buffer should provide:

• tight interfaces with the host rock within a reasonable time.

Competing requirements on buffer density are balanced in the design process. For example, excessive density would lead to a correspondingly high swelling pressure and to a risk of damage to the rock. It would also offer less protection of the canisters from rock movements. On the other hand, insufficient density would lead to the possibility of colloid-facilitated radionuclide transport. The choice of MX-80-type bentonite as a buffer material with a design target for saturated density of 2,000 kg/m^3 is made with a view to balancing these various requirements.

The filling blocks are not considered part of the buffer and are not assigned any long-term safety functions - i.e. they are not required to contribute directly to the isolation of the spent fuel and containment of radionuclides. On the other hand, in the current design, they have the same properties as the buffer as they are likely, in practice, to contribute to the limitation and retardation of the release of any radionuclides from the canisters, should any canisters be damaged.

During the saturation of the repository, high hydraulic pressure gradients and gradients in buffer swelling pressure may develop along the drifts, which could potentially lead to phenomena such as piping and erosion of the buffer and displacement of the distance blocks and supercontainers. The distance blocks and filling blocks, together with the compartment and drift end plugs, have the important design function of keeping the adjoining buffer in place, and not allowing any significant loss or redistribution of buffer mass by piping and erosion during the operational period and subsequent period of buffer saturation. The fixing rings also have the short-term safety-related design function of preventing displacement of a distance block while the adjoining components are installed. The distance blocks and filling blocks have a low hydraulic conductivity at saturation and will develop swelling pressure against the drift wall, such that friction will resist buffer displacement. Furthermore, each compartment plug is designed to stay in place under the applied loads (i.e. no significant displacement are allowed) until the next compartment is filled and a further compartment plug or drift end plug installed. Likewise, the drift end plug is designed to stay in place under the applied loads (no significant displacement allowed) until the adjoining transport tunnels are backfilled. Issues of piping and erosion and of displacement of the distance blocks and supercontainers are discussed further in the KBS-3H Process and Evolution Reports /Gribi et al. 2007, Smith et al. 2007a/.

The temperature of the buffer is kept below 100ºC to avoid significant chemical alteration of the buffer that could undermine its ability to satisfy the above requirements. This in turn imposes requirements on buffer layout and dimensioning (Section 2.2.7 of the KBS-3H Evolution Report; /Smith et al. 2007a/).

A.2.4 Design requirements to support the safety functions of the host rock

Unlike the engineered component of the repository, the implementer has no control over the undisturbed properties of the host rock, except in as far as by grouting of intersecting transmissive fractures during construction to avoid drawdown of surface waters and upconing of saline groundwaters, and by adaptation of the depth and layout of the repository, for example, to avoid unacceptable features (see, e.g. Section 2.2.7 of the KBS-3H Evolution Report, /Smith et al. 2007a/). It should be noted, however, that grouting also affects the rock mass properties. Futhermore it should be noted, however, that backfilling and sealing of the repository cavities support the safety functions of the host rock, being carried out with the main purpose of preventing the formation of water conductive flow paths, and making the inadvertent human intrusion to the repository more difficult. Requirements on the host rock related to site selection are similar to those for the KBS-3V design and will not be further discussed here.

A.2.5 Design requirements related to the issue of repository gas

The repository must be designed so as to avoid the build-up of potentially damaging pressures due to repository-generated hydrogen gas § This does not imply that the drifts and access tunnels need to be gas permeable, provided that gas can escape to from the drift by other routes, e.g. via transmissive fractures in the rock. The issue of gas pressurisation in the repository near field is discussed in the KBS-3H Process and Evolution Reports /Gribi et al. 2007, Smith et al. 2007a/.

A.3 Safety function indicators and criteria

A.3.1 Use of safety function indicators in safety assessment

To assess the performance and safety of a KBS-3H or KBS-3V repository, it is necessary to assess the conditions under which the identified safety functions will operate as intended, and the conditions under which they will fail, or operate with reduced effectiveness. Following the methodology adopted in the Swedish SR-Can safety assessment /SKB 2006ab/, KBS-3H safety studies make use of the concept of safety function indicators and associated criteria. One or more safety function indicators are assigned to each safety function. A safety function indicator is a measurable or calculable property of the system that is critical to a safety function being fulfilled. If the safety function indicators fulfil certain criteria, then the safety functions can be assumed to be provided. If, however, plausible situations can be identified where the criteria for one or more safety function indicators are not fulfilled, then the consequences of loss or degraded performance of the corresponding safety function must be evaluated in the safety assessment.

It is important to distinguish design requirements from the criteria on safety function indicators. In general, design requirements refer to attributes that the repository is ensured to have by design at the time of emplacement of the first canister, or during the early evolution of the repository in the period leading up to saturation, although some design requirements also affect the long-term evolution of the system. Repository design also aims to ensure that the criteria on the safety function indicators are fulfilled over the required time frames, but this is seen as a target, rather than as a design requirement.

Adherence to design requirements is primarily the concern of design studies, whereas safety studies focus more on the fulfilment of safety function indicator criteria, taking into account the associated uncertainties. It is emphasised that, if there are plausible situations where one or more the criteria on safety function indicators are not satisfied, this does not imply that the system as a whole is unsafe. Such situations must, however, be carefully analysed, for example by means of radionuclide release and transport calculations, as described in the Radionuclide Transport Report /Smith et al. 2007b/.

A.3.2 Safety function indicators and criteria for the canisters

Four fundamental modes have been identified by which, in principle, one or more canisters could fail to provide their safety function of complete containment of spent nuclear fuel and associated radionuclides /SKB 2006a/: i) initial, penetrating defects, ii) failure due to corrosion of copper shell, iii) rupture due to rock shear and the transfer of shear stresses from the rock via the buffer to the canister (in particular, in the event of post-glacial earthquake), and iv) collapse due to isostatic loading.

Safety function indicators for the canister are (i), minimum copper thickness – failure occurs if this is zero at any point on the canister surface, due to the presence of an initial defect that penetrates the entire thickness of the shell or due to localised and general corrosion processes leading to the gradual thinning of the shell, (ii), the isostatic pressure on the canister – failure occurs if this exceeds the isostatic pressure for collapse, and (iii), the shear stress on the canister – failure occurs if this exceeds the rupture limit. The canister safety function indicators and associated criteria, as presented in SR-Can /SKB 2006a/, are summarised in Table A-1.

Table A-1. Safety function indicators and criteria for the canister (after Figure 7-2 of /SKB 2006a/).

Safety function indicator	Criterion	Rationale
Minimum copper thickness	> 0 mm	Zero copper thickness anywhere on the copper surface would allow relatively rapid water ingress to the canister interior and radionuclide release
Isostatic pressure on canister	< pressure for isostatic collapse (varies between canisters, but probability of collapse at 44 MPa is vanishingly small)	An isostatic pressure on the canister greater than 44 MPa would imply a more significant possibility of failure due to isostatic collapse
Shear stress on canister	< rupture limit	A shear stress on the canister greater than the rupture limit would imply failure due to rupture

A.3.3   Safety function indicators and criteria for the buffer

Three broad modes can be envisaged by which a bentonite buffer could conceivably cease to perform its safety functions fully: loss or redistribution of buffer mass, mineral alteration of the buffer, freezing of the buffer.

1. Loss or redistribution of buffer mass

The loss or redistribution of buffer mass due, for example, to piping and erosion by flowing water could in principle lead to:

- a loss of swelling pressure at the drift wall, which could, if sufficiently large, lead to a loss of tightness of the contact between the buffer and the rock, and, in turn, enhance the transfer of mass (dissolved corrosive agents - especially sulphide - and radionuclides) between the rock and the buffer and thus compromise or reduce the ability of the buffer to perform any of its three safety functions;

- a loss of swelling pressure at the drift wall, could also lead to enhanced thermal spalling due to reduction in confining pressure associated with time-dependent degradation of rock strength;

- a more general loss of swelling pressure, which could, if sufficiently large, lead to increased microbial activity within the buffer, potentially increasing the rate of canister corrosion by reducing dissolved sulphate to sulphide, and, for still larger losses in swelling pressure, the possibility of canister sinking;

- an increase in buffer hydraulic conductivity, which, if sufficiently high, could lead to advective transport of dissolved corrosive agents and radionuclides in the buffer and hence compromise the ability of the buffer to perform any of its three safety functions (note that isolated regions of higher hydraulic conductivity around the canisters would have a less significant affect);

- a reduction in buffer density, which, if sufficiently large, could lead to the possibility of colloid-facilitated radionuclide transport in the buffer and reduce the ability of the buffer to limit and retard radionuclide releases (note again that isolated regions affected in this way would have a less significant affect); and

- an increase in buffer density at some locations along the drift, which, if sufficiently large, could lead to mechanical damage of the rock, and compromise the ability of the buffer to protect the canisters from rock shear movements of less than 10 cm.

2. Mineral alteration of the buffer

Mineral alteration of the buffer due, for example, to high temperatures around the canisters or to chemical interactions between the buffer and the steel or cementitious components could in principle lead to:

- a change to a less plastic material, which, if it affected a significant proportion of the buffer between the canisters and the drift wall, could compromise the ability of the buffer to protect the canister from rock movements, including shear displacements at canister locations;

- a loss of swelling pressure, with potential consequences as described above in the context of loss or redistribution of buffer mass; and

- a loss of self-healing capacity, which could lead to fracturing of the buffer and an increase in hydraulic conductivity, again with potential consequences as described above in the context of loss or redistribution of buffer mass.

3. Freezing of the buffer

Freezing of the buffer as a result, for example, of the deep penetration of permafrost following a major climate change would, if it were to occur, detrimental changes in buffer properties that could compromise its capacity to protect the canister and to limit and retard radionuclide releases from a failed canister. According to present knowledge based on past glaciations, the permafrost layer is not expected to reach more than 180 metres below ground at Olkiluoto /Hartikainen 2006/ and is thus not considered as a potential cause of major loss of buffer safety functions in the present study. The possibility that conditions at Olkiluoto could in the future differ significantly compared with those during the past glaciations and lead to buffer freezing may, however, require further consideration in future studies.

Consideration of these three possible modes for loss or degradation of the buffer safety functions leads to the safety function indicators and associated criteria that are summarised in Table A-2. Most are taken directly from SR-Can. It should be noted that the criterion given in Table A-2 that there is a negligible impact on the rheological and hydraulic properties of the buffer due to mineral alteration subsumes the SR-Can criterion for a Swedish KBS-3V repository that buffer temperature remains below 100°C. The potential chemical processes that may occur at elevated temperature are, for example, silica dissolution close to the canister followed by transport outwards by diffusion to colder parts and precipitation, as well as buffer cementation due to the dissolution, transport and precipitation of silica or aluminosilicate minerals. But neither experimental or natural analogue studies have shown that these processes will actually occur. The effect of buffer cementation due to silica precipitation is, however, an issue for further work. The present criterion takes account of the concern that the buffer of a KBS-3H repository may be more affected by certain chemical interactions, and particularly those between the corrosion products of steel components external to the canisters and bentonite and those between cementitious materials and bentonite, than is the case for a KBS-3V repository.

Table A-2. Safety function indicators and criteria for the buffer (adapted for KBS-3H from Figure 7-2 of /SKB 2006a/).

Safety function indicator	Criterion	Rationale
Bulk hydraulic conductivity	$< 10^{-12}$ m/s	Avoid advective transport in buffer
Swelling pressure at drift wall	> 1 MPa	Ensure tightness, self sealing
Swelling pressure in bulk of buffer	> 2 MPa*	Prevent significant microbial activity
	> 0.2 MPa	Prevent canister sinking
Saturated density	> 1,650 kg/m^3	Prevent colloid-facilitated radionuclide transport (note, however, that higher densities may be required to fulfil the above criteria on swelling pressure - see Section A.5)
	< 2,050 kg/m^3	Ensure protection of canister against rock shear
Mineralogical composition	No changes resulting in significant perturbations to the rheological and hydraulic properties of the buffer (e.g. from iron or cement interaction or related to temperature)	See main text
Minimum buffer temperature	> –5°C	Avoid freezing

* Although developed for KBS-3V, this criterion is also expected to be applicable to KBS-3H, and is likely to be more conservative for this alternative since, in KBS-3H, the weight of the canister is distributed over a larger horizontal area compared with KBS-3V.

A.3.4   Safety function indicators and criteria for the host rock

Loss or degradation of the isolation function of the host rock would occur if the Precambrian Shield were to erode away sufficiently to expose the repository at the surface (this situation, which concerns the farthest future, is discussed in Chapter 9 of the KBS-3H Evolution Report; /Smith et al. 2007a/. Loss or degradation of the protective function of the host rock could occur if chemical conditions in the groundwater become unfavourable to buffer and canister longevity, or if a fracture intersecting the deposition drifts near a canister location were to slip sufficiently to cause rupturing of the canister. Finally, there are several rock properties that can favour its performance as a radionuclide transport barrier (for example, absence or low frequency of highly transmissive fractures, low hydraulic gradient, mineralogical and geochemical characteristics giving high retention by sorption). Safety-related aspects of the hydraulic properties of fractures intersecting a drift at canister and buffer emplacement locations are discussed in Appendix A.4. Some safety-relevant properties may vary over time (especially geochemical characteristics), potentially leading to some degradation of the host rock as a transport barrier.

The host rock safety function indicators and associated criteria as presented in SR-Can and are summarised in Table A-3.

A.4   Hydraulic properties of fractures intersecting a drift at canister and buffer emplacement locations

In determining where along a deposition drift canisters and buffer can be emplaced, a key consideration is the avoidance of significant buffer loss or redistribution by piping and erosion phenomena during saturation. The potential for transient water flows to cause piping and erosion is described in Section 5.5.6 of the KBS-3H Evolution Report /Smith et al. 2007a/. There, it is noted that laboratory and modelling studies indicate that, for the current reference design, piping will not occur provided the inflow rate to a supercontainer drift section comprising a supercontainer plus a distance block during saturation is 0.1 litres per minute or less, and provided there is no significant deformation and displacement of the distance blocks relative to the supercontainers (this is an issue addressed on ongoing design developments).

There are, however, considerations related to the evolution of the repository subsequent to saturation that also have a bearing on the suitability of particular drift sections as emplacement locations. In particular, it is at least desirable that any flow through the intersecting fractures be such that:

- there is no significant long-term erosion of the buffer by flowing water that could affect its barrier function;
- the rate at which species with the potential to corrode the copper shell of the canister can migrate from the rock via the buffer to the canister surface does not lead to an unacceptable rate of loss of copper coverage, and hence early canister failure by corrosion; and
- the rock provides an effective barrier to the transport of released radionuclides in the event of canister failure.

It is also clearly desirable that canister positions are not intersected by fractures capable of undergoing potentially damaging slip as a result of large earthquakes. The buffer is expected to protect the canisters from shear displacements smaller than 0.1 m. The issue of potential larger shear movements caused by large, post-glacial earthquakes is discussed in Section 7.4.5 of the Evolution Report /Smith et al. 2007a/.

The rate of groundwater inflow to the drift during saturation is related to the transmissivity and frequency of fractures intersecting the drift. Hence, it is also related to the long-term flow subsequent to saturation (the relationship is, however, complicated by a number of factors, as discussed below). The purpose of the scoping calculations presented in this appendix is to discuss how design requirements related to the saturation period and, in particular, the requirement that inflow is 0.1 litres per minute or less, compare to desirable properties related to the post-closure evolution and performance of the repository, and especially fracture transmissivity.

Table A-3. Safety function indicators and criteria for the host rock (adapted for KBS-3H from Figure 7-2 of /SKB 2006a/).

Safety function indicator	Criterion	Rationale
Redox conditions	No dissolved oxygen	The presence of measurable O_2 would imply oxidising conditions
Minimum ionic strength	Total divalent cation concentration > 10^{-3} M	Avoid buffer erosion
Maximum chloride concentration or minimum pH	pH^{GW} > 4 or	
	$[Cl^-]^{GW}$ < 3 M	Avoid chloride corrosion of canister
Limited alkalinity	pH^{GW} < 11	Avoid dissolution of buffer smectite
Limited salinity (expressed in terms of total dissolved solids, TDS)	[NaCl] < 100 g/l (or other compositions of equivalent ionic strength)	Avoid detrimental effects, in particular on swelling pressure of buffer and distance block
Limited concentration of detrimental agents for buffer, distance block and canister	Applies to HS^-, K^+ and Fe(II)/Fe(III). The lower the better (no quantitative criterion)	Avoid canister corrosion by sulphide, avoid illitisation (K^+) and chloritisation (Fe) of buffer and distance block
Limited rock shear at canister/distance block locations in deposition drift	< 10 cm	Avoid canister failure due to rock shear in deposition drift

The calculations assume that the system is implemented as planned. Perturbing features and processes, such as the presence of initial defects in the canisters, poor emplacement of the buffer and the possibility of processes that could disturb the buffer / rock interface (rock spalling and iron / bentonite interaction, cement-bentonite interaction) are assumed to be of negligible importance or avoided by design. Such features and processes are, however, taken into account in the overall description of system evolution in the Evolution Report.

A.4.1 Hydrodynamic relationships

Inflow and transmissivity

Assuming that saturation in a drift section occurs principally due to radial inflow from the rock (rather than water migration parallel to the drift), a relationship between fracture transmissivity and the rate at which a drift section saturates with water in the early phase of evolution may be obtained from Darcy's law in a radial configuration (Thiem's equation). Assuming that **n** fractures intersect the section:

$$Q = 2\pi \frac{\Delta P}{\rho_w g \ln(l_h / r_t)} \sum_{i=1}^{n} T_i ,$$
(Eq. A-1)

with:

Q   inflow from the **n** intersecting fractures [m³/s].

T   fracture transmissivity [m²/s].

ΔP magnitude of the maximum hydraulic pressure difference between the drift and the undisturbed rock during saturation (about 4 MPa for a 400 m repository depth).

l_h hydraulic length (from drift to nearest major fracture zone – assumed here to be about 50 m, consistent with the modelling reported in /Lanyon and Marschall 2006/.

r_t drift radius (0.925 m).

According to this equation, a single fracture with a transmissivity 3×10^{-9} m²/s will deliver an initial inflow of about 0.1 litres per minute, which is currently taken to be the maximum allowable value if the possibility of piping and erosion is to be avoided.

There are, however, other factors that may affect the initial inflow from transmissive fractures such that fractures with transmissivities above 3×10^{-9} m^2/s could potentially give initial inflows of less than 0.1 litres per minute. Firstly, it may be possible to reduce the initial inflow through some larger aperture fractures by injecting grout, such that significant piping and erosion do not occur during the operational period and subsequent buffer saturation, but this grout is likely to become degraded and ineffective in reducing flow in the longer term (in view of current uncertainties in the performance of any grout, an inflow of less than 0.1 litres per minute prior to grouting is used as a criterion for a drift section to be suitable for the emplacement of canisters and buffer in deriving a preliminary repository layout). Furthermore, initial inflows may also be reduced by drawdown of the water table, which will give a reduction in the hydraulic pressure at repository depth, by the impact of other open repository tunnels and drifts, and potentially by mineral precipitation and degassing in the fracture. These are generally transient effects which do not affect flow in the longer term, once the drifts are saturated. Finally, inflow is determined not only by the hydraulic properties of fractures intersecting the drift, but also by those of other connected fractures in the wider fracture network.

The impact of fracture network effects on the initial rate of inflow to a drift at canister and buffer emplacement locations is illustrated by the results of the discrete fracture network (DFN) modelling of /Lanyon and Marschall 2006/. Lanyon and Marschall constructed a series of model variants in which one or more KBS-3H drifts were positioned within a network of deterministically positioned major fracture zones and stochastically generated local fracture zones and discrete water-conducting fractures in the background rock, each with a distribution of transmissivities based on field measurements at Olkiluoto. Based on the above consideration of Thiem's equation, fractures intersecting the drift with transmissivities above about 3×10^{-9} m^2/s were considered unsuitable as canister and buffer emplacement locations, but were rather assumed to be sealed using filling blocks or compartment seals. Flow simulations were carried out to evaluate, among other issues, the time to fill the supercontainer gap volumes (assumed to be 1.38 m^3). From these times, the inflow rates[4] to drift sections containing supercontainers, which are intersected by one or more fractures with transmissivities of 3×10^{-9} m^2/s or less can be evaluated (Table A-4).

In none of the simulations did the inflow rate to the gap around a supercontainer exceed about 0.05 litres per minute, implying a 0.1 litre per minute maximum inflow rate to a drift section containing a supercontainer plus distance block. In most cases, inflow was significantly less than this. This indicates that the initial inflow criterion of 0.1 litres per minute might be satisfied if it were possible to exclude fractures with transmissivities above 3×10^{-9} m^2/s at canister and buffer emplacement locations. It does not, however, necessarily show that avoiding locations with inflows greater than 0.1 litres per minute will ensure that there are no intersecting fractures with

Table A-4. Inflow rates to the gap around a supercontainer calculated for four single drift models (derived from Table 5-6 in /Lanyon and Marschall 2006/).

Drift	Number of supercontainers	Number intersected by features in model	Inflow rate [litres per minute]		
			Max.	Av.	Min.
W01T01	23	6	0.048	0.015	0.009
W01T12	25	9	0.019	0.006	0.003
W01T22	19	5	0.025	0.011	0.005
W01T23	17	4	0.022	0.017	0.007

---

[4] The inflow rate will, in reality, decrease with time as the gap is filled and the pressures of the fluids (water and air) inside the gap increase. The storage model used in the calculations was, however, set up in such as way that this decrease was small (high compressibility while the gap volumes are being filled).

transmissivities greater than 3×10^{-9} m²/s. In practice, characterisation of fractures intersecting the drift is likely to be based largely on observations made at the drift wall, including inflow. It must further be kept in mind that the impact of repository excavation on the rock matrix pore pressure around the drift, and hence on inflow, was not been considered in the model used to generate Table A-4. Nor have the possibilities of mineral precipitation and degassing reducing initial inflow been considered. All these issues require further investigation. Thus, the possibility that, in reality, some higher transmissivity fractures are present must be acknowledged.

In the following sections and in the majority of radionuclide transport calculations in the safety assessment of a KBS-3H repository at Olkiluoto /Smith et al. 2007b/, the flow around a deposition drift is calculated based on the assumption that the drift section containing the canister under consideration is intersected by a fracture with a transmissivity of 3×10^{-9} m²/s. This is viewed as a moderately pessimistic assumption, but is not necessarily the "worst case". Intersection of the drift by a higher transmissivity fracture at the location of a failed canister is, however, considered in some variant cases in radionuclide transport calculations.

Transmissivity and aperture

Fracture transmissivity and aperture are clearly related, although the form of the relationship depends on the geometry of the fracture (the presence of constrictions, etc). For the purposes of this appendix, following /Lanyon and Marschall 2006/, it is assumed that the fracture half-aperture b_v [m] is related to transmissivity via the equation:

$$b_v = \frac{\sqrt{T}}{2c},$$ (Eq. A-2)

where c is a constant (2 seconds$^{-1/2}$).

Flow around a deposition drift

In the following sections, it is assumed that a fracture (transmissivity 3×10^{-9} m²/s) intersects the drift at a canister location with the fracture plane perpendicular to the drift and aligned with the regional hydraulic gradient, taken to be 0.01 in current safety studies. In reality, more than one fracture may intersect a drift section, which will tend to increase overall flow, whereas flow will tend to be reduced by the dip of the fractures with respect to the regional gradient. Furthermore, fractures that will intersect the drift at a range of angles and other connected fractures will have a perturbing effect on the flow. These effects are again illustrated in the DFN modelling of /Lanyon and Marschall 2006/, where DFN models variants with different cut-off transmissivities are used to evaluate the flow into and out of a cylindrical volume of rock around a drift element containing a supercontainer, with its outer surface 0.5 m from the drift wall (1.425 m from the drift centre line). Values obtained by Lanyon and Marshall vary significantly between drift sections, but are never more than 4×10^{-11} m³/s (Table A-5). A single 3×10^{-9} m²/s fracture aligned with the regional gradient and with the fracture plane perpendicular to the drift axis would give rise to a similar flow of $\sim 4 \times 10^{-11}$ m³/s into and out of this cylindrical volume (3×10^{-9} m²/s $\times$ 0.01 $\times 2 \times 0.66$ m)[5]. It is therefore concluded that basing the flow around a deposition drift on a single fracture with the properties described above represents a reasonable assumption in safety assessment.

---

[5] The solution of Darcy's Law for flow around an impermeable circular drift shows that the fluid velocity in a fracture along a line passing through the drift centre and normal to the flow direction is $v = V(1+r_t^2/r^2)$ for $r > r_t$, where r is distance from the drift centre, r_t is drift radius and V is the undisturbed water velocity at large distances from the drift. By integrating v with respect to r between $r = r_t$ and $r = r_t + 0.5$ m, it can be shown that, because of distortion of the flow by the drift, the flow passing through the cylindrical volume is equivalent to the flow passing through a fracture of width 2×0.66 m in the undisturbed rock.

Table A-5. Flows across supercontainers calculated from steady state DFN flow models for two model drifts (after Table B-1 in /Lanyon and Marschall 2006/).

Drift	Model transmissivity cut-off [m²/s]	Supercontainers not intersected	Flow [× 10⁻¹¹ m³/s] Max.	Av.
W01T01	10^{-10}	15	4	1.5
W01T01	10^{-11}	1	4	0.6
W01T02	10^{-10}	14	5	0.2

A.4.2 Buffer erosion

The swelling pressure of the buffer of a KBS-3H repository following saturation may be sufficient to cause bentonite to be extruded into open fractures intersecting the drift. The advancing clay front will be composed of a soft clay gel, which may potentially be eroded by flowing groundwater. There are two broad ways in which this might happen:

- mechanical erosion, in which the viscous force exerted by the flowing water on the particles of the clay gel exceeds the average particle bond strength; and,

- chemical erosion, in which the concentration of cations in solution at the gel / water interface falls below the value required to maintain the stability of the gel (e.g. as a result of the penetration of dilute waters to repository depth in association with glaciation).

Either of these mechanisms may in principle cause the gel to break up and disperse in the form of colloids. They are discussed in turn below.

a. Mechanical erosion

The shear stress (traction) exerted by a laminar flow through a fracture on the buffer, τ [Pa], is given by Newton's law of viscosity:

$$\tau = \mu \frac{dv}{dy} \qquad \text{(Eq. A-3)}$$

where v [m s⁻¹] is the groundwater velocity in the fracture, averaged across its aperture, y [m] is normal distance from the buffer / rock interface and μ [Pa.s] is the viscosity of water (about 10^{-3} Pa.s). The influence of the interface on the water velocity in the fracture extends to a distance of a few fracture apertures from the interface /Liu and Neretnieks 2006/. The velocity gradient perpendicular to the buffer / rock interface is therefore of the order:

$$\frac{dv}{dy} \cong \frac{v}{b_v} \cdot \qquad \text{(Eq. A-4)}$$

Considering a single fracture intersecting the deposition drift, and neglecting the distortion in the streamlines caused by the cylindrical shapes of the buffer, the groundwater velocity in the fracture away from the influence of the interface is given by:

$$v = \frac{T \cdot i_0}{2b_v} \cdot \qquad \text{(Eq. A-5)}$$

where i_0 is hydraulic gradient (0.01).

From Eq. A-3 to A-5:

$$\tau \cong \frac{\mu T i_0}{2b_v^2} \cdot \qquad \text{(Eq. A-6)}$$

If a fracture intersecting the drift at supercontainer and distance block emplacement locations is assumed to have a transmissivity of 3×10^{-9} m²/s, then, according to Eq. A-2, the fracture half-aperture is in the order of 10^{-5} m. For a hydraulic gradient of 0.01, Eq. A-6 gives a shear stress in the order of 10^{-4} Pa. In practice, the fracture aperture is likely to vary locally around the buffer / rock interface, giving some corresponding variability in the shear stress, which may be higher or lower than the 10^{-4} Pa indicated above. However, while a locally smaller aperture will, according to Eq. A.2-6, give rise to a higher shear stress, this does not take account of the mitigating effect of channelling – i.e. flow will tend to be channelled around any local constrictions, offsetting to some extent the effect of the smaller aperture on shear stress.

The typical Bingham yield stress of the gel front is strongly dependent on the composition of the clay and ionic strength of the water, but a review of experimentally determined values by /Liu and Neretnieks 2006/ indicates that 1.0 Pa may be taken as a conservative estimate of the minimum shear stress required for mechanical erosion. The expected shear maximum stress is around four orders of magnitude smaller than this once the influence of transient pressure gradients associated with repository saturation has passed, which implies that no mechanical erosion will occur once the repository is saturated, in spite of the uncertainties noted above associated with the variability of aperture, the effects of channelling and the possibility that fractures with transmissivities greater than 3×10^{-9} m²/s will intersect the drift at canister and buffer emplacement locations. Some limited erosion associated with piping during the saturation phase cannot, however, currently be excluded.

b. Chemical erosion

The next glacial retreat, and hence the next possibility for penetration of glacial meltwater to repository depth, is assumed to be in 70,000 years time, according to the Weichselian-R climate scenario. Penetration of glacial meltwater to repository depth could lead to some chemical erosion of the buffer (see Section 7.4.7 of /Smith et al. 2007a/).

Significant erosion is here defined as that required for advective conditions to occur within the buffer. /Börgesson and Hernelind 2006/ have calculated the buffer swelling pressure for cases where, in the KBS-3V alternative, one, two and three entire bentonite rings surrounding the canister have been omitted, to illustrate the effects of a local loss of large amounts of bentonite. The conclusion was that a mass loss of 1,200 kg to a fracture intersecting the deposition hole would lead to conditions where advective conditions in the buffer must be considered. Due to the similarity between the deposition hole diameter in KBS-3V (1.75 m) and the deposition drift diameter of in KBS-3H (1.85 m), this conclusion can be taken to apply to both alternatives.

A model of chemical erosion has been developed by SKB for SR-Can. If the model is applied to a KBS-3H repository at Olkiluoto, the results indicate that significant erosion could occur in a single glacial cycle if fractures intersecting the buffer have transmissivities in excess of about 3×10^{-8} m²/s. The SKB model is, however, tentative (a new model is currently under development by SKB / KTH) and model uncertainties are probably too great to draw any firm conclusions regarding those fractures that should be avoided in emplacing supercontainers and distance blocks.

A.4.3   Canister corrosion

A model for the time required for canister failure by corrosion to occur for a given set of flow conditions around the drift and a given groundwater sulphide concentration is given in Appendices B.8 and B.9 of the Evolution Report /Smith et al. 2007a/. Assuming that no processes occur that lead to detrimental perturbations to the buffer or buffer / rock interface, canister lifetime (t_a [s]) is given by:

$$t_a = \frac{d}{c_{local} \dot{j}_a},$$ (Eq. A-7)

with:

d   thickness of the copper canister shell (0.05 m).

c_{local}   factor for uneven corrosion of copper [–] (50, note – a lower value of 5 was used in earlier studies in Finland – p. 94 of /Vieno et al. 1992/; a higher and more conservative value is, however, consistent with current understanding, as described, for example, in SR-Can, where a factor of about 35 is used).

j_a   copper corrosion rate [m/s].

Noting that 2 moles of copper are corroded per mole of sulphide arriving at the canister surface, the maximum rate of uniform copper corrosion is given by:

$$j_a = \frac{2 f_{max}}{\rho_c} \frac{N_c}{N_s}, \tag{Eq. A-8}$$

with:

ρ_c density of copper (8,900 kg/m^3).

N_c molar weight of copper (64 g/mol).

N_s molar weight of sulphide (33 g/mol).

f_{max} rate of arrival of sulphide at the canister surface at the location where this is the highest (directly opposite the fracture/drift line of intersection) [mol/s].

f_{max} is given by:

$$f_{max} = \frac{\pi D_e C_s}{2(r_t - r_c)} \frac{1}{\log_e \left(\frac{2(r_t - r_c)}{b_v} \right)} \frac{Q_b}{Q_b + Q_f}, \tag{Eq. A-9}$$

with:

D_e effective diffusion coefficient of anions in the saturated buffer (10^{-11} m^2/s; Table A-11 of /SKB 2006b/).

r_t drift radius (0.925 m).

r_c canister radius (0.525 m).

b_v fracture half aperture (from Eq. A-2).

C_s concentration of sulphide in groundwater approaching the drift [kg/m^3] (see below).

Q_b [m^3/s] and Q_f [m^3/s] are transfer coefficients given by:

$$Q_b = \frac{A_{frac}}{\pi} \sqrt{\frac{2 D_w T \cdot i_0}{r_t b_v}}, \tag{Eq. A-10}$$

and

$$Q_f \approx \frac{\pi D_e A_{frac}}{2 b_v \log_e \left(\frac{2(r_t - r_c)}{b_v} \right)}. \tag{Eq. A-11}$$

D_w [m^2/s] is the diffusion coefficient of ions in free water (2×10^{-9} m^2/s) and A_{frac} [m^2], the area of intersection of the fracture with the drift, is given by:

$$A_{frac} = 4 \pi b_v r_t, \tag{Eq. A-12}$$

In deriving Eq. A-9, it is assumed that the buffer has uniform transport properties from the canister surface to the drift wall. In reality, there are a number of features and processes that could perturb mass transfer in the buffer and at the buffer / rock interface. The impacts of such features and processes are considered in Appendix B.7 of the Evolution Report /Smith et al. 2007a/.

Figure A-2 shows the calculated canister lifetime as a function of the transmissivity of a fracture assumed to intersect the drift adjacent to a canister position, for different values of groundwater sulphide concentration:

• 12 mg/l (the highest currently observed value);

• 42.5 mg/l (the maximum value calculated for future times – see /Pastina and Hellä 2006/).

The results show that the canister lifetime exceeds the minimum design lifetime of 10^5 years by one to two orders of magnitude in the case of a transmissivity of 3×10^{-9} m²/s. It continues to exceed the minimum, though by a reduced margin, as fracture transmissivity is increased. This is because, even at high transmissivities, the barrier to sulphide transport provided by the buffer severely limits the rate at which sulphide can reach the canister surface. Consideration must, however, be given to the possibility of chemical erosion of the buffer at high transmissivities, as discussed in Section (iii) (this and the impact of other possible perturbations to the buffer and the buffer / rock interface are discussed in Appendix B.7 of /Smith et al. 2007a/).
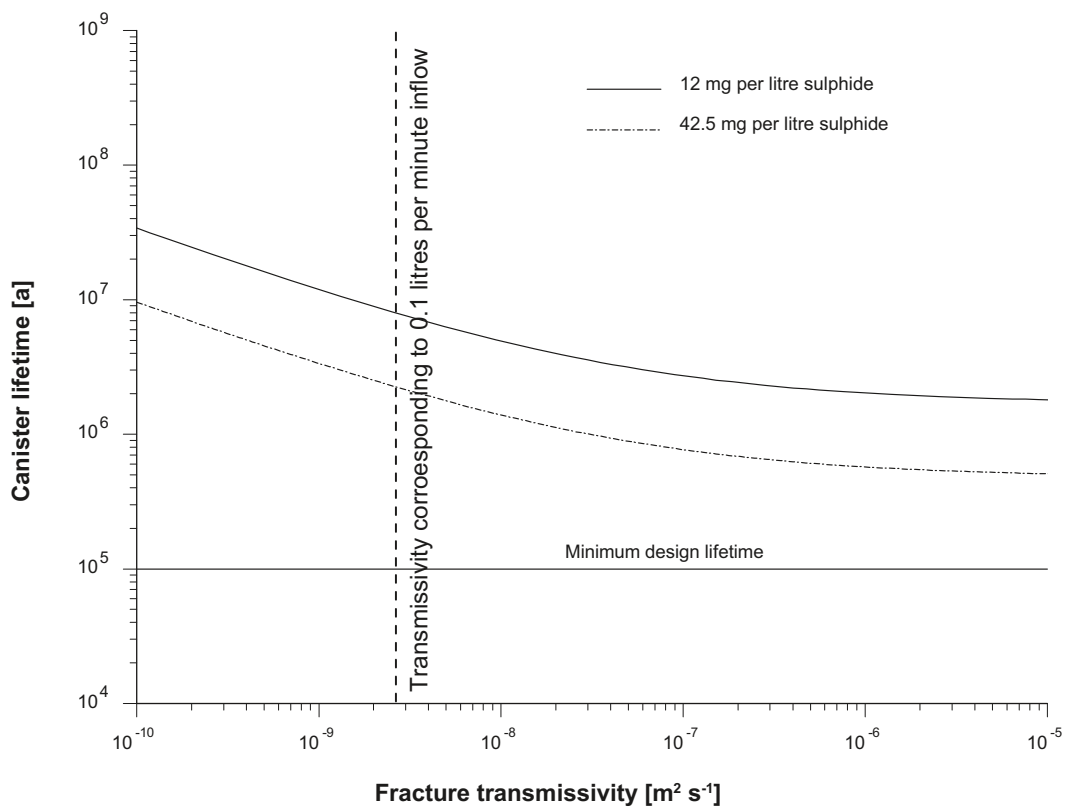
Figure A-2. *Canister lifetime as a function of fracture transmissivity for two different groundwater sulphide concentrations.*

127

A.4.4   Geosphere transport barrier

In terms of the hydrogeological properties of the rock, the effectiveness of the geosphere and a transport barrier to radionuclides released in the event of canister failure is a function of the "transport resistance", defined as W / Q, where W [m] is the width of a representative transport path within the fracture network, L [m] is the transport distance along this path and Q [m³/a] is the flow through the path. Experience from past Posiva safety assessments is that a value of WL / Q of a few thousands or more years per metre provides an effective barrier to the transport of many safety relevant radionuclides (the median value for all sites given in TILA-99 is 5×10^4 years m^{-1} - see Section 11.6 in /Vieno and Nordman 1999/).

The transport resistance of a single fracture may also be expressed in terms of transmissivity:

$$\frac{WL}{Q} = \frac{L}{Ti_0} \, . \tag{Eq. A-13}$$

In a heterogeneous geosphere, the transport resistance is additive along different sections of the overall transport path. It is, however, likely that, where the migrating radionuclides encounter higher-transmissivity features, low transmissivity fractures between the near-field / geosphere interface and some point within the geosphere, perhaps a few tens of metres away, dominate the transport resistance.

Figure A-3 shows transport resistance plotted against transmissivity for transport path lengths of 10 m, 50 m and 100 m, where transmissivity is to be understood as the transmissivity of fractures intersecting the drift near a canister emplacement position, and transport path length is the assumed distance from the drift to the most highly transmissive features along the transport path.

The figure shows that, for a pessimistic transport path length of 10 m to the nearest higher-transmissivity fracture, a transmissivity of about 3×10^{-9} m²/s provides a transport resistance of the order of 10,000 years per metre, and thus a effective geosphere transport barrier for many safety-relevant radionuclides (this is roughly equivalent to the transmissivity giving rise to a maximum 0.1 litre per minute inflow during saturation).
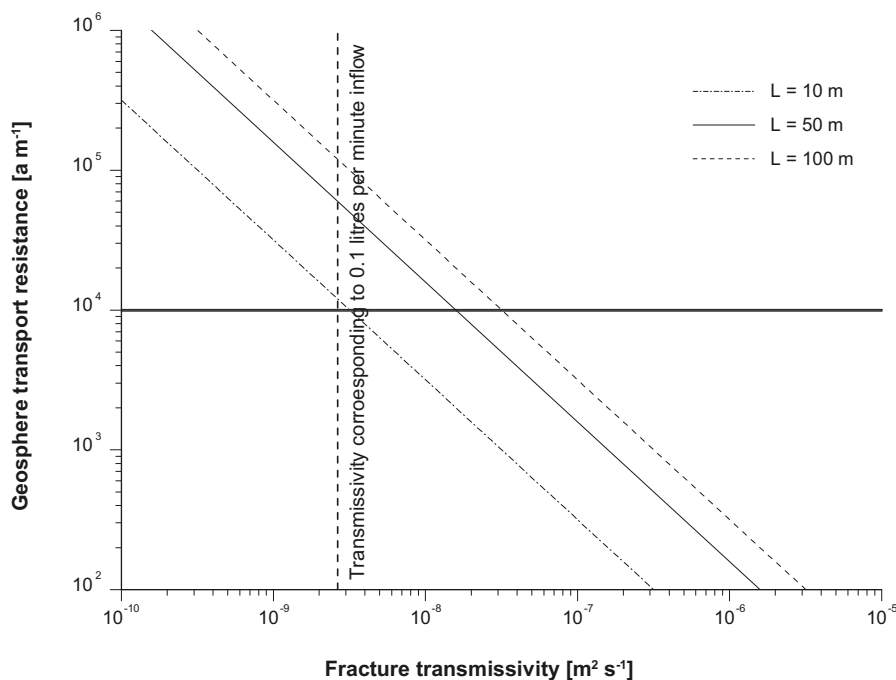
Figure A-3. *Transport resistance plotted against transmissivity for different transport path lengths. The figure indicates the fracture transmissivity which is assumed to give rise to a maximum 0.1 litre per minute inflow during saturation (see, however, the caveats given in Section (ii)).*

/Lanyon and Marschall 2006/ carried out steady state flow modelling using their discrete fracture representation of the Olkiluoto site, and evaluated transport resistances from various supercontainer deposition locations to the outer boundary of their model, 50 m from the modelled deposition drift. Histograms of the results for model drift W01T01, which were obtained using particle tracking, are shown in Figure A-4. The results show that none of the particle tracks gave transport resistances less than about 5×10^4 years m^{-1}, the highest value being obtained for supercontainer location W01T01:CO16. The results for other modelled drifts gave still higher minimum transport resistances (see Figure B-3 parts b-d in /Lanyon and Marschall 2006/. Figure A-5 shows particle tracks from which the lowest transport resistance was calculated (supercontainer location W01T01:CO16, which is circled in red). In this realisation of the DFN model, supercontainer location W01T01:CO16 is separated by a distance block from a 10 m section of filling blocks intersected by a fracture with a relatively high transmissivity of about 10^{-7} m^2/s. Even in this location, although the smallest transport resistance is about 5×10^4 years m^{-1}, the mean is about an order of magnitude higher.

This discussion suggests that an assumption of a transport resistance of 5×10^4 years m^{-1} is conservative for the purposes of geosphere transport modelling, and is assumed in analysing many of the assessment cases in the Radionuclide Transport Report /Smith et al. 2007b/.
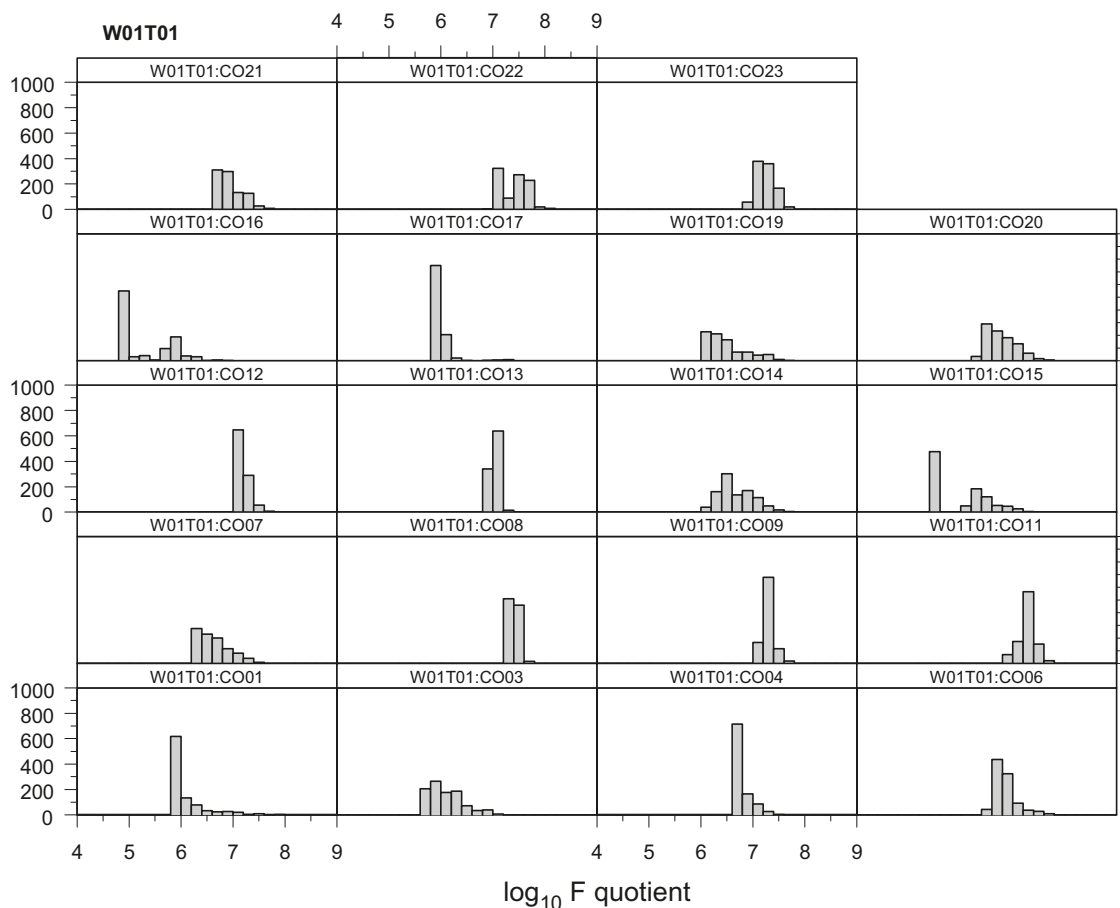
Figure A-4. *Histograms of transport resistances (termed here F quotient) from particles released at different supercontainer locations in a DFN model of the Olkiluoto site (after Figure B-3 of /Lanyon and Marschall 2006/).*
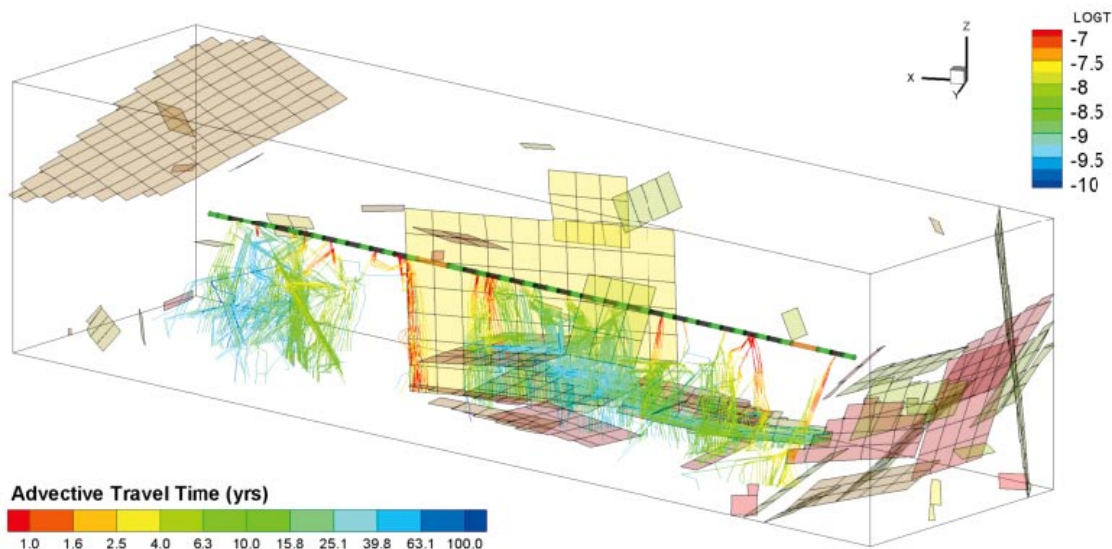
Figure A-5. *Particle tracks from supercontainer drift elements. Supercontainer location W01T01:CO16, which gives the lowest calculated transport resistances, circled in red. Tracks coloured by travel time. Features coloured by log transmissivity, only features with transmissivity greater than 10^{-8} m^2/s are shown (after Figure B-1 of /Lanyon and Marschall 2006/).*

A.4.5 Conclusions on the transmissivity criteria

The scoping calculations presented some above illustrate the potential impact of fracture transmissivity on various processes relevant to long-term safety.

Considering the possibility of failure by corrosion, the canister lifetime will remain well in excess of the minimum design lifetime of 100,000 years, irrespective of fracture transmissivity (the impact of perturbations to the buffer on canister lifetime is considered in App. B.7 of the Evolution Report, /Smith et al. 2007a/. Mechanical erosion of the buffer is shown to be irrelevant even at high transmissivities. In the case of chemical erosion due to the penetration of dilute glacial meltwater to repository depth, model uncertainties are probably too great to draw any firm conclusions regarding those fractures that should be avoided in emplacing supercontainers and distance blocks. It should, however, be noted that the next possibility for penetration of glacial meltwater to repository depth is in 70,000 years time and, even if advective conditions then become established in parts of the buffer, it will take time for canister failure to occur - thus the minimum design lifetime may still be achieved.

In terms of the transport barrier provided by the geosphere, a 10 m long transport path having a transmissivity of about 3×10^{-9} m^2/s provides a transport resistance in the order of 10,000 years per metre, which corresponds to an effective geosphere transport barrier for many safety-relevant radionuclides. This is also roughly the transmissivity giving rise to a maximum 0.1 litre per minute inflow during saturation - i.e. the maximum inflow if the possibility of piping and erosion is to be avoided - see, however, the caveats given in Section (ii).

Overall, it is concluded that a transmissivity limit of about 3×10^{-9} m^2/s for fractures intersecting the drift at canister and buffer emplacement locations desirable from the point of view of long-term safety. This criterion is derived in the first place from considerations of the geosphere transport barrier, being the most restrictive of those described in this appendix. In practice, however, it is unlikely that a transmissivity criterion can be applied directly in selecting locations for canister and buffer emplacement. Characterisation of fractures intersecting the drift is likely to be based largely on observations made at the drift wall, and other quantities including inflow, that can be measured directly, rather than on transmissivities inferred from a model that are therefore subject to greater uncertainty.

There are various mechanisms, such as erosion by transient water flows, whereby some loss or redistribution of buffer mass may occur during the saturation of a KBS-3H repository – Sections 5.4 and 5.5 of the KBS-3H Evolution Report /Smith et al. 2007a/. The magnitude of the resulting changes in density affects whether many of the safety function indicator criteria on the buffer remain satisfied. Buffer density is a safety function indicator. The hydraulic conductivity and swelling pressure of the buffer, which are also safety function indictors, are functions of buffer density. They are also, however, functions of buffer pore water salinity, which will vary over time due to transient changes in the groundwater. This appendix discusses how, in the case of a KBS-3H repository at Olkiluoto, provided the saturated buffer density remains in the range of about 1,890 to 2,050 kg/m³ (the design density is 2,000 kg/m³), changes in swelling pressure and hydraulic conductivity caused by salinity variations are expected to be minor, and the criteria on the buffer safety function indicators will continue to be met.

A.5 Range in buffer densities ensuring that relevant safety function indicators are satisfied for a KBS-3H repository at Olkiluoto

The upper bound for saturated buffer density that the buffer can be assumed to perform its safety functions (2,050 kg/m³) is taken directly from Table A-2 and is based on the requirement on the buffer to protect the canisters in the event of rock shear movements. The lower bound of 1,890 kg/m³ is derived firstly from the requirement on the buffer to prevent significant microbial activity. The corresponding safety function indicator criterion given in Table A-2 is a swelling pressure of 2 MPa. Studies indicate that bacterial activity will be suppressed, and both culturability and viability will decrease, at swelling pressures exceeding 2 MPa /Stroes-Gascoyne et al. 2006, Masurat 2006/. It is likely that microbes are barely active under these conditions (although this is an issue that is still under investigation). Below about 2 MPa, however, significant microbial activity cannot be excluded. This lower bound for swelling pressure is met for 0.3 M NaCl solution (corresponding roughly to the present-day 10–20 g per litre total dissolved solids – TDS – at Olkiluoto) if the dry density is above about 1,300 kg/m³ (1,830 kg/m³ saturated) (see Figure 4-7 of /SKB 2006a/). A conservative estimate of the maximum salinity that could occur at a depth of about 550 m at Olkiluoto at future times is 30–45 g per litre. There is currently about 12 g per litre of TDS at repository depth (420 m below ground), which may rise transiently to around 25 g per litre as a result of the upconing associated with excavations, before decreasing again as a result of continuing post-glacial uplift (Figure 4-1 of /Smith et al. 2007a/. For a 1 M NaCl solution (which corresponds to about 60 g per litre TDS) a 2 MPa swelling pressure is achieved at a dry density of about 1,400 kg/m³ (1,890 kg/m³ saturated).

In addition to preventing significant microbial activity, a saturated density of 1,890 kg/m³ will prevent colloid-facilitated radionuclide transport (Table A-2 of the present appendix – see also Section 2.5.4 of /SKB 2006c/ for further discussion). Furthermore, since the swelling pressure will never be less than 2 MPa, irrespective of salinity variations in the expected range, it will also prevent the possibility of canister sinking and ensure tightness at the drift wall and self sealing capability (Table A-2). Finally, it will ensure diffusion-dominated transport in the buffer, given that hydraulic conductivities of less than 10^{-12} m²/s are measured in MX-80-type bentonite in saline conditions at dry densities above about 1,200 kg/m³ (1,760 kg/m³ saturated) (see Figure 4-8 of SKB 2006a). Diffusion dominates over advection as a transport process at these low conductivities.

References

Börgesson L, Hernelind J 2006. Consequences of loss or missing bentonite in a deposition hole. SKB TR 06-13. Svensk Kärnbränslehantering AB, Sweden.

Gribi P, Johnson L, Suter D, Smith P, Pastina B, Snellman M, 2007. Safety assessment for a KBS-3H spent nuclear fuel repository at Olkiluoto - Process Report, POSIVA 2007-09 and SKB R-08-36. Posiva Oy, Olkiluoto, Finland and Svensk Kärnbränslehantering AB, Sweden.

Hartikainen J, 2006. Numerical simulation of permafrost depth at Olkiluoto. Posiva Working Report 2006-52. Posiva Oy, Olkiluoto, Finland.

Lanyon G W, Marschall P, 2006. Discrete fracture network modelling of a KBS-3H repository at Olkiluoto. POSIVA 2006-06 and SKB R-08-26. Posiva Oy, Olkiluoto, Finland and Svensk Kärnbränslehantering AB, Sweden.

Liu J, Neretnieks I, 2006. Physical and chemical stability of the bentonite buffer. SKB R-06-103. Svensk Kärnbränslehantering AB, Sweden.

Masurat P, 2006. Potential for corrosion in disposal systems for high-level radioactive waste by Meiothermus and Desulfovibrio. Doctoral thesis. Göteborg University, Sweden.

Pastina B, Hellä P, 2006. Expected evolution of a spent fuel repository at Olkiluoto. Posiva 2006-05. Posiva Oy, Olkiluoto, Finland.

Posiva, 2006. Nuclear Waste Management of the Olkiluoto and Loviisa Power Plants: Programme for Research, Development and Technical Design for 2007-2009. TKS-2006. Posiva, Olkiluoto, Finland.

SKB, 2006a. Long-term safety for KBS-3 repositories at Forsmark and Laxemar – a first evaluation – Main report of the SR-Can project. SKB TR-06-09. Svensk Kärnbränslehantering AB, Sweden.

SKB, 2006b. Data report for the safety assessment SR-Can. SKB TR-06-25. Svensk Kärnbränslehantering AB, Sweden.

SKB, 2006c. Buffer and backfill process report for the safety assessment SR-Can. SKB TR-06-18. Svensk Kärnbränslehantering AB, Sweden.

Smith P A, Johnson L H, Snellman M, Pastina B, Gribi P, 2007a. Safety assessment for a KBS-3H spent nuclear fuel repository at Olkiluoto – Evolution report. Posiva 2007-08 and SKB R-08-37. Posiva Oy, Olkiluoto, Finland and Svensk Kärnbränslehantering AB, Sweden.

Smith P, Nordman H, Pastina B, Snellman M, Johnson L, 2007b. Safety assessment for a KBS-3H spent nuclear fuel repository at Olkiluoto – Radionuclide transport report. Posiva 2007-07 and SKB R-08-38. Posiva Oy, Olkiluoto, Finland and Svensk Kärnbränslehantering AB, Sweden.

Stroes-Gascoyne S, Hamon C J, Kohle C, Dixon D A, 2006. The effects of dry density and porewater salinity on the physical and microbiological characteristics of highly compacted bentonite. Ontario Power Generation Report No: 06819-REP-01200-10016-R00.

Vieno T, Nordman H, 1999. Safety assessment of spent fuel disposal in Hästholmen, Kivetty, Olkiluoto and Romuvaara TILA-99. Posiva 99-07. Posiva Oy, Helsinki, Finland.

Vieno T, Hautojärvi A, Koskinen L, Nordman H, 1992. TVO-92 Safety Analysis of Spent Fuel Disposal. Report YJT-92-33E. Nuclear Waste Commission of Finnish Power Companies, Helsinki, Finland.

Pressure increase rate in KBS-3H deposition drifts

Project 67060267.SAFCA

By Pirjo Hellä, Pöyry Environment Oy. 2006.

B.1 Introduction

This document presents estimates of the possible pressure increase rate in a single supercontainer section of the KBS-3H layout adaptation. The estimates are based on Olkiluoto specific data to the extent possible. The estimates are primarily derived for the planning of buffer tests commencing during the year 2006 the pressure increase rate being one significant test parameter.

The work has been conducted to KBS-3H design subproject managed by J. Autio (Saanio & Riekkola Oy).

This appendix has been edited by Pirjo Hellä based on the contributions by Jorma Autio, Saanio & Riekkola Oy (KBS-3H Repository Design and Problem Description), Lasse Koskinen, VTT Processes (Analytical solution), Antti Poteri VTT Processes (Appendix 1), Henry Ahokas, Pöyry Environment Ltd (Olkiluoto field data and interpretation of field data) and Joonas Klockars, Pöyry Environment Ltd (data processing). Comments by Aimo Hautojärvi, Posiva Oy; Bill Lanyon, Fracture Systems; Sven Follin, SF GeoLogic and Ingvar Rhén, Sweco and discussions on meeting organized at Saanio & Riekkola April 3, 2006 have been taken into account.

B.2 General description of KBS-3H repository design

KBS-3H design is a variation of KBS-3 method and an alternative to KBS-3V design. KBS-3H design is based on emplacement of spent fuel canisters in horizontal direction in contrary to KBS-3V design where the canisters are emplaced in vertical direction, see Figure 1. The repository is planned to be build at the depth of –420 m below sea level.

In KBS-3H design, the canister and buffer are placed in a perforated steel container, and together constitute the "supercontainer" (see Figure 2), which is emplaced in a long horizontal drift. A distance plug of compacted bentonite is emplaced between each supercontainer to obtain proper mutual thermal spacing and isolation.

One of the most important functions of the distance block is to seal the drift section between the supercontainers in order to prevent flow and advective transport along the drift. The sealing and plugging is assumed to occur when the distance block absorbs water (saturates), swells and obtains proper swelling pressure.
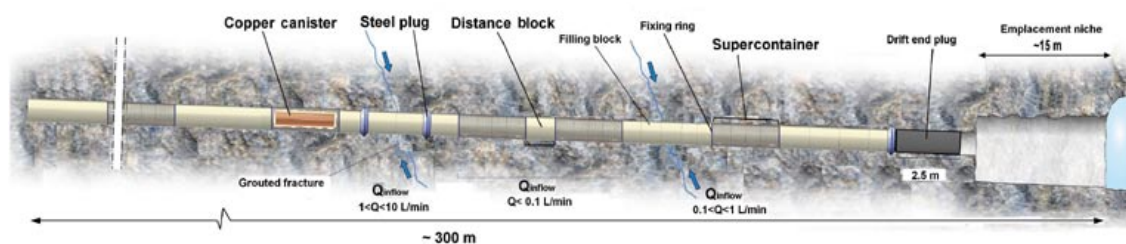

Figure 1. *Principle of KBS-3H drift. The canister is copper coloured.*
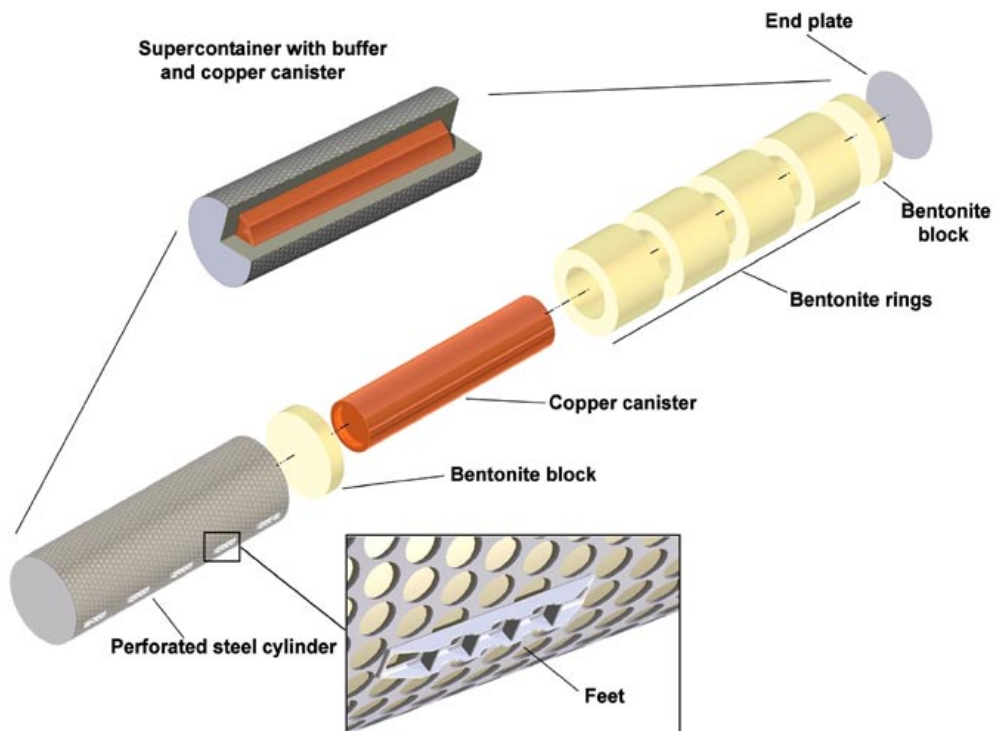
Figure 2. *The buffer and canister are embedded in a steel supercontainer in KBS-3H design.*

There are two different variations (called candidate designs) of KBS-3H design: a) Basic Design (BD) and b) design based on Drainage, Artificial Watering and air Evacuation (DAWE). BD alternative is based on assumption that the distance blocks will seal the supercontainer units in wet sections stepwise in sequence independently of each other. In DAWE design the drift is filled with water after plugging and sealing the drift compartment and the distance blocks will swell and isolate the supercontainer units simultaneously. These two KBS-3H candidate designs are at the moment being developed to proper level of details based on Olkiluoto bedrock data in order to evaluate the feasibility of the KBS-3H alternative in 2007.

B.3   Pressure increase rate, problem description

The research and development of distance block design in BD alternative has shown that it is possible that channelled flow (referred later as piping) through the distance block adjacent to the rock interface may occur if the distance block design is not proper /Börgesson et al. 2005/. This has been specified as one critical issue to be resolved and is addressed in present buffer tests /Autio et al. 2006/. The development of proper design is very sensitive to inflow rates (Q) from rock into the open volume (V, of the order of couple cubic meters) between supercontainer units (filling time of the open volume) and pressure increase rate and time until the full hydrostatic pressure is obtained after the volume has been filled with water, see Figure 3.

In this memo, an estimate for the pressure increase from the initial atmospheric pressure to full hydrostatic pressure of 4 MPa with time in the supercontainer section is derived based on two simplified cases. In the first case, a) the supercontainer section is assumed to be tight with no air escape and the other case b) considers the saturated case with no trapped air. The two idealised cases are illustrated in Figure 4. The interest is to study the early behaviour of the supercontainer sections with highest allowable inflows in the range of 0.1 l/min to 1 l/min.

In these cases, it has been assumed that the supercontainer package is stiff and the effect on pressure increase is insignificant on the basis that the water absorption rates to supercontainer are small (order of 0.01 l/min, about 1% of largest inflow rates of 1 l/min) and the buffer blocks inside the supercontainer have been compressed at 100 MPa pressure without significant defor-
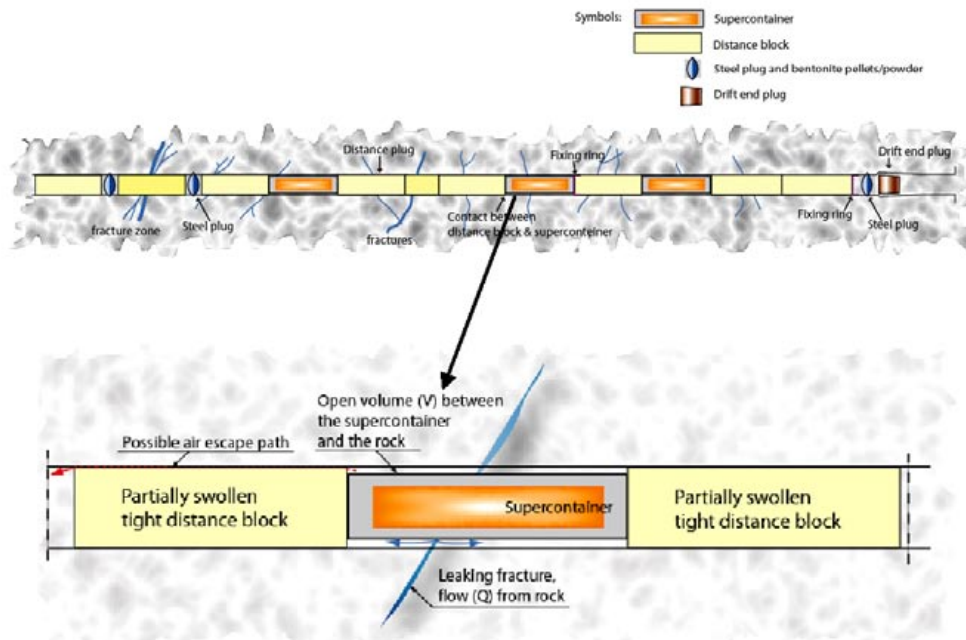
Figure 3. *The function of distance blocks depends on inflow rates buffer and canister is embedded in a steel supercontainer in KBS-3H design.*

mation during removal from form. Therefore no storage is assumed to be related to bentonite. Considering case a) only the void space in the tunnel is taken into account as it is assumed that the flowing water will flush the air from the fractures. Also, temperature effects are neglected. Despite the many simplifications, it is thought the two cases give an idea of the factors affecting the pressure increase.

B.4   Field data and observations

The repository will be placed in a heterogeneous, fractured rock, where the inflow to the drifts will take place mainly from single fractures. Posiva Flog Log /Öhberg and Rouhiainen 2000/ has been systematically used to measure the hydraulic conductivity in the rock and the method enables detection of single flowing features even in the fracture scale. The theoretical lower limit of the Posiva Flow Log is in the order of 30 ml/h, but in practice the detection limit can be vary due to the applied draw-down and borehole conditions e.g. to borehole wall roughness, solid particles and gas bubbles in water and high flow rate along the borehole (see e.g. /Pöllänen et al. 2005/) meaning that that the lower limit of transmissivity is in the order of 10^{-9} m²/s. The flow data available from boreholes at the repository depth have been summarized by /Hellä et al. 2006/. The transmissivity of the test sections in this depth range are mainly below the detection limit, but occasionally transmissivities up to 10^{-6} m²/s are observed. Based on design requirements on the maximum allowable inflow, the highest transmissivities in the supercontainer sections are in the order of 10^{-8} m²/s. This estimate is based on the relationship between inflow and transmissivity given by the Thiem's equation (Equation 2), assuming steady state radial flow with constant head, radius of influence of 50 m and drift radius of appr. 1 m.

In the following, few examples are given on the observed responses of the rock on the pressure changes. It can be assumed that the pressure and flow field in the hydraulic tests in the boreholes is similar to those in the saturated drift. Naturally the dimensions of a borehole and applied test sections (2 m) are not comparable to the drift. Furthermore, some storage is likely related to the packers. The examples consider pressure build-up tests /Öhberg et al. 2006ab/ in the pilot holes and observed pressure recovery in constant head injection tests carried out as a part of the standard characterization programme /Hämäläinen 1997a–d, 2003a–c, 2004, 2005/. The referred reports describe the measurements and applied techniques in detail.
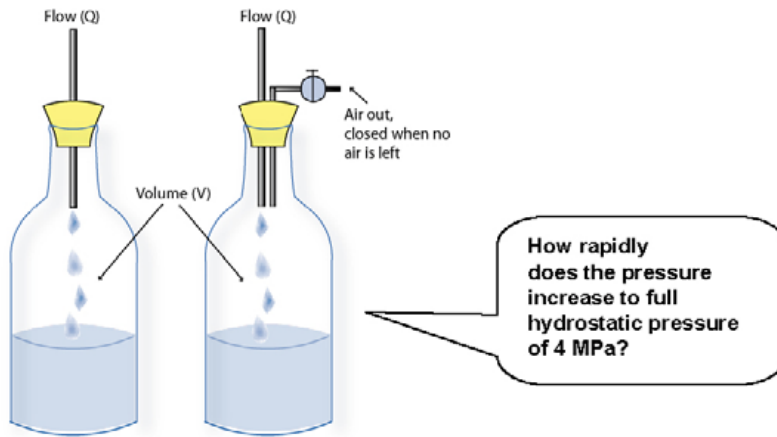
Figure 4. *Simplification of the two cases for pressure increase: a) Air remains in the supercontainer section (on left) and b) air escapes from the supercontainer section (on right). Note: Q is of the order from 0.1 to 1.0 l/min and V is of the order of a couple cubic metres. The maximum pressure of flow and therefore the final pressure in bottle is the full hydrostatic pressure of 4 MPa.*

Pressure buildup tests in pilot holes

Pressure build up tests were done in two pilot holes in ONKALO, OL-PH3 and OL-PH4. OL-PH3 is sub-horizontal, 150 m long borehole in depth range –60 to –70 m below sea level. OL-PH4 is sub-horizontal, 75 m long borehole in depth range –77 to –84 m below sea level. Diameter of both of the boreholes is 76 mm. The pressure build-up observed in the tests is shown in Figure 5. There are uncertainties related to the tests. In OL-PH4 the flow was not necessarily stabilized before the buildup phase, the last measured value was close to 85 l/min. From OL-PH3 there is no data available of the pressure in the borehole prior to the buildup phase. In OL-PH3 the flow was likely stabilized prior to the pressure buildup phase and was 6.2 l/min. In both of the tests the pressure increase was nearly instantaneous, several hundreds kPa within seconds in OL-PH4 and within minutes in OL-PH4. The results are not very representative for the deposition drift or the supercontainer position, because the inflows are so high and they summarize the flow from several fractures along the whole borehole with length corresponding to several supercontainer sections. The flow field in the upper parts of the rock is likely different from the repository depth. Still, the tests indicate that the pressure increase can be very rapid. Based on the straight-line part of OL-PH3, the head of 50 m is reached within about 3 minutes meaning pressure increase about 10 MPa/hour.
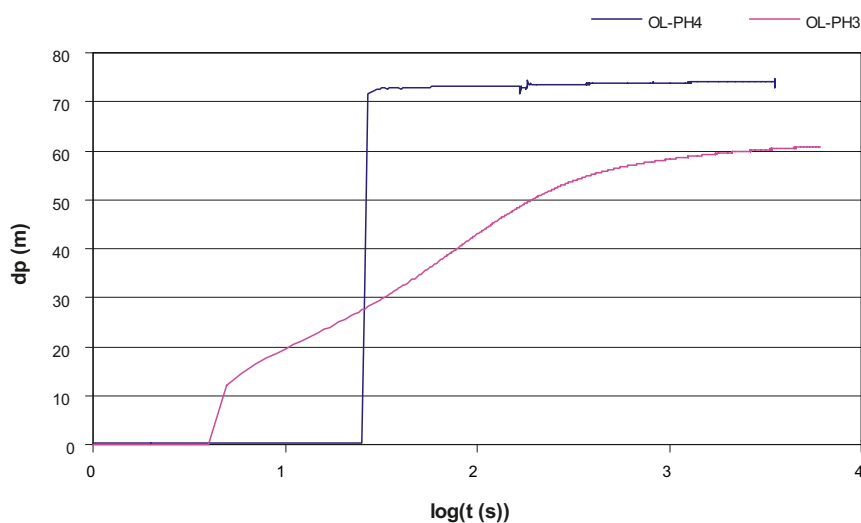

Figure 5. *Pressure increase in the pressure build-up tests in pilot holes OL-PH3 (flow prior to build-up phase 6.2 l/min) and OL-PH4 (flow prior to build-up phase 83 l/min).*

136

Pressure decrease in constant head injection tests

During a constant head injection tests (HTU-tests), there is an overpressure in the test section, typically around 200 kPa. The flow and pressure during the injection and fall of phases are monitored. An example of typical flow and pressure curves observed in HTU-measurements are presented in Figure 6. For the estimation of the pressure increase rate some representative test section were selected for a brief analysis. The selected intervals (data from / Hämäläinen 1997a–d, 2003a–c, 2004, 2005/):

- have T at highest in the order of 10^{-8} m²/s,
- have only one single flowing fracture or a narrow zone,
- are located in depth range of 400 – 500 m and outside deformation zone and.

The selected field data from the constant head injection tests (HTU) and flow logging are summarized in Table 1. Note that the observed transmissivity of the test section is the sum the all flowing features in the test section, but due to the similarity of the results of HTU- and Posiva flow log measurements and the way these sections were selected, the flow most likely comes from a single fracture.

Summary of the observed pressure decrease rates in the selected HTU-test sections is shown in Figure 7. The pressure decrease rate shows a rather large variety and is not clearly dependent on the conductivity of the interval. The decrease of pressure can be in the order of 150 to 200 kPa in about 2 minutes i.e. around 5 to 10 MPa/h even for fractures having transmissivities in the order $10^{-9} – 10^{-8}$ m²/s.

OLKR1 569.03-571.03 m
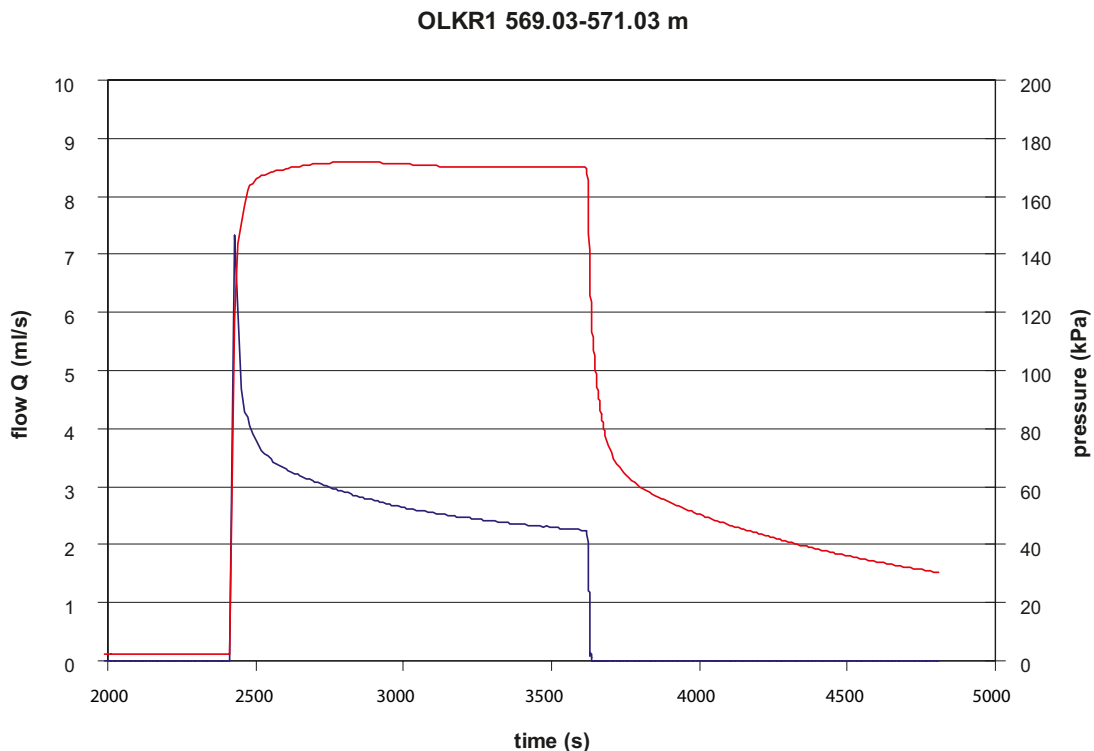
Figure 6. *An example of typical flow (in blue) and pressure (in red) curve in HTU measurement. Transmissivity in this section is 4–5×10⁻⁸ m²/s (data from /Hämäläinen 1997a/).*

Table 1. Selected test intervals and their transmissivity. Length of the test sections in HTU measurements was 2 m (data from /Hämäläinen 1997abcd, 2003abc, 2004, 2005/ (HTU and /Rouhiainen 2000, Pöllänen and Rouhiainen 2001, 2002/ (Posiva flow log)).

| Borehole | Ø mm | HTU | | | Posiva flow log | |
		Start length (m)	end length (m)	T_{2m} (m²/s) calculated from K_{Moye}	Depth (m)	T (m²/s)
OL-KR1	56	569,03	571,03	7,40E–08	568,6	5,19E–08
		368,00	370,00	2,00E–09	368,1	–
OL-KR2	56	610,11	612,11	1,50E–08	613,9	5,11E–09
		631,15	633,15	2,60E–09	630,4	7,38E–10
		542,90	544,90		543,5	2,36E–09
OL-KR4:	56	508,15	510,15	2,60E–08	510,2	1,79E–08
		562,23	564,23	7,40E–09	564,1	1,22E–08
OL-KR7:	56	414,00	416,00	1,92E–09	414,8	2,85E–09
OL-KR10:	76	320,52	322,52	7,00E–09	320,9	5,97E–09
		366,59	368,59	2,20E–09	367,2	3,96E–09
		416,68	418,68	6,40E–09	417,1	7,73E–09
		496,80	498,80	9,60E–09	499,7	6,93E–09
		366,00	368,00	4,40E–09	367,2	3,96E–09
		416,00	418,00	1,04E–08	417,1	7,73E–09
		498,00	500,00	1,24E–08	499,7	6,93E–09
OL-KR13:	76	325,00	327,00	1,36E–08	325,5	2,41E–08
		365,00	367,00	2,40E–09	363,9	6,46E–08
		415,00	417,00	1,42E–08	417,9	7,05E–09
OL-KR14:	76	329,00	331,00		329,9	3,00E–09
		447,00	449,00		448,2	1,69E–08
		475,00	477,00		476,8	3,10E–09
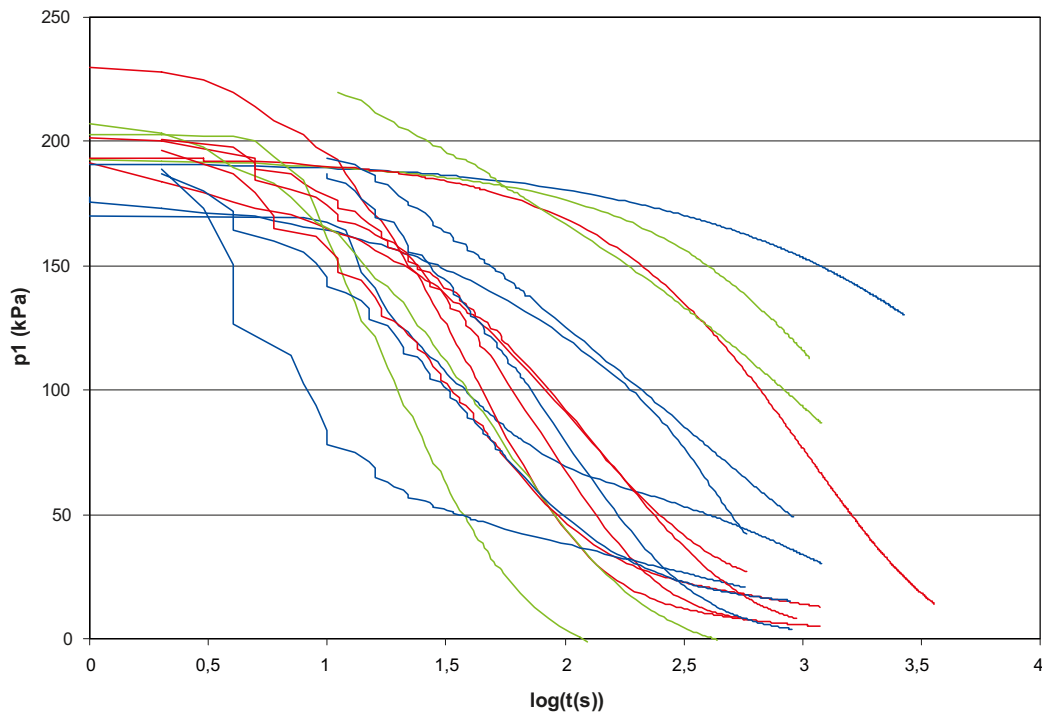
Figure 7. *Pressure decrease in the selected 2 m test intervals in HTU measurements as function of logarithm of the time (t = 0 is the start of pressure recovery). In blue intervals with T = 10⁻⁸ – 10⁻⁷ m²/s, in green intervals with T = 5×10⁻⁹ – 10⁻⁸ m/s and in red intervals with T < 5×10⁻⁹ m/s.*

B.5 Estimates based on Theis's and Thiem's equation assuming radial flow

The rate of pressure change after closing a KBS-3H tunnel may be estimated with the well known Theis's equation that describes a transient pressure/hydraulic head field s induced by a fixed pumping rate applied at a point-like source/sink in an infinite aquifer. No storage term is assumed, thus the estimate gives the upper limit of the pressure increase rate. Neither the skin factor is taken into account, in reality due to the skin effect the inflow into open tunnel will be less than the one observed in the boreholes. This estimation is related to the case b) in Chapter 3 and Figure 4.

The Theis's solution, describing a radial field, is written as

$$s = \frac{Q_w}{4\pi T} W(u); \quad W(u) = \int_u^\infty \frac{e^{-y}}{y} \, dy; \quad u = \frac{r^2}{4t}\left(\frac{S}{T}\right) \qquad \text{Equation 1}$$

where Q_w is the strength of the sink/source (flow rate), S is the storativity, T is the transmissivity, r is the distance from the well or tunnel and t is the time. The pumping rate may be estimated, in turn, with the Thiem's equation

$$Q_w = \frac{2\pi T \Delta h}{\ln(r/r_w)} \qquad \text{Equation 2}$$

It can be seen from the equations above that the behaviour of the head is determined by the storativity to transmissivity ratio S/T. With small S/T ratio, the pressure increase is rapid and the larger the ratio is the slower the pressure increase.

There are hardly any site-specific estimates of storativity needed for the analytical solution (Equation 1). Most relevant data for transmissivities in the order of 1×10^{-8} m^2/s is based on interference tests at Äspö where up to 80 observation sections were used and means of the results together with theoretical limit are shown in Figure 8. The theoretical limit is based on equation where compressibility range of rock and fluid together with other parameters are taken into account (see details in /Rhén et al. 1997/ p. 216 in TR97-06).
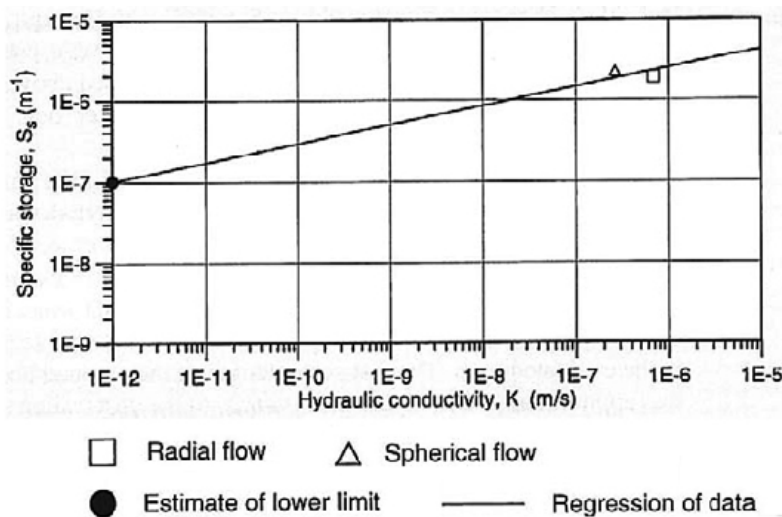

Figure 8. *Relationship between specific storativity S_s and hydraulic conductivity K according to /Rhén et al. 1997/.*

Based on Figure 8, the range of S/T ranges from 15 to 500 for T-values between 1×10^{-9}–1×10^{-7} m²/s correspondingly. For T = 1×10^{-8} m²/s the S/T is appr. 100. These values can likely be considered as an upper limit. SKB has revised the applied relation between the storativity and transmissivity and use now the following relationship /SKB 2005/:

$$S = 7E\text{–}4 \cdot T^{0.5} \qquad\qquad\qquad \text{Equation 3}$$

Equation 3 results in S/T to be in range from 2 to 20, if T is in range of $1\times10^{-9} - 1\times10^{-7}$ m²/s. The relationship is based on larger and minor zones, and give lower values of S for low T-values than estimated based on e.g. Figure 8. Based on the data from Prototype Repository at Äspö Rhén has proposed also following relationships between S and T, which would be more appropriate for fracture scale, but not applicable to larger fracture zones:

$$S = 0.0269 \cdot T^{0.64} \qquad\qquad\qquad \text{Equation 4}$$

$$S = 2.18 \cdot T^{0.919} \qquad\qquad\qquad \text{Equation 5}$$

These estimates are based on the assumption of radial flow around the tunnel. According to Equations 4 and 5, S/T is estimated to be in range from 8 to 50, if T is in range of 1×10^{-9}–1×10^{-7} m²/s, i.e. somewhat higher than based on Equation 3. The results are uncertain and in reality storativity S could be in range of 0.1S to 10*S. As a result in the transmissivity range of interest, the S/T is likely to be in range from 1 to 1,000.

Thus assigning following values to Equation 2:

r = 500 m,

rw = 0.925 m equal to the drift radius,

Δh = 500 m equal to present approximated maximum repository depth, and

T = 10^{-8} m²/s, estimated to be in the order of largest transmissivities observed in the drifts.

one obtains Q_w = 0.3 litres/min. With this flow rate we now calculate the response s for the values of S/T = 1, 10, 100, 1,000 s/m² according to Equation 1, see Figure 9. For the second case (S/T = 100 s/m²), an approximate rate of change Δs/Δt is calculated with Matlab's diff function (Figure 10). The maximum rate of change with S/T = 100 s/m² is 0.7 m/s corresponding to appr. 25 MPa/h. Correspondingly, for S/T = 1 s/m² the maximum pressure increase rate would be 2,500 MPa/h and for S/T = 1,000 s/m² 2.5 MPa/h.

The analytical solution, Theis's equation (Equation 1) is valid for a pointlike sink and it has limited applicability in a case like this as the sink, the gap in supercontainer section is a finite-diameter circle. The early behaviour of the pressure corresponding of Theis's solution reflects a time lag needed by the pressure response to reach the distance of r_w from the point-like source at the origin. Still the results are representative for the time period describing the pressure increase taking place after the void space is being filled with inflowing water. This has been confirmed by comparing the analytic solution and numeric results obtained with COMSOL Multiphysics (v. 3.2), showing that the results do not differ significantly after the very early phases and before long times. After a long time Theis solution departs from the numerical one as the former is not limited in time. In the analytic solution based on Theis's equation, the flow rate has been assumed to be constant, whereas in the numerical solution head relative to the depth has been instantaneously changed to no flow boundary condition. So neither of the solution takes into account the gradually reducing flow rate occurring in the natural conditions and therefore the maximum pressure increase rates overestimate the ones to be observed in the real tunnel. A considerable uncertainty is related also to the S/T values.
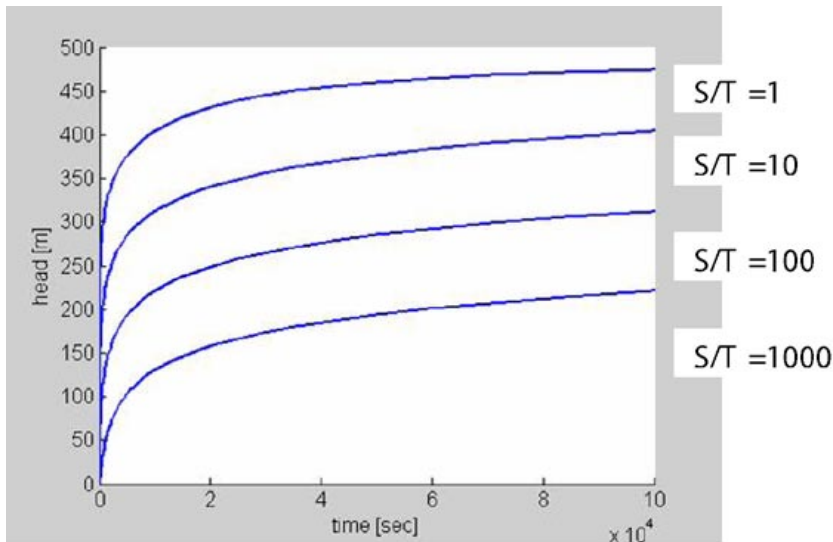
Figure 9. *The time evolution of the head with respect to the z = –500 m datum for S/T values of 1, 10, 100 and 1,000 s/m².*
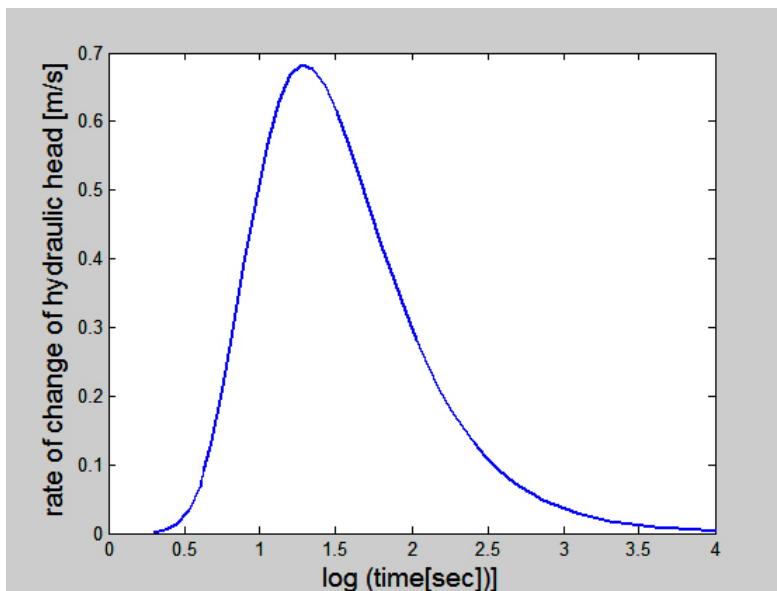

Figure 10. *Approximate rate of change of the drawdown for S/T = 100 s/m².*

B.6 Estimate based on pressure build-up assuming no gas escape from the supercontainer section

A case where water flow into a closed section of tunnel is discussed below. At the beginning the tunnel is not saturated by water. The pore space is filled by air that is not able to escape from the closed tunnel section. This situation can be conceptualised by a closed container that is filled by the inflowing water (Figure 11). It is assumed that the inflowing water comes along a fracture that is connected to a large reservoir of water that is able to maintain constant pressure (P_r). The evolution of the water inflow rate and build-up of the pressure inside the closed section of the tunnel is governed by the compression of the air.

It is assumed that the trapped air behaves as a perfect gas. It is also assumed that there is no gas in the fractures (i.e. the flowing water flushes the gasses away from the fractures). Dissolution of the gas/air into the water is not taken into account because it is regarded to be a slow process compared to the water inflow.

The closed section of tunnel contains bentonite. Water leakage to the bentonite is not taken into account. The leakage is assumed to be small, and on the other hand, the bentonite swells about the amount of water intake. This means that leakage to the bentonite does not affect the pressure build-up process considered in this study.

It is assumed that at the beginning there is a pressure P_o in the void space. The volume of the void space is V_o. Water flows to the void space through a fracture that is connected to a constant pressure of P_r in the bedrock. Then the flow rate to the tunnel is

$$\frac{dV(t)}{dt} = k\,\Delta P(t) = k\,(P_r - P(t)),\tag{1}$$

where $P(t)$ is the time dependent pressure in the void space of the tunnel and k is the conductance of the fracture. The flowing groundwater fills up the void space in the tunnel. This causes a pressure build-up in the void space, because the void space is filled by the inflowing water

$$P(t) = \frac{P_o V_o}{V_o - V(t)},\tag{2}$$

where $V(t)$ is the total volume of water that has entered tunnel during the time [0,t].

Substituting (2) to (1) and solving the equation for the initial condition $V(0) = 0$ gives

$$V(t) = \frac{V_o}{P_r}\left\{ P_r - P_o - P_o\,\mathbf{W}\!\left[\frac{P_r - P_o}{P_o}\,\mathbf{Exp}\!\left[\frac{P_r(V_o - k\,P_r t)}{P_o V_o} - 1\right]\right]\right\},\tag{3}$$

where $\mathbf{W}(x)$ is a solution for W in $x = w\,\mathbf{Exp}(w)$.

Flow rate to the void space is calculated as a time derivate of (3)

$$\frac{dV(t)}{dt} = k\,P_r\left\{ 1 - \frac{1}{1 + \mathbf{W}\!\left[\frac{P_r - P_o}{P_o}\,\mathbf{Exp}\!\left[\frac{P_r(V_o - k\,P_r t)}{P_o V_o} - 1\right]\right]}\right\},\tag{4}$$

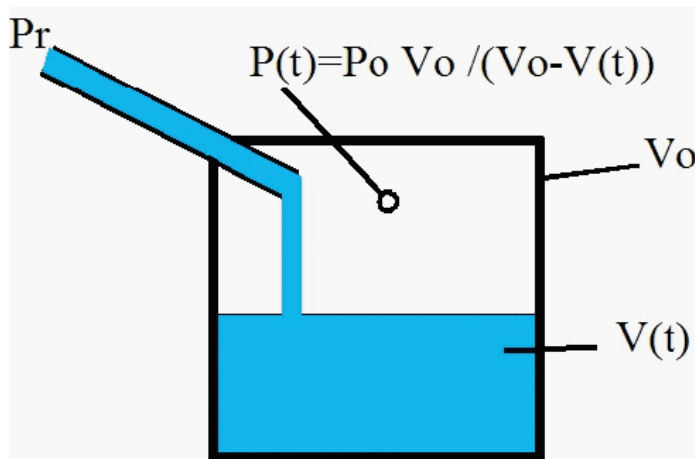Pressure in the void is given from (2) (or more easily using (1) and (4))

Figure 11. *Conceptualisation of the groundwater flow to open tunnel.*

$$P(t) = \frac{P_r}{1 + \mathbf{W}\left(\dfrac{P_r - P_o}{P_o} \mathbf{Exp}\left[\dfrac{P_r(V_o - kP_r t)}{P_o V_o} - 1\right]\right)} \quad ,$$ (5)

then the pressure build-up rate can be calculated as a time derivate of (5)

$$\frac{dP(t)}{dt} = \frac{kP_r^3}{P_o V_o} \frac{\mathbf{W}\left(\dfrac{P_r - P_o}{P_o} \mathbf{Exp}\left[\dfrac{P_r(V_o - kP_r t)}{P_o V_o} - 1\right]\right)}{1 + \mathbf{W}\left(\dfrac{P_r - P_o}{P_o} \mathbf{Exp}\left[\dfrac{P_r(V_o - kP_r t)}{P_o V_o} - 1\right]\right)} \quad ,$$ (6)

Equations (3) to (6) are below plotted for following cases:

Void space in the atmospheric pressure at the beginning and at the depth of 500 metres below the surface:

V_o = 1,500 litres

P_r = 5 MPa

P_o = 0.1 MPa.

Two different leakage rates are considered:

K = 60/5 litres/hour/MPa, this gives a leakage of about 60 litres/hour at the initial state

K = 6/5 litres/hour/MPa, this gives a leakage of about 6 litres/hour at the initial state.

The rationale to select these flow rates is that we cannot allow a leakage that is higher that 1 litre/min and a leakage that is smaller than 0.1 litre/min is not a problem.

Figures 12 and 13 show the integrated inflow to the void space with a leakage rate of 60 and 6 litres/hr, respectively.

Figure 14-15 shows the inflow rate with an initial leakage rate of 60 and 6 litres/hour, respectively. Figure 16-17 shows the pressure in the void space with a leakage rate of 60 and 6 litres/hour, respectively.

Figures 18 and 19 show the pressure buildup rate, with a leakage rate of 60 and 6 litres/hour respectively.

Assuming initial void space to be 1,500 l and either 1 l/min or 0.1 l/min initial inflow, the maximum pressure buildup rate is 1.6 MPa/h or 0.16 MPa/h respectively. The solution does not take into account the flow field.
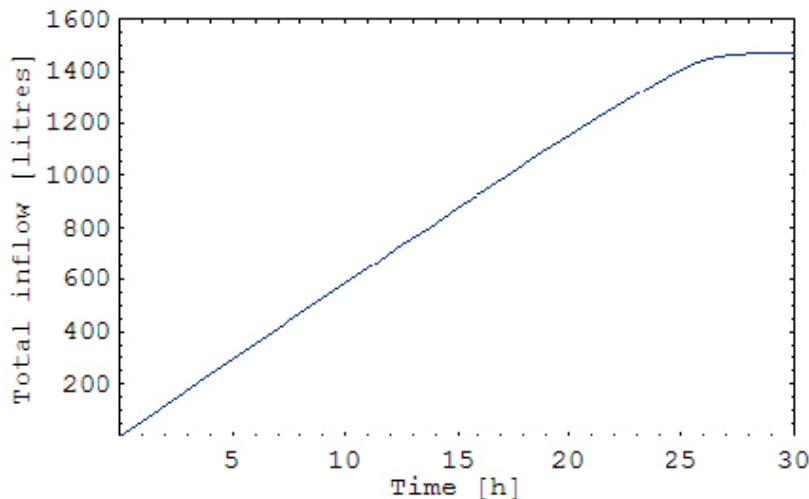

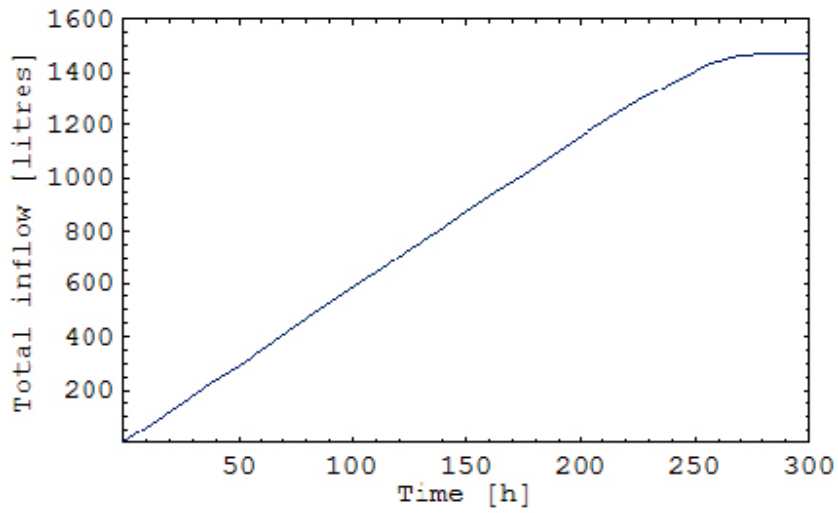**Figure 12.** *Integrated inflow to the void space. Leakage rate 60 litres/hour.*

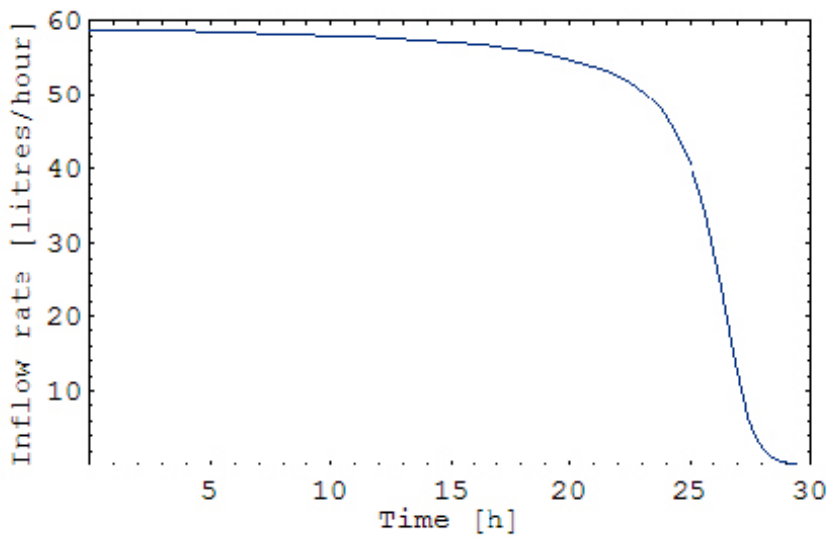***Figure 13.*** *Integrated inflow to the void space. Leakage rate 6 litres/hour.*

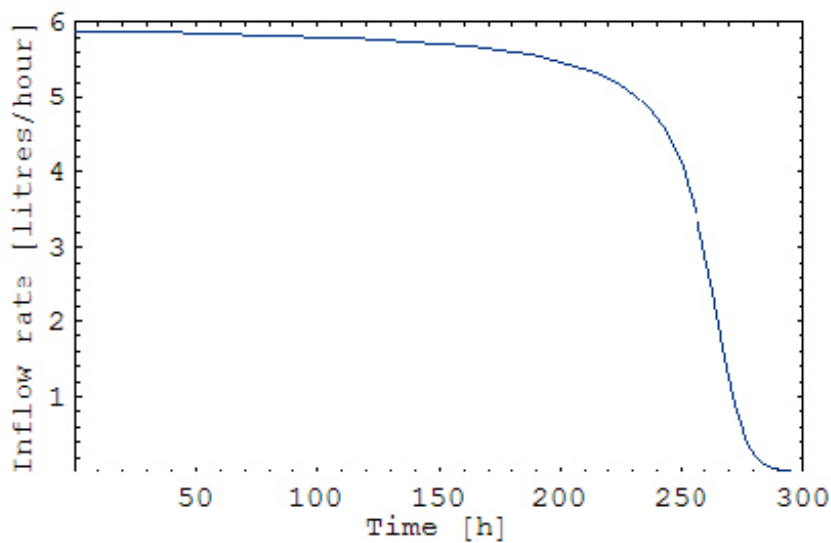***Figure 14.*** *Inflow rate. Leakage rate at the beginning 60 litres/hour.*

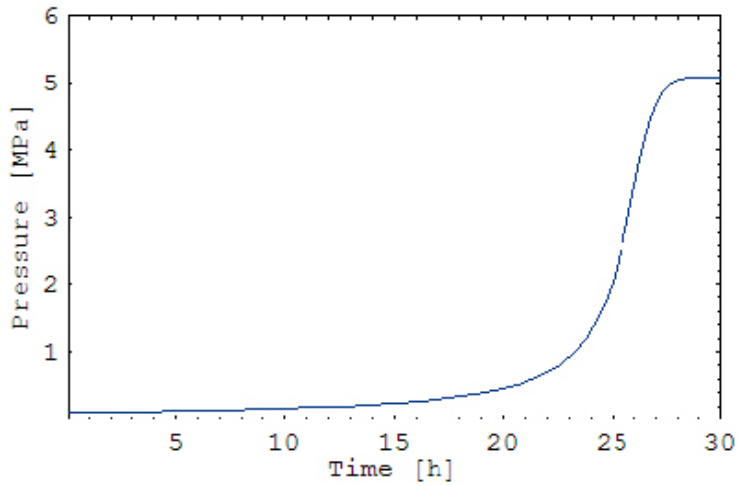***Figure 15.*** *Inflow rate. Leakage rate at the beginning 6 litres/hour.*

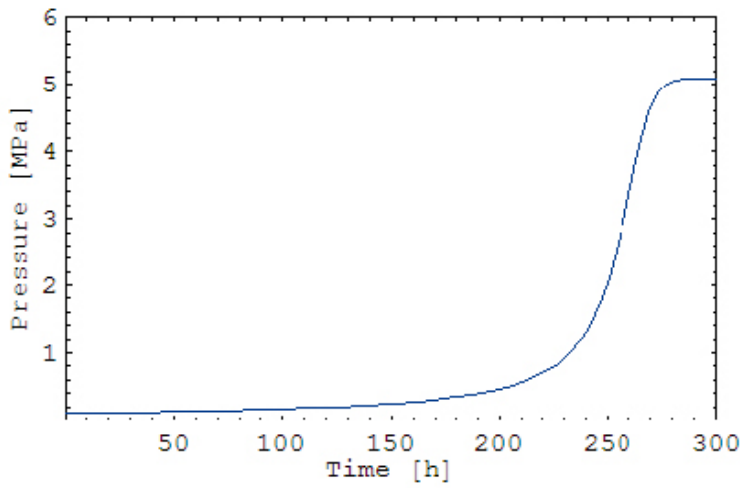**Figure 16.** *Pressure in the void space. Leakage rate at the beginning 60 litres/hour.*

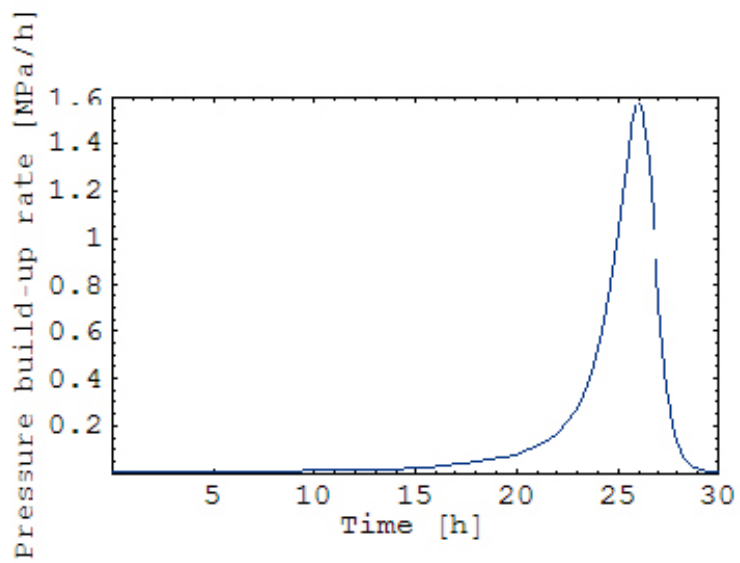**Figure 17.** *Pressure in the void space. Leakage rate at the beginning 6 litres/hour.*

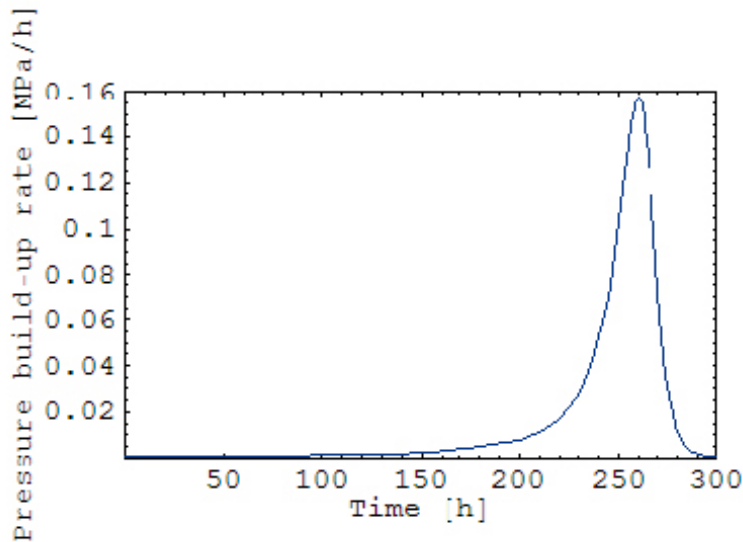**Figure 18.** *Pressure build-up rate. Leakage rate at the beginning 60 litres/hour.*

Figure 19. *Pressure build-up rate. Leakage rate at the beginning 6 litres/hour.*

B.7   Summary

This appendix presents some background data from the Olkiluoto and estimates of the possible pressure increase rates in the supercontainer section in KBS-3H type repository. High pressure increase rates are related to higher T-values, which are likely to be occasionally observed in the deposition drifts and supercontainer positions. High flows and rapid pressure changes can have detrimental effects on buffer and may lead to piping and transport of bentonite by erosion. All the estimates assume that the initial void space is filled with water gradually and the swelling of bentonite will not divide the initial void space to smaller compartments. This assumption can be considered reasonable as the interest is in the early behaviour of the supercontainer section and in sections with the largest allowable inflows, in the range of 0.1 l/min to 1 l/min.

In the pressure build-up tests in pilot holes and the constant head injection test (HTU), pressure changes in the order of 1 to 10 MPa/h have been observed. It can be assumed that the pressure and flow fields in the hydraulic tests in the boreholes are similar to those in the saturated drift. Naturally the dimensions of a borehole and applied test sections in HTU (2 m) are not comparable to the drift. The observed flow in the HTU tests is in the range of interest, but in the pressure-built up test the flow was clearly higher than expected in the supercontainer sections in real repository conditions.

Estimates of the pressure build-up were calculated assuming two cases a) a closed supercontainer section with no gas escape and b) considering the increase of hydraulic pressure after escape of the air (see Figure 4). Both estimates assume the supercontainer with the bentonite to remain rigid and not take the swelling into account. In case a) and assuming the initial void space to be equal to open space between the supercontainer and the drift wall, the maximum pressure build-up rate is 1.6 MPa/h (inflow 1 l/min) or 0.16 MPa/h (inflow 0.1 l/min). In case b) the estimate is based on the solution of Theis's equation and assuming radial flow, the estimate is depending on the storativity to transmissivity ratio S/T, which assumed to be in the range from 1 to 1,000. In case of S/T equal to 100, a value relevant for the drifts considering the estimated storativity and possible transmissivities of the fractures, the maximum pressure build-up rate can be as high as 25 MPa/h with lower S/T even higher. With larger S/T ratio value i.e. in practice lower transmissivity, the pressure build-up rate is decreased. The value of storativity is uncertain and site-specific data is lacking causing uncertainties in the estimations. Furthermore, the analytic solution does not take into account the changing flow rate, which means that the resulting pressure increase rates are upper limits for a given S/T value. The pressure increase rate is changing during the filling of supercontainer sections. In case b) (Figure 4) the pressure increase is very rapid after the air has escaped, whereas in case a) where there is significant

amount of trapped gas in the supercontainer section, the pressure increase starts significantly earlier and at slower rate than in the case when the air leaks out of the section.

It can be concluded that the presented values of pressure increase are rough estimates based on simplified cases neglecting many phenomena e.g. skin actually occurring in the drift, which can retard the actual pressure increase. Still, the estimates are considered to give an idea of the possible range of the pressure increase rate.

References

Autio J, Börgesson L, Sandén T, 2006. KBS-3H Buffer test plan 2005-2007 to resolve critical design and early evolution issues. Memorandum PROJEKTI-798-15/2006. Saanio & Riekkola Oy.

Börgesson L, Sandén T, Fälth B, Åkesson M, Lindgren E, 2005. Studies of buffer behaviour in KBS-3H concept. Work during 2002–2004. SKB R-05-50. Svensk Kärnbränslehantering AB, Sweden.

Hellä P, Ahokas H, Palmén J, Tammisto E, 2006. Analysis of geohydrological data for design of KBS-3H repository layout. Posiva Working Report 2006-16 and SKB R-08-27. Posiva Oy, Olkiluoto, Finland and Svensk Kärnbränslehantering AB, Sweden.

Hämäläinen H, 1997a. Measurements of hydraulic conductivity at Olkiluoto in Eurajoki, borehole OL-KR1. Working Report 97-03 (Vol 1 and 2). Posiva Oy, Helsinki, Finland (in Finnish).

Hämäläinen H, 1997b. Measurements of hydraulic conductivity at Olkiluoto in Eurajoki, borehole OL-KR2. Working Report 97-21 (Vol 1 and 2). Posiva Oy, Helsinki, Finland (in Finnish).

Hämäläinen H, 1997c. Measurements of hydraulic conductivity at Olkiluoto in Eurajoki, borehole OL-KR4. Working Report 97-45 (Vol 1, 2 and 3). Posiva Oy, Helsinki, Finland (in Finnish).

Hämäläinen H, 1997d. Measurements of hydraulic conductivity at Olkiluoto in Eurajoki, borehole OL-KR10. Working Report 97-47. Posiva Oy, Helsinki, Finland (in Finnish).

Hämäläinen H, 2003a. Complementary hydraulic conductivity measurements at Eurajoki, Olkiluoto, borehole OL-KR1. Working report 2003-27 b(Vol 1 and 2). Posiva Oy, Helsinki, Finland (in Finnish with an English abstract).

Hämäläinen H, 2003b. Complementary hydraulic conductivity measurements at Eurajoki, Olkiluoto, borehole OL-KR7. Working report 2003-47 (Vol 1 and 2). Posiva Oy, Helsinki, Finland (in Finnish with an English abstract).

Hämäläinen H, 2003c. Complementary hydraulic conductivity measurements at Eurajoki, Olkiluoto, borehole OL-KR10. Working report 2003-54 (Vol 1 and 2). Posiva Oy, Helsinki, Finland (in Finnish with an English abstract).

Hämäläinen H, 2004. Hydraulic conductivity measurements with HTU at Eurajoki Olkiluoto, borehole OL-KR13. Working report 2004-40 (Vol 1 and 2). Posiva Oy, Helsinki, Finland.

Hämäläinen H, 2005. Hydraulic conductivity measurements with HTU at Eurajoki Olkiluoto, borehole OL-KR14. Working report 2004-42 (Vol 1 and 2). Posiva Oy, Helsinki, Finland.

Pöllänen J, Rouhiainen P, 2001. Difference flow and electric conductivity measurements at the Olkiluoto site in Eurajoki, boreholes KR6, KR7 and KR12. Working Report 2000-51. Posiva Oy, Olkiluoto, Finland.

Pöllänen J, Rouhiainen P, 2002. Difference flow and electric conductivity measurements at the Olkiluoto site in Eurajoki, boreholes KR13 and KR14. Working Report 2001-42. Posiva Oy, Olkiluoto, Finland.

Pöllänen J, Pekkanen J, Rouhiainen P, 2005. Difference Flow and electric Conductivity Measurements at the Olkiluoto Site in Eurajoki, Boreholes KR19-KR28, KR19B, KR20B, KR22B, KR23B, KR27B and KR28B. Working Report 2005-52. Posiva Oy, Olkiluoto, Finland.

Rhén I, Gustafsson G, Wikberg P, 1997. Geoscientific evaluation 1997/5. Models based on site characterization 1986-1995. Technical Report TR-97-06. Svensk Kärnbränslehantering AB, Sweden (pages 214–217, 240–242).

Rouhiainen P, 2000. Electrical conductivity and detailed flow logging at the Olkiluoto site in Eurajoki, boreholes KR1-KR11. Working Report 99-72. Posiva Oy, Olkiluoto, Finland.

SKB, 2005. Preliminary Site description. Simpevarp sub-area – version 1.2. SKB R-05-08. Svensk Kärnbränslehantering AB, Sweden.

Öhberg A, Rouhiainen P, 2000. Posiva Groundwater Flow Measuring Techniques. Posiva-2000-12. Posiva Oy, Olkiluoto, Finland.

Öhberg A, Heikkinen E, Hirvonen H, Kemppainen K, Majapuro J, Niemonen J Pöllänen J, Rautio T, Rouhiainen P, 2006a. Drilling and the Associated Drillhole Measurements of the Pilot Hole ONK-PH4. Working Report 2006-71. Posiva Oy, Olkiluoto, Finland.

Öhberg A, Heikkinen E, Hirvonen H, Kemppainen K, Majapuro J, Niemonen J, Pöllänen, J, Rouhiainen P, 2006b. Drilling and Associated Borehole Measurements of the Pilot Hole ONK-PH3. Working Report 2006-20. Posiva Oy, Olkiluoto, Finland.

Appendix C

Deposition equipment, Supercontainer assembly, Drawing M-011-C
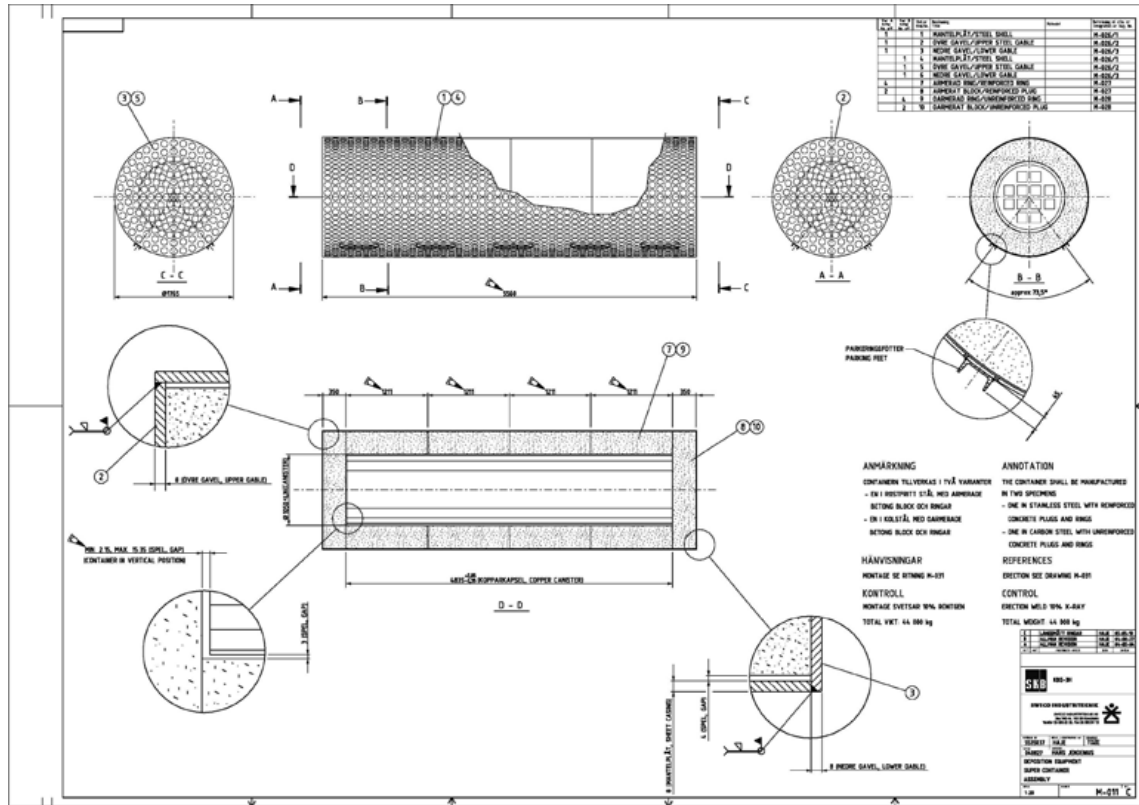
List of input parameters

The purpose of this appendix is to list the input data used in this report and in the other KBS-3H long-term safety study reports. Data used in this report are based on the preliminary information available at the time of the writing of the long-term safety reports (2006–2007). Design data are to be considered preliminary as the KBS-3H design work is still in progress. The information for design provided in this table is mostly based on the information given in the main text and other Appendices of this report. A generic report on data, models, codes, and databases that would apply both to the KBS-3V and KBS-3H will be produced at a later time.

D.1   Origin of input data

The data in Table D-1 is based on different origins, as discussed below. The references are in the table next to the data. Design data are to be considered as preliminary as the design work is still in progress.

- Repository depth: the values are from the preliminary design for a KBS-3V repository in Olkiluoto.

- Deposition drift: the drift diameter is from the buffer design studies and design descriptions 2006 and 2007 (the latter for tolerances). Drift length and separation between drifts are from the Layout Adaptation report. The drift dip appeared first in the KBS-3H summary report 2004. The drift orientation is from the Layout adaptation report and the main principal stress is from the Olkiluoto Site Description 2004.

- Canister and insert: dimensions are from the canister design report for all fuel types. The 2006 spent fuel inventories for Posiva's fuel types are from the KBS-3V Evolution Report.

- Supercontainer shell: supercontainer shell material, dimensions and surface areas (including hole edges and feet) are from the DD-2006. Carbon steel composition is from the European Structural Steel Standard /EN 10025/. Shell diameter and steel thickness as well as perforation hole diameter and degree of perforation are from KBS-3H buffer studies. Alternative values for other fuel types (VVER and EPR) are from the Layout Adaptation report and the Canister Design report.

- Buffer rings and end blocks: Initial water content of the buffer ring is 10% after KBS-3H buffer studies (Buffer study report 2002-2004). Buffer block length and gap to canister are also from the same studies. Other buffer dimensions are from the DD-2006. The saturated porosity of the buffer is from SKB's SR-97 Process report and the swelling pressure is from SR-Can Main report. The reference value of buffer porosity is used in scoping calculation in this report and in the Evolution Report. The alternative value was used in the radionuclide transport calculations, according to SR-Can.

- Distance blocks: all data concerning the Basic Design is from the DD-2006 and references therein. Data concerning the DAWE design is partly from KBS-3H buffer studies.

- Fixing rings: Data is from the DD-2006, the *assumption* on the number of fixing rings in a drift (4-5) is from the Residual Materials report.

- Filling blocks: all data is from the DD-2006. Filling blocks have not yet been designed in detail so the information is very preliminary at this stage.

- Plugs: all data is from the DD-2006. The composition of the low-heat high performance cement is from AECL (Canada) but this type of plug has not been tested yet in the Olkiluoto conditions.

- Spray and drip shields: the description is from the DD-2006, the *assumption* on the inventory is from the Residual Materials report. In these reports, the thickness of these shields is not

reported. In the present report, the *assumption* on the thickness (1 mm) was made to calculate the amount of gas generated per shield (see Section 5.5.1).

- Backfill: the *assumptions* on backfill inventories for the deposition niches and the access tunnels are from the Residual Materials report. The backfill material has not yet been selected.

- Cement and colloidal silica: the *assumptions* on cement inventory for the deposition niches and the access tunnels are from the Residual Materials report. Grouting estimates are based on ONKALO grouting experience, scaled to the relevant drift size. Grouting cement composition is *measured* on samples from ongoing cement tests in ONKALO. The composition of colloidal silica used for grouting is *measured* and comes from the Silica Sol supplier (BASF via EKA Chemicals).

- Bentonite: MX-80-type bentonite composition is from SR-Can Main report.

- Steel: steel corrosion rate for the supercontainer shell and the cast iron insert is from *experimental work* on steel corrosion rates in presence of bentonite. *Expert judgment* has been exercised in selecting the long-term steel corrosion rate based on experimental studies and natural analogues information available in the literature. The rationale for rate selection is described in Section 2.5.1 and Section 5.7.1 of the present report.

- Rock properties:
  - Geochemical properties: TDS (Total dissolved solids) data in present day conditions is from the Olkiluoto Site Description 2006 and is a sum of concentrations of cations and anions *measured* at the repository depth (400–500 m). Hydrochemical data are from the OIVA database. This database is continuously updated along with the new data collected from Olkiluoto, as described in /Pitkänen et al. 2007/. The data table used for this report was from the file called "uusiOIVA_10032006.xls". Future evolution of the TDS is from the KBS-3V Evolution Report and they are the result of *modelling* work and *expert judgment*. pH, redox potential, dissolved metals, dissolved gases are *measured* data. Solubilities of gases were taken from the literature.

  - Geological properties: Fractures are from the geological *model* presented in the Site Description 2006. Fracture density and transmissivity are *calculated/assumed* statistical analyses of vertical borehole data from depths of 300–700 m at Olkiluoto /Hellä et al. 2006/. The hydraulic conductivity range of mica gneiss and gneiss is *estimated (expert judgement)* from a range of rock conditions. Rock porosity, gas effective diffusion constant and gas intrinsic permeability are *measured* on Gneissic tonalite in the Research Tunnel at Olkiluoto. Hydraulic conductivity was *calculated* from the gas permeability values using a scaling factor to convert to diffusivity of heavier molecules in water- saturated samples by 1/35000 /Autio et al. 1999/. EDZ properties are from *observations and measurements* in the Research Tunnel at Olkiluoto. EDZ properties at repository depth are still highly uncertain at present.

  - Hydraulic properties: leakage rates in a drift without sealing are *estimated* based on statistical analyses of borehole data. The leakage after grouting in a drift is from the KBS-3H DFN model /Lanyon and Marschall 2006/. The maximum inflow *calculated* in all realisations is about 15 L/min with less than 1% of drifts exceeding 10 L/min. The saturation time for the drift is *calculated* from buffer studies. The hydraulic gradient is based on site-scale groundwater flow modeling results /Löfman 1999/.

  - Mechanical properties: stress state is from in situ borehole measurements at relevant depths, as reported in the Olkiluoto Site Description 2006. Rock strength values (including spalling strength) are *estimated* based on laboratory tests on core samples from Olkiluoto and in situ observations from the Äspö Pillar Stability Experiment. Some *expert judgment* was applied in deriving the Olkiluoto in situ rock strength from laboratory results and Äspö observations.

  - Thermal properties: the temperature of the Olkiluoto rock at repository depth has been *measured*.

Table D-1. Input parameter values for the KBS-3H Process Report and in other KBS-3H long-term safety reports.

PARAMETER	Unit	Symbol	Reference value	Alternative values	Reference
REPOSITORY DEPTH					
one-storey	m		400–420		/Saanio et al. 2004/
two-storeys	m			420 and 500–520	/Saanio et al. 2004/
DEPOSITION DRIFT					
Diameter	mm	$2\,r_t$	1,850 0/–10 mm	1,840	/Börgesson et al. 2005, tolerances are from this present report
Length	m		300 (272 mean)	100–300	/Johansson et al. 2007/ The total length includes the deposition niche.
separation between drifts	m	d	25	40	/Johansson et al. 2007/
Drift dip	°		2± 1		/Thorsager and Lindgren 2004/
Drift orientation	°		120 ± 10, parallel to main principal stress		/Johansson et al. 2007, Posiva 2005/
CANISTER					
Reference case					
Posiva, BWR 1,700 W					
outer diameter	mm	$2\,r_c$	1,050 $^{+2,35}/_{-2,35}$		/Raiko 2005/, tolerances are from this report
Length	mm	l_c	4,800	4,835 $^{+2,85}/_{-2,35}$	/Raiko 2005/, tolerances are from this report
thickness	m		0.05		/Raiko 2005/
total number of canisters			1,210		/Pastina and Hellä 2006/
total amount of spent fuel	tU		2,530		/Pastina and Hellä 2006/
Cast iron insert					
dimensions of fuel channels	m		4.45 × 0.16 × 0.16		/Raiko 2005/
number of fuel channels per insert	–		12		/Raiko 2005/
mass of iron and steel	kg		13,400		/Raiko 2005/
void space	m³		0.95		/Raiko 2005/
Alternative cases					
Posiva VVER 1,370 W					
outer diameter	m	$2\,r_c$		1.05	/Raiko 2005/
length	m	l_c		3.60	/Raiko 2005/
thickness	m			0.05	
total number of canisters				700	/Pastina and Hellä 2006/
total amount of spent fuel	tU			1,020	/Pastina and Hellä 2006/
Posiva EPR 1,830 W					
outer diameter	m	$2\,r_c$		1.05	/Raiko 2005/
length	m	l_c		5.25	/Raiko 2005/

PARAMETER	Unit	Symbol	Reference value	Alternative values	Reference
thickness	m			0.05	
total number of canisters				930	/Pastina and Hellä 2006/
total amount of spent fuel	tU			1,980	/Pastina and Hellä 2006/
Overall Posiva inventory					
Total number of canisters			2,840	3,000	/Pastina and Hellä 2006/. A rounded up value of 3000 canisters was used in scoping calculations in the Evolution Report (Smith et al. 2007).
Total amount of spent fuel	tU		5,530		/Pastina and Hellä 2006/
COPPER PROPERTIES					
density	kg m^{-3}	ρcu	8,900		/CRC 2007/
molar weight	g mol^{-1}		64		/CRC 2007/
SUPERCONTAINER SHELL, SC					
A SC + distance block unit can be placed in the drift in sections with water inflow rate < 0.1L/min					
Container materials and dimensions					
Reference case -Posiva, BWR 1,700 W					
Shell material			carbon steel S235JRG2		
Fraction of total mass of elements	%				/EN 10025/
C			< 0.17		
Si - Mn			< 0.14		
P			< 0.045		
S			< 0.045		
Cr,Ni,Al,Cu			–		
Shell, total mass	kg		1,031, with feet 1,071	890	The alternative value corresponds to an older shell design.
Shell, length	mm	l_{sc}	5,525	5,556 $^{+5}/_0$	Tolerances are from this report
feet, total mass (10 feet per SC)	kg		40.2		
Shell, outer diameter	mm	$2\,r_{sc}$	1,765 $^0/_{-2}$		/Börgesson et al. 2005/
inner diameter	mm		1,749		/Börgesson et al. 2005/
steel, thickness	mm		8		/Börgesson et al. 2005/
Void volume to canister and around a SC before saturation	mm		5		See definition of gaps below under Bentonite blocks in the SC
SC surface area					
External+ internal surface area+ hole edges surface area+ feet	m^2		41.52	41.39 (min)	

PARAMETER	Unit	Symbol	Reference value	Alternative values	Reference
External+ internal surface area+ feet	m²		35.73	35.6 (min)	
shell, degree of perforation	%		62		/Börgesson et al. 2005/
End plate, no perforation	%		0		
steel thickness	mm		8		
Alternative cases					
Posiva VVER 1,370 W					
Total mass	kg			880	
Length	mm	l_{sc}		4,330	/Raiko 2005/
Posiva EPR 1,830 W					
Total mass	kg			1,140	
Length	mm	l_{sc}		5,980	/Raiko 2005/
STEEL PROPERTIES					
Steel corrosion rate for the supercontainer shell	µm a⁻¹	R	1	2	/Smart et al. 2004/ Section 5.7.1 in /Gribi et al. 2007/
Steel corrosion rate for the cast iron insert	µm a⁻¹	R	1	10 (only for sensitivity analysis purposes)	/Smart et al. 2004/ Section 2.5.1 in /Gribi et al. 2007/
Density of iron/steel	kg m⁻³		7,800		/CRC 2007/
Molar weight of iron	g mol⁻¹		56		/CRC 2007/
Bentonite blocks in the SC					
Bentonite, MX-80					
ring blocks					
initial water content	w–%		10		/Börgesson et al. 2005/
initial dry density	kg m⁻³		1,885	1,789–1,977	
saturated density after swelling	kg m⁻³		2,000	1,950–2,050	
end blocks					
initial water content	w–%		10		
initial dry density	kg m⁻³		1,753	1,667–1,837	
saturated density after swelling	kg m⁻³		2,000	1,950–2,050	
ring and end blocks					
saturated porosity after swelling	%	ε_b	44	43	/SKB 1999/
swelling pressure	MPa		7–8		/SKB 2006/
Block dimensions					
Gap to canister (radial)	mm		5		/Börgesson et al. 2005/
gap to supercontainer (radial)	mm		5		
diameter end blocks	mm		1,739	1,740 $^{+1}/_{-2}$	Tolerances are from this report
outer diameter ring blocks	mm		1,739	1,740 $^{+1}/_{-2}$	Tolerances are from this report
inner diameter ring blocks	mm		1,058 $^{+1}/_{-1}$		Autio et al. 2008
length end blocks	mm		700 (2×350) $^{+2}/_{-2}$		/Börgesson et al. 2005/, tolerances are from this report

PARAMETER	Unit	Symbol	Reference value	Alternative values	Reference
length ring blocks	mm		4,810 (4 × 1,202.5)	4,844 $^{+4}/_{-4}$ (4×1,211 $^{+1}/_{-1}$)	Modified to the reference length (4,844 –> 4,810 mm). The alternative value and tolerances are from this report.
Bentonite,total mass in one SC	kg		16,445		
DISTANCE BLOCKS					
Reference case -Posiva, BWR 1,700 W, 25m separation between drifts					
Basic Design, BD					
Distance block					
Total length	mm		5,475		
Distance block unit is composed of "tight" and "loose" component					
"Tight" component					
Diameter	mm		1,850	1,840	
Length	mm		1,000		
block slices of thickness of 500 mm					
Bentonite MX-80					
initial water content	w–%		24		
initial dry density	kg m^{-3}		1,559	1,570	Alternative value is from Fig 4.8 in Sr-Can /SKB 2006/
saturated density after swelling	kg m^{-3}		2,000		
saturated porosity after swelling	%	ε_b	44		
"Loose" component					
Diameter	mm		1,820		
Length	mm		4,475		
block slices of thickness of 500 mm					
Centred blocks					
Supporting feets, material type and design, not done	–				
Bentonite MX-80					
initial water content	w–%		24	26	
initial dry density	kg m^{-3}		1,610		
saturated density after swelling	kg m^{-3}		2,000		
saturated porosity after swelling	%	ε_b	44		
Total amount of bentonite (dry mass)/distance block	kg		22,940		
DAWE					
Distance blocks					
Diameter	mm			1,765	/Börgesson et al. 2005/
Length	mm			5,475	

PARAMETER	Unit	Symbol	Reference value	Alternative values	Reference
void slot	mm			37.5–42.5	/Börgesson et al. 2005/
Centred blocks					
Supporting feet, material type	–			steel	
Feet, 4 feet per block	kg			13.9	
Bentonite, MX-80					
initial water content	w–%			21	
Dry density	kg m^{-3}			1,712	
saturated density after swelling	kg m^{-3}			2,000	
Total amount of bentonite (dry mass) /distance block	kg			22,940	
FIXING RINGS, BD to prevent movement of distance blocks, in every position where the inflow to SC+DB unit is larger than 0.01 L/min					
material type	–		10 mm thick steel plate		
mass	kg		600		
fixing material, low pH cement					
cement	kg		23		
SiO2	kg		1.5		
organic material	kg		0.009		
Total number of fixing rings in a drift			4.5	4–5	/Hagros 2007a/
SUPERCONTAINER +DISTANCE BLOCK UNIT					
BD AND DAWE					
Reference case -Posiva, BWR 1,700 W, 25 m separation between drifts					
Length (pitch, centre to centre distance)	m	p_c	11.0		
Gap between DB and SC (BD)	mm		5	max. 7	
Void volume within and outside a SC and DB unit	m^3		1.5		Appendix B.3 of KBS-3H Evolution report (Smith et al. 2007). Void space excludes unsaturated buffer pores and spaces
Alternative cases					
Posiva VVER 1,370 W					
Length (pitch, centre to centre distance)	m	p_c		9.1	/Raiko 2005/
Gap between DB and SC (BD)	mm			5 (max. 7)	
Posiva EPR 1,830 W					
Length (pitch, centre to centre distance)	m	p_c		10.6	/Raiko 2005/
Gap between DB and SC	mm			5 (max. 7)	

PARAMETER	Unit	Symbol	Reference value	Alternative values	Reference
FILLING BLOCKS, BD AND DAWE					
Distance block units (defined above)					
placed in positions were gw inflow before sealing is > 0.1 l/min and < 1L/min (after sealing)					
Dimensions and properties as for corresponding distance blocks in BD/DAWE					
Length per position	mm		10,000		
PLUGS, BD and DAWE					
Steel compartment plugs					
Compartment plugs will be used to isolate a section of the drift with higher inflow than 1L/min					
material type, steel	–		10 mm steel plate, S355J0		
Compartment plug components:					
fastening ring	kg		400		
collar	kg		1,250		
cap	kg		440		
bolts, steel	kg		20		
total mass of one single-sided plug	kg		2,110		One-sided plugs were considered in the residual material inventory /Hagros 2007a/. Double-sided plugs are used in this report.
mass of one double-sided plug	kg		2,550		
fixing material, low-pH cement					
cement	kg		300		
SiO2	kg		40		
organic material	kg		0.2		
Total mass, steel 2 plugs	kg		5,100		
Total mass, cement 2 plugs	kg		600		
Filling adjacent to steel compartment plug					
Bentonite pellets, MX-80					
Dry bulk density	kg m^{-3}		950		
Bulk density (for individual pellets)	kg m^{-3}		1,830		
Sand filling in compartment plug	m^3		1		
Transition blocks to compen-sate for the density reduction in the filled open volume					
"Loose" distance block					

PARAMETER	Unit	Symbol	Reference value	Alternative values	Reference
Diameter	mm		1,820		
Length	mm		4,475		
slices of thickness of 500 mm					
Centred blocks					
Supporting feet, material type and number of not designed	–				
Filling between steel compartment plugs					Not designed
Permeable filling material in the leaking fracture intersection					
crushed rock with proper grading					
In other parts compacted bentonite					
Total section length	mm		30,000		
Drift en d plug					
Steel-reinforced concrete plug (reference design)					
Length	mm		2,000		
Steel mass	kg		860		
low-pH concrete	m³		8		LHHPC, /Martino et al. 2002/
low-pH concrete (mixture: LHHP cement)	kg		19,200		/Martino et al. 2002/
cement	kg		780		
silica	kg		2,300		
coarse aggregates	kg		8,320		
sand	kg		7,160		
organics (SP)	kg		82		
cooling and grouting pipes	mm		123,000		
Rock plug					
Length	mm			2,000	
Steel mass	kg			200	
low-pH concrete	m³			1	
low-pH concrete	kg			1,900	
Fixing ring + steel compart-ment plug included in all drift end plug options					
Compartment plug					
steel mass	kg		2,110		One sided plug with bolts
Fixing material, low-pH cement					
cement	kg		300		
silica, SiO2	kg		20		
organic material	kg		0.1		
Fixing ring (as defined above)					

PARAMETER	Unit	Symbol	Reference value	Alternative values	Reference
Total length of fixing ring + Compartment plug	mm		1,000		
SPRAY AND DRIP SHIELDS, BD and DAWE					
Material type			steel		
Weight of one drip shield	kg		0.600		
Number of drips shields in one drift			5	4–6	/Hagros 2007a/
Thickness	mm		1		Assumption used for gas generation values (Section 5.5.1 in /Gribi et al. 2007/)
Total amount per drift	kg		3		/Hagros 2007a/
DRAINAGE, ARTIFICIAL WATERING AND AIR EVACU-ATION PIPES (DAWE)					These are removed from drift
Watering pipes					one pipe in each SC section
Material				steel	
Diameter	mm			17.2	
Air evacuation system					one/two pipes in the drift
Material				steel	
Diameter	mm			10	
BACKFILL PER DRIFT					
The first 10–15 m of the drift which has a wider diameter will be backfilled	m³		750(max)		
Backfill crushed rock/ bentonite	w %		70/30		/Hagros 2007a/
Bentonite			MX-80		
Density, dry (average)	kg/m³		2,150		
85 % of the volume					
In addition the first 5 meters of the drift with the diameter 1.85 m will be backfilled with compacted bentonite					
CEMENT IN A DRIFT (excluding the first 15 m emplacement section)					
Basic Design, BD					
Cement in compartment plugs, end plug (**reference LHHP plug**), fixing rings	kg		2,140		/Hagros 2007a/
Cement in compartment plugs, end plug for the **alternative grouted rock plug,** and fixing rings				2,960	
Composition of low-pH cement (mixture: LHHP see drift end plug)			See drift end plug		/Martino et al. 2002/
Low-pH cement for grouting	kg			500	
Composition (mixture: P308B)					

PARAMETER	Unit	Symbol	Reference value	Alternative values	Reference
cement	kg/m³			335	/Ahokas et al. 2006/
SiO₂	w%			52.8	/Ahokas et al. 2006/
Organic materials	w%			4	/Ahokas et al. 2006/
Density	kg/m³			1,354	/Ahokas et al. 2006/
Total amount of cement in a drift (excl. the first 15 m)	kg		2,140	3,460	/Hagros 2007a/
Reference material, Silica Sol for grouting					
Silica Sol	l		100–500		
Silica Sol	kg		130–670		
Composition (mixture: MEYCO MP320)					
SiO₂	w%		33.5		/Hagros 2007b/
Accelerators (NaCl)	w%		1.7		/Hagros 2007b/
organic materials (biocides)	w%		< 0.01		/BASF 2007/
Density	kg/m³	ρ	~ 1,300		/Ahokas et al. 2006/
CEMENT IN THE DRIFT (the first 15 m emplacement section)					
Support bolts, anchor bolts, shotcrete, grouting - remaining amount					/Hagros 2007a/
Low-pH shotcrete					
Cement	kg		320	320	
Other cement bearing components	kg		170	170	
Total cement for first 15 m of a drift		490	490		
TOTAL AMOUNT OF CEMENT IN A DRIFT (BD)	kg		2,630	3,950	
DAWE					
Total amount of cement in a drift	kg			3,700	/Hagros 2007a/
BENTONITE					
Bentonite MX-80			MX-80		/SKB 2006/
Montmorillonite	w %		87		
Na-			72 %		
Ca-			18 %		
Mg-			8 %		
K-			2 %		
pyrite	w %		0.07		
Gypsum	w %		0.7		
calcite+ siderite	w %		0–1		
Quartz	w %		3		
Cristobalite	w %		2		
Mica	w %		4		
Albite	w %		3		
Dolomite	w %		0		
Anorthoclase	w %		0		
organic carbon	w %		0.2		

PARAMETER	Unit	Symbol	Reference value	Alternative values	Reference
CEC	meq/100g		75		
ROCK PROPERTIES					
Geochemical conditions (at 400–500 m depth)					
Salinity (TDS, Total dissolved solids)					
Present level	g l^{-1}		10–13	10–20	/Andersson et al. 2007, Pastina and Hellä 2006/
Post-emplacement	g l^{-1}		10–25(420 m depth)	25–45 (550 m depth)	/Pastina and Hellä 2006/, max. at 100 years after disposal
pH			7.5–8.2		/Pitkänen et al. 2004/
Redox potential	mV		–300..–250	$\approx -250..-200$	/Pitkänen et al. 2004/
Dissolved Fe(II)	mg l^{-1}		0.11(median)	0.01–0.72	OIVA database (file name: "uusiOIVA_10032006.xls"). (see text)
Dissolved sulphide	mg l^{-1}		0.25 (median)	12 (max)	ibid
Dissolved gases					
H$_2$	ml l^{-1}		< 1	20–25 (< 800 m)	/Pitkänen and Partamies 2007/
CH$_4$	ml l^{-1}		< 400	920 (< 800 m)	/Pitkänen and Partamies 2007/
Solubilities of gases at 30 °C (after $\approx$ 2000a) at 0.1MPa					/SKB 1999/ p. 100
H$_2$	mol m^{-3}		0.77		/Himmelblau 1960/
	ml l^{-1}		19		/Himmelblau 1960/
CH$_4$	mol m^{-3}		1.3		/Himmelblau 1960/
	ml l^{-1}		33		
Geological properties					
Gneiss (migmatitic gneiss): fracture properties					
fracture type	–		fractures	vein-like	/Andersson et al. 2007/
orientation	–		several sets		
density	m^{-1}	N	1--3	3–10	/Hellä et al. 2006/
aperture	mm	a	calc. from T-distribution		
transmissivity	m^2 s^{-1}	T	10^{-14}–10^{-7}		
hydraulic conductivity	m s^{-1}		10^{-8}–10^{-15}		Estimated range of rock hydr. cond. in /Börgesson et al. 2005/
Gneiss: average matrix properties					
porosity	%	ε_m	0.14	0.1–0.2	/Autio et al. 2003/
hydraulic conductivity	m s^{-1}		10^{-14}	$\approx < 10^{-15}$	Estimated range of tightest rock hydr.cond. in /Börgesson et al. 2005/
gas effective diffusion constant	m^2 s^{-1}		2.63 10^{-10}		/Autio et al. 2003/
intrinsic gas permeability	m^2		5.16 10^{-21}		/Autio et al. 2003/
EDZ: properties of crushed zone (0–4 mm)					
thickness (radial extent)	mm		4		/Autio et al. 2003/

PARAMETER	Unit	Symbol	Reference value	Alternative values	Reference
porosity	%		0.64	2–4	/Autio et al. 2003/
fracture type	–		open cracks		/Montoto et al. 2003/
mean fracture aperture	µm		2		/Montoto et al. 2003/
small fractures (< 5.4 µm)	%		90		/Montoto et al. 2003/
larger fractures (> 5.4 µm)	%		10		/Montoto et al. 2003/
EDZ: properties of microfractured zone (4–9 mm)					
thickness (radial extent)	mm		5		/Autio et al. 2003/
porosity	%		0.34		/Autio et al. 2003/
fracture type	–		open cracks		/Autio et al. 2003/
mean crack specific surface	µm^{-1}		0.004		/Montoto et al. 2003/
small fractures (< 2.16 µm)	%		60 %		/Montoto et al. 2003/
EDZ: properties of zone of minor damage (9–23 mm)					
thickness (radial extent)	mm		14		/Autio et al. 2003/
fracturation	–		similar as in undisturbed rock		/Autio et al. 2003/
EDZ: average properties (0–23 mm)					
thickness	mm		23		Combined thickness of crushed zone, microfractured zone and zone of minor damage
porosity	%	ε_{EDZ}	0.34		/Autio et al. 2003/
gas effective diffusion constant	m^2 s^{-1}		3.97 10^{-9}		/Autio et al. 2003/
intrinsic gas permeability	m^2		2.96 10^{-19}		/Johnson et al. 2005, Appendix C/ in /Gribi et al. 2007/
max hydraulic conductivity	m s^{-1}	K_{EDZ}	3 x 10^{-12}		The maximal hydraulic conductivity of the EDZ was indirectly calculated by taking the average intrinsic gas permeability (see line above) as an upper bound for the transport of water in the EDZ.
Hydraulic properties					
<u>Leakage rates for 300 m drift without sealing</u>	L/min				/Hellä et al. 2006/
long dry sections			"tight"		
Zones with 1-3 local fractures			> 4		one fracture per 250 m
a few fractures or fracture zones			0.4–4		one fracture per 100 m
six 5 m long sections (per 300 m)			> 0.1		
four to five 10 m long sections (per 300 m)			> 0.1		

163

PARAMETER	Unit	Symbol	Reference value	Alternative values	Reference
total leakage into a drift			10		/Hellä et al. 2006/, the likely range of inflow into a drift
Leakage after grouting for a 300 m drift (successful grouting to a T< 10–8 m²/s)					
Inflow	l/min		< 10 (99 %)	< 10 (99 %)	/Lanyon and Marschall 2006/, max. inflow in all realisations is about 15 l/min with less than 1% of drifts exceeding 10 l/min
Saturation time for a supercontainer section in the drift	a		10	12,000	Figure 8-14 in /Börgesson et al. 2005/
Hydraulic gradient (post-closure phase)	%		0.01	0.01 – 1	/Löfman 1999/
Hydraulic length (from drift to the nearest major fracture zone)	m		50		/Lanyon and Marschall 2006/. Assumed distance to constant head hydrostatic boundary in discrete fracture network modelling.
Mechanical properties at repository depth					
Main horizontal stress	MPa	$\sigma 1$ or σH	5+0.021z min 10+0.042z max		/Andersson et al. 2007/, 300< z < 800 m
Secondary horizontal stress	MPa	$\sigma 2$ or σh	0.021z min 5+0.027z max		Ibid.
Vertical stress	MPa	$\sigma 3$ or σv	0.015z min 0.030z max		Ibid.
Spalling strength	MPa		65		/Hakala et al. 2008/, Table 2.3
Thermal properties					
Ambient temperature	°C	T_0	+10.5 °C (400m)	0	/Ikonen 2003/, gradient 1.5 °C/100 m
Heat output	W				
BWR canister, OL 1-2			1,700		/Raiko 2005/
PWR canister				1,370	/Raiko 2005/
EPR Canister				1,830	/Raiko 2005/
Thermal conductivity (gneiss)	$Wm^{-1}K^{-1}$		2.7		/Posiva 2003/, p. 114, for a temperature 22°C
Heat capacity (gneiss)	$J\,kg^{-1}K^{-1}$		797		/Posiva 2003/, p. 114
Thermal diffusivity (gneiss)	$m^2\,s^{-1}$		$1.23\ 10^{-6}$		/Posiva 2003/, p. 114
Thermal conductivity (bentonite)	$Wm^{-1}K^{-1}$		1.0		/Ikonen 2003/
Maximum temperature at canister surface (for thermal dimensioning)	°C		90		10° below the design basis max. of 100°, /Ikonen 2003/

D.2   References

Ahokas H, Hellä P, Ahokas T, Hansen J, Koskinen K, Lehtinen A, Koskinen L, Löfman J, Mészáros F, Partamies S, Pitkänen P, Sievänen U, Marcos N, Snellman M, Vieno T, 2006. Co ntrol of water inflow and use of cement in ONKALO after penetration of fracture zone R19. Working Report 2006-45. Posiva Oy, Olkiluoto, Finland.

Andersson J, Ahokas H, Hudson J A, Koskinen L, Luukkonen A, Löfman J, Keto V, Pitkänen P, Mattila J, Ikonen A I T, Ylä-Mella M, 2007. Olkiluoto Site Description 2006. POSIVA 2007-03. Posiva Oy, Olkiluoto, Finland.

Autio J, Kirkkomäki T, Siitari-Kauppi M, Timonen J, Laajalahti M, Aaltonen T, Maaranen J, 1999. Use of 14C-PMMA method and He-gas methods to characterize excavation disturbance in crystalline rock. POSIVA 99-22, Posiva Oy, Helsinki, Finland.

Autio J, Hjerpe T, Siitari-Kauppi M, 2003. Porosity, Diffusivity and Permeability of EDZ in Crystalline Rock and Effect on the Migration in a KBS-3 Type repository. Proceedings of a European Commission Cluster conference and workshop on Impact of the excavation disturbed or damaged zone (EDZ) on the performance of radioactive waste geological repositories, Luxemburg, 3 to 5 November 2003, EUR 21028 EN, p. 149–155.

Autio J, Anttila P, Börgesson L, Sandén T, Rönnqvist P E, Johansson E, Hagros A, Eriksson M, Halvarsson B, Berghäll J, Kotola R, Parkkinen I, 2008 . KBS-3H design description 2007. POSIVA 2008-01 and SKB R-08-44. Posiva Oy, Olkiluoto, Finland and Svensk Kärnbränslehantering AB, Sweden.

BASF, 2007. MEYCO MP320 Data sheet. Available at: http://www.basf-cc.com.au/acrobat/meymp320.pdf.

Börgesson L, Sandén T, Fälth B, Åkesson M, Lindgren E, 2005. Studies of buffers behaviour in KBS-3H concept – Work during 2002-2004. SKB R-05-50, Svensk Kärnbränslehantering AB, Sweden.

CRC 2007. CRC Handbook of Chemistry and Physics, 88th Edition (CRC Handbook of Chemistry and Physics). D.R. Lide (ed.). 88th Edition. The Chemical Rubber Company (CRC), Boca Raton, USA.

EN 10025. European Structural Steel Standard 10025.

Gribi P, Johnson L, Suter D, Smith P, Pastina B, Snellman M, 2007. Safety assessment for a KBS-3H spent nuclear fuel repository at Olkiluotoa – Process Report. Posiva Report 2007-09. Posiva Oy and SKB R-08-36. Posiva Oy, Olkiluoto, Finland and Svensk Kärnbränslehantering AB, Sweden.

Hagros A, 2007a. Estimated quantities of residual materials in a KBS-3H repository at Olkiluoto. Posiva Working Report 2007-104 and SKB R-08-33. Posiva Oy, Olkiluoto, Finland and Svensk Kärnbränslehantering AB, Sweden.

Hagros A, 2007b. Foreign materials in the repository – Update of the estimated quantities. Working Report 2007-17. Posiva Oy, Olkiluoto, Finland.

Hakala M, Hudson J A, Harrison J P, Johansson E, 2008. Assessment of the Potential for Rock Spalling at the Olkiluoto Site. Working Report 2008-83. Posiva Oy, Olkiluoto, Finland.

Hellä P, Ahokas H, Palmén J, Tammisto E, 2006. Analysis of geohydrological data for assessment of the alternative repository layout KBS-3H. Working report 2006-16. Posiva Oy, Olkiluoto, Finland.

Himmelblau D M, 1960. Solubilities of inert gases in water. J. Chem. Eng., Vol. 5/1, January 1960.

Ikonen K, 2003. Thermal Analyses of KBS-3H Type repository. Posiva 2003-11, Posiva Oy, Olkiluoto, Finland.

Johansson E, Hagros A, Autio J, Kirkkomäki T, 2007. KBS-3H layout adaptation 2007 for the Olkiluoto site. Working Report 2007-77. Posiva Oy, Olkiluoto, Finland.

Johnson L, Marschall P, Wersin P, Gribi P, 2005. HMCBG Processes Related to the Steel Components in the KBS-3H Disposal Concept. Working Report 2005-09 and SKB R-08-25. Posiva Oy, Olkiluoto, Finland and and Svensk Kärnbränslehantering AB, Sweden.

Lanyon G W, Marschall P, 2006. Discrete fracture network modelling of a KBS-3H repository at Olkiluoto. POSIVA 2006-06 and SKB R-08-26. Posiva Oy, Olkiluoto, Finland and Svensk Kärnbränslehantering AB, Sweden.

Löfman J, 1999. Site Scale Groundwater Flow in Olkiluoto. POSIVA 99-03. Posiva Oy, Olkiluoto, Finland.

Martino J B, Chandler N A, Read RS, Baker C, 2002. Response of the tunnel sealing experiment concrete bulkhead to pressurization. Report No: 06819-REP-01200-10085-R00. Ontario Power Generation, Toronto, Canada.

Montoto M, Rodriguez-Rey A, Autio J, 2003. Microfractographic characterization of the excavation damage caused by boring of the experimental full scale deposition holes in the Research tunnel at Olkiluoto. Proceedings of a European Commission Cluster conference and workshop on Impact of the excavation disturbed or damaged zone (EDZ) on the performance of radioactive waste geological repositories, Luxemburg, 3 to 5 November 2003, EUR 21028 EN.

OIVA data file, see Pitkänen et al, 2007.

Pastina B, Hellä P, 2006. Expected evolution of a spent fuel repository at Olkiluoto, POSIVA 2006-05. Posiva Oy, Olkiluoto, Finland.

Pitkänen P, Partamies S, Luukkonen A, 2004. Hydrogeochemical Interpretation of Baseline Groundwater Conditions at the Olkiluoto site. POSIVA 2003-07. Posiva Oy, Olkiluoto, Finland.

Pitkänen P, Partamies S, 2007. Origin and Implications of Dissolved Gases in Groundwater at Olkiluoto. POSIVA 2007-04. Posiva Oy, Olkiluoto, Finland.

Pitkänen P, Ahokas H, Ylä-Mella M, Partamies S, Snellman M Hellä P, 2007. Quality Review of Hydrochemical Baseline Data from the Olkiluoto Site. POSIVA 2007-05. Posiva Oy, Olkiluoto, Finland.

Posiva, 2003. Baseline conditions at Olkiluoto. POSIVA 2003-02. Posiva Oy, Olkiluoto, Finland.

Posiva, 2005. Olkiluoto Site Description 2004. POSIVA 2005-03. Posiva Oy, Olkiluoto, Finland.

Raiko H, 2005. Disposal canister for spent nuclear fuel – Design report. POSIVA 2005-02. Posiva Oy, Olkiluoto, Finland.

Saanio T, Kirkkomäki T, Sacklén N, Autio J, Kukkola T, Raiko H, 2004. Spent nuclear fuel repository at Olkiluoto – Preliminary design – Stage 1. Working Report 2003-74. Posiva Oy, Olkiluoto, Finland. (In Finnish)

SKB, 1999. SR 97 – Processes in the repository evolution. SKB TR-99-07, Svensk Kärnbränslehantering AB, Sweden.

SKB, 2006. Long-term safety for KBS-3 repositories at Forsmark and Laxemar – a first evaluation – Main report of the SR-Can project. SKB TR-06-09, Svensk Kärnbränslehantering AB, Sweden.

Smart N R, Rance A P, Werme LO, 2004. Anaerobic corrosion of steel in bentonite. Mat. Res. Soc. Symp. Proc. 807, 441-446.

Smith P A, Johnson L H, Snellman M, Pastina B, Gribi P, 2007. Safety assessment for a KBS-3H spent nuclear fuel repository at Olkiluoto – Evolution report. POSIVA 2007-08 and SKB R-08-37. Posiva Oy. Olkiluoto, Finland and Svensk Kärnbränslehantering AB, Sweden.

Thorsager P, Lindgren E, 2004. KBS-3H summary report of work done during Basic Design. SKB R-04-42, Svensk Kärnbränslehantering AB, Sweden.

Canister spacing in Finnish KBS-3H and KBS-3V repositories and length of distance blocks

INSINÖÖRITOIMISTO SAANIO & RIEKKOLA OY		KBS-3H Design 1 (9) PROJEKTI-798-16/2006
Author Jorma Autio	Reviewed by Margit Snellman	Approved by Reijo Riekkola
date 19.7.2006 (11.4-07)	date 11.4.07	date 13.4.2007

CANISTER SPACING IN FINNISH KBS-3H AND -3V REPOSITORIES AND LENGTH OF DISTANCE BLOCKS

1 BACKGROUND

The site utilization degree is in general lower in KBS-3H concept than in KBS-3V. The difference utilization degree of KBS-3H versus KBS-3V concepts is of the order from 0% in Posiva's evaluation to a maximum of 26% in SKB's evaluation, see Table 1 (i.e. 26% difference in the length of required deposition drift in KBS-3H versus deposition tunnel in KBS-3V). Utilization degree has impact on the feasibility of the concept.

The reasons for the significantly lower site utilization degree of KBS-3H concept in SKB's design and large difference between Posiva's and SKB's utilization degree are discussed.

There has also been some confusion in the canister spacing values. Therefore the present canister spacing and length of distance blocks in the Finnish KBS-3H design are presented to be used as basis in KBS-3H design and lay-out adaptation.

2 CANISTER SPACING AND DISTANCE BLOCK LENGTH

The present canister spacing and length of distance blocks together with the division of Posiva's different fuel canister types are presented in tables 1, 2 and 3 on the basis of what has been presented in Appendix 1. Supercontainer is assumed to be 0.725 m longer than canister (note: differs from Appendix 1) based on design drawings of super container by Halvarsson 2005, consisting of 0.35 m of buffer on both sides of canister, 10 mm thick steel endplates on both sides and total of 5 mm in gaps.

Table 1. Canister spacing (center to center) at Olkiluoto in KBS-3V and -3H repositories at 25 m drift/depositiontunnel separation in one storey at −420 m level. The values for SKB's canister spacing are at 40 m drift/depositiontunnel separation.

Fuel	Spacing KBS-3V [m]*	Spacing KBS-3H [m]**	Difference between 3V and 3H [%]
Posiva BWR 1700 W	11.0	11.0	0.0
Posiva VVER 1370 W	8.6	9.1	5.8
Posiva EPR 1830 W	10.6	10.6	0.0
SKB BWR 1700 W***	6.35	7.30-7.95	15.0-25.2

* Ikonen, K., 2003a for Posiva fuel.

** Ikonen, K., 2003b for Posiva fuel

*** Hökmark & Fälth 2003 for all SKB fuel

DISTRIBUTION: ark/S&R, www.projectplace.com
E-mail: E. Thurner

Table 2. Canister spacing (center to center) and length of distance blocks in KBS-3H repository at 25 m drift separation in one storey –420 m level at Olkiluoto. SKB values are based on 40 m drift separation.

Fuel	Canister spacing [m]	Canister length [m]	Super container length* [m]	Distance Block length [m]**	Distance block length with 5 mm gaps [m]
Posiva BWR 1700 W	**11.0**	4.8	5.53	5.475	5.465
Posiva VVER 1370 W	**9.1**	3.6	4.33	4.775	4.765
Posiva EPR 1830 W	**10.6**	5.25	5.98	4.625	4.615
SKB BWR 1700 W	7.30-7.95	4.835	5.56	1.74-2.39	1.73-2.38

*   The supercontainer is 0.725 m longer than canister (drawing by B. Halvarsson, 2005).

**   No gaps included, a gap of 5 mm on both sides would reduce the length by 0.01 m

Table 3. Division of Posiva's 2993 spent fuel canisters * .

Source of fuel canister	Quantity	Proportion	
Olkiluoto 1&2 fuel	1256	42.0	%
Olkiluoto 3 fuel	1039	34.7	%
Loviisa 1&2 fuel	698	23.3	%
Total	2993		

*   Malmlund, H., Äikäs, K. & Hagros, A. 2003.

3   EVALUATION OF PRESENT BASIS AND CONCLUSIONS

3.1   DIFFERENCES BETWEEN KBS-3H AND KBS-3V CONCEPTS

The reason for longer canister spacing in KBS-3H when compared to KBS-3V in general originates evidently from the geometry of the canister. The shorter the canister spacing, the larger is the effect on heat distribution when the canister orientation is changed from vertical to horizontal, see Figure 1. The larger the drift separation, the shorter the canister spacing. SKB's drift separation is 40 m (compared to Posiva's 25 m), which results in clearly shorter canister spacing and therefore the effect of the orientation of canister becomes more significant.

3.2   DIFFERENCES BETWEEN POSIVA'S AND SKB'S DESIGNS

The canister spacing is the same in KBS-3V and –3H alternatives at Olkiluoto in case of BWR and EPR spent fuel. In case of VVER fuel there is a 6% difference, which means that 6% more drift length is needed for the same amount of canisters.

In SKB's design the difference in canister spacing between KBS-3V and 3H is 17-27% According to Hökmark & Fälth 2003, which differs clearly from Posiva's corresponding value as seen in Table 1.

In the thermal dimensioning calculations (Hökmark & Fälth 2003) and (Ikonen 2003b) there are some differences due to different site properties, e.g. the thermal conductivity in higher in

Swedish site candidates than in Olkiluoto, as well as the ambient temperature of the repository rock. Furthermore, the effect of air gaps around the canister and around the supercontainer is modelled partly in a different way. These differences lead to different canister distances in different sites.

Also, there is a difference between the KBS-3H and KBS-3V repository analyses. The gaps are of different width and in 3H case the rock-supercontainer interface is assumed to be air filled whereas in 3V case the rock-bentonite gap is assumed to be water filled.

In KBS-3H case the interaction between adjacent canisters in the tunnel is the greater the closer to each other the canisters are. Therefore the main reason for the significant difference originates from the larger 40 m drift separation in SKB's design when compared to Posiva's 25 m, which results in shorter canister spacing, which intensifies the effect of canister orientation.

If the rock conductivity is higher (as is the case in SKB site candidates) the canisters can be located closer to each other and the interaction between adjacent canisters is higher in 3H case than in 3V case. In Olkiluoto site the rock conductivity is lower and the canister distances somewhat greater than in SKB sites. The greater distance lowers also the interaction of adjacent canisters in 3H case and thus the different cases 3H and 3V differ less in Olkiluoto case from each other than in case of SKB candidate sites.

3.3   VVER FUEL

If the spacing between canisters is the same (or close to it) in both KBS-3V and –3H alternatives, there is no significant difference in site-utilization efficiency in that perspective. However in case of Loviisa VVER fuel, which is 23% of the total amount, the canister spacing is 17% smaller than in case of Olkiluoto BWR fuel, will improve slightly the site utilization efficiency presented in the previous lay-out adaptation study, where the spacing has been assumed to be constant 11 m regardless of the spent fuel type.

3.4   CANISTER SPACING

The canister spacing is function of drifts separation and it can be optimised with respect to cost and site utilization. Smaller drift separation results in better site utilization than longer separation and the lay-out becomes more compact. However, as the utilization becomes better, the cost may increase depending on the cost of backfilling and sealing of central tunnels versus the cost of distance blocks.

The shortest distance block is 1.7 m (SKB) and the longest is 5.5 m (Posiva). The longer block is about 3.2 times longer than the shortest block and it is possible that the lengthening of distance blocks has positive impact on the function.

It is proposed that the present drift separation and canister spacing is re-evaluated when the functional impacts of canister spacing are resolved, the cost of backfilling and buffer are known and the importance of site utilization is understood.

It is proposed that the canister spacing and distance block lengths presented in this document are used as input for KBS-3H design and long term safety related studies.
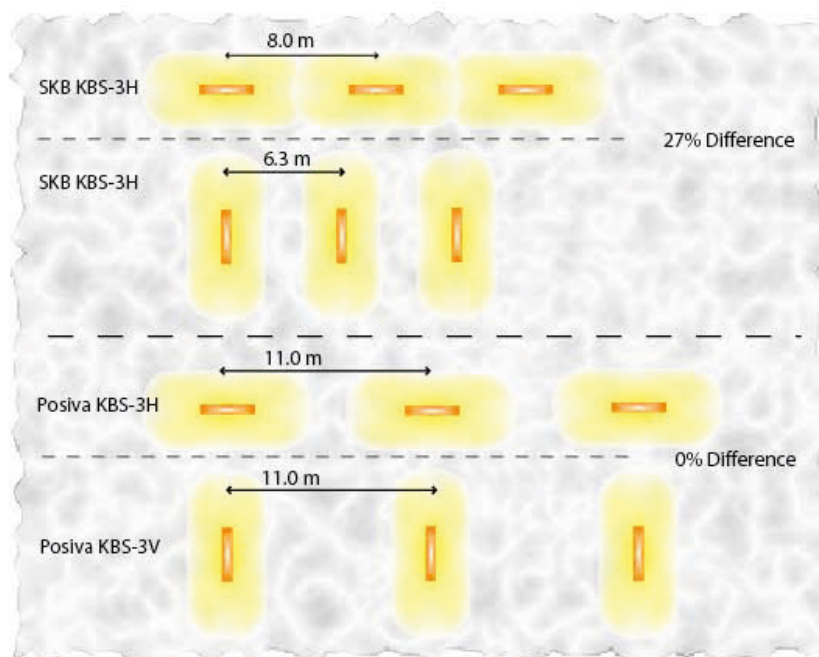
Figure 1. Illustration of the effect of initial canister spacing and orientation in KBS-3V design on spacing in KBS-3H design.

REFERENCES

Halvarsson, B. 2005. Based on drawings M-011C.pdf, M-025C.pdf, M-026_revA.pdf, M-027B.pdf, M-028B.pdf, M-029Bpdf, and M-030B.pdf, (at Projectplace)

Hökmark, H. & Fälth, B. 2003. Thermal dimensioning of the deep repository. Influence of canister spacing, canister power, rock thermal properties and near field design on the maximum canister surface temperature. Clay Technology AB. SKB Report TR-03-09. 82 p. ISSN 1404-0344.

Malmlund, H., Äikäs, K. & Hagros, A. 2003. Layout adaptation examples for a KBS-3V repository at Olkiluoto. Olkiluoto, Finland: Posiva Oy. Working Report 2003-68.

Ikonen K. 2003a. Thermal analysis of spent nuclear fuel repository. Report POSIVA 2003-4. Posiva Oy, Olkiluoto. 61 p. ISBN 951-652-118-5.

Ikonen, K. 2003b. Thermal Analyses of KBS-3H Type Repository. Report POSIVA 2003-11, Posiva Oy, Olkiluoto. 43 p. ISBN 951-652-125-8.

CANISTERS AND CANISTER DISTANCES IN KBS-3H REPOSITORY LAYOUT

Summary

This memo summarizes the main dimensions and distances in the repository of the various types of canisters in Posiva and SKB disposal systems, KBS-3H and KBS-3V.

Canister types and main dimensions

Posiva's disposal system has 3 different canister types. They are VVER 440 type, BWR type and EPR type. SKB has 2 types of canisters; BWR type that is, in practice, identical with the Posiva BWR type canister and PWR canister that is suitable for Westinghouse type PWR-fuel of Ringhals 2, 3 and 4 units' fuel bundles. SKB PWR canister is different from VVER 440 and EPR type canisters. See Figure 1 for Posiva type canisters.

FIGURE 1. *Artist's view of the Posiva type canisters, VVER 440 type left, BWR type middle, and EPR type right.*

Canister main dimensions are given in Table 1. The outside dimensions of the 2 SKB type canisters, BWR and PWR are identical. The total length of the Posiva BWR canister depends a little on the copper shell bottom manufacture. If the bottom is welded, the total length is some centimetres longer than in case the bottom is integrated (made by pierce & draw). This is the reason for a slight difference in the total length of Posiva and SKB BWR canisters. In practice, they are identical.

TABLE 1. *Main dimensions, design heat load and number of fuel elements in various canister types.*

CANISTER TYPE	Posiva VVER 440	Posiva BWR	Posiva EPR	SKB BWR	SKB PWR
Outside diameter [m]	1.050	1.050	1.050	1.050	1.050
Total length [m]	3.6	4.8	5.25	4.83	4.83
Design heat load [W]	1370	1700	1830	1700	1700
Number of fuel elements [ex]	12	12	4	12	4

Design heat loads of the canisters

The decay heat generation in canisters (Anttila 2005) depends on the amount, burn-up and cooling time of the fuel. The initial decay heat generation in a BWR canister will be 1700 W or less; 1370 W or less in a VVER 440 canister and 1830 W or less in an EPR canister.

Canister temperature in repository

The maximum temperature on canister surface is reached within 10 to 15 years after the disposal. According to Olkiluoto site-specific thermal dimensioning the canisters are planned to be emplaced in disposal tunnels with a spacing of 9.1 m for VVER 440 canister, 11 m for BWR canister and 10.6 m for EPR canister. The distance between parallel tunnels is 25 m in planned reference case. If the tunnel distance to each other is increased to 40 m, the canister spacings are 7.0, 8.7 and 7.8 m, respectively. Thermal dimensioning and optimisation of the Olkiluoto repository is made for KBS-3V in (Ikonen 2003a), for KBS-3H in (Ikonen 2003b) and for EPR-fuel canisters in KBS-3V repository in (Ikonen 2005). EPR-canisters are not analyzed separately for KBS-3H repository, but the canister distances are assumed to be the same as for KBS-3V case.

In Olkiluoto site the ambient rock temperature is assumed to be +10.5 C and the average rock conductivity 2.61 W/m/K. Bentonite conductivity is assumed to be 1.0 W/m/K. The 5

mm + 42.5 mm gaps between bentonite, supercontainer steel and rock, and the 5 mm gap between canister and bentonite is assumed to be dry and air filled. The calculation model includes the handling of air gaps between canister and bentonite buffer and between buffer and rock. The air gap heat transfer is modelled as parallel coupled conduction and radiation. The canister distances are taken so that the calculated maximum temperature on the canister surface is +90 C. Ten degrees C between the design temperature +100 C and the nominal calculated temperature of +90 C is taken as a safety marginal due to uncertainties and scattering in rock and bentonite properties and in the decay heat estimates of the spent fuel inside each canister.

The SKB-specific thermal dimensioning calculations are presented in (Hökmark & Fälth 2003). The report gives a large variety of results calculated with variations of many relevant properties of the cooling system. In site specific chapter 11 (page 71), some calculation examples are given for Forsmark site. There, the initial parameters are: ambient temperature +12 °C, thermal conductivity 3 W/(mK) and thermal capacity 2.08 MJ/(m³K). The result for KBS-3V is 6.35 m and for KBS-3H 7.3 m or 7.95 m depending on the assumption of wetting of the supercontainer/rock interface. In every case the SKB calculations refer to tunnel spacing of 40 m intead of the tunnel spacing of 25 m used in Olkiluoto specific calculations. Furhermore, (Hökmark & Fählt 2003) gives an assessment that KBS-3H requires 16 to 26 % more total tunnel length than KBS-3V.

Differences between SKB and Posiva repository dimensioning

In the thermal dimensioning calculations (Hökmark & Fälth 2003) and (Ikonen 2003b) there are some differences due to different site properties, for ex. the thermal conductivity in higher in Swedish site candidates than in Olkiluoto, as well as the ambient temperature of the repository rock. Furthermore, the effect of air gaps around the canister and around the supercontainer is modelled partly in a different way. These differences lead to different canister distances in different sites.

Also, there is a difference between the KBS-3H and KBS-3V repository analyses. The gaps are of different width and in 3H case the rock-supercontainer interface is assumed to be air filled whereas in 3V case the rock-bentonite gap is assumed to be water filled. The gap between canister and bentonite is assumed to be air-filled in both concepts.

In KBS-3H case the interaction between adjacent canisters in the tunnel is the greater the closer to each other the canisters are. If the rock conductivity is higher (as is the case in SKB site candidates) the canisters can be located closer to each other and the interaction between adjacent canisters is higher in 3H case than in 3V case. In Olkiluoto site the rock conductivity is lower and the canister distances somewhat greater than in SKB sites. The greater distance lowers also the interaction of adjacent canisters in 3H case and thus the different cases 3H and 3V differ less in Olkiluoto case from each other than in case of SKB candidate sites.

In Table 2, there are summarized the calculated canister distances in SKB and Posiva repository concepts for various canister types.

Summary of canister spacing in KBS-3H repository

The KBS-3H repository design is 0 to 26 % less effective in use of repository area or need of tunnel length than the KBS-3V repository in case of various canister types and various sites.

TABLE 2. The calculated distances between canisters in Olkiluoto and SKB candidate site Forsmark for various canister types. EPR canister distances are analyzed only for KBS-3V case. In Posiva case, the supercontainer length is assumed to be canister length + 0.9 m.

	Posiva VVER 440	Posiva BWR	Posiva EPR	SKB BWR (40 m tunnel separation)
Distance (m) in KBS-3H, tunnel separation 25 m	9.1 (Ikonen 2003b)	11.0 (Ikonen 2003b)	~10.6	7.3 - 7.95 (Hökmark & Fälht 2003)
Canister length (m)	3.6	4.8	5.25	4.83
Supercontainer length (m)	4.5	5.7	6.15	5.546
Block length, nominal (m)	4.4	5.6	4.45	1.75 – 2.40
Distance (m) in KBS-3V, tunnel separation 25 m	8.6 (Ikonen 2003a)	11.0 (Ikonen 2003a)	10.6 (Ikonen 2005)	6.35 (Hökmark & Fälht 2003
Difference of 3H distance when compared to 3V distance (%)	+12 (Ikonen 2003b)	+/-0 (Ikonen 2003b)	~0	+16 – 26 (Hökmark & Fälht 2003

REFERENCES

Anttila, M., 2005. Radioactive Characteristics of the Spent Fuel of the Finnish Nuclear Power Plants. Posiva Working Report 2005-71. Posiva Oy, Olkiluoto. 310 p.

Hökmark, H. & Fälth, B. 2003. Thermal dimensioning of the deep repository. Influence of canister spacing, canister power, rock thermal properties and near field design on the maximum canister surface temperature. Clay Technology AB. SKB Report TR-03-09. 82 p. ISSN 1404-0344.

Ikonen K. 2003a. Thermal analysis of spent nuclear fuel repository. Report POSIVA 2003-4. Posiva Oy, Olkiluoto. 61 p. ISBN 951-652-118-5.

Ikonen, K. 2003b. Thermal Analyses of KBS-3H Type Repository. Report POSIVA 2003-11, Posiva Oy, Olkiluoto. 43 p. ISBN 951-652-125-8.

Ikonen K. 2005. Thermal Analysis of Repository for Spent EPR-type Fuel. Report POSIVA 2005-06. Posiva Oy, Olkiluoto. 36 p. ISBN 951-652-138-X.

KBS-3H basic design, deposition drift for demonstration, permissible variations, boundary conditions, drawing KBS-3H 003B
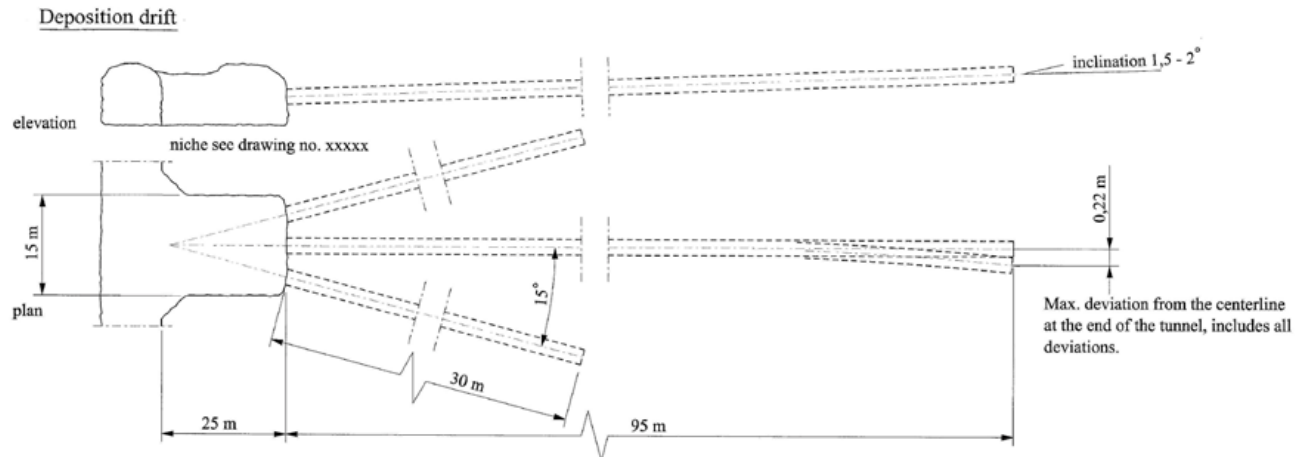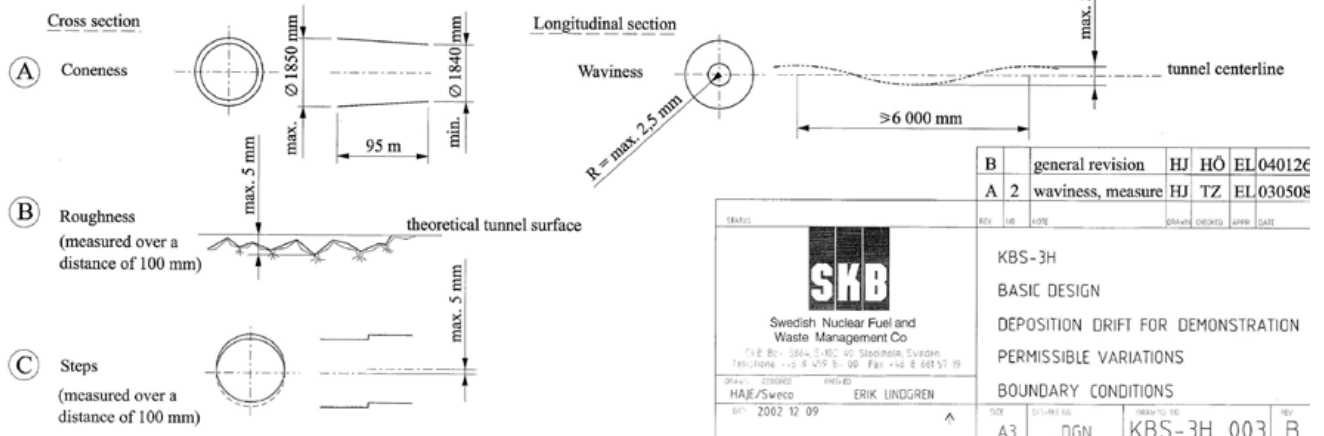
Design basis for design of steel plug, KBS-3H design

INSINÖÖRITOIMISTO		Muistiotunnus	1(4)
SAANIO & RIEKKOLA OY		PROJEKTI-798-7/2006	
Laatija Jorma Autio	Tarkastaja Margit Snellman	Hyväksyjä	
pvm. 16.1..2006	pvm. 2.2.2006	pvm. 2.2.2006	

DESIGN BASIS FOR DESIGN OF STEEL PLUG, KBS-3H DESIGN

A list of design basis as input parameters to be used in the detailed design of steel compartment plug is presented in this document as a table. These parameters will be checked and updated during the detailed design of the steel plug.

The preliminary design, design requirements and design components of KBS-3H repository, which form the basis for this document have been presented in the Design Description 2005 document (Autio, J. 2005). The design is based on installing a steel collar structure in rock before deposition operation starts. The collar is attached in the rock surface and sealed during installation by using concrete. The centre part of the plug is installed during operation in a rapid manner.

The functional requirement of the steel plug is to isolate the "good quality" deposition compartment from "bad quality" water bearing fracture zones, which may have detrimental effect on the distance blocks and supercontainer during saturation. The design requirements are:

a) Sealing of the drift by prevention of flow through the plug including the rock plug interface in order to prevent detrimental flow which could cause erosion of buffer. The flow should be reduced to the same order of magnitude as the flow through the rock. The plug is positioned in good quality rock sections in drift.

b) The plug will tolerate and is capable of maintaining a full hydrostatic pressure in the drift at 400 m level after operation.

c) Support the supercontainers and other components in position during operation phase by forming a confining surface. It is assumed that these forces will be equal or less than hydrostatic pressure during operation.

The plug is positioned so that flow from the drift into the surrounding open tunnels is small enough to eliminate possible erosion.

The design is the same in principle for the BD and DAWE design alternatives, with the exception of lead-throughs for pipes, which are only part of the DAWE design as indicated in the table below. The preliminary design basis and design of the steel plug has been presented in Design Description 2005 Document (Autio, J.). The data has been reviewed and checked by Jorma Autio, Paul-Erik Rönnqvist, Bo Halvarsson and Margit Snellman.

Design Basis, Steel Design, BD and DAWE Candidate Design

Id	Parameter	Unit	Value	Range	Ref.	Comment	Action
A	**Deposition drift**						
A.1	Drift diameter	mm	1850	1835-1850	Autio 2005	Range includes possible 10 mm reduction in diameter and 5 mm stepwise unevenness	
A.2	Surface unevenness	mm	+-5	0-10 mm	Autio 2005		
A.3	Drift inclination	°	2	1-3	Autio 2005		
B	**Pressure**						
B.1	Hydrostatic pressure exerted on plug surface	MPa	5	2-5	Autio 2005	On one surface or on both surfaces as preferable option	The dimensioning basis is fixed after evaluation of alternative solutions
C	**Rock**						
C.1	Elastic modulus, E	GPa	50	30-70		Values are defined for Olkiluoto rock, use of Äspö values is preferred	Äspö values are defined
C.2	Poisson's ratio	v	0.3	0.25-0.35			
C.3	Density	Kg/m3	2700	2650-2850			
C.4	Main principal stresses	MPa	Sxx 15 Syy 25 Szz 11				
C.5	Estimated displacement of rock surface	mm	0.1			Displacement outwards at 5 MPa pressure	
C.6	Hydraulic conductivity	m s^{-1}	10^{-12}	$10^{-8}-10^{-15}$			

Issue	Description	Comment	Action
I.1 Steel			
I.1.1	Steel material	Most common types of carbon steel and cast iron are acceptable. Use of other steel materials have to accepted.	
I.1.2	Steel thickness	It is beneficial if the corrosion of steel plugs occur during the same time range as the corrosion of supercontainer units. Therefore it is beneficial if the thickness of steel is of the same order as thickness of supercontainer (8 mm) being of the order of centimetres.	
I.1.3	Corrosion properties	The expected average life-time corrosion rate is 1 μm a^{-1}.	

I.1.4	Steel quantity	Corrosion of steel produces hydrogen gas, which can cause problems during the evolution of the system. The quantity of gas is dependent on the total amount of steel. Therefore it is beneficial to minimize the total quantity of steel. The present rough estimate is that quantities in the range of 2500 – 5000 kg are allowed.	The quantity of steel in design is defined in the design documents

1.2 Concrete

I.2.1	Concrete material	High pH (11 or higher) concrete may introduce some adverse effects on the behaviour of buffer.	Follow up of the R&D on low pH concrete.
I.2.2	Concrete quantity	Concrete may introduce some adverse effects on the behaviour of buffer. Low-pH concrete (pH less than 11) might have some detrimental effect due to high amount of silica. Therefore the quantity should be minimized. Therefore the quantity should be minimized.	
I.2.3	Additives	Use of concrete additives is restricted according to section 1.3 "other materials". No organic additives are allowed.	

1.3 Other materials

I.3.1	Organic or foreign materials (excluding steel, cast iron, copper, low pH concrete)	No organic or foreign materials are accepted, e.g. rubber and polymers are prohibited. Small amounts of inorganic materials may be accepted after verification but is beneficial to design process not to use such materials because of approval of such materials.	Approval of small quantities of foreign materials if required.
I.3.2	Copper	Copper is assumed to be used in seals between steel components. Use of copper (at the moment presumably of order of 5-500 kg) is allowed.	

I.4 Construction procedure

I.4.1	Installation time during operation	The installation time of the steel plug during operation should be as short as possible. It has been assumed that the plug can be installed in 24 hours or less during operation.	
I.4.2	Installation time before operation	The attachment of steel structures and collars on rock can be installed before operation without time restrictions.	
I.4.3	Free open diameter during operation	A free open diameter, which corresponds to the nominal drift diameter has to remain during operation phase before the steel plug is emplaced. All notches and cavities on the floor shall be filled with low pH concrete to provide even surface for deposition equipment.	
I.4.4	Filling of cavities before operation	All notches and cavities on the drift surface shall be filled with low pH concrete to provide even surface for deposition equipment.	Follow up of the development of low pH concrete.
I.4.5	Filling of cavities after operation	All cavities adjacent to the steel plug shall be filled with bentonite to provide even buffer density in drift after saturation. The penetration of buffer in remaining cavities is compensated by increasing the amount of highly compacted buffer adjacent to cavities.	The compensation of remaining cavities is designed in buffer development acitivity.

I.5 Life time			
I.5.1	Life time	The steel plug should function during a time period when large hydraulic gradient occur. Therefore the plug should function during the operation period until the central tunnels have been backfilled and sealed and have been filled with water. Therefore the expected life time is 100 years.	

I.6 Lead-throughs and fittings			
I.6.1	Lead-throughs	There shall be two lead-throughs for 10 mm diameter air evacuation pipes and four for diameter 17.2 mm wetting pipes based on design with several small diameter pipes. The pipes are described in Design description 2005.	
I.6.2	Filling cap	The open cavities behind the steel plug shall be filled with bentonite (presumably powder and pellets). Therefore the plug is fitted with a filling hole with a cap. It is beneficial if the cap is in the upper part of the plug. The present assumption for the diameter of the filling hole is 150 mm or less.	Size of filling hole to be defined in buffer development activity.

References:

Autio, J. 2005. KBS-3H Design Description, June 2005. Draft.

KBS-3H Steel plug, design specification

Finnmap Consulting
FMC GROUP

REPORT 1

PL 88, Ratamestarinkatu 7 A 00521 Helsinki	PB 88, Banmästargatan 7 A 00521 Helsingfors	P.O. Box 88, Ratamestarinkatu 7 A 00521 Helsinki, Finland	☎ 0207 393 300 ☎ +358 207 393 300	Fax 0207 393 396 Fax +358 207 393 396
Rev	Date	Author	Inspected by	Approved by
	31.5.2006	Ilpo Parkkinen	Jarno Berghäll	Jorma Autio

KBS-3H
STEEL PLUG

STEEL PLUG, DESIGN SPECIFICATION

1. General description

The structure described in this document constitutes a waterproof steel plug in a round horizontal drift of 1.85 metre diameter bored to bedrock. In the drift copper canisters, in which spent nuclear fuel is encapsulated, are being emplaced inside a perforated steel cylinder of ca. 6 metres of length and embedded in bentonite clay between the perforated cylinder and canister. The space between the steel cylinder and the drift will be filled by bentonite swelling through the perforation after the bentonite inside the supercontainer has been saturated sufficiently. The drift will be sealed with the plug thus allowing filling in the forepart of the drift to continue even if the rear of the drift is closed and becoming filled with water.

The principle of the usage of a steel plug is presented in Figure 1.
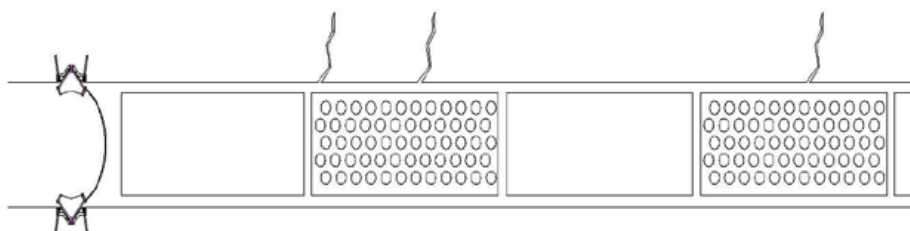
Figure 1. The principle of the usage of a steel plug.

In the basic case a full water pressure is acting on one side of the plug only, the other side being under no pressure. In situation where the buffer in a plugged "tight" drift section absorbs all the water available, pressure may decrease from the initial hydrostatic pressure. In that case two steel plugs are used to isolate highly water leaking fractures, one on each side of the leaking fracture set. When a second plug is installed, water leakage from transmissive fractures into to the space between the steel plugs fills the empty space between plugs and pressure raises rapidly between the plugs to a full hydrostatic pressure. Thereby in certain possible situations the firstly installed plug has to be able to withstand water pressure affecting either way.

2. Structure of the plug

The plug consists of a V-shaped groove excavated to the drift and a matching steel ring (fastening ring), a collar mounted against the ring, and a cap installed on the collar. The space between the ring and the rock is filled with grouting.
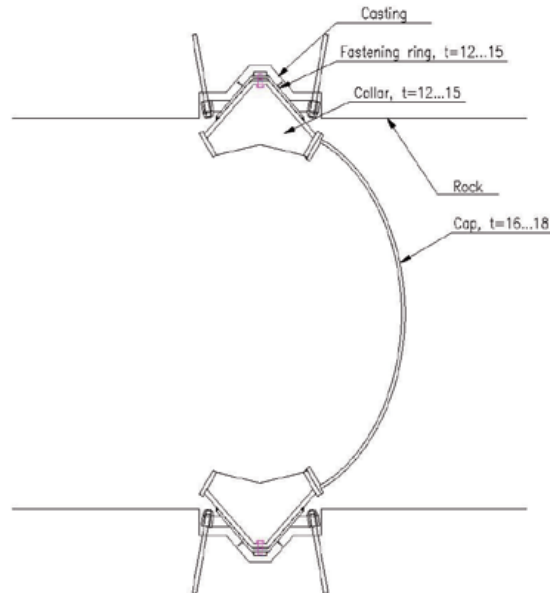
Figure 2. Structure of the plug (one-sided plug, one collar)

2.1 Structure of the cap

The cap has a shape of a dome attached to a flange. The shape of the cap has been chosen so that the stress distribution in the cap would be as even as possible. The height of the cap is 400 mm.

2.2 Two-way pressure loading, V-shaped collar (figure 3)

Construction with which a two-sided plug can be configured with the least number of parts consists of a symmetric groove in the rock and a symmetric fastening ring and collar. This way the behaviour of these parts is similar in either of the two possible directions of the acting force.
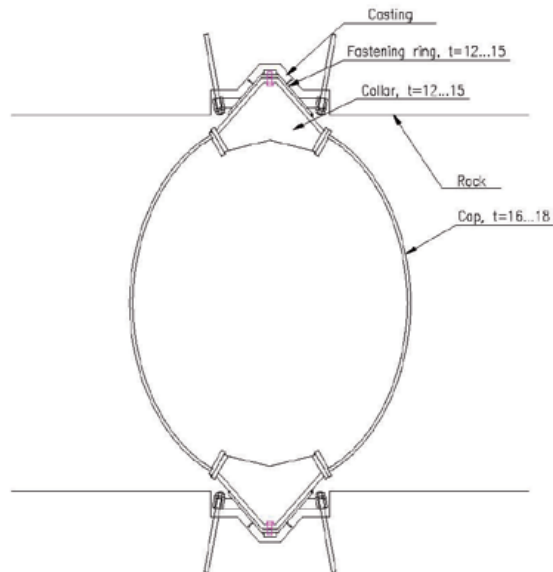
Figure 3. Two-sided plug, one collar

In this construction all or almost all joints are sealed by welding. The fastening ring and collar parts are welded together to form the final parts, and the collar itself is welded to the fastening ring. The rear side cap that is installed first may alternatively be fastened with bolts, but the front side cap is at this stage considered to be fastened and secured by welding.

2.3 Manufacturing

2.3.1 Requirements

The required precision of the parts is very high, especially concerning surfaces to be in connection.

Steel flanges to be inter-connected have shapes of a cone and they will be manufactured using a lathe. Welding of parts produces slight alteration in dimensions, and therefore the compatibility between parts is to be ensured by lathing after the parts have been welded. The compatibility is to be assured by preassembling the parts at the workshop.

Final steel weights of the fabricated parts:

Fastening ring 400 kg
Collar 1250 kg
Cap 440 kg.

The approximate total steel weight of a one-sided plug without bolts is 2090 kg. The bolts add ca. 20 kg to the weight. The grade of the steel used is general structural steel S355J0.

2.3.2 Manufacturing of the fastening ring

The profile of the fastening ring is a blunt-headed V-shape, and bending such a profile to form a circular shape isn't feasible. Therefore, the profile is practical to produce as three sections, which are welded together after having been bent. Thus, the fabrication of the fastening ring is assumed to be performed in six steps:

- prefabrication of the straight sections of the profile
- welding to form the blank
- preliminary lathing of the ring
- welding of the guide parts of the joint and other buildup, cutting the ring into installation parts, and machining of the joint surfaces
- final machining of the connected parts into the finished shape and smoothness
- cutting the welding joint preparations.

The order of the steps may differ from the abovementioned; e.g. weld joint preparations may be cut before final machining.

The joints will be equipped with guides to help position and keep the parts tightly in their position during welding. The guides will be utilised during the final lathing as well. The ring will originally be made oversized to compensate the loss of material in the cutting.

Sufficient extra needs to be provided for the necessary lathing and machining phases.

The slenderness of the final profile may require use of a supporting jig or temporary stiffeners to ensure attainment of the required tolerances.

2.3.2 Manufacturing of the collar

Manufacturing of the collar includes the same fabrication steps as does that of the fastening ring, with the exception of the guides of the joints, which aren't used. The stiffening ribs are welded prior to the final machining, and therefore a separate supporting jig isn't considered necessary due to the already stiff structure.

2.3.3 Manufacturing of the cap

The dome of the cap is pressed and drawn from a flat steel plate of at least the nominal thickness to reach the required tolerances. The flange is manufactured by conventional machine workshop methods, leaving sufficient extra in the first step. The dome and the flange are welded together to form the cap. Finally the flange is machined to reach the required tolerances and surface smoothness.

2.4 Installation

Installation of the steel plug takes place in two phases. In the first phase the fastening ring is seated to its position and the space between the ring and the rock is cast with concrete. This can be done in advance and the time for this phase is not limited. During the second phase, when the supercontainers holding the spent fuel and adjacent distance and filling blocks are installed behind the steel plug, the collar and the cap are being installed.

2.4.1 Installation of the fastening ring

The parts that constitute the ring are assembled together in the final position of the ring. The parts or the ring aren't tied up at this point, but the ring is loose in the groove instead. The parts are placed against each other with help of guides and bolted together. The last part is a short one and it can be slid in its position with help of guides, too.

When the ring is assembled, its centricity, verticality and perpendicularity to the drift are assured and the ring is preliminarily locked to its position with wedges. Holes for anchoring bolts of the ring are then drilled as through drilling and the bolts installed and tightened. At this point the wedges can be removed. The butt joints of the sections are welded and the weld is polished to a degree corresponding the required smoothness of the surface.

After positioning of the ring, the space between the ring and the rock is cast with concrete. All gaps are first sealed with wooden formwork. A tube used for casting is placed to lowest part of the ring, auxiliary cast tubes to the middle and an air outlet pipe is placed to the highest past of the groove. A post grouting pipe of perforated sheet metal will be used to seal possible microfractures caused by shrinkage of cement. A bentonite sealing band inserted to the bottom of the groove is as an option if found acceptable. They may, however, contain polymers which prevent their use. Finally the groove on the bottom of the drift is filled with concrete and the surface is levelled according to the surrounding rock to produce smooth surface for the deposition equipment. Concrete adhesion to the bottom of the fastening ring during the levelling of the surface is hindered e.g. by plastic, thus ensuring easy removal of the concrete prior to installation of the collar.

The required amount of concrete for casting the space between the ring and rock is ca. 190 litres.
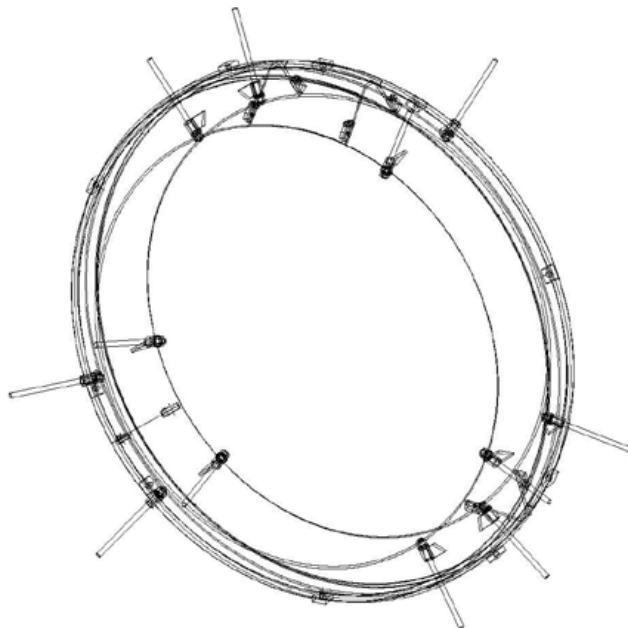
Figure 4. Fastening ring and its division into subparts.
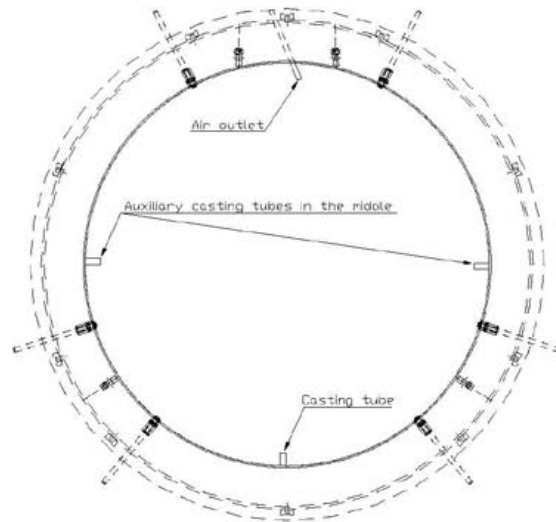
Figure 5. Casting tubes.
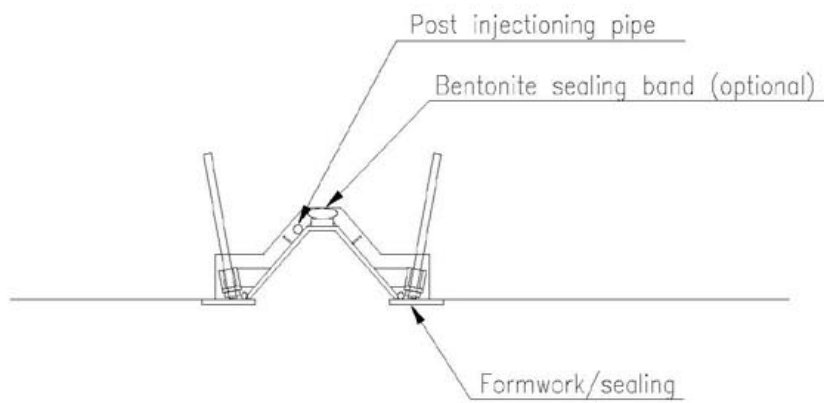
Figure 6. Fastening ring, cross section of the casting arrangement.

2.4.2 Installation of the collar

Before installation of the collar the rear side cap needs to be transported past the plug position beforehand. At the full scale test the cap can be transported e.g. with a pallet truck.

Collar sections are positioned one by one against the fastening ring, and bolts to fastening ring are tightened preliminarily. When the parts are at exact positions in respect of each other, bolts between the parts are tightened. The collar is installed in four sections as well, the last section being a short one that can be slid into its position (figure 7). If considered necessary, appropriate snugness of the last part can be ensured by manufacturing the part to be 1–2 millimeters oversized and using portable machining equipment for removing the excess after fitting. When all sections are in their positions, bolts are tightened to their final tightness and sections welded to each other. The installation is finalised by welding the collar to the fastening ring with a fillet weld around the perimeter. The fillet locations are shown in figure 8.
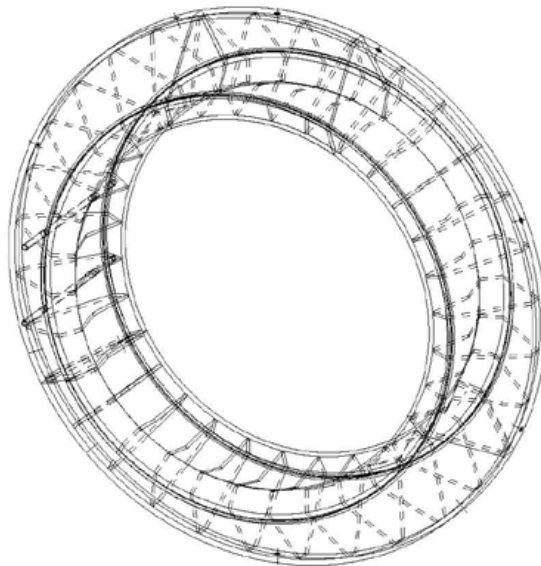
Figure 7. Collar and its division into subparts.
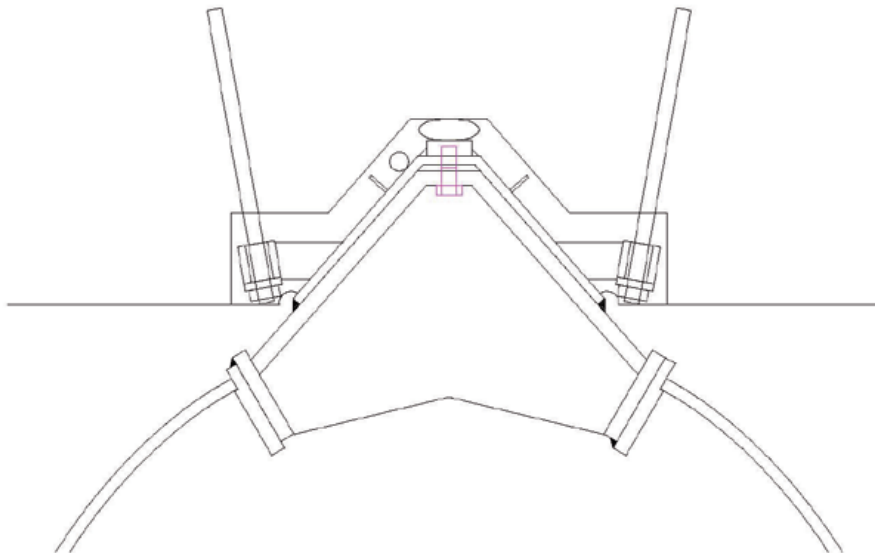
Figure 8. Sealing by welding, fillet locations.

2.4.3 Installation of the cap

The cap is positioned against the collar and eventual installation bolts are tightened. The final fastening is done by applying fillet welding around the cap.

2.4.4 Welding

Welding of the plug parts involves some issues that need to be addressed. A welding method is to be chosen with which the heat involved in the process is minimised. Welding deformations are prone to cause gaps between the fastening ring and the rock thus increasing risk of transmissive cracks and decreased water-tightness.

According to consultation with Welding Engineer EWE (Mr Kari Saaranen) from Ruukki Oy, possible means to restrict unfavourable deformations during welding include symmetrical tack weld placement and welding with back-step sequences to minimise deformations. When welding around the cap, tack welds of length 50 mm with intervals of 200–500 mm are required. A fillet of 5 mm is estimated to be sufficient to guarantee water-tightness. The fillet weld may be inspected with penetration liquid. It is estimated that the four butt welds of the collar reduces the length of the collar by a few millimetres. Straightness of the collar can be preserved by symmetrical execution of the welding. Groove shapes in butt welds as well as the need for backing bars are to be assessed.

Time required for welding was evaluated to ensure that it can be carried out according to requirements. The length of one fillet weld around the collar is ca. 5.7 m. The total amount of fillet weld for a one-sided plug (two weld seams) is ca. 11.4 m.The estimated welding velocity in manual welding is 20 cm/min and

the effectiveness factor is estimated to be 20–50 %, and thereby the duration of the welding process does not constitute a problem. The welding process can also be mechanised.

The welding procedure in general needs to be carefully planned by a welding expert to minimise negative effects.

The plug structure has four contact surfaces that need to be sealed. To ensure tightness between the fastening ring and the rock, the grouting should be of a quality as free from shrinkage as possible and with as good adhesion to the rock as possible. As an extra security a bentonite clay band fitted between the fastening ring and the rock may be used. When getting moist, the bentonite swells and fills the unevenness and cracks of the surfaces. The optimum location for the bentonite seal would be at the bottom of the groove. However, bentonite bands, which are common in many applications, often contain organic material such as polymers, which makes them inappropriate in this application. However, use of small quantities of these or e.g. bitumen type sealing material would facilitate the sealing significantly.

Tightness between steel surfaces can easiest and most reliably be ensured by welding. Some amount of welding is in every case needed when utilising a shared collar for the two caps. Thus, welding is to be used for sealing. If necessary, attaching the cap to the collar with bolts is still possible. If the cap is attached with bolts, a spring seal fitted to a groove (e.g. Helicoflex, www.garlock.net) would be advisable for sealing the joint.

4. Strength calculations

The strength calculations of the plug are performed using Algor software (www.algor.com), which is a Finite Element (FEM) program. Either 6 or 8 node brick elements and either linear or nonlinear material models have been used in the calculations.

4.1 Loads, materials, and safety factors

A pressure of 5.0 MPa representing the pressure of a 500 m high water column, acting perpendicular to the plug surface, has been used as a load in the calculation. The swelling pressure of the bentonite has not been added. It has been assumed that by the time the swelling pressure to develop, the drift will be filled and sealed.

As the material of the plug normal structural steel S355J0 with yield limit of 355 MPa has been used. The following safety factors according to European steel code EC3 have been used:

- the steel material factor $\gamma_s = 1.1$
- the load partial safety factor $\gamma = 1.35$.

4.2 The geometry of the dome

The geometry of the dome has significant influence on stress distribution of the dome. Several different geometries have been tested by modelling and calculating stress distribution for the dome alone. Were the load unidirectional, the most optimal shape for the dome would probably be a parabola, but the load being perpendicular to the surface somewhat changes the situation. Of the potential shapes, an ellipse, a pure parabola and a modified parabola have been considered, in addition to experimental shapes that have been estimated to render a favourable response to the applied load. The observation in general is that a

geometry, whose curvature follows the radial bending moment distribution when considering a plate structure, yields to most advantageous results.

4.3 Calculation model of the entire structure

A calculation model of the entire structure has been built as well. The cap, collar, fastening ring, rock and the casting between the ring and the rock have been included in the model. Contact surfaces have been defined between the cap and the collar, the collar and the fastening ring and the ring and the casting. Continuity has been assumed between the casting and the rock.

The structural alternative that has been modelled is a two-sided plug with one collar.

4.4 Stability

Sufficient safety against loss of stability of the cap needs to be assessed. Eventual means of stability loss include buckling and puncture. These have been examined for the final chosen structure.

4.5 Sensitivity to deviations in form

The cap part will probably be manufactured by pressing and drawing and therefore there may eventually be at least the following form deviations:

- curvature differences from what was planned
- imperfect symmetry
- fluctuation in plate thickness.

These deviations may induce differences between real stresses and those calculated according to theoretical shape and constant thickness, and the consequences of these deviations are studied separately.

FINNMAP CONSULTING OY

Appendices:

Appendix 1: Dimensional drawing of a two-sided plug, cross-section.
Appendix 2: Perspective drawings of a one-sided plug.
Appendix 3: Detailed drawings of the plug parts.   Not included

Finnmap Consulting
FMC GROUP

Appendix 1. Dimensional drawing of a two-sided plug, cross-section.

- Post injectioning pipe (optional)
- Bentonite sealing band (optional)
- Casting
- Fastening ring, t=12...15
- Collar, t=12...15
- Rock
- Cap, t=16...18

20
20

1390

1850

Finnmap Consulting
FMC GROUP
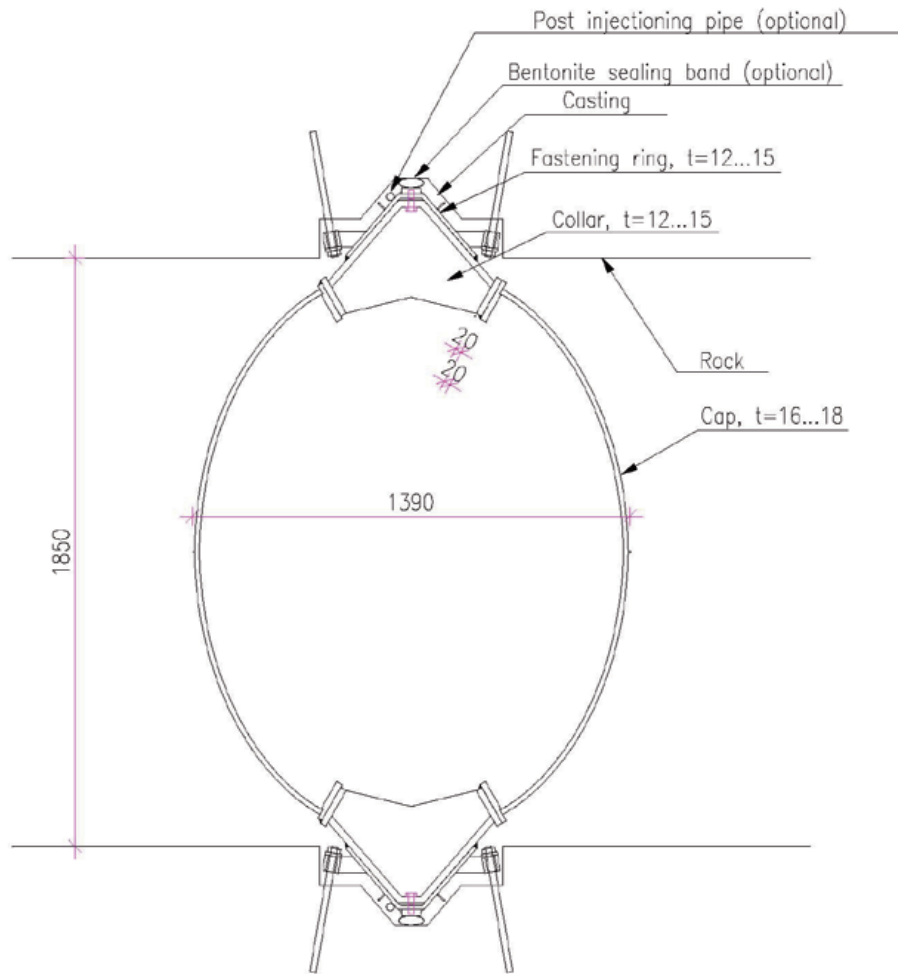
Appendix 2. Perspective drawings of a one-sided plug.
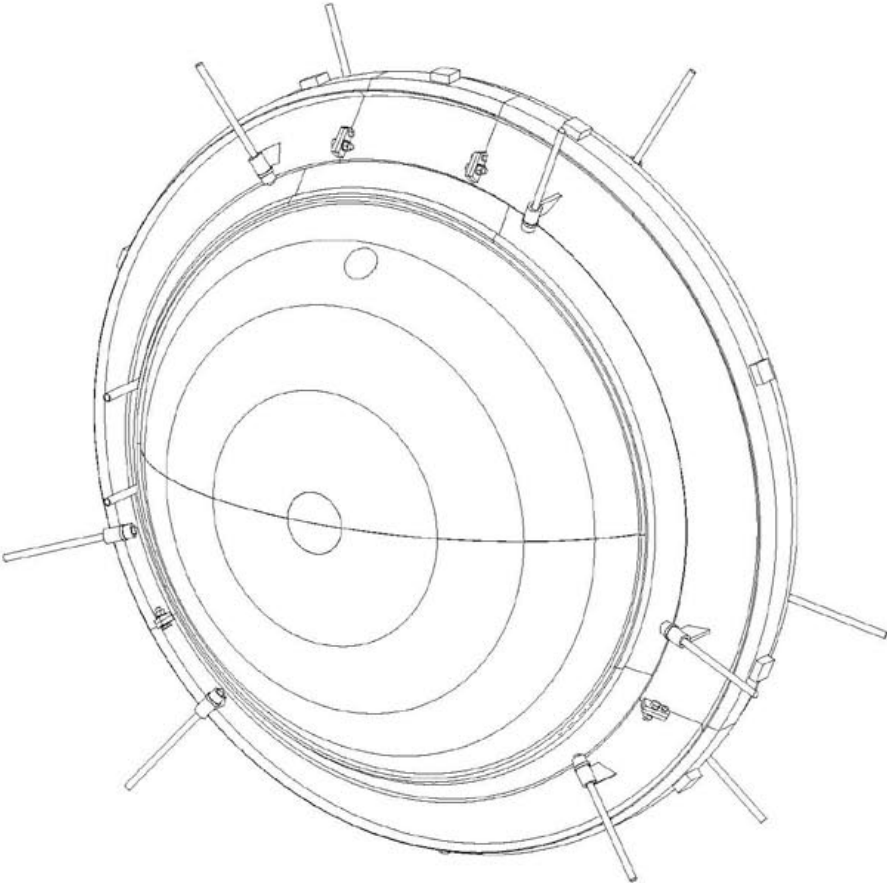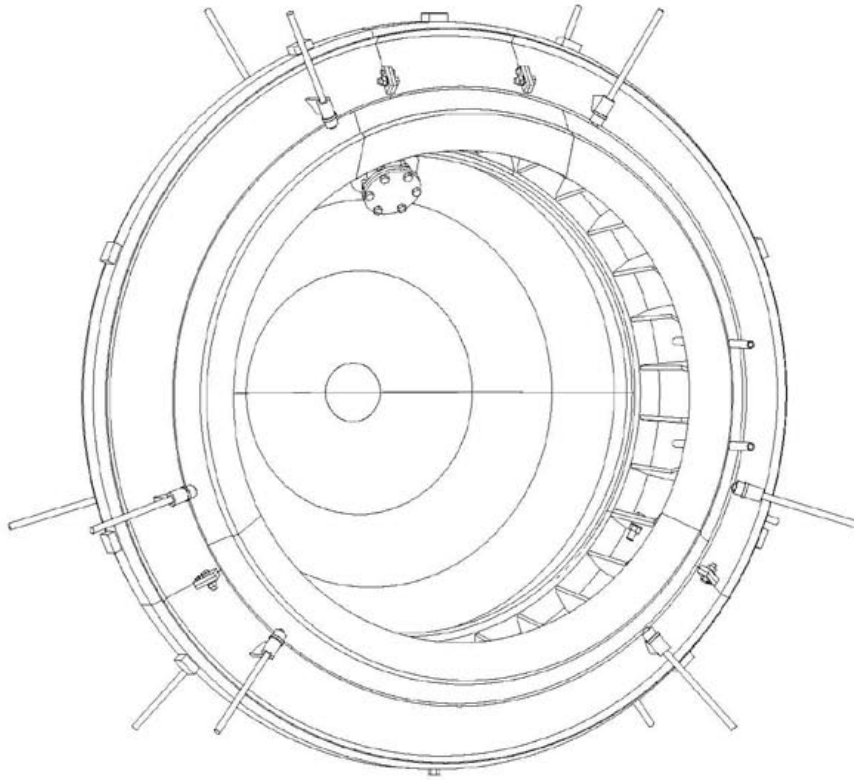
Explosion drawing:

KBS-3H Steel plug, calculation Report of the Steel Plug Structure

Finnmap Consulting FMC GROUP   REPORT   1

PL 88, Ratamestarinkatu 7 A 00521 Helsinki	PB 88, Banmästargatan 7 A 00521 Helsingfors	P.O. Box 88, Ratamestarinkatu 7 A 00521 Helsinki, Finland	☎ 0207 393 300 ☎ +358 207 393 300	Fax 0207 393 396 Fax +358 207 393 396
Rev	Date	Author	Inspected by	Approved by
	12.4.2006	Ilpo Parkkinen	Jarno Berghäll	Jorma Autio

**KBS-3H
STEEL PLUG**

Calculation Report of the Steel Plug Structure

Contents

1.   General

The structure to be analysed is a watertight steel plug positioned into a round horizontal drift bored to the bedrock. The diameter of the drift is 1.85 metres. After the drift has been sealed with the plug, water pressure against the plug will develop to a full hydrostatic pressure, thus necessitating the plug to resist a pressure corresponding to 500 metres of water.

The analysis has been carried out using a general FEM program Algor (Algor Inc., www.algor.com). The structure has been modelled wit either 8- or 6-noded brick elements. Due to symmetry, a quarter of the plug is usually modelled.

1.1   Structure

A cross-section of the plug structure is shown in Figure 1.
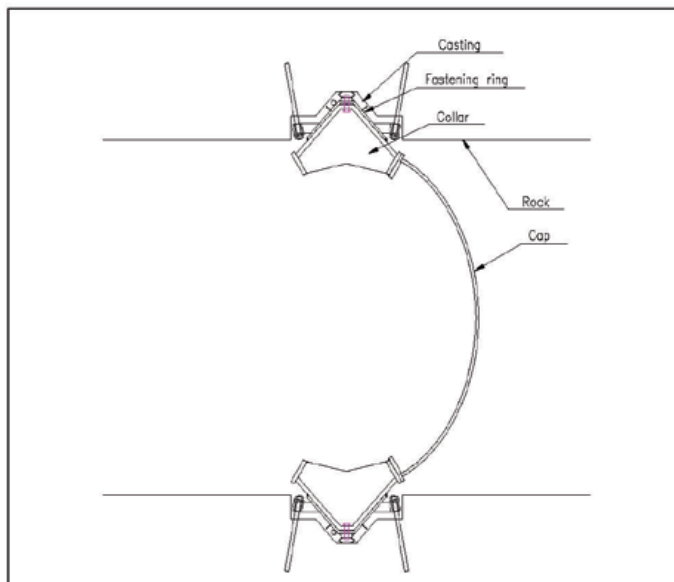
Figure 2. Cross-section of the analysed structure.

The plug consists of three distinct parts. Outermost there is a fastening ring that is mounted to a groove in the rock and attached to the rock. Forces from the cap that comprises the actual water barrier are transferred to the fastening ring and thence to the rock through a steel collar. The collar is stiffened with rib plates.

The diameter of the cap is 1650 mm and the height is 400 mm. The exact structure is shown in drawings RT100–RT207.

1.2 Materials

The whole structure FEM model consists of three different material layers. Outermost is the rock, for which an elastic modulus of E = 50 GPa has been used. For steel parts the standard values E = 210 GPa and υ = 0.3 have been used. The space between the rock and the fastening ring is filled with concrete casting, for which an elastic modulus of E = 35.5 GPa has been used.

The steel grade used in the steel parts is structural steel S355 with nominal strength of 355 MPa.

1.3 Loads and coefficients

The basic load acting on the surface of the cap is 5 MPa corresponding to pressure of 500 metres of water. The direction of the load is perpendicular to the surface. A load safety factor γ = 1.35 and a material safety factor γ = 1.1 according to Eurocode 3 have been used.

Below is a summary of the design data.

Design data		Geometry	
Pressure	5 MPa	Diameter of the membrane	1650 mm
Load safety factor	1.35	Height of the membrane	400 mm
Material safety factor	1.1	Thickness of the membrane	16 mm
Material	Steel S355	Collar main plates thickness	20 mm
Grout elastic modulus	35.5 GPa	Thickness of the grout layer	40 mm
Rock elastic modulus	50 GPa	Thickness of the rock layer	60 mm
Steel elastic modulus	205 GPa		
Poisson's coefficient	0.3 (0.15 grout)		

The calculation strength of the steel is f_d = 355 MPa / 1.1 = 323 MPa.

2. Stress and displacement study of the dome

The optimum shape for the dome has been searched by modelling only a quarter of the dome itself without any surrounding parts such as the flange. Several different geometries for the dome have been studied, including an ellipse, a parabola, a 3rd degree curve, and different curves based on trial and error.

2.1 Model geometry and restraints

The dome element mesh includes a quarter of the dome. The perimeter of the dome is considered to be rigidly fixed. Symmetry boundary condition is applied on the other boundaries.

The shape for the dome is chosen from the candidates by obtaining a shape with which the maximum peak stress value is lowest. The chosen shape for the dome is derived by trial and error and it is shown in Figure 2.
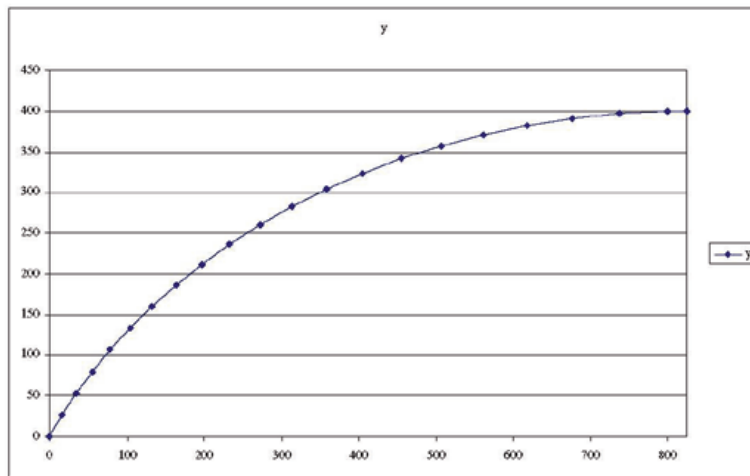
Figure 2. The chosen shape for the dome.

2.2 Loads

The load of the dome is defined as surface load acting perpendicular to the top surface of the dome. There is only one load case with pressure load 5 MPa and load factor 1.35.

2.3 Results

The von Mises stress distribution is shown in Figure 3 and displacements of the dome in Figure 4.
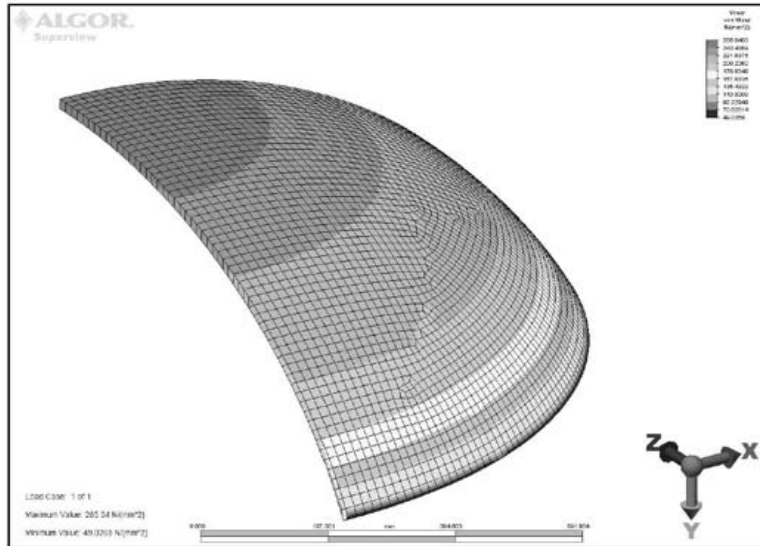
Figure 3. The von Mises stress distribution.
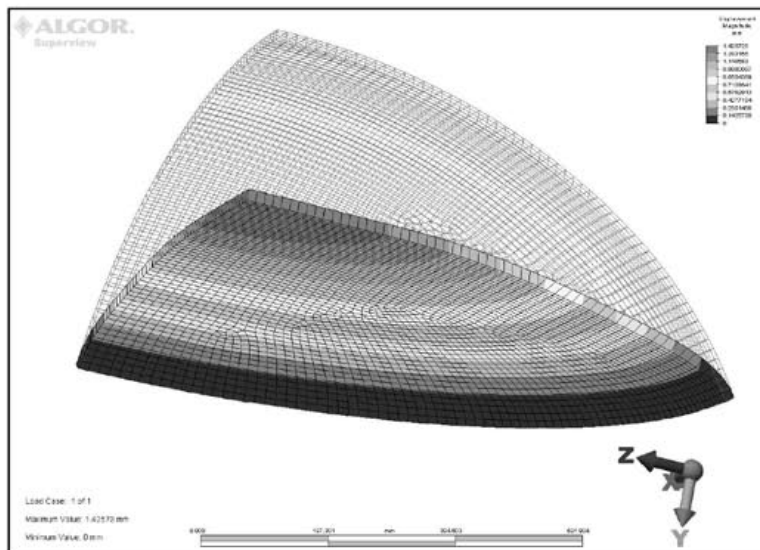
Figure 4. Displacements.

As can be seen in Figure 3, highest stresses occur at the centre of the dome. Some stress concentration can be seen at the perimeter of the dome, where there is a fixed boundary condition. The von Mises stresses are below the calculation strength $f_d = 323$ MPa, and hence the stresses are on an acceptable level.

Maximum displacement at the centre of the dome is 1.4 mm with a load factor of 1.35, and thereby the displacement with the nominal load of 5 MPa is ca. 1 mm.

3.   Evaluation of the complete structure

In the model of the complete structure, the dome is supported by a collar through cone-shaped flanges. Forces from the collar are transmitted by contact surfaces to the fastening ring and thereafter to the casting and rock.

3.1   Model geometry and restraints

The model of the whole structure includes all steel parts, rock, and the concrete cast between the rock and the steel. The model geometry is shown in figure 5.
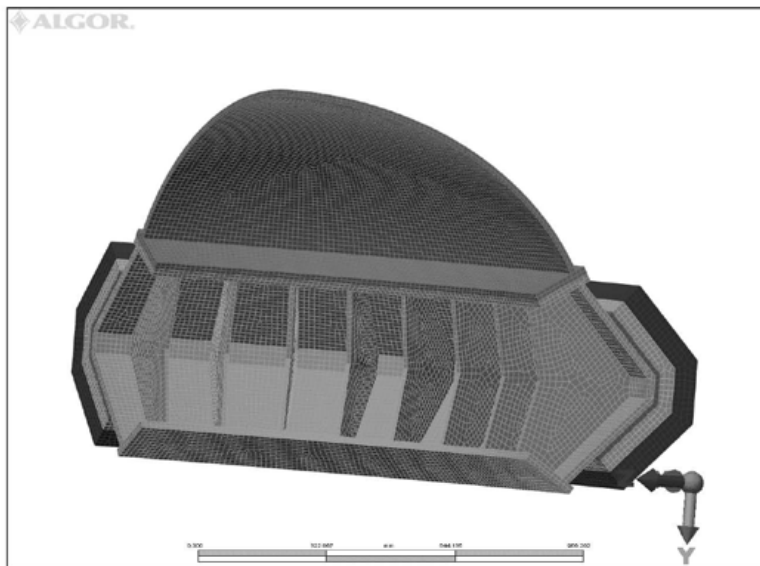
Figure 5. Model geometry.

In figure 5, each different part is represented by a different colour. A contact surface allowing parallel movement of the parts in respect of each other is defined between parts. Between the concrete casting (grey) and rock adhesion is assumed, therefore a fixed connection between the surfaces is defined.

Symmetrical boundary conditions are applied on the cut planes of the model. A fixed boundary condition is applied on the outer surface of the rock.

3.2 Loads

The pressure load of 5 MPa with a load multiplier of 1.35 is acting on the dome equally with the dome model. In addition to that, the load is acting on the narrow strip of the collar exposed to water.

3.3 Results

The displacements of the structure are shown in figure 6. The load factor 1.35 is included in the values. The displacements outside the dome are of a magnitude of tenths of millimetres.
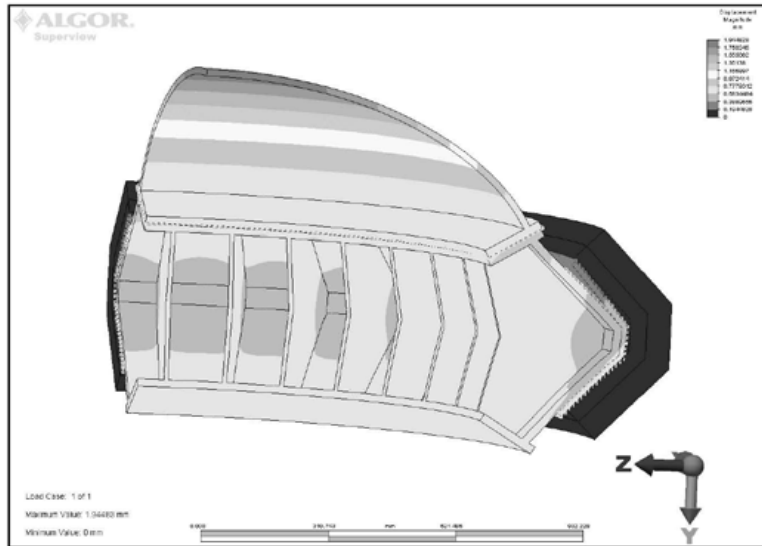
Figure 6. Displacements.

Von Mises stresses are shown in figure 7. Outside the dome, which is covered by the distinct model, highest stresses appear in the stiffening ribs. The stress level (maximum stress 230 MPa) is, however, well below the calculation strength of the steel.
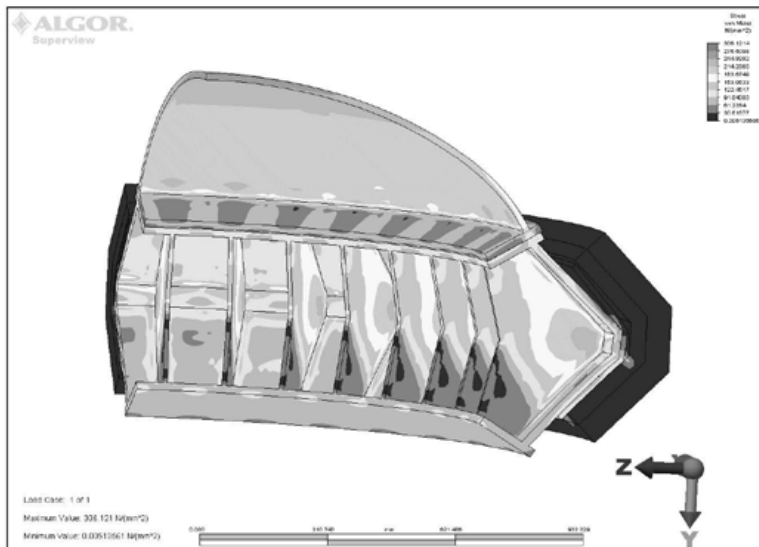
Figure 7. Von Mises stress.

Compression stresses in the concrete cast are shown in figure 8. Stress peaks can be seen at the intersection points of the collar profile and stiffening ribs. The maximum stresses in general are ca. 100 MPa. Stress peaks are somewhat higher than that, but the area where stresses above 100 MPa occur is negligible.
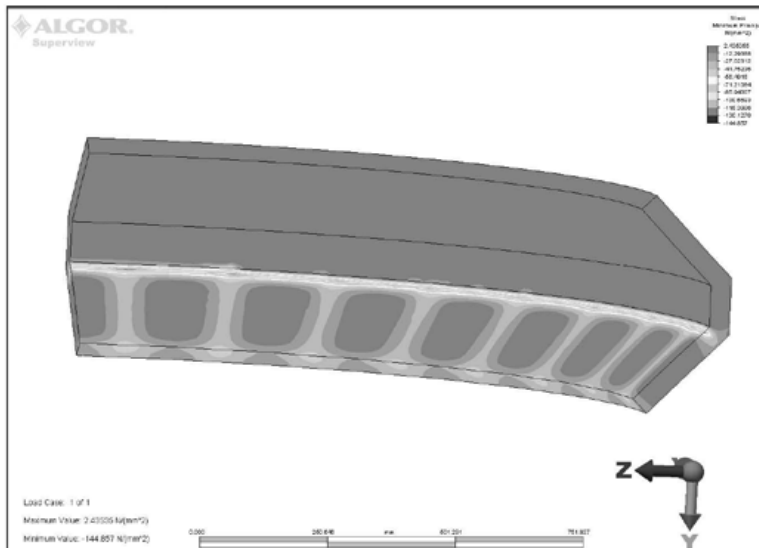
Figure 8. Minimum principal stress in the concrete cast.

The compression is evening out rapidly in the concrete cast. In the rock, at the bottom of the groove, highest compression stress values are ca. 32 MPa. The stresses are shown in figure 9.
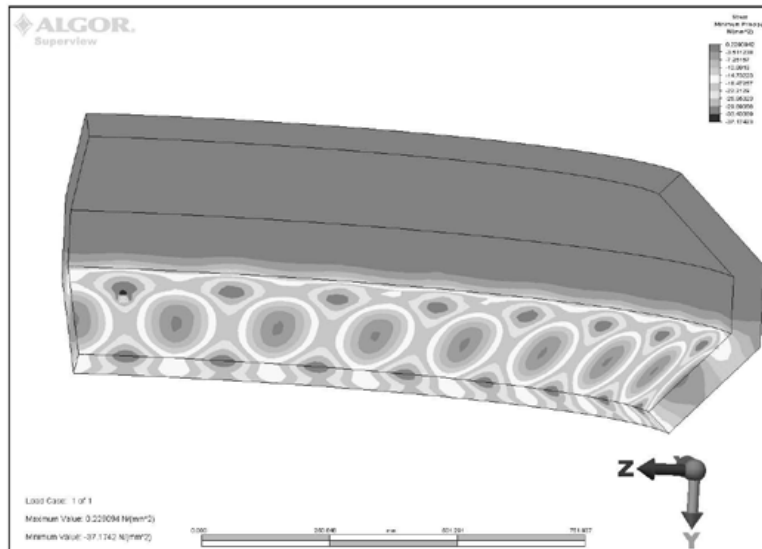
Figure 9. Minimum principal stress in rock at the bottom of the groove.

4.   Snap-through

Resistance against snap-through was evaluated with a nonlinear Mechanical Event Simulation solver. Both material and geometric nonlinearity were used. The load was applied stepwise. The time vs. load multiplier curve is shown in figure 10. Load multiplier 1.0 represents the nominal load 5 MPa.
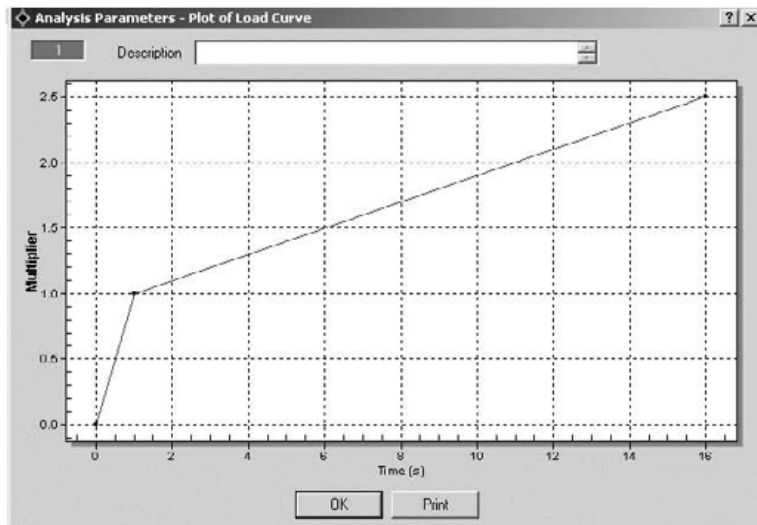
Figure 10. Load curve.

The material model was von Mises with isotropic hardening. The yield limit was 355 MPa and the strain hardening modulus 100 MPa. A small value for strain hardening modulus was chosen to represent material whose stress remains nearly constant above the yield limit.

In the iteration, Combined Newton without line search was used as the iteration method and displacement as the convergence criteria. Due to the complexity of the calculation process, only the dome was included in the model. Boundary conditions were equal with the first model, where static stresses of the dome were analysed.

The initial calculation time step was chosen to be 1/10 of a second. However, if the calculation ceases to converge, the program automatically decreases the time step until convergence is regained. Due to the abrupt nature of the phenomenon, the convergence is easily disrupted close to the snap point. Since the post-snap behaviour isn't of interest here, the possibly impaired accuracy after the snap-through doesn't constitute a problem.

In figure 11 the displacement of the centre of the dome against time is shown.
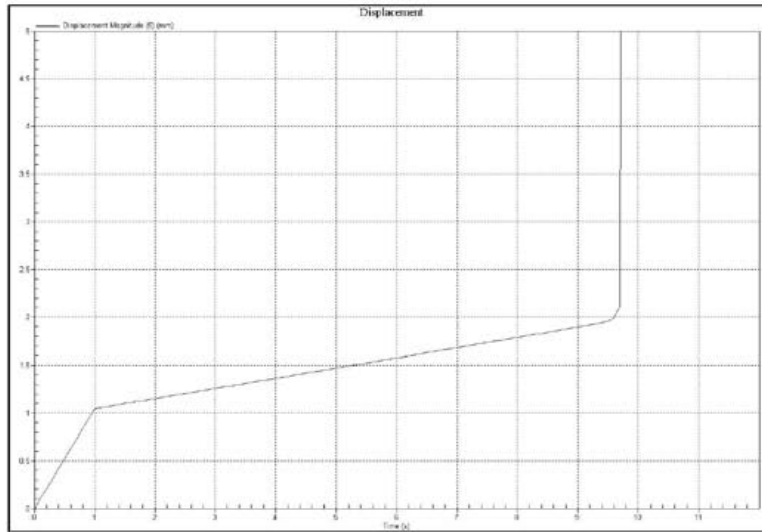
Figure 11. Displacement as a function of time.

In figure 11, it can be seen that the displacement follows the applied force linearly up to ca. 9.8 seconds. At that point the displacement increases rapidly as the dome reaches the snap-through point. The load factor corresponding $t = 9.8$ sec is ca. 1.8, therefore safety against snap-through is 1.8. The displaced shape of the dome after the snap-through is shown in figure 12. Note that the displacement value is unreliable, since there are numerous error sources due to the abruptness of the event.
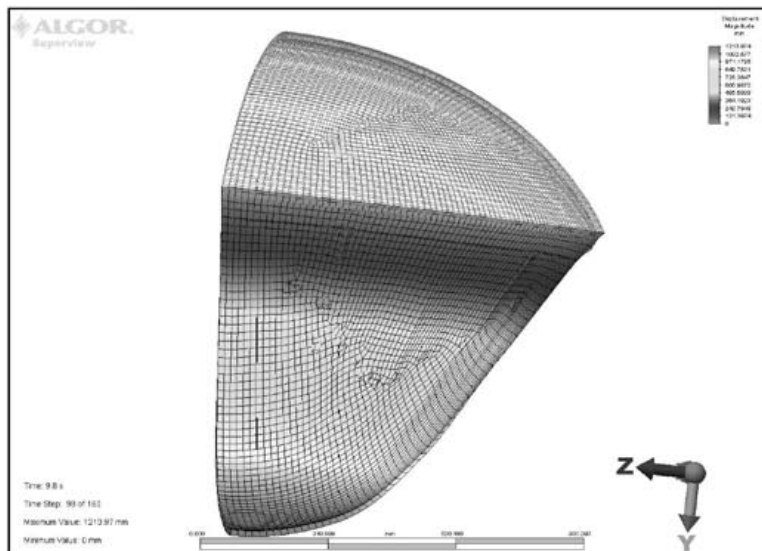
Figure 12. Deflected shape after snap-through.

5. Effect of shape deviations of the dome

To examine the effect of eventual shape imperfections produced in the manufacturing process, a two-phase approach has been used. Firstly, a load is applied on the dome that results to a distorted shape. Secondly, the distorted shape is used as a base geometry, and the original load of 5 MPa is applied on the distorted surface. Two different shapes have been examined. In initial shape deviation 1 there is a depression with a depth of 5 mm at halfway of the radius of the dome. The diameter of the depression is ca. 300 mm. In initial shape deviation 2 the centre of the dome has shifted sideways. Maximum deviation from the theoretical shape is 5 mm as in shape 1. The two shapes are shown in figures 13 and 14. Note that the shape deformations are strongly exaggerated in the figures.
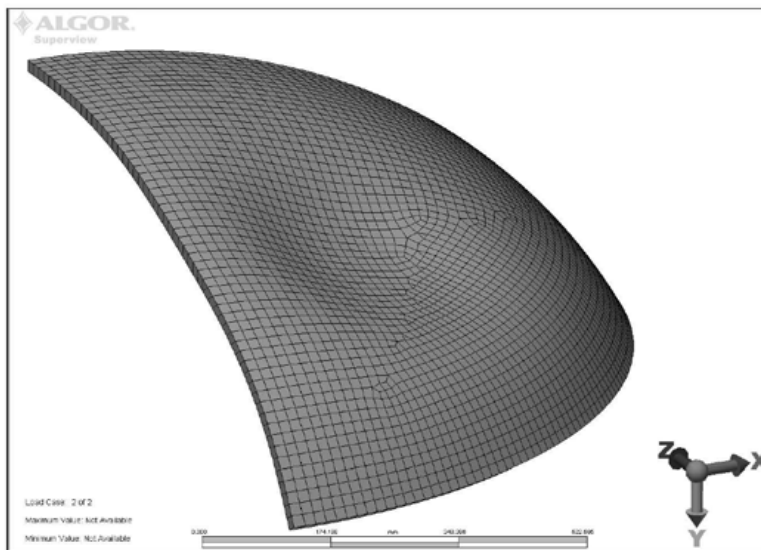
Figure 13. Initial shape deviation 1.
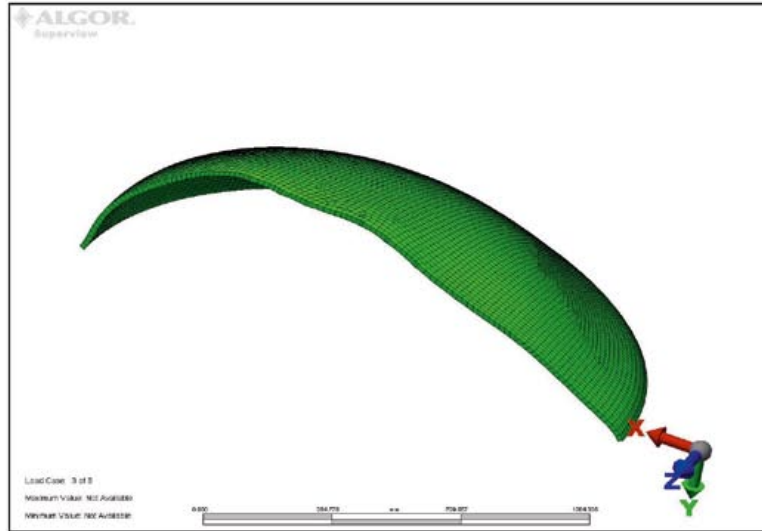
Figure 14. Initial shape deviation 2.

5.1 Effect on stresses

The von Mises stresses resulting from the shape deviations are shown in figures 15 and 16.
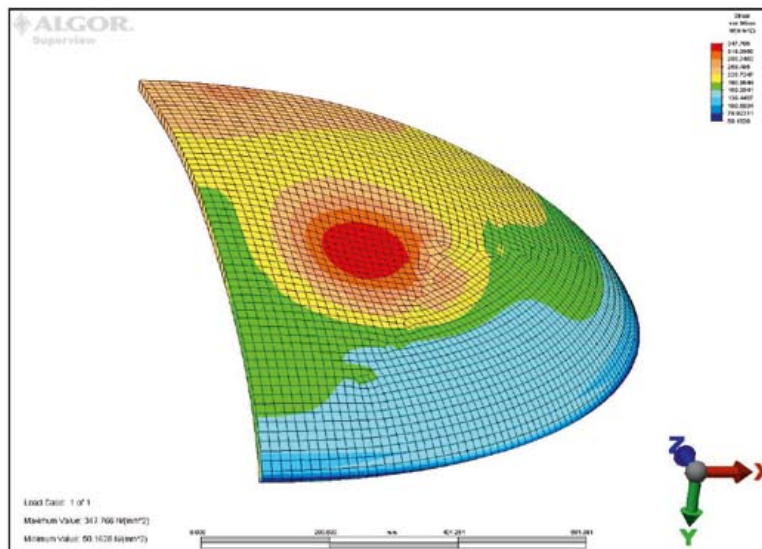
Figure 15. Von Mises stresses, initial shape deviation 1.
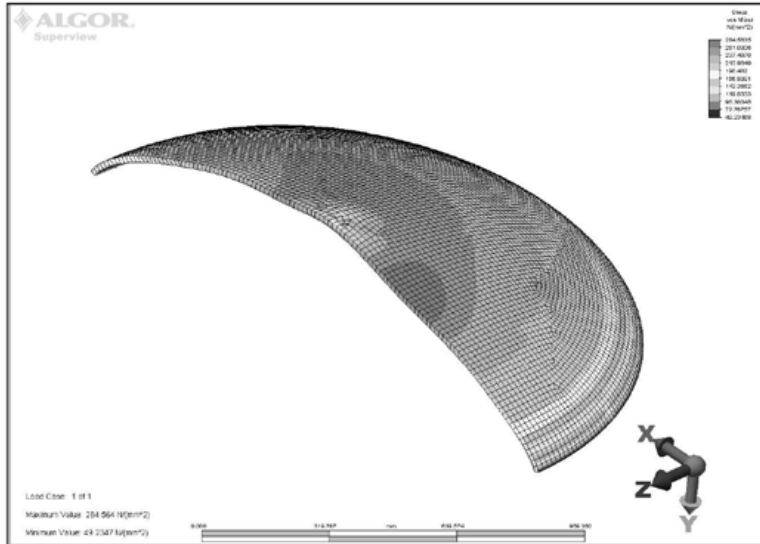
Figure 16. Von Mises stresses, initial shape deviation 2.

As shown in figure 15, the maximum von Mises stress is 348 MPa, which is slightly over the calculation stress of 323 MPa, but still below yield limit. Von Mises stresses from initial shape deviation 2 are shown in figure 16. Here the maximum stress is 285 MPa, which is well below the calculation strength of the steel.

It can be concluded that minor deviations (less than 5 mm) in shape do not cause excessive stresses.

5.2 Effect on snap-through

A nonlinear analysis was conducted for both of the deformed shape models. Except for the shape of the dome, the models were identical with the one presented in section 4.

In the calculation, the iteration of the model with initial shape deformation 1 stopped converging at time step t = 8.8 seconds corresponding a load of 1.7 times the nominal load. The deflection of the dome at that point is shown in figure 17.
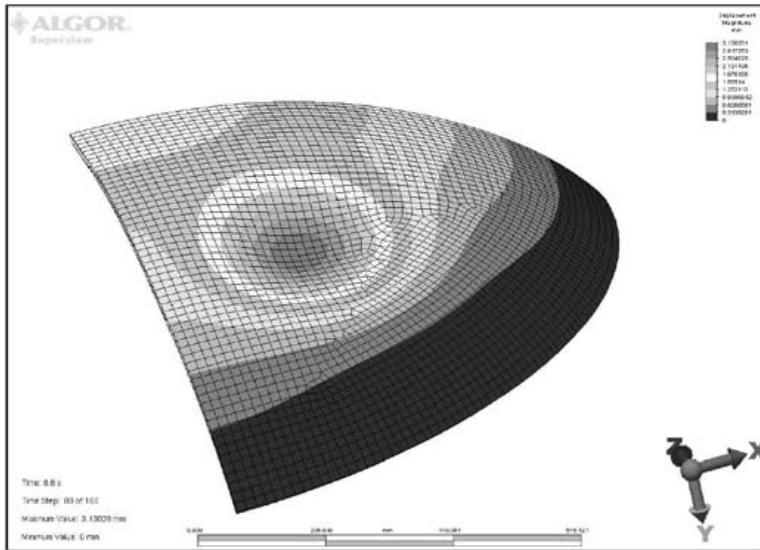
Figure 17. Nonlinear calculation, deflection of initial shape deviation 1.

The deflection vs. time plots of midpoint of the dome and bottom of the depression are shown in figures 18 and 19, respectively.
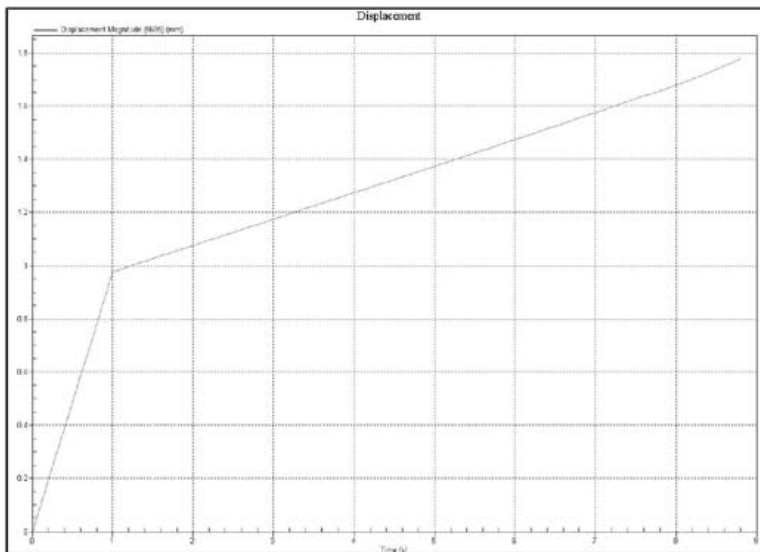
Figure 18. Initial shape deviation 1, deflection of midpoint of the dome.
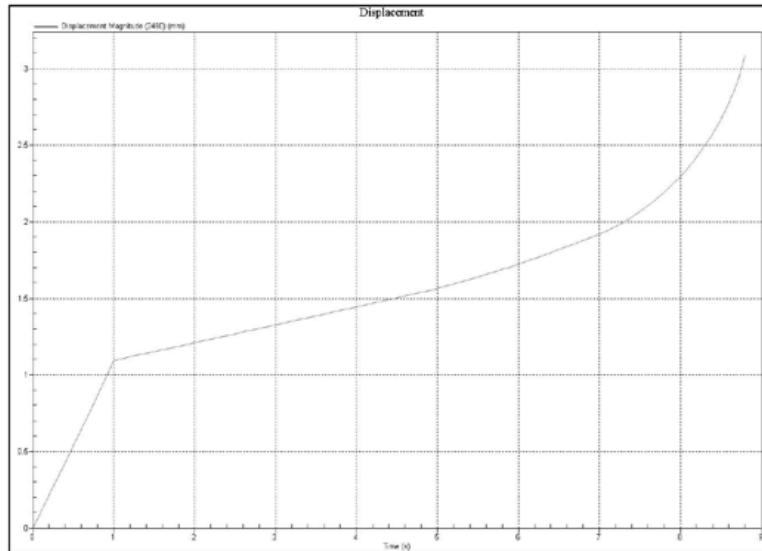
Figure 19. Initial shape deviation 1, deflection of bottom of the depression.

It can be seen from figures 18 and 19 that nonlinear effects concentrate on the locale of the depression. This is most likely due to abrupt changes in geometry which are caused by the small area of the depression. It is, however, not likely that such abrupt changes exist after manufacturing, but the deviations are expected to be smoother instead. Nonetheless, load resistance is almost the same as that of the theoretical structure. Figure 18 also denotes that the snap point of the whole dome is not yet reached.

The snap-through load of the model with initial shape deviation 2 is practically the same as that of the theoretical structure. The deformations prior to the snap point are shown in figure 20.

Finnmap Consulting
FMC GROUP
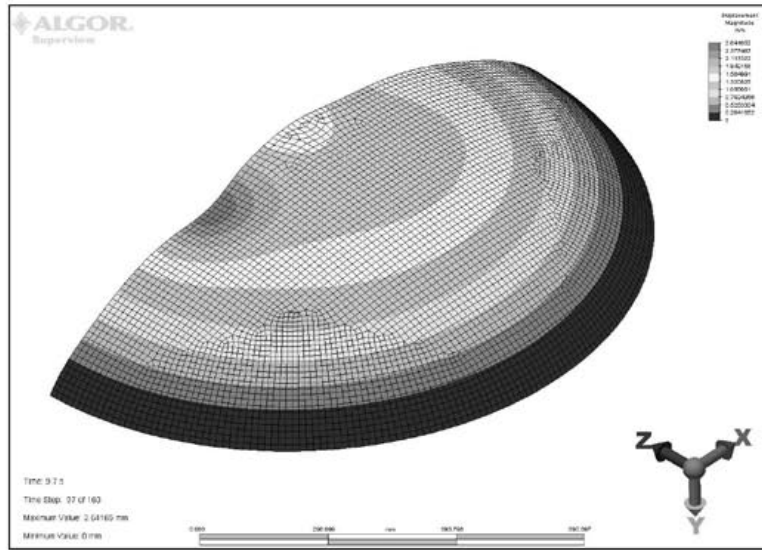
Figure 20. Initial shape deviation 2, deflections prior to snap point.

Design of buffer components and Distance blocks for the KBS-3H design alternative

By Lennard Börgesson and Torbjörn Sandén, Clay Technology AB. March 2007.

J.1 Introduction

The KBS-3H alternative implies a number of buffer components:

1. **Bentonite blocks inside the supercontainer.** Bentonite blocks of two types, ring shaped along the canister and cylindrical at the ends, will be installed in each supercontainer.

2. **Distance blocks.** Between each supercontainer section, distance blocks will be placed in order to seal every section hydraulically. Different designs are suggested.

3. **Fixing ring.** If the water inflow rate into a supercontainer section is of a certain rate, it is possible that the section is filled with water in a short time and a hydrostatic pressure starts to build up on the distance block. A fixing ring is a supporting steel ring, which is fixed mechanically to the rock in order to prevent movements of the distance block.

4. **Filling blocks.** Filling components are used next to plugs and in sections with high water inflows.

This report describes the design of the different buffer components i.e. dimensions, initial density and water ratio.

J.2 Buffer block in supercontainer

J.2.1 General

A main part in the KBS-3H alternative is the use of a "supercontainer". Bentonite blocks will be installed inside the supercontainer, surrounding the copper canister. The final average density at saturation of the blocks after having swelled through the perforated steel container and filled the volume between the container and the rock should be between 1,950–2,050 kg/m³ (dry density 1,481–1,637 kg/m³). Two types of block will be installed: ring shaped blocks around the canister and cylindrical blocks at each end of the container. The initial density of the blocks, before emplacement, will vary depending on block type.

J.2.2 Initial conditions

The suggested design requires blocks with high initial density depending on the rather large slots that should be filled. The production of the blocks is described in Chapter J.5. Table 2-1 shows the dimensions used for the calculations and also the calculated dry density of the blocks. In Figure 2-1 the dry density of the blocks is plotted vs. the saturated density after swelling and homogenisation. The tolerances of the dry density on the manufactured blocks are rather large (1,791–1,979 kg/m³ for the ring shaped blocks and 1,665–1,841 kg/m³ for the cylindrical end blocks) in order to get an average density at saturation between 1,950–2,050 kg/m³ in the tunnel.

Table 2-1. Table showing the dimensions used in the calculations. The table also shows the calculated dry density of the blocks that will be used in the supercontainer.

Dimensions

Rock

Diameter tunnel, mm	1,850

Super container

Outer diameter, mm	1,765
Inner diameter, mm	1,749
Thickness of container and end plate, mm	8
Degree of perforation	62%
Length, mm	5,546

Canister

Outer diameter, mm	1,050

Ring shaped block

Outer diameter, mm	1,739
Inner diameter, 1060	1,060

Cylindrical end block

Outer diameter, mm	1,739

Calculated block data

Ring shaped block

Target average density at saturation, kg/m³	2,000
Initial block dry density, kg/m³	1,885
Initial block void ratio	0.480

Cylindrical end block

Target average density at saturation, kg/m³	2,000
Initial block dry density, kg/m³	1,753
Initial block void ratio	0.592
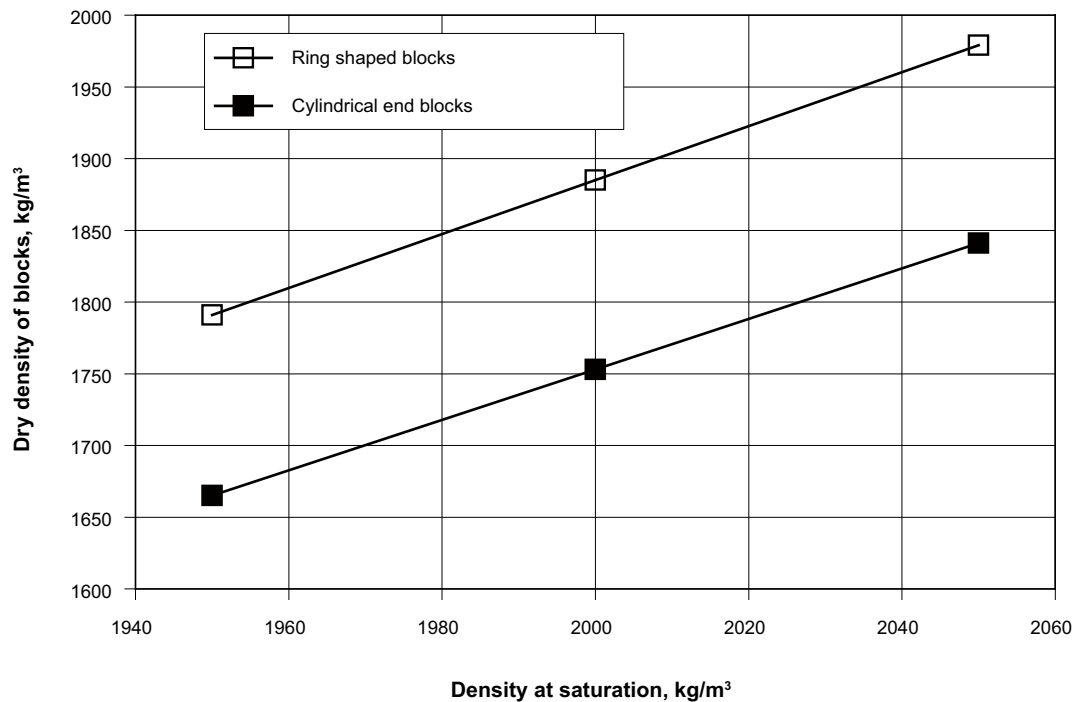
Figure 2-1. *Diagram showing the dry density of the blocks (dimensions according to Table 2-1) plotted vs. the density at saturation in the tunnel after swelling and homogenisation. The two different block types in the supercontainer (ring shaped and cylindrical) are shown in the diagram.*

J.2.3 Sensitivity for variations of the tunnel diameter

The calculations are done using the nominal diameter of the disposal tunnel i.e. 1,850 mm. The diameter will however vary and this will influence the density at saturation in the system. The diagram in Figure 2-2 shows how the density at saturation will vary with different tunnel diameters. The figures in the diagram assume a density at saturation of 2,000 kg/m³ at the nominal tunnel diameter (1,850 mm).

J.2.4 Sensitivity for corrosion of the supercontainer

Investigations are going on regarding the behavior of the steel in the supercontainer during corrosion. Calculations of some extreme mechanical effects of complete corrosion have been done for three different cases:

1. The volume of the emplaced steel is the same after corrosion.
2. The volume of the corroded steel is zero.
3. The volume of the emplaced steel has been doubled after corrosion.

In Table 2-2 the results from the calculations are shown for both block types. The influence is limited for the ring shaped blocks but larger for the end blocks depending on the rather large end plate of the container.

Table 2-2. Table showing how corrosion of the supercontainer influences the final average density of the buffer. Three different cases have been calculated: the steel volume is the same after corrosion, the steel has no volume and the steel volume is doubled.

| Block type | Saturated density for the different volume cases | | |
	Same volume kg/cm3	No volume kg/cm3	Double volume kg/cm3
Ring shaped block	2000	1991	2009
Cylindrical block	2000	1982	2016
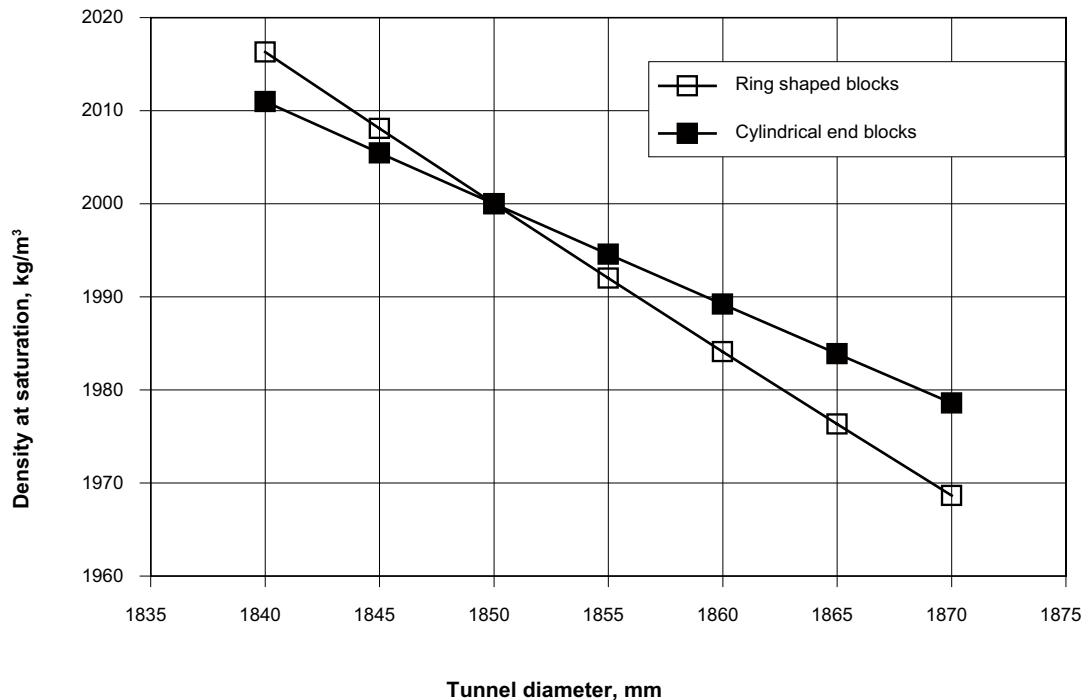
Figure 2-2. Diagram showing the density at saturation in the tunnel after swelling and homogenisation (intended density at saturation 2,000 kg/m³) plotted vs. various tunnel diameters. The earlier calculations are done using the standard diameter 1,850 mm, but there will probably be variations in the real case.

J.3   Distance blocks design alternatives

J.3.1   General

An important component in the KBS-3H design is the distance block. The distance blocks are required to prevent water flow between the supercontainer sections. The function of distance blocks was identified as a critical design issue in the KBS-3H test plan, Figure 3-1. The influence of the hydraulic conditions in the surrounding rock is very strong i.e. water inflow rate and water pressure increase rate.

The design and function of distance blocks in the KBS-3H alternative has been investigated in a number of laboratory tests /Börgesson et. al. 2005/ and Appendix K of this report). Most of the tests have been performed in scale 1:10 in order to save time and money. The investigations have yielded that the alternative is feasible but also that additional tests are needed. The scale effect is an example of an issue that has to be more carefully studied.

The laboratory investigations have so far resulted in four different suggested alternatives for design of the distance blocks. It is probably necessary and also feasible to have a number of different designs depending on the actual rock conditions.

The alternatives have so far not dealt with the problems regarding the installation technique.

The reference case for the first studies was:

• An inflow rate of 0.1 l/min in a supercontainer section.

• When the inflow was stopped, a water pressure increase rate of 0.1 MPa/h up to maximum 2 MPa.

Later hydrological studies /Hellä 2006/ have shown that the water inflow and the water pressure increase rates can be much higher. Therefore, additional test series have been performed simulating these extreme cases, which thus deviate from the reference case. The values simulated in this test series was:

• An inflow rate of 1 l/min in a supercontainer section.

• When the inflow was stopped, a water pressure increase rate of 1 MPa/h up to maximum 5 MPa.

These conditions are very tough for the distance blocks to handle, but on the other hand, a distance block design that can seal for these high water inflows and withstand the fast pressure increase rate is a very robust design for most of the cases. For the reason of robustness only the designs that can withstand these conditions have been proposed.
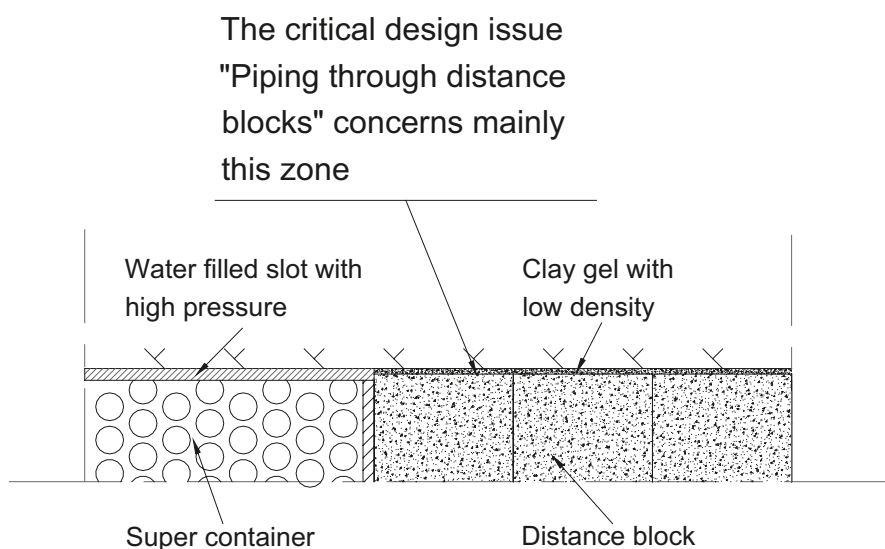
Figure 3-1. *Figure showing a schematic drawing of the critical issue "piping through distance block"*

J.3.2 Design alternative 1 (5 mm slot)

A number of tests have been performed in scale 1:10 (diametrical) and with a test length of 1 metre. In the test series several parameters have been varied such as slot widths, centred and non-centred blocks, pellets filling in the slot and also a pre-wetting of the slot. The results showed that a slot of 5 mm can be accepted under these conditions if the slot is pre-wetted. A design that seems to work for these extreme conditions is shown in Figure 3-2. Tests with this design and conditions were repeated three times in the laboratory.

Layout:

• Centred blocks with 5 mm slot to the rock
• Pre-wetting of the slot
• 3.5% salt in the water.

The layout demands that special sealings are made around the inner distance block against the supercontainer and also at the outermost block against the fixing-ring due to the pre-wetting of the gap bentonite/rock. The sealings can be rather simple, perhaps made of bentonite, since its only purpose is to withstand the pressure from the water when filling up the slot (the pre-wetting).

The difference in diameter between the deposition drift and the distance blocks is only 10 mm. The small gap and the demand to centre the block radially could be a problem for the installation. The laboratory experiments indicate that this is the maximum gap that can be allowed for these extreme conditions without controlling the water pressure.

J.3.3 Design alternative 2 (10 mm slot and controlled water pressure)

Tests have also been made in a similar test device with the test length 3 meter. In this device a design with artificial control of the water pressure inside the distance blocks was tested. A drainage tube leading into the supercontainer section was installed in the slot under the distance blocks, see Figure 3-3. This drainage tube made it possible to control the water pressures in the supercontainer section and by that also give the bentonite more time for maturation (water uptake and swelling). This technique has also made it possible to increase the slot width from 5 to 10 mm which will facilitate the installation of the distance blocks.

An issue discussed with this layout has been the retrieval of the drainage tube. This was also tested with good results. The technique used was to pull the tube out in steps (Tested with 1 meter/step and 24 hours) giving the bentonite time to seal the remaining volume. This design has been repeated two times in the laboratory at these extreme conditions.
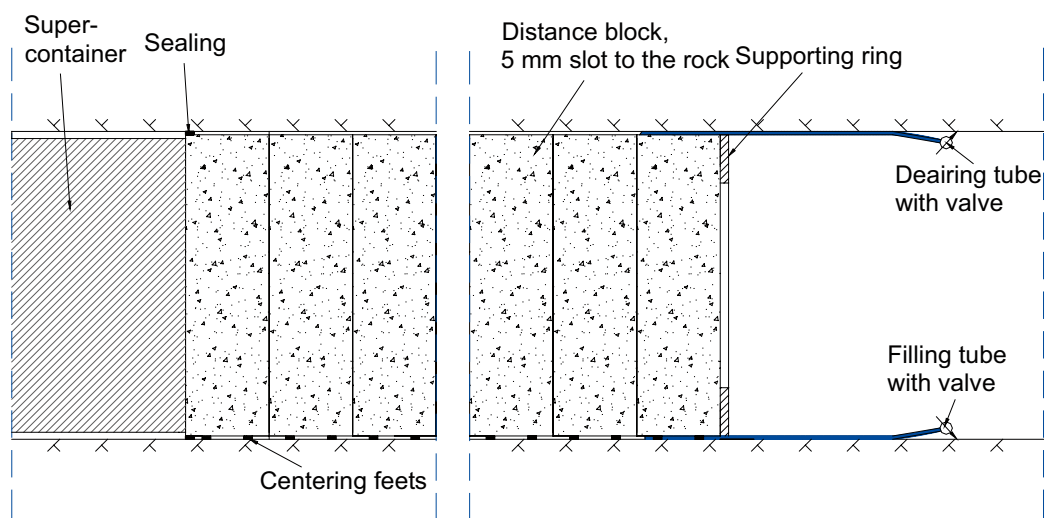
Figure 3-2. Figure showing a schematic drawing of layout alternative 1.
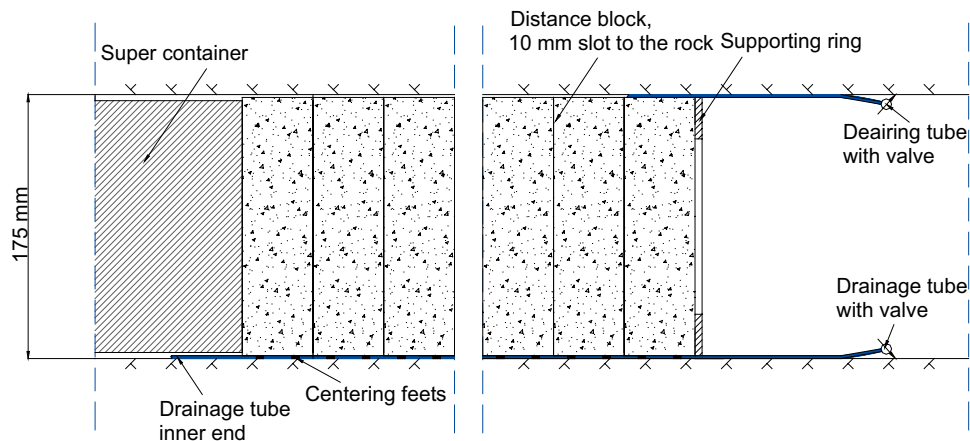
Figure 3-3. *Figure showing a schematic drawing of Alternative 2.*

Layout:

- Centred blocks with 10 mm slot to the rock.
- Pre-wetting of the slot.
- 3.5% salt in the water.
- Drainage tube through the distance blocks into the supercontainer section in order to control the water pressure.

A temporary sealing is needed around the outermost block facing the fixing-ring. The sealing can be rather simple, perhaps made of bentonite, since its only purpose is to withstand the pressure from the water when filling up the slot (the pre-wetting).

The difference in diameter between the deposition drift and the distance blocks is in this layout increased from 10 mm (Layout alternative 1) to 20 mm. This will facilitate the installation of the distance blocks but it is still rather tight.

The layout is rather time consuming. The bentonite needs about 14 days before it can withstand 5 MPa including withdrawal of the tubes. This time can perhaps be decreased if the technique is optimised.

J.3.4   Design alternative 3 (block split in three parts)

Design alternative 3 is to use a block divided in three parts in order to fit the rock tightly to the rock, see Figure 3-4. The surfaces of the blocks are inclined which means that the parts could be pushed in position and the bentonite will be in contact with the rock surface. This design could be used for the entire length of the distance block section.

An alternative version is to use solid distance blocks, with a diameter 40–100 mm smaller than the deposition drift and have divided distance blocks only for the last meter.

This layout is not yet tested in any laboratory experiments.

Layout:

- Tight distance block; the block is divided in three parts, which means that the block will be installed very tight to the rock.

J.3.5   Design alternative 4 (block divided in one central part and an outer ring)

This design is a variation of design alternative 3.
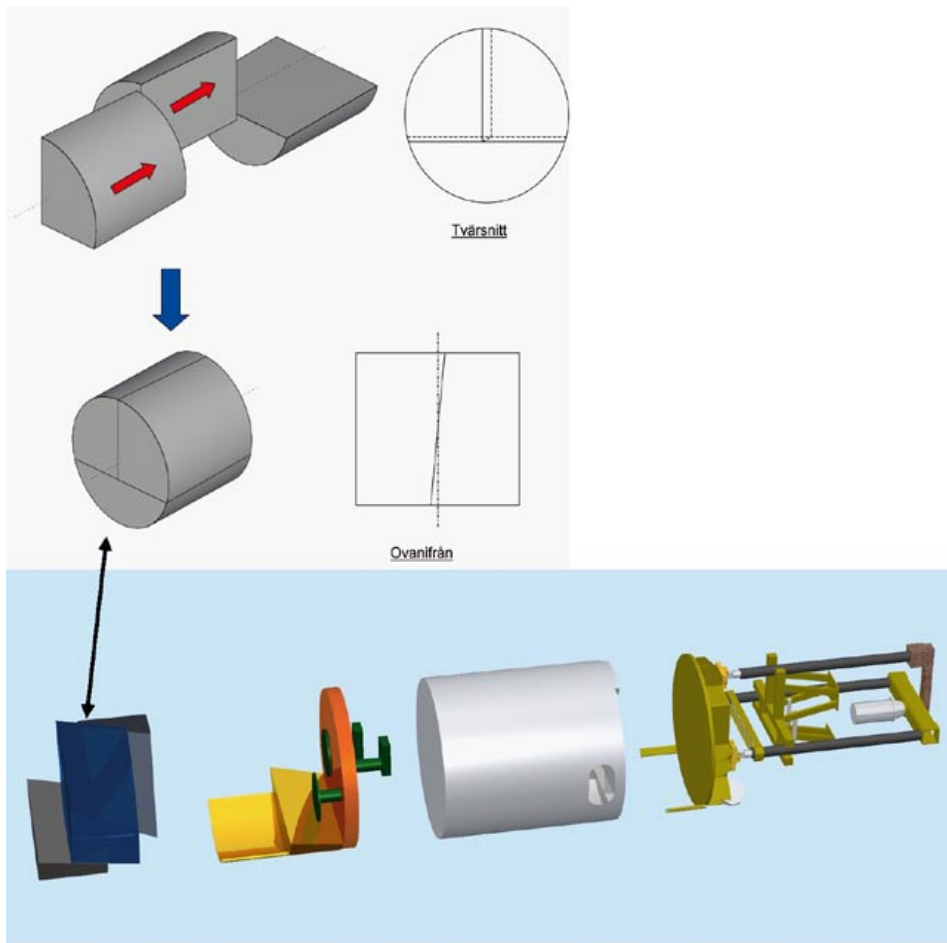
Figure 3-4. Figures showing a schematic drawing of Alternative 3. The picture shows the divided block to the left and an example of special designed installation device.

Layout:

- The same idea as alternative 3 with tight fitting blocks, but the distance block consists of a central, somewhat conical block, with a number of outer minor fitting blocks placed in contact with the rock, see Figure 3-5. This solution means that the sealing ability is high since the block is mainly in contact with the rock.

- The outer block is proposed to be made with a thickness of 1 meter. The distance blocks inside can be made with a slot of 5 cm to the rock, which facilitates their installation.

- The fitting blocks will be made slightly larger than the slot and the jutting part after installation will be cut off.

J.3.6   Initial conditions of distance blocks

The final average density at saturation of the distance block section should be between 1,950–2,050 kg/m^3 (dry density 1,481–1,637 kg/m^3). The initial density of the distance blocks, before emplacement, will vary somewhat for the different designs depending on the different dimensions.

The suggested designs request blocks that only yield a small slot bentonite/rock which means that the initial density of the blocks must be rather low. In order to produce blocks of good quality with this low dry density, it will probably be necessary to compact them with high initial water content, see Chapter J.5.
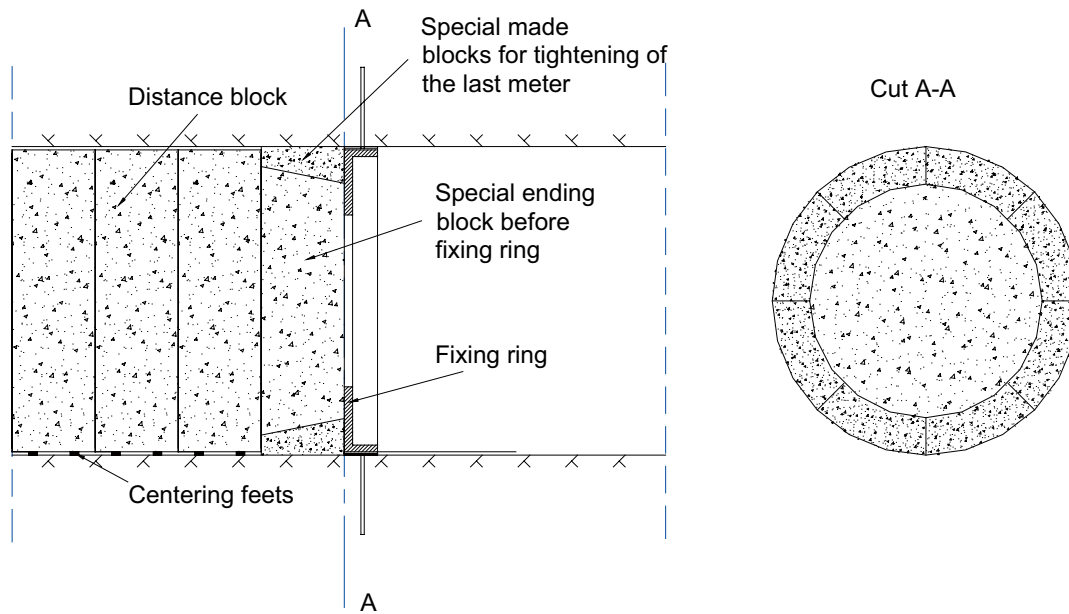
Figure 3-5. *Figure showing a schematic drawing of layout alternative 4.*

Table 3-1 shows the dimensions and block data. In Figure 3-6 the dry density of the blocks is plotted vs. the average density at saturation after swelling and homogenisation. The tolerances of the dry density on the manufactured blocks are rather large (1,513–1,673 kg/m³ for the design with 10 mm gap and 1,481–1,637 kg/m³ for the design with split block) in order to get an average density at saturation between 1,950–2,050 kg/m³ in the tunnel.

Table 3-1. Table showing the data used in the calculations of average density after swelling and saturation. The table also shows the calculated dry density of the distance blocks for the suggested designs.

Dimensions	
Rock	
Diameter tunnel, mm	1,850
Tight distance block, 5 mm gap (Alt. 1)	
Outer diameter, mm	1,840
Tight distance block, 10 mm gap (Alt. 2)	
Outer diameter, mm	1,830
Tight distance block, split block (Alt.3 and 4)	
Outer diameter, mm	1,850
Calculated block data	
Tight distance block, 5 mm gap (Alt. 1)	
Target average density at saturation, kg/m³	2,000
Initial block dry density, kg/m³	1,576
Initial block void ratio	0.771
Tight distance block, 10 mm gap (Alt. 2)	
Target average density at saturation, kg/m³	2,000
Initial block dry density, kg/m³	1,593
Initial block void ratio	0.752
Tight distance block, split block (Alt.3 and 4)	
Target average density at saturation, kg/m³	2,000
Initial block dry density, kg/m³	1,559
Initial block void ratio	0.790
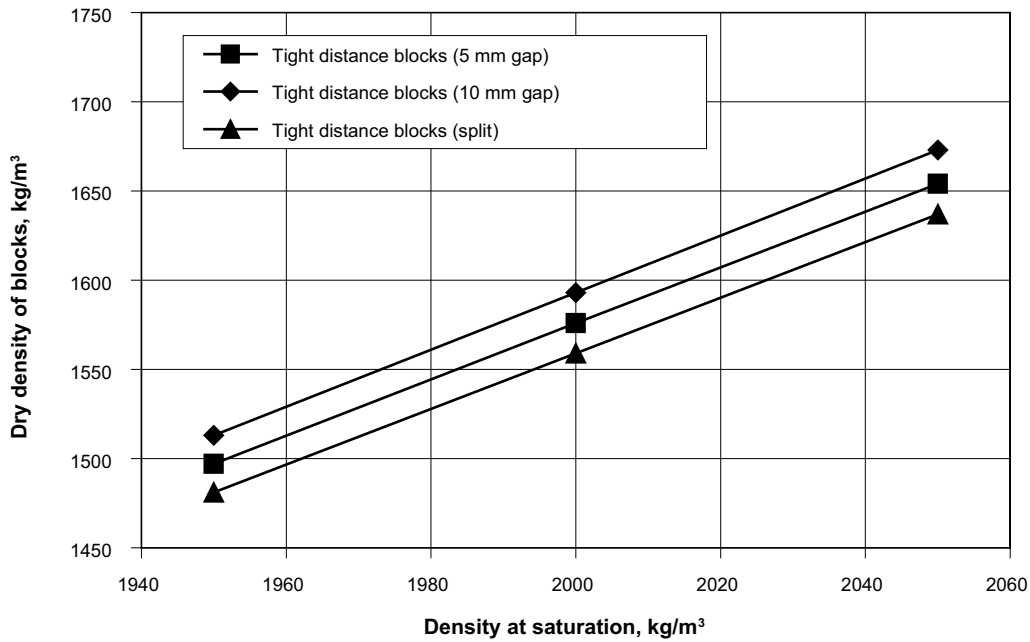
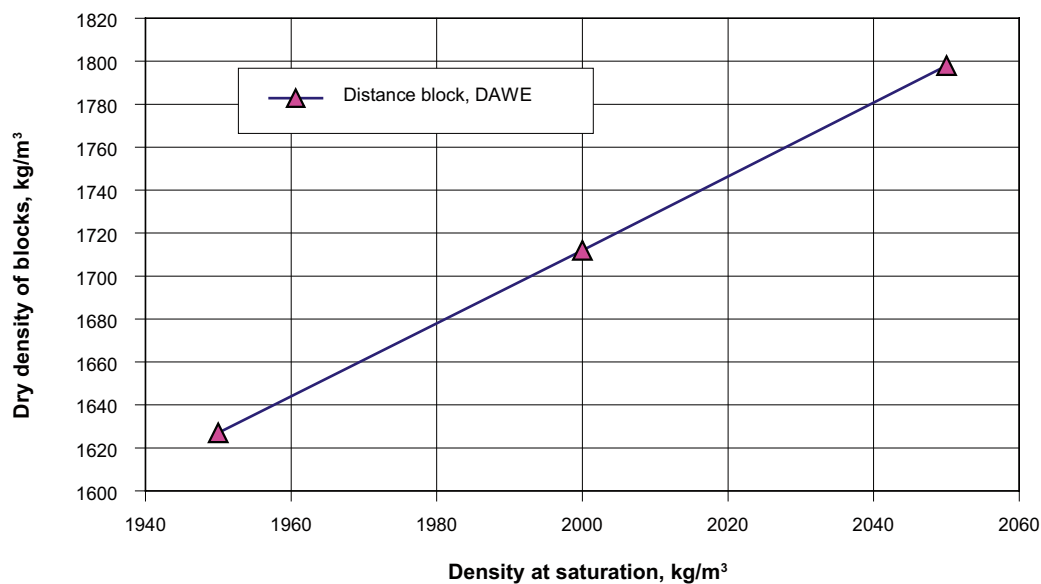***Figure 3-6.*** *Diagram showing the dry density of the blocks (dimensions according to Table 3-1) plotted vs. the average density at saturation in the tunnel after swelling and homogenisation. Data for two of the suggested designs are plotted in the diagram.*

J.3.7 Sensitivity for variations of the tunnel diameter

The required block densities are calculated are done using the nominal diameter of the disposal tunnel i.e. 1,850 mm. The diameter will however vary and this will influence the final density in the system. The diagram in Figure 3-7 shows how the average density at saturation will vary with tunnel diameter. The diagram assumes an average density at saturation of 2,000 kg/m³ at the nominal tunnel diameter (1,850 mm).
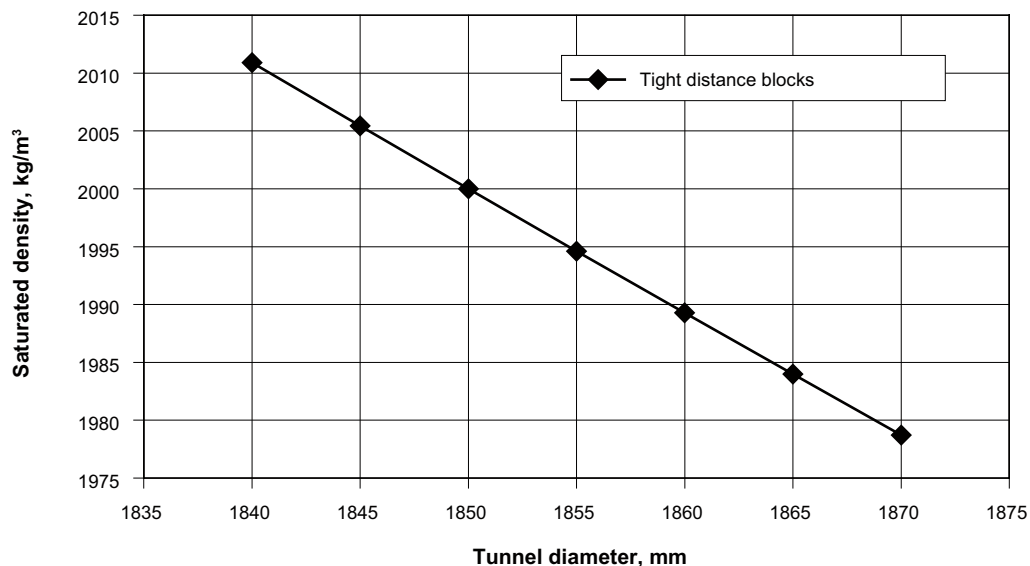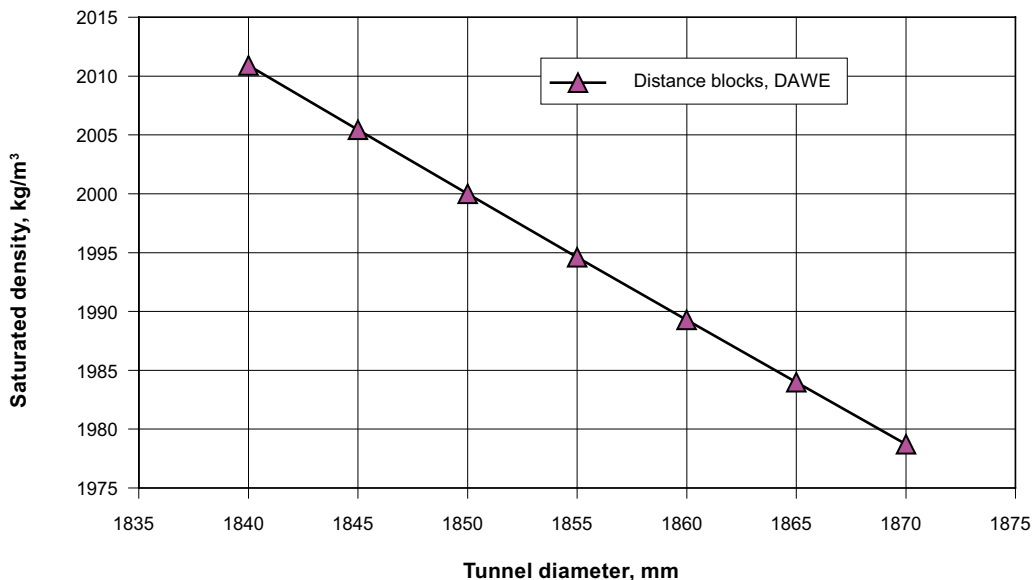

Figure 3-7. *Diagram showing the average density at saturation in the tunnel after swelling and homogenisation (target density at saturation 2,000 kg/m³ at the tunnel diameter 1,850 mm) plotted vs. various tunnel diameter.*

225

J.4 Distance blocks in the DAWE alternative

J.4.1 General

The distance blocks in the DAWE alternative are not intended to seal and prevent water flow between sections during the installation phase. The main idea is instead to let water flow freely along the tunnel until the end plug is placed and sealed.

J.4.2 Initial conditions

The final average density at saturation of the distance blocks is between 1,950–2,050 kg/m³ (dry density 1,481–1,637 kg/m³). The distance blocks in the DAWE alternative are assumed to have the same initial diameter as the supercontainer.

Table 4-1 shows the dimensions used for the calculations and also the calculated dry density of the blocks. In Figure 4-1 the dry density of the blocks is plotted vs. the density after swelling and homogenisation. The tolerances of the dry density on the manufactured blocks are rather large (1,627–1,798 kg/m³) in order to get a density at saturation between 1,950–2,050 kg/m³ in the tunnel.

Table 4-1. Table showing the dimensions used in the calculations. The table also shows the calculated dry density of the distance blocks for the DAWE design.

Dimensions	
Rock	
Diameter tunnel, mm	1,850
Distance block	
Outer diameter, mm	1,765
Calculated block data	
Distance block DAWE	
Target average density at saturation, kg/m³	2,000
Initial block dry density, kg/m³	1,712
Initial block void ratio	0.629

Figure 4-1. *Dry density of the blocks (dimensions according to Table 4-1) plotted vs. the average density at saturation in the tunnel after swelling and homogenisation.*

J.4.3 Sensitivity for variations of the tunnel diameter

The required block densities are calculated using the nominal diameter of the disposal tunnel i.e. 1,850 mm. The diameter will however vary and this will influence the final density in the system. The diagram in Figure 4-2 shows how the average density at saturation will vary with tunnel diameter. The diagram assumes an average density at saturation of 2,000 kg/m³ at the nominal tunnel diameter (1,850 mm).

J.5 Manufacturing of buffer blocks

J.5.1 General

The different buffer positions and designs request bentonite blocks of different quality. The blocks placed in the supercontainer have a limited initial space and the slots to fill are rather large. These blocks have to be produced using bentonite with low water ratio in order to achieve a high dry density of the blocks. On the other hand, the suggested designs regarding the distance blocks request blocks that only yield a small slot bentonite/rock which means that the initial density of the blocks should be rather low. In order to produce blocks of good quality with low dry density, it will probably be necessary to compact them with high initial water content. Figure 5-1 shows a diagram where reached dry density is plotted versus water ratio for different compaction pressures. The bold black line is the saturation line. This line shows the highest possible water ratio for a certain dry density.

Experience from manufacturing of bentonite blocks shows that in order to get blocks of good quality, the compaction pressure should be at least 40 MPa and the water ratio should not exceed 26%. The figure shows the block density for some block types and design alternatives. The figure thus shows that e.g. the ring shaped blocks inside the supercontainer needs to be compacted with 100 MPa pressure at the water ratio 10% in order to yield a density high enough while the distance blocks with large diameter must have a very high water content (~ 26%) in order to not have too high density.

Figure 4-2. *Average density at saturation in the tunnel after swelling and homogenisation (intended average density at saturation 2,000 kg/m³) plotted vs. tunnel diameter.*
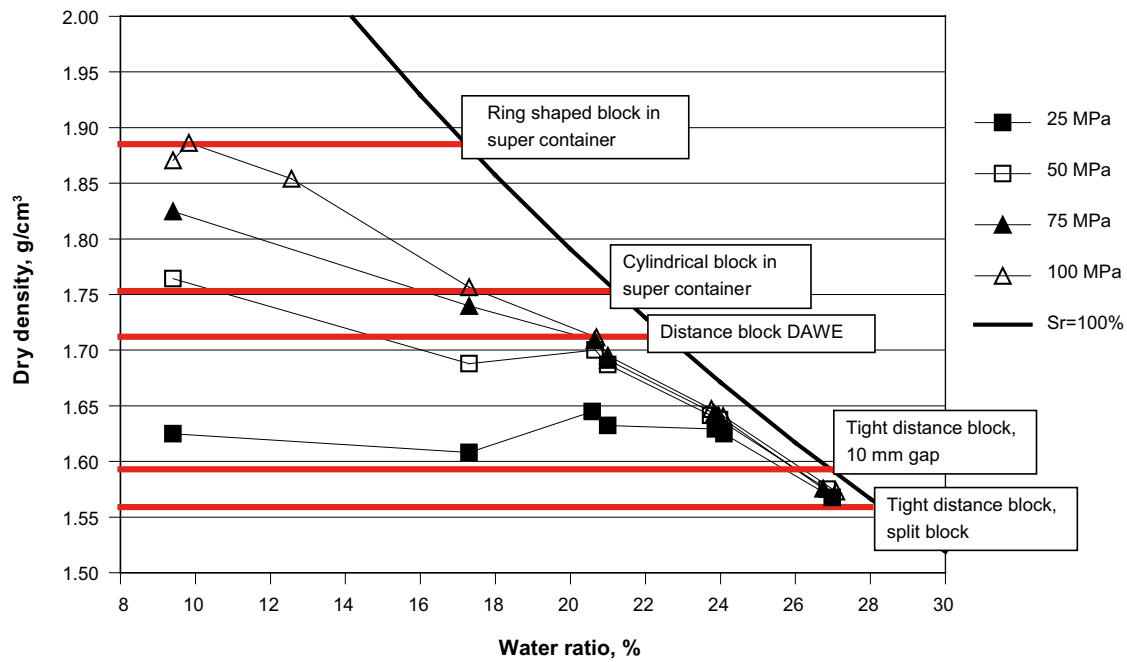
Figure 5-1. *Reached dry density of compaction tests plotted versus water ratio for different compaction pressures. The requested dry density of the blocks for the different designs and positions are also shown in the diagram.*

J.6   Reference design for the distance block in BD

J.6.1   General

Four distance block designs are suggested, see Chapter J.3. The designs are based on laboratory tests performed at Clay Technology AB.

Two main problems are decisive for the design:

• The ability to seal the slot between the block and the rock surface

• The radial penetration of water pressure between the block and supercontainer (or between blocks).

J.6.2   Design alternatives

J.6.2.1   Alternative 1

Layout (see also Chapter J.3.2):

• Centred blocks

• 5 mm slot buffer/rock

• Pre-wetting of distance block slot.

Advantages:

• The design is simple and straight forward.

Disadvantages:

• Difficult to install depending on the rather small slot buffer/rock (5 mm).

J.6.2.2   Alternative 2

Layout (see also Chapter J.3.3):

- Centred blocks
- 10 mm slot to buffer/rock
- Pre-wetting of distance block slots and filling of container section
- Control of water pressure in the container section
- Stepwise removal of the drainage tube
- About two weeks are required for the complete installation.

Advantages:

- Controlled conditions (water inflow and water pressure increase rate)
- Solves the problem with rapid water pressure increase rate
- Best way to reduce forces on the fixing ring.

Disadvantages:

- Difficult to install depending on the rather small slot buffer/rock (10 mm)
- The installation requires two weeks.

J.6.2.3   Alternative 3

Layout (see also Chapter J.3.4):

- Three-piece block
- Contact block-rock surface
- 1 m thick block.

Advantages:

- Known excellent sealing properties (not yet tested with divided blocks)
- Rapid installation.

Disadvantages:

- Difficult to avoid inside slot
- Blocks difficult to produce. Requires careful manufacturing.
- Possible strength problems due to the fracturing.

J.6.2.4   Alternative 4

Layout (see also Chapter J.3.5):

- Central slightly conical block
- Small wedge shaped blocks fitted in the slot
- 1 m thick block
- Contact buffer-rock surface.

Advantages:

- Known excellent sealing properties (not yet tested with divided blocks)
- Rapid installation
- No inside slot.

Disadvantages:

- Blocks difficult to produce. Requires careful manufacturing.

- Possible strength problems due to the fracturing.

- Can radial slots be avoided.

J.6.3 Comments to the distance block design

- All alternatives have been tested for piping at the extreme scenario (1 l/min and 1 MPa/h) and seem to work. Design alternative 3 and 4 is not yet tested with divided blocks.

- All alternatives require a fixing ring to withstand water pressure built up in the container section

- A remaining problem is to determine the magnitude of the force on the fixing ring. Laboratory tests are running where this phenomena is studied in detail. Earlier investigations have shown that the problem can be handled at the reference conditions (0.1 l/min, 0.1 MPa/h and maximum 2 MPa) but it could be a problem at the extreme conditions (1 l/min, 1 MPa/h and maximum 5 MPa). It is also possible that there are mechanical problems with alternative 3 and 4 due to the splitting of the blocks. Additional tests and calculations will be needed.

J.6.4 Suggested distance block reference design

Design alternative 2 is believed to function well especially at extreme conditions with high water inflows and fast water pressure increase rates. Due to the disadvantages regarding the rather difficult and time consuming installation with this design has however design alternative 3 (or 4) been chosen as reference design. The design is proven to withstand the extreme conditions (1 l/min and 1 MPa/h) and the installation is judged to be feasible. Another advantage is that the design will take care of the spalling problem if it is used in the entire distance block section. The design could be motivated in all distance block sections. It is also possible to combine the two design alternatives i.e. install distance blocks according to design alternative 3 but also install a drainage tube. The advantages of pre-wetting i.e. filling all empty space with water are seen in several laboratory tests. This will of course extend the installation time somewhat mainly due to the fact that the drainage tube has to be retrieved which is supposed to take some days. The retrieval technique is tested in laboratory but could probably be improved.

J.7 Water filling of a supercontainer section after installation

J.7.1 General

In the Basic Design the empty space in a supercontainer section will act as a water storage that delays the time until a water pressure starts to build up, giving the distance blocks time to swell and seal of the drift. The achieved time depends on the available volume and on the water inflow rate in the section. Calculations using the dimensions shown in Table 6-1 yield that and the empty space around a supercontainer is 1,656 litres (the volume between the ring shaped blocks and the canister is not included, since it will probably not be filled during this first period). A water inflow rate of 0.1 l/min yields a filling time of 11.5 days.

Table 6-1. Table showing the dimensions used in the calculations.

Dimensions	
Rock	
Diameter tunnel, mm	1,850
Super container	
Outer diameter, mm	1,765
Inner diameter, mm	1,749
Thickness of end plate, mm	8
Degree of perforation	62%
Length, mm	5,546
Canister	
Outer diameter, mm	1,050
Ring shaped block	
Outer diameter, mm	1,739
Inner diameter, 1060	
Cylindrical end block	
Outer diameter, mm	1,739

Reference

Börgesson L, Sandén T, Fälth B, Åkesson M, Lindgren E, 2005. Studies of buffers behaviour in KBS-3H concept - Work during 2002–2004. SKB R-05-50, Svensk Kärnbränslehantering AB, Sweden.

Hellä P, 2006. Pressure increase rate in KBS-3H deposition drifts. Memorandum PROJEKTI-822-5/2006, Saanio & Riekkola Oy.

<div align="right">**Appendix K**</div>

Status report regarding activities described in APTDMLH3-06-036. Buffer tests to resolve critical design and early evolution issues

By Torbjörn Sandén, Lennart Börgesson, Ann Dueck, Reza Goudarzi, Margareta Lönnqvist, Ulf Nilsson, Clay Technology AB. April 2007.

K.1   Introduction

The KBS-3H Test plan /Autio et al. 2006/ identifies a number of critical design issues. Laboratory investigation regarding some of the issues is described in an Activity Plan, APTDMLH3-06-036. This status report is a summary of the present situation regarding the activities described in the Activity Plan.

K2   Humidity induced swelling of distance blocks

K.2.1   Small scale tests

K.2.1.1   General

The test series were described in detail in a Test plan /Autio et al. 2006/ where the issue addressed by the experiments was described together with the objectives and the expected output parameters. A test description is also given in the activity plan /Sandén and Börgesson 2006/.

The objective was to define the water absorption rates, swelling rates and cracking of the buffer surfaces with respect to time in realistic conditions and geometries at different inflow conditions.

K.2.1.2   Terminology

Water ratio is defined as mass of water per mass of dry substance. The dry mass is obtained from drying the wet sample at 105°C for 24 hours.

K.2.1.3   Material

The material used in the test series is MX-80 bentonite powder. MX-80 is a commercial product of sodium bentonite. The powder is delivered with a water ratio about 10%. Higher water content was produced by adding a predetermined mass of tap water and mixing it with a mixer in order to get a homogenous material.

K.2.1.4   Evaluation

All the compacted samples were weighed and measured with a slide caliper before and after the test. During the test period the samples were weighed in a hook below the balance at least once a week. For some of the samples the increase in height and diameter was evaluated from measurements with the slide caliper at least once a week. After ending the test each sample was divided into three slices, which were used for determination of water ratio and density. The density was calculated from a volume determined by weighing the sample above and submerged into paraffin oil. The data were noted manually and stored in excel files.

The amount of absorbed water, i.e. the increase in weight determined at prescribed intervals, was used for calculation of the absorption rate.

K.2.1.5 Experimental set-up of the small scale tests

In order to investigate the block behaviour i.e. water absorption, swelling and cracking, experiments were done in different scales. In the following the experimental set up for the small scale tests is described.

Compacted samples with different initial water ratios were exposed to a high relative humidity. Water uptake and swelling (volume expansion) were measured continuously and the cracking of the surfaces was studied. The idea was to compact samples with different compaction pressures (25, 50, 75 and 100 MPa). The water ratio (and by that the degree of saturation) of the samples was varied between 10–25%. The dry density of the samples in the test series then varied between 1.60–1.9 g/cm^3, but due to the number of tests it should be possible to compare samples with the same dry density. Three identical samples were made for every compaction pressure and water ratio; one sample was used for determination of the water absorption rate, one for studying the swelling/volume expansion and one was used for measurement of the obtained dry density and water ratio. The complete test matrix is rather large, but after having performed a number of initial tests, limited number of tests was selected.

Test equipment

Determination of the water absorption rate. The bentonite sample was hung in a special glass or Plexiglas vessel with a tight lid, see Figure 2-1. The sample was covered with a rubber sealing only exposing one of the ends. The bottom of the vessel was filled with pure water or a salt solution. The sample was hung by a rod, which was led through the lid. This made it possible to weigh the sample without taking the sample out of the jar. A washer was mounted on the upper part of the rod, above the lid, in order to seal off the hole when no weighing was performed. The distance between the exposed bentonite surface and the water surface was held constant during the test period. The main part of the planned tests was performed at room temperature but a number of tests were also performed in climate chambers in order to have deviating and constant temperatures. These samples were taken out of the chamber for the weighing.

Studying the swelling/volume expansion and cracking. These tests were identical to the previous tests but the samples were taken out of the jar to be measured at prescribed intervals. The surfaces were studied for cracking.

Test matrix

The complete test matrix regarding compaction pressure, initial water ratio of the samples and the prescribed gap between the bentonite and water surface is shown in Table 2-1a. From this matrix a number of tests were selected with main focus on the most relevant parameter values i.e. above 20% water ratio and with a gap between the bentonite and the water surface of 45 mm, which is the distance between the bentonite blocks and the rock in the DAVE alternative (60 mm is the expected gap bentonite/rock for the blocks inside the supercontainer).

A number of additional tests were performed for checking the influence of the following parameters:

1. **Influence of humidity.** All tests in the matrix were performed using pure water in the vessel, which gives an *RH* just above the water surface of 100%. Additional tests were performed using a saturated KCl solution which gives an *RH* of about 85% just above the water surface.

2. **Influence of test temperature.** All tests shown in the matrix were performed at room temperature. In order to study the influence of the temperature, some additional tests were performed at 30°C and at 10°C.

3. **Influence of air movements.** It is assumed that the vapour transport rate in air is the limiting factor for the water absorption rate. In the planned test series air movements inside the vessels that may increase the vapour transport rate were avoided. In order to check the sensitivity to such effects, some additional tests were performed at the same conditions but with a magnetic stirrer in the water to provoke water movements and resulting air movements.
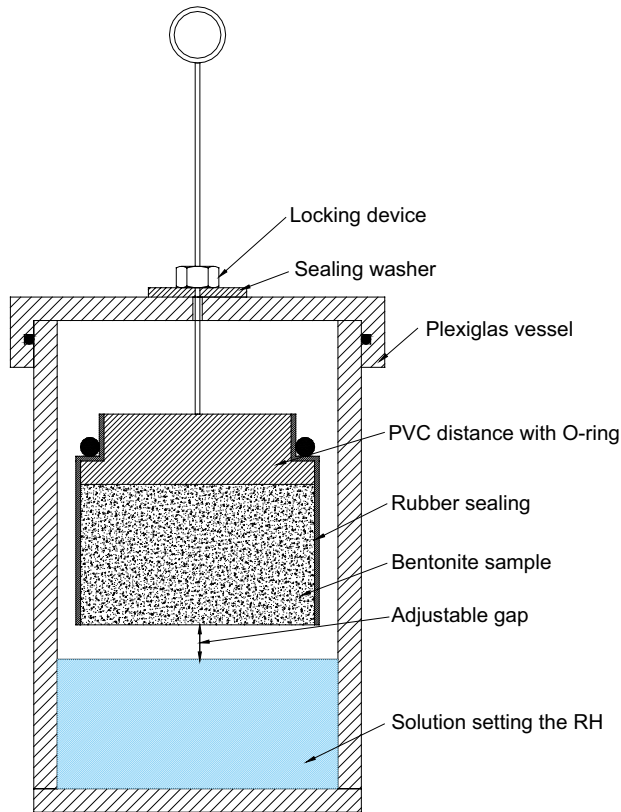
Figure 2-1. *Schematic view showing the test equipment.*

The additional tests were performed on samples with the same initial conditions as sample S222, Table 2-1b. In addition to the factors mentioned above, the influence of prevented radial swelling and of a gap size of 20 mm were also tested.

Preparation

Powder with prescribed water ratio was compacted with prescribed compaction pressures according to Table 2-1a. The compacted samples had diameters of 5 cm and they were cut to a height of 3 cm. With few exceptions the samples were hung with the cut side upwards and the uncut side towards the water surface in the equipment shown in Figure 2-1.

Table 2-1a. Table showing the test matrix for the small scale tests.

Humidity induced swelling - test matrix for the small scale test											
	Compaction pressure										
w initial	25 MPa			50 MPa			75 MPa			100 MPa		
%	Gap bentonite/water			Gap bentonite/water			Gap bentonite/water			Gap bentonite/water		
	10 mm	45 mm	60 mm	10 mm	45 mm	60 mm	10 mm	45 mm	60 mm	10 mm	45 mm	60 mm
10	S110	S120	S130	S210	S220	S230	S310	S320	S330	S410	S420	S430
15	S111	S121	S131	S211	S221	S231	S311	S321	S331	S411	S421	S431
20	S112	S122	S132	S212	S222	S232	S312	S322	S332	S412	S422	S432
22	S113	S123	S133	S213	S223	S233	S313	S323	S333	S413	S423	S433
24	S114	S124	S134	S214	S224	S234	S314	S324	S334	S414	S424	S434

235

Table 2-1b. Table showing additional small scale tests.

Humidity induced swelling - test matrix for the small scale test					
	Additional tests starting from sample S222				
w initial %	RH = 85%	T = 10 degC	T = 30 degC	Air movement	Gap 20 mm	No radial swelling
20	S222_H	S222_T10	S222_T30	S222_A	S222_g20	S222_Dr0

K.2.1.6 Preliminary results from the small scale tests

All results refer to the normal sample represented by sample S222 which is shown in all diagrams. This sample represents initial water content of 20%, compaction pressure of 50 MPa, a gap of 45 mm between the bentonite and water surface and placed at room temperature i.e. about 20°C. In the diagrams the legends for most of the samples contain information about the compaction pressure, the size of the gap and the initial water content, respectively. In all diagrams the colour (purple, green, red, light blue, dark blue) denote the initial water content (10%, 15%, 20%, 22%, 24%) and the shapes of the marks (x, ♦, ■, ▲) denote the compaction pressures (25, 50, 75, 100) MPa. Initial and final water content and density are presented for all samples in Table 2-2 (water content) and Table 2-3 (density). The tests were performed during about 2,000 h or 84 days and the samples were supposed not to have reached steady state.

Water absorption

Absorption in terms of increase in mass was investigated according to Chapter 2.1.5. The most influencing factors were the following:

• initial water content which is illustrated in Figure 2-2,

• size of the gap which is illustrated in Figure 2-3,

• temperature which is illustrated in Figure 2-4.
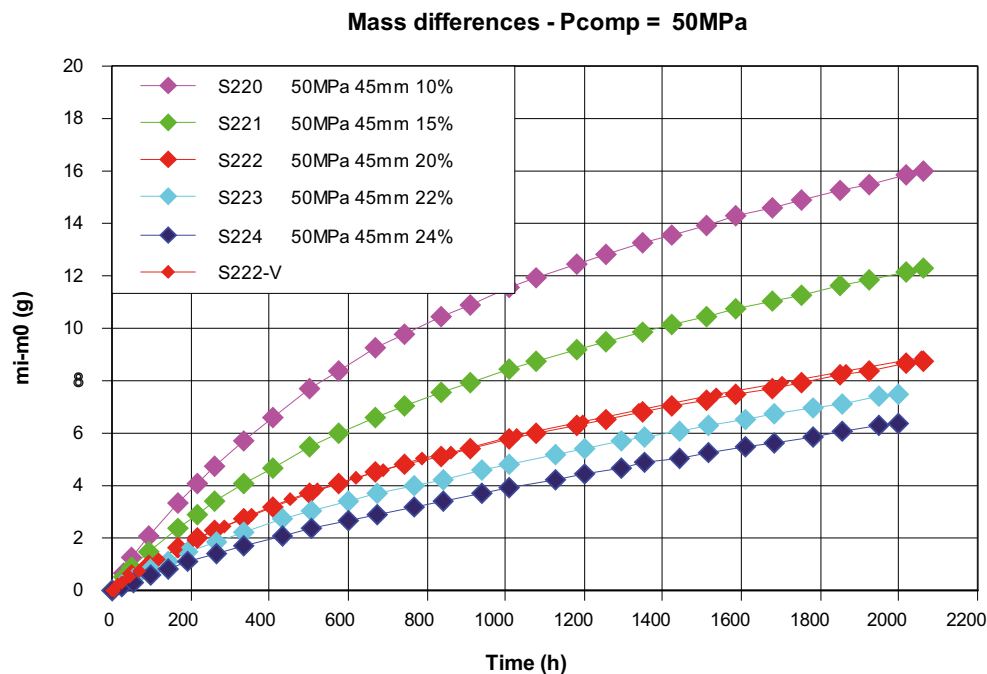
Figure 2-2. Water absorption as a function of time. Influence of initial water content. All samples were compacted at 50 MPa.

Mass differences - gap and stir
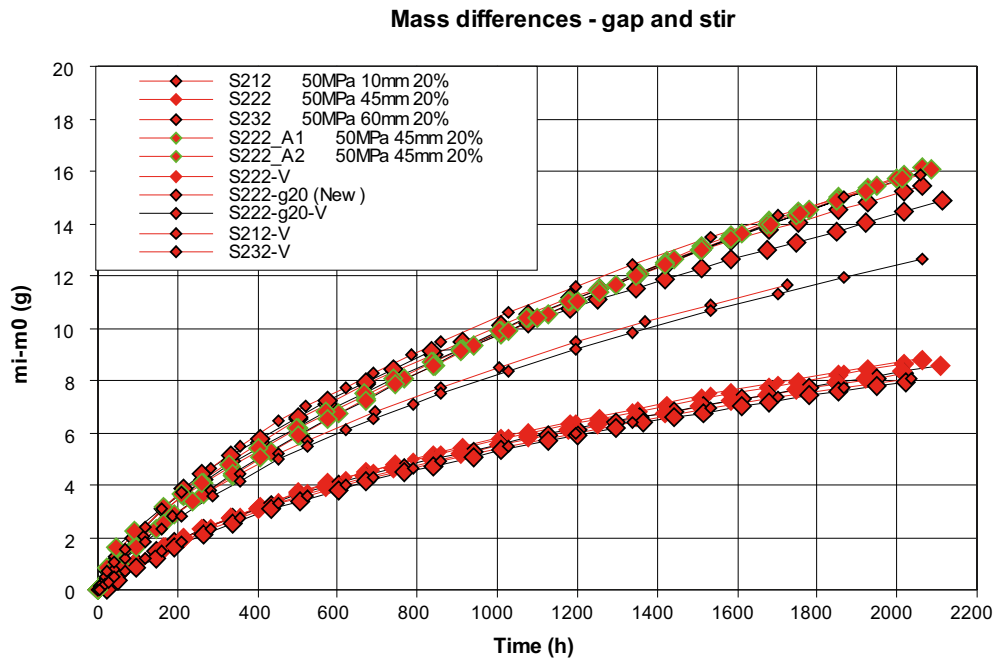
Figure 2-3. *Water absorption as a function of time. Influence of size of the gap between the water surface and the sample. Also shown are results with samples placed in jars with air movement (_A). All samples were compacted at 50 MPa with an initial water content of 20%.*

According to Figure 2-2 the absorption rate is higher the less initial water is present. In Figure 2-3 the influence of the size of the gap between the sample and water surface is shown. The samples placed 10 mm from the water surface and the samples placed 45 mm from the surface with air movement show the largest and almost the same water uptake. The samples placed 20 mm from the water surface show a water absorption rate between the samples placed 10 mm and the base case representing a gap size of 45 mm. The absorption from samples with a gap size of 60 mm coincides with the base case.

The influence of temperature is shown in Figure 2-4. A first attempt to investigate the influence of low temperature (10°C) was made by placing the jars in cold boxes, S222_T10a and S222_T10b. The samples were taken out of the boxes and weighed at 20°C which caused visible condensation on the membranes covering the samples and on the bottom surface of the samples. The results from those samples are not shown in Figure 2-4. New samples were placed in a climate room with temperature control, S222-10c and S222-10d (◊). In this case the balance was placed inside the climate room and the samples were not exposed to any temperature change during weighing. However, the samples exposed to 30°C were still taken out of the climate chamber and weighed at 20°C. This might have induced a small error in the absorption of these samples but no water droplets were visible on the samples.

Regarding the compaction pressure a small influence was seen and almost no influence at all was observed at initial water contents larger than 20%, see Table 2-2. The influence of preventing radial swelling was also investigated. These samples started with the same condition as the normal sample S222 and it was shown that preventing radial swelling has no effect on the amount of absorbed water.

The absorption rate can be calculated from the tangent of the time curves. The absorption rates for samples compacted at 50 MPa but with different initial water contents are shown in Figure 2-5.

Mass differences - temperature part I and II
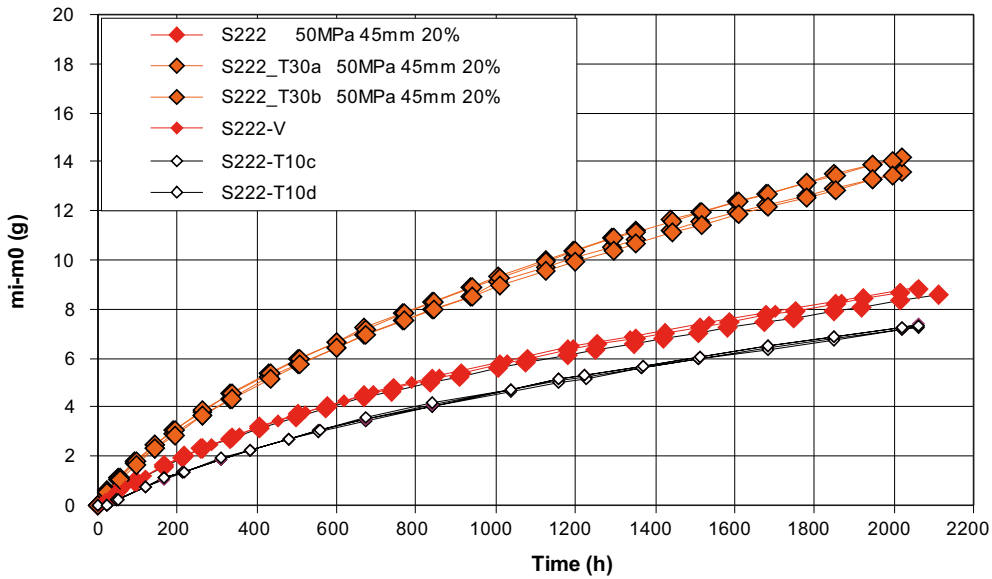
Figure 2-4. *Water absorption as a function of time. Influence of temperature. All samples were compacted at 50 MPa with an initial water content of 20%.*
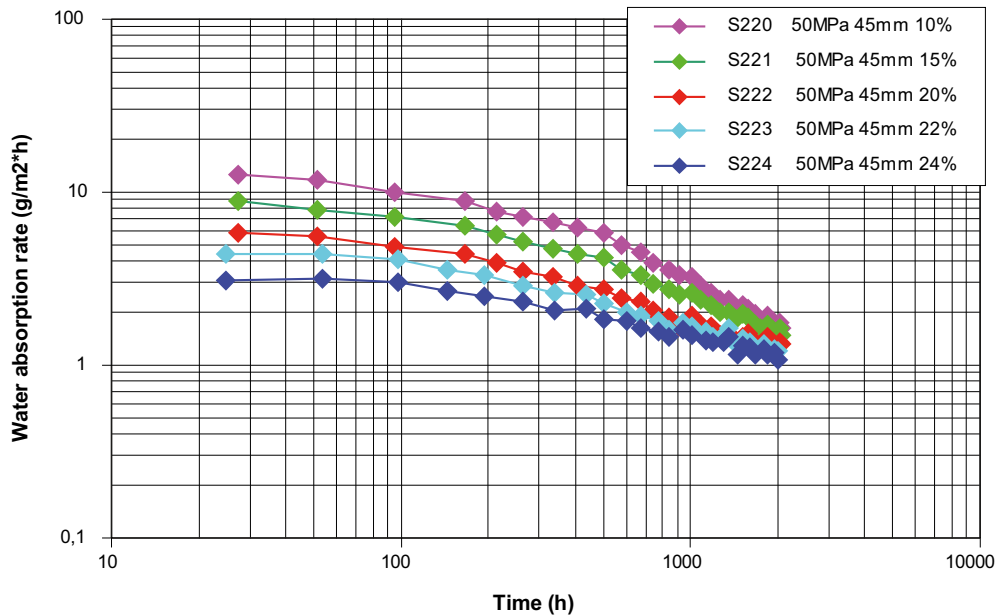
Water absorption rate Pcomp = 50 MPa

Figure 2-5. *Absorption rate evaluated from the results shown in Figure 2-2.*

In Table 2-2 the initial and final water contents for all samples are shown and in Figure 2-6 the initial and final water contents of the main part of the samples are shown. Since each sample was divided into three slices each sample has values representing the upper/middle/lower part of the sample. Both initial and final values are shown. The initial values were measured on extra samples made only for the determination of initial values of water content and density.

The number of tests performed on each sample is shown in Table 2-2. If more than one sample was tested the value represents the average. If the number of tests is zero this means that the initial value refers to the normal sample S222.

Table 2-2. Initial and final water contents for all samples.

Water content (%)	Initial Upper	Middle	Lower	No.	Final Upper	Middle	Lower	No.
S210	10,3	10,5	10,4	1	31,1	31,9	33,6	1
S122	19,5	19,5	19,5	1	27,1	27,0	27,9	2
S124	23,8	23,7	23,6	1	28,9	29,3	29,1	2
S212	19,6	19,6	19,5	1	33,7	34,4	36,1	2*
S220	10,5	10,6	10,5	1	24,8	25,2	26,1	2
S221	15,1	14,9	15,0	1	25,7	26,2	27,0	2
S222	19,4	19,5	19,5	2	27,5	28,0	28,6	2
S223	21,7	21,9	21,9	1	28,1	28,5	29,1	2
S224	23,8	23,8	23,7	1	29,0	29,3	29,9	2
S232	19,5	19,5	19,5	1	26,8	27,1	27,7	2
S322	19,6	19,6	19,4	2	27,5	27,9	28,6	2
S323	21,8	21,8	21,7	2	28,4	28,8	29,4	2
S420	10,5	10,5	10,5	1	24,8	25,4	26,3	2
S421	16,6	15,0	15,1	1	26,1	26,5	27,2	2
S422	19,6	19,6	19,5	2	27,7	28,2	28,8	2
S222_H	19,4	19,4	19,4	0	20,3	20,3	20,3	2
S222_A	19,4	19,4	19,4	0	33,7	34,4	35,6	2
S222_T10	19,4	19,4	19,4	0	34,6	36,0	38,5	4
S222_T30	19,4	19,4	19,4	0	31,9	32,5	33,2	4
S222_T10	19,5	19,5	19,6	0	26,3	26,9	27,7	4
S222_Dr0	19,5	19,5	19,6	0	27,1	27,7	28,6	2
S222_g20	19,5	19,5	19,6	0	30,9	31,5	32,4	2

* The final water content of the lower part includes a value from a wetter and darker part of the surface towards the water.
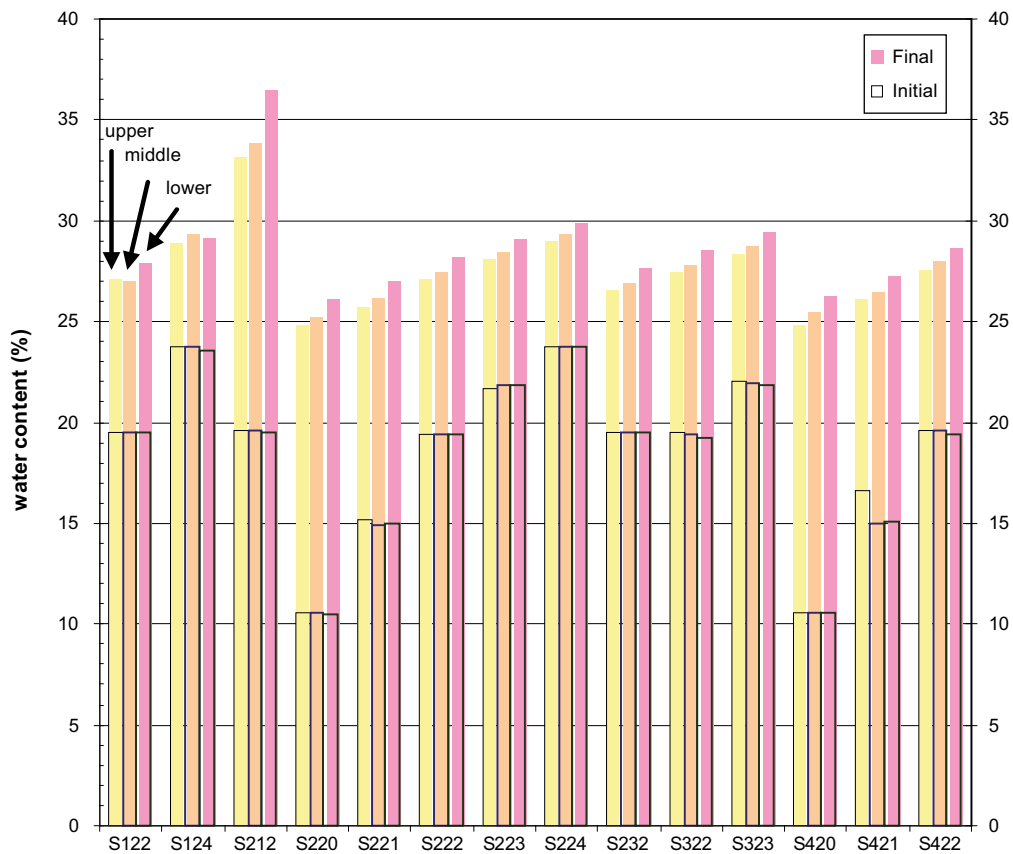
Figure 2-6. *Initial and final water content of samples from Table 2-1a.*

Each sample started with homogeneous water content but showed a gradient in water content at termination. This can be seen in Figure 2-6 where the three columns representing the initial water contents of each sample have almost the same height while the columns representing the final water contents of each sample differ in height.

For some of the samples placed near the water surface (S212) a dark area was seen, probably from water droplets. Additional samples were done in order to check this but droplets were not seen on the additional samples.

Swelling/volume expansion

The most influencing factors for the swelling were the initial water content, the size of the gap to the water surface and the temperature. The increase in sample height is shown in Figures 2-7 to 2-9.

The results shown in Figure 2-7 follow the water absorption shown in Figure 2-2, i.e. the lower initial water content the larger absorption and the larger increase in height. In Figure 2-8 the influence of gap size is shown. The results indicate that gaps of 60 mm and 45 mm between the sample and the water surface yield approximately the same increase in height with time which is in accordance with the absorption results shown in Figure 2-3.

Figure 2-8 shows that the two samples representing a gap size of 10 mm do not coincide. A total of three samples were placed 10 mm from the water surface. All three samples showed the same absorption in Figure 2-3. The height and diameter were measured on two of the samples during the test period. The measured increase in diameter with time was the same for the two samples but the increase in height was different, according to Figure 2-8 (see sample S212-V*). After the test all samples were dismantled and the height and diameter were measured. From the initial height and diameter of the samples a second value of the final increase in height and diameter were calculated. For all samples the difference between the two evaluated increases in height was about ± 0.5 mm except for sample S212-V*. For this sample the final increase in height according to Figure 2-8 is 5.8 mm while the corresponding value from initial and final measurements was 2.3 mm less i.e. 3.5 mm. This indicates that some error was involved in the calculated increase in height of S212-V* in Figure 2-8.

Height increase - Pcomp = 50 MPa

Legend:
- S220_V   50MPa 45mm 10%
- S221_V   50MPa 45mm 15%
- S222_V   50MPa 45mm 20%
- S223_V   50MPa 45mm 22%
- S224_V   50MPa 45mm 24%
- S222-V
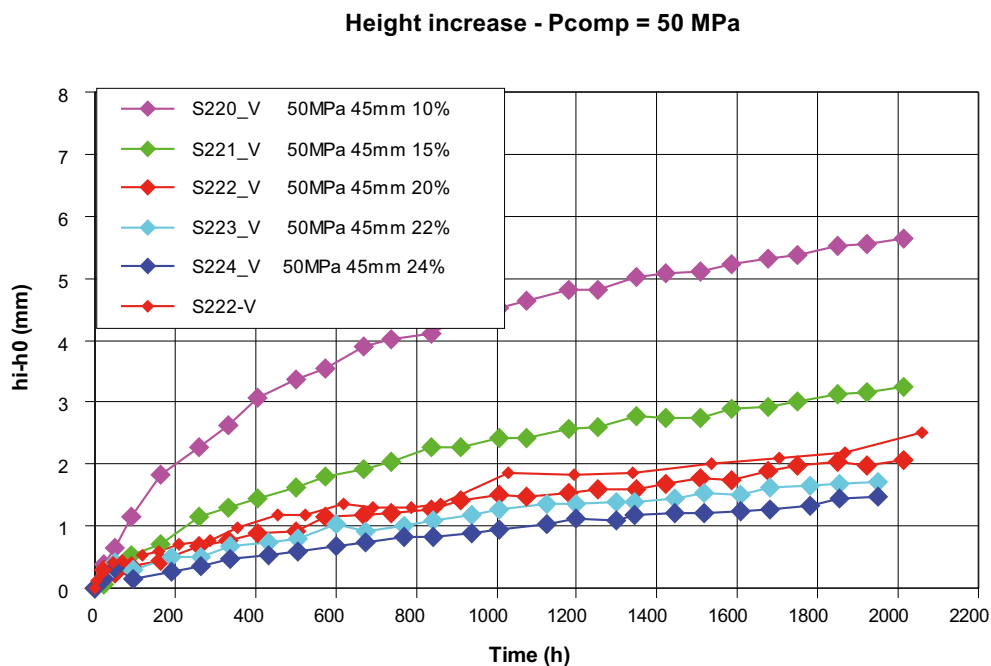
Figure 2-7. Increase in sample height as a function of time. Influence of initial water content. All samples were compacted at 50 MPa.

Height increase - gap and stir
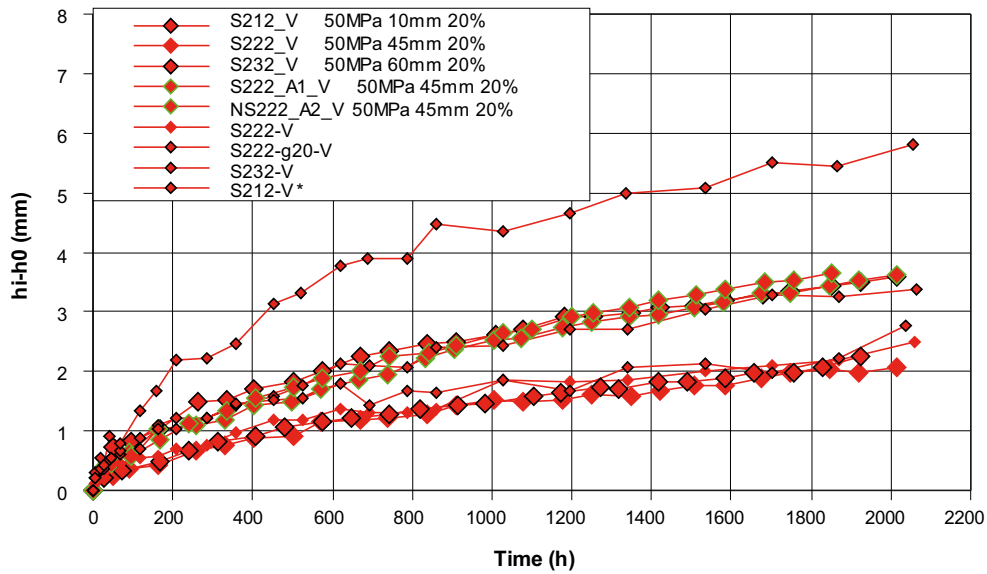
Figure 2-8. *Increase in sample height as a function of time. Influence of size of the gap between the water surface and the sample. Also shown are samples placed in jars with air movement (_A1_V and _A2_V). All samples were compacted at 50 MPa with an initial water content of 20%.*

According to Figure 2-8 no difference is seen between samples placed 20 mm from the water surface and samples placed 45 mm from the surface with air movement. If test S212-V* is not taken into account the same increase is also seen in the sample placed 10 mm from the water surface.

In Figure 2-9 the influence of temperature is shown. Approximately the same increase in height was seen for samples placed at 20°C and 10°C. The samples placed at 30°C increased more in height. The first series of samples placed at 10°C suffering from condensation, mentioned earlier, is not plotted in Figure 2-9.

Height increase - temperature part I and II
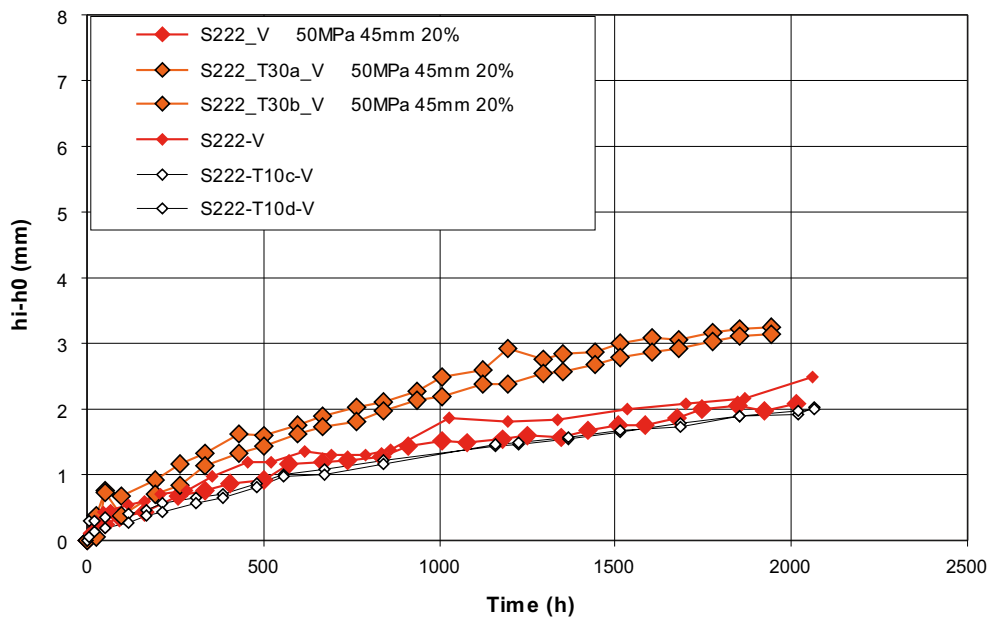
Figure 2-9. *Increase in sample height as a function of time. Influence of temperature. All samples were compacted at 50 MPa with an initial water content of 20%.*

241

In Table 2-3 the initial and final densities for all samples are shown. Since each sample was divided into three slices each sample has values representing the upper, the middle and the lower part of the sample. Both initial and final values are shown. The initial values were measured on extra samples made only for the determination of initial values of water content and density. In Figure 2-10 the initial and final densities of the main part of the samples are shown.

The number of tests performed on each sample is shown in Table 2-3. If more than one sample was tested the value represents the average. If the number of tests is zero this means that the initial value refers to the normal sample S222.

Each sample started with a gradient in density over the sample and at termination the gradient was less but in almost all samples the part nearest the water had a marked less density. This can be seen in Figure 2-10 where the three columns representing the initial densities of each sample differ over the sample while the columns representing the final density of each sample differ less in height.

Cracking

Cracking was most marked on samples starting with low water content. Small radial cracking was seen on some of the S222 and S422 samples starting with 20% water content but not on S223 and S224 samples starting with water contents 22% and 24%, respectively. There is some uncertainties regarding S323 also starting from 22% in water content. Further evaluations of results will be done regarding cracking.

Uncertainties

For quantification of the swelling and absorption uncertainties should be taken into account. This can be done by comparison of doublet samples and by comparison of calculations based on different measurements already done. The accuracy in the methods used for the measurements should be analyzed.

Table 2-3. Initial and final densities for all samples.

Density kg/m3	Upper	Middle	Lower	No.	Upper	Middle	Lower	No.
S210	1923	1969	1995	1	1585	1542	1569	1
S122	1952	1976	1982	1	1859	1857	1860	1
S124	2019	2026	2025	1	1933	1934	1922	1
S212	2050	2064	2072	1	1833	1833	1818	2
S220	1927	1965	1993	1	1665	1660	1661	1
S221	2005	2024	2036	1	1808	1822	1809	1
S222	2065	2069	2074	2	1922	1923	1912	2
S223	2068	2070	2065	1	1955	1951	1937	1
S224	2045	2047	2047	1	1960	1956	1943	1
S232	2066	2077	2080	1	1934	1936	1926	2
S322	2014	2096	2097	2*	1944	1941	1924	2
S323	2073	2073	2074	2	1953	1949	1938	2
S420	2087	2113	2128	1	1736	1738	1734	1
S421	2152	2150	2135	1	1887	1875	1851	1
S422	2098	2102	2101	2	1946	1942	1925	2
S222_H	2062	2075	2083	0	2023	2034	2038	2
S222_A	2062	2075	2083	0	1827	1822	1808	2
S222_T10	2062	2075	2083	0	1819	1807	1773	4
S222_T30	2062	2075	2083	0	1850	1848	1832	4
S222_T10	2069	2063	2065	0	1946	1947	1936	4
S222_Dr0	2069	2063	2065	0	1949	1943	1913	2
S222_g20	2069	2063	2065	0	1875	1873	1859	2

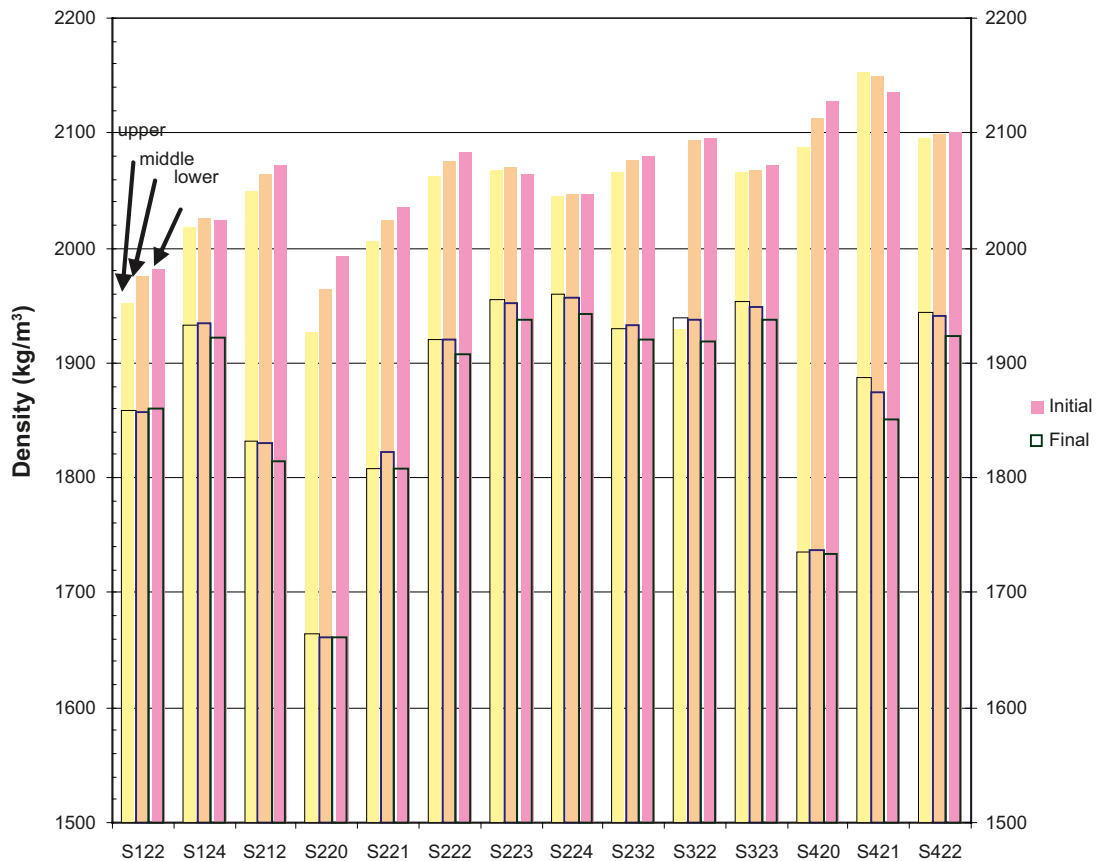* The initial density of the upper part is probably not correct.

Figure 2-10. *Initial and final density of samples from Table 2-1a.*

K.2.1.7   Discussion of results from the small scale tests

All of the tests in the test plan have been carried out. The following preliminary conclusions can be drawn:

•   The lower the initial water content, the higher the absorption and swelling

•   Small influence of compaction pressure (density)

•   The size of the gap between the sample and the water surface influenced the absorption and swelling in a logical way

•   The smaller the size of the gap, the larger the absorption rate and most probably also the larger swelling rate

•   Air movement increased the absorption and swelling

•   Cracking is most obvious on samples starting with low initial water content.

Further work

The test results are still preliminary. For quantification of swelling and absorption rates uncertainties should be further analyzed from the measurements. Further studies of notes and photos should be made regarding cracking.

Modeling and evaluation of the water absorption rate and possibly also the swelling rate will be done.

K.2.2 Medium scale tests

K.2.2.1 General

As a complement to the small scale tests described in Chapter 2.1, an additional test series has been performed on a larger scale. Blocks with a diameter of 280 mm and a height of 100 mm were compacted with desired water ratio and compaction pressure. The blocks were placed in special made vessels where the distance from the outer block surface to the wall was set to a prescribed value. The wall in the vessels, simulating the rock, was kept wet in order to simulate a real worst case.

K.2.2.2 Test equipment

A schematic view of the test equipment is shown in Figure 2-11. The end faces of the block were covered with rubber mats and the outer periphery surface was exposed to a high relative humidity. The blocks were taken out at prescribed intervals in order to be weighed, measured and inspected for investigating possible cracking. In order to facilitate the inspections, the vessels were placed in a special frame where the lids could be locked or removed in an easy way, Figure 2-12.

K.2.2.3 Test matrix

Table 2-4 shows the complete test matrix. The shaded boxes mark the performed tests. All blocks/samples were compacted with a pressure of 100 MPa except for the sample with the highest water ratio, M153, which was compacted with 50 MPa. At high water ratios there is no advantage in having a high compaction pressure. The final block density will be the same and the higher pressure only makes the manufacturing more difficult. Three tests, M150, M152 and M153, were performed with the same gap to the rock (45 mm) and with the same relative humidity (100%) but with different initial water ratio (13, 20 and 24%). Two tests, M142 and M162, were made in order to study the influence of the slot width (10 andd 60 mm respectively) and one test, M120, was made in order to study the influence of the Relative Humidity (85%) in the slot.
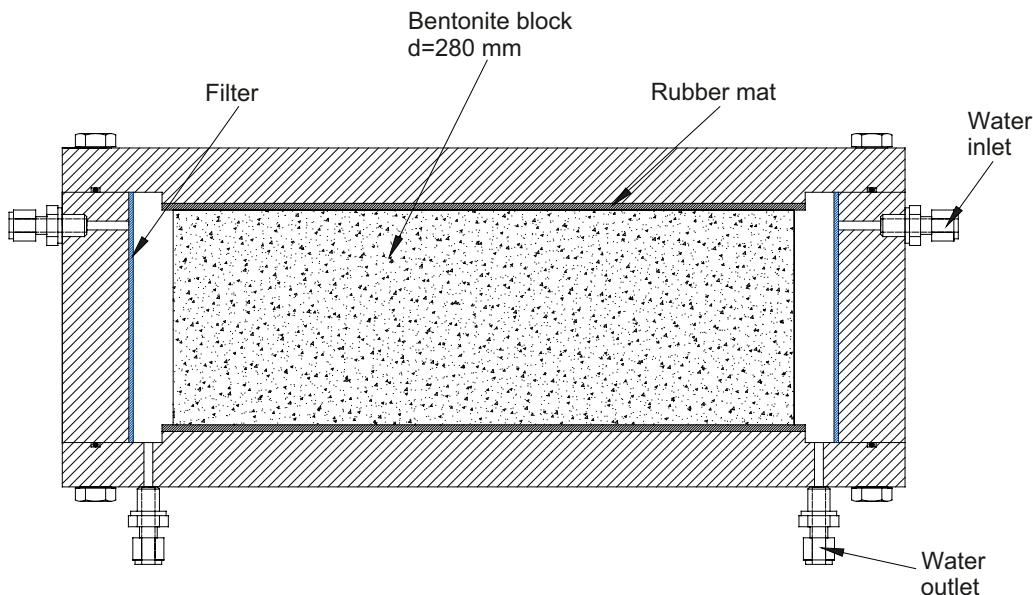
Figure 2-11. *Schematic view of the test equipment. The bentonite block had a prescribed gap between the outer block surface and the inner wall of the vessel. The wall was covered with a filter which was kept wet by circulating water through four inlets and four outlets. The filter was made of paper and the water was spread capillary on the surface which means that the whole "rock" surface was kept wet. The blocks were taken out at regular intervals in order to be weighed, measured and inspected to determine possible cracking on the surface.*

Figure 2-12. *Picture showing three of the test vessels after emplacement in the special made frame.*

Table 2-4. Suggested test matrix for the medium scale tests. The shaded boxes mark the performed tests.

Humidity induced swelling - test matrix for the medium scale tests						
	RH 85%			RH 100%		
w initial, %	Gap bentonite/water			Gap bentonite/water		
	10 mm	45 mm	60 mm	10 mm	45 mm	60 mm
13	M110	M120	M130	M140	M150	M160
15	M111	M121	M131	M141	M151	M161
20	M112	M122	M132	M142	M152	M162
24	M113	M123	M133	M143	M153	M163

K.2.2.4   Test results

Water uptake and swelling

The water absorption from the initial state is shown in Figures 2-13 and 2-14. Figure 2-13 shows the weight increase during the first 30 hours of the tests. Two of the tests, M120 (w $_{ini}$ = 13%, RH = 85%) and M150 (w $_{ini}$ = 13%, RH = 100%) were terminated after 8 and 24 hours respectively, due to very strong cracking which made it impossible to continue the measurements, see Figure 2-16. The diagram in Figure 2-13 also shows that these two samples had the largest water uptake rate. Two of the samples M162 (w $_{ini}$ = 20%, RH = 100%, gap = 60 mm) and M153 (w $_{ini}$ = 24%, RH = 100%, gap = 45 mm) had a test duration of three months and was still after this time in rather good shape. During the test time the diameter of the blocks was also measured at decided intervals, Figure 2-15.
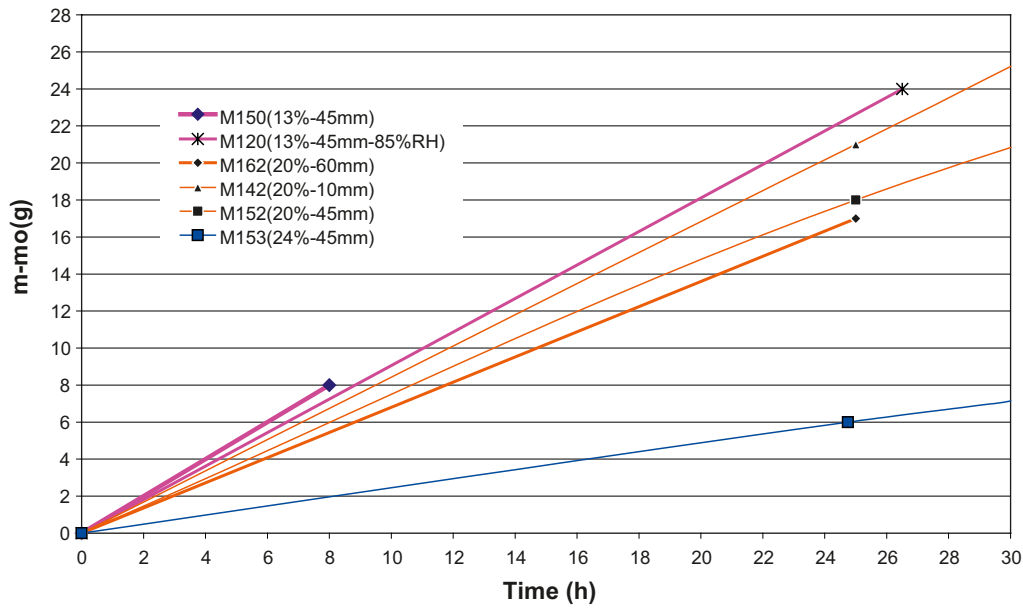
Figure 2-13. *Diagram showing the water absorption as a function of time for the six samples during the first 30 hours.*
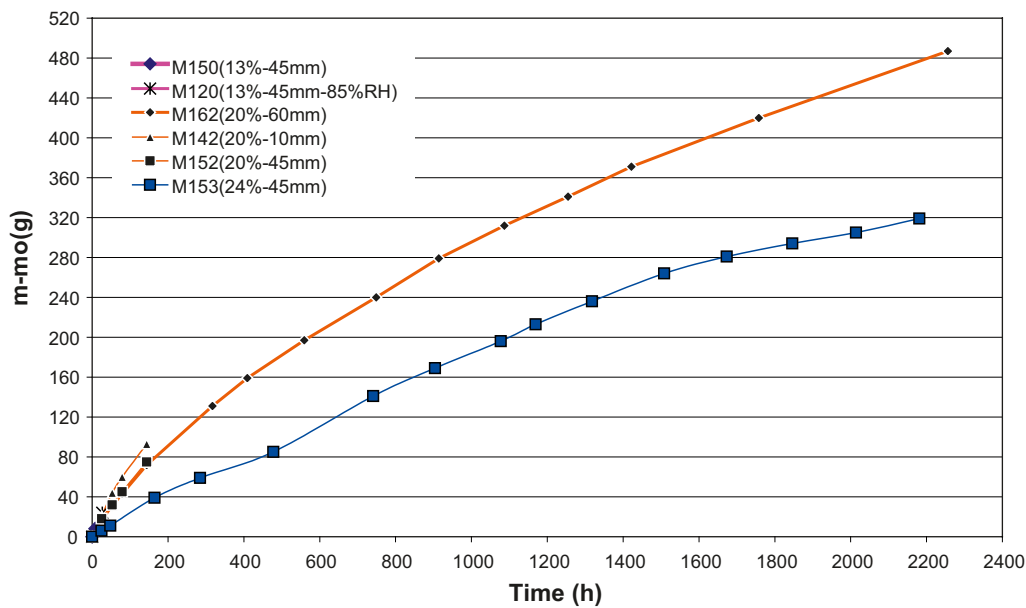
Figure 2-14. *Diagram showing the water absorption as a function of time for the six samples.*

Cracking

The tests show that the blocks sensitivity to cracking was very dependent on the initial water ratio and also on the distance to the wet surface. The two samples with the lowest initial water ratio (13%) were cracked in pieces during the first 24 hours. Two of the three samples with an initial water ratio of 20% and smallest gap (10 and 45 mm) had both a diametrical crack within one weeks test duration. The third sample with an initial water ratio of 20% had a gap to the rock of 60 mm. After about one month testing a diametrical crack could be seen but still after three months test the sample was in one piece, Figure 2-18. The sample with an initial water ratio of 24% was after three months test unaffected by cracking, Figure 2-19.

Changes in diameters M162-M153 (three months)
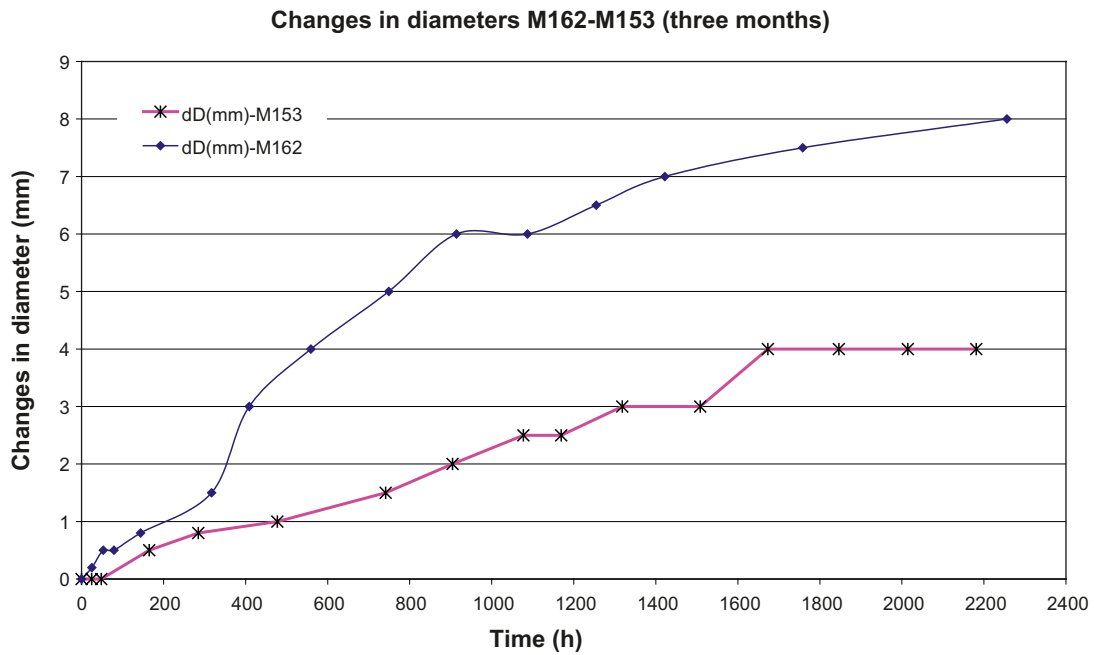
Figure 2-15. *Diagram showing the measured change in diameter for the samples M162 (w_{ini} = 20%, RH = 100%, gap = 60 mm) and M153 (w_{ini} = 24%, RH = 100%, gap = 45 mm) plotted vs. time.*

Figure 2-16. *Picture showing block sample M150 (w_{ini} = 13%, RH = 100%, gap = 45 mm) after 8 hours test duration.*

Sample M120, (w_{ini} = 13%, RH = 85%, gap = 45 mm). The sample had cracked completely after 24 hours test duration.

Sample M150, (w_{ini} = 13%, RH = 100%, gap = 45 mm). The sample had cracked completely after 8 hours test duration, Figure 2-16.

Sample M142, (w_{ini} = 20%, RH = 100%, gap = 10 mm). Diametrical crack after 6 days test duration.

Figure 2-17. *Picture showing block sample M152 (w $_{ini}$ = 20%, RH = 100%, gap = 45 mm) after 7 days test duration.*

Figure 2-18. *Picture showing block sample M162 (w $_{ini}$ = 20%, RH = 100%, gap = 65 mm) after 3 months test duration. The block was still in one piece but there was an evidently diametrical crack which occurred after about one months test duration.*

Figure 2-19. *Picture showing block sample M153 after 3 months test duration. No cracks could be seen on the surface.*

Sample M152, (w $_{ini}$ = 20%, RH = 100%, gap = 45 mm). Diametrical crack after 7 days test duration, Figure 2-17.

Sample M162, (w $_{ini}$ = 20%, RH = 100%, gap = 60 mm). The block was after three month test duration still in one piece but there was a very evidently diametrical crack which occurred after about one month testing, Figure 2-18.

Sample M153, (w $_{ini}$ = 24%, RH = 100%, gap = 45 mm). No cracks could be seen after three months test duration, Figure 2-19.

K.2.2.5   Discussion of results from the medium scale tests

The following preliminary conclusions can be drawn:

Cracking is more marked on the samples starting with low water content. This is in accordance with the results from the small scale tests.

Cracking seems to depend on the size of the gap; the smaller size of the gap the more cracking.

After about 2,000 h the water absorbed from the sample with an initial water content of 24% is about 2/3 of the water absorbed from the sample with an initial water content of 20%. This ratio is almost the same as in the small scale tests if the influence of gap size is not considered.

Further work

The performed test series is done with ring shaped LOT blocks (D = 280 mm, d = 110 mm) i.e. they have a central hole. A similar test series using solid blocks is under consideration.

K.3   Piping through distance blocks

K.3.1   General

After the emplacement of distance blocks, the bentonite will take up water, swell and seal the drift. If high water pressures are built up in a short time just after the sealing, a piping scenario could occur i.e. water may pipe through the bentonite and a flow of water and bentonite will take place, see Figure 3-1. It has been observed in previous tests that piping may occur at certain design and inflow conditions. It has also been observed that internal piping seems to be a fundamental process, which enables transport of water in the buffer and improves efficient saturation of the blocks.

When piping starts, bentonite may erode and reduce the density of buffer locally. The erosion and transport of bentonite depends on several factors, the flow velocity being one of the most important ones.

Experiments have been performed in three different test equipments:

- Scale 1:10, test length 1meter.
- Scale 1:10, test length 3 metre.
- Transparant tube, d = 0.1 metre and length = 1 metre.

K.3.2   Experiments in the 1 metre long test equipment

K.3.2.1   General

The function of distance blocks has been tested in three different test series in scale 1:10 (radial scale) in a 1 metre long test equipment. The results from the first two test series were presented in the report Studies of buffer behaviour in KBS-3H alternative /Börgesson et al. 2005/ In this third test series so far 13 tests have been made. The principle test layout in this test series is shown in Figure 3-2. The tests have been performed with a strong deviation from the reference case in order to assess the sensitivity of the system to varying conditions. The test conditions examined have been (current reference case conditions are shown in parentheses):

- Inflow rate: 1 l/min, corresponding to filling time of 1 day (0.1 l/min).
- Water pressure increase rate: 1,000 kPa/h (low 100 kPa/h, high 5,000 kPa/h)
- Total water pressure: 5 MPa (2 MPa).
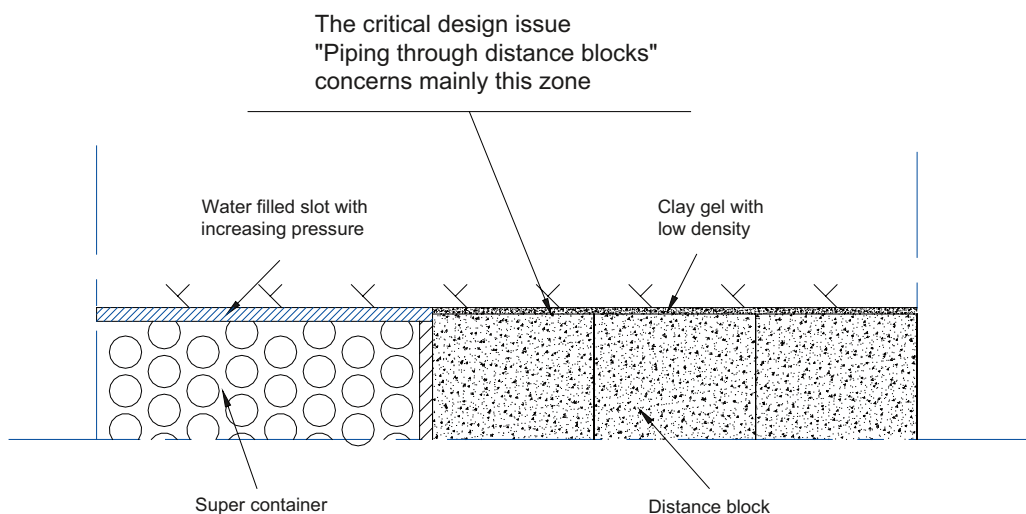
Figure 3-1. *Schematic drawing showing a part of a vertical view of the KBS-3H layout. The critical design issue "Piping through distance blocks" concerns mainly the slot between distance blocks and rock.*
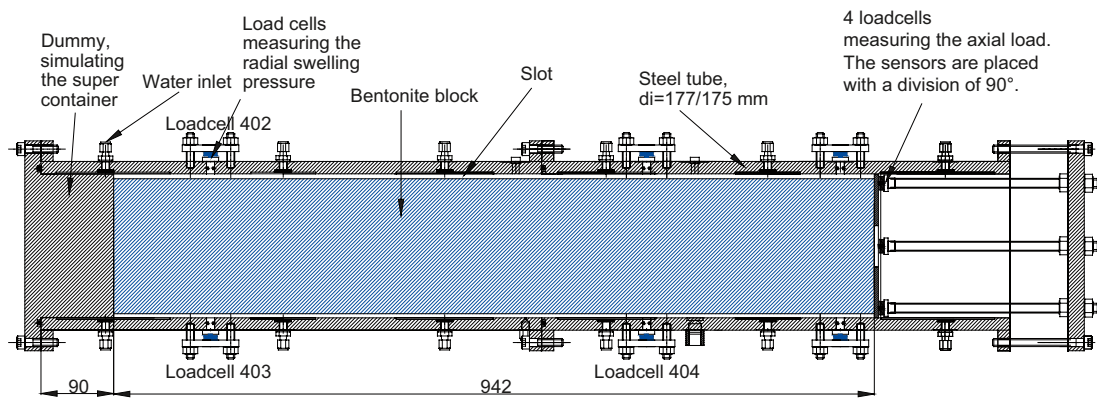
Figure 3-2. *Schematic view showing the test equipment used in the latest test series in scale 1:10.*

The test variables have been the following:

• Different slot widths

• Pellet filled slot or not

• Salt content in the water

• Pre-wetting of the slot or not.

During the tests the following has been measured:

• Water pressure of the injected water

• Water volume injected

• Axial load on the end of the distance plug (four points)

Swelling pressure of the bentonite (three points).

Table 3-1 shows a compilation of all tests performed in the 1-meter equipment.

Test III-1 and III-6. These tests were performed with centred blocks and a pellets filled slot with a width of 35 and 15 mm respectively. Tap water was used in these tests.

Result. In none of the tests could the bentonite seal and withstand the water pressure built up. The samples could after 2–3 days withstand a water pressure of 150 kPa (III-1) and 450 (III-6).

Test III-2. The blocks were placed on the bottom with a 2 mm slot at the top. Tap water was used in this test. After a filling time of two days a pressure ramp of 5 MPa/h was applied up to maximum 5 MPa.

Result. After some internal piping the bentonite could withstand the applied water pressure.

Test III-3. The layout in III-2 can handle the extreme test conditions. An installation of distance block with these small slots is however probably very difficult. In order to improve the layout and test the limits, the block diameter was decreased giving a slot of 5 mm at the top. Tap water was used also in this test. After a filling time of two days a pressure ramp of 5 MPa/h was applied.

Result. Internal piping occurred during the pressure ramp. The bentonite could not withstand a maximum water pressure higher then 820 kPa.

Test III-4. The same test layout and test conditions as in test III-3. In order to improve the possibilities for the bentonite to seal it was decided to pre wet the slot at test start and by that give the whole bentonite surface around the distance block access to water during 24 hours, before applying the water pressure ramp (in the earlier test water was filled up from the supercontainer section bottom and reaching the upper parts after 24 h).

251

Table 3-1. Table showing the tests performed in the 1 metre long test equipment. The tests marked with grey background are performed with pellets in the slot and the ones marked with purple background are performed with 3.5% salt in the water.

Test	Arrangement	Slot up/down mm	Test length m	Filling time days	Filling rate scale 1:1 l/min	Water pressure increase rate kPa/h	Maxiamal pressure kPa	Water type	Comments
III-1	35 mm slot filled with pellets	35/35	0.94	1.6	0.63		350	Tap water	After filling, a constant flow of 5 l/24h was applied. **The system did not seal.**
III-2	Tight distance block, d bentonite 173 mm	2/0	0.94	1.9	0.53	1000	5000	Tap water	Some "internal piping" during the pressure ramp. **The system seals.** Water penetration 71cm in bottom.
III-3	Tight distance block, d bentonite 170 mm	5/0	0.94	1.9	0.53	1000	820	Tap water	"Internal piping" continoued with piping. **The system did not seal.** The outer surface completely wet.
III-4	Tight distance block, d bentonite 170 mm Pre saturated bentonite	5/0	0.94	1	1	1000	5000	Tap water	Some "internal piping" during the pressure ramp. **The system seals.**
III-5	Tight distance block, d bentonite 165 mm Pre saturated bentonite	10/0	0.94	1	1	1000 / 100	4200	Tap water	The system can not stand the fast pressure build up. The bentonite can withstand 4.2 MPa after 2 weeks
III-6	15 mm slot filled with pellets Pre saturated bentonite	15/15	0.94	1	1	1000 / 100	1800	Tap water	The system can not stand the pressure build up. The bentonite can withstand 1.8 MPa after 2 weeks
III-7	Tight distance block, d bentonite 170 mm Pre sat.bentonite+salt	5/0	0.94	1	1	1000	5000	3.5 % salt	The salty water increases the swelling rate and by that also the sealing effect. **The system seals.**
III-8	Tight distance block, d bentonite 165 mm Pre sat.bentonite+salt	10/0	0.94	1	1	1000	1600/3600	3.5 % salt	Piping at 1600 kPa. After 12 h resttime new pressure ramp. Clay pressed out at 3600 kPa.
III-9	Tight distance block, d bentonite 165 mm Pre sat.bentonite+salt	5/5	0.94	1	1	1000	5000	3.5 % salt	Some "internal piping" during the pressure ramp. **The system seals.**
III-10	Tight distance block, d bentonite 165 mm Pre sat.bentonite+salt	5/5	0.94	1	1	1000	4600	3.5 % salt	Repeating test III-9 "Internal piping" during the pressure ramp. **The system could not take 5 MPa.**
III-11	Tight distance block, d bentonite 165 mm Pre sat.bentonite+salt	5/5	0.94	1	1	1000	5000	3.5 % salt	Repeating test III-9 "Internal piping" during the pressure ramp. **The system seals.**
III-12	Tight distance block, drainage tube under block Pre sat.bentonite+salt	10/10	0.94	Controlled (7days)	Controlled	1000	1700/800	3.5 % salt	Pre test with drainage tube. The system can not stand the fast pressure build up. Max 800 kPa after 20 days.
III-13	Tight distance block, Pre sat.bentonite+salt	10/10	0.94	-	-	1000	5000	3.5 % salt	After pre wetting of the slot, has sample no access to additional water. Test has influence on spalling issue.

252

Result. Internal piping took place a number of times during the pressure ramp. The bentonite could withstand a maximum water pressure of 5 MPa after about 30 hours.

Test III-5. The same test layout and test conditions as in test III-4 but the initial slot at the top was increased to 10 mm.

Result. The sample can not withstand the water pressure. New pressure ramps were applied a number of times during two weeks. After two weeks the sample could withstand 4.2 MPa.

Test III-7. The same test layout and test conditions as in test III-4 (5 mm slot at the top) but instead of tap water, water with 3.5% salinity was used.

Result. The sample can withstand the water pressure. The salt water increases the swelling rate and by that also the sealing effect. At these rather high densities it could be favourable to use salt water. This effect should be investigated more carefully.

Test III-8. Again was the upper slot increased to 10 mm (same test layout as in III-5) but now the test was performed with salt water.

Result. The sample can withstand 1,600 kPa. After 12 hours of rest time a new pressure ramp was applied. The sample can now take 3,600 kPa. At this pressure clay gel was squeezed out around the fixing ring.

Test III-9. Same test condition as in III-8 but the block is now centred in the tunnel (5 mm slot).

Result. The sample can withstand 5 MPa. There was some internal piping during the pressure increase.

Test III-10 and III-11. Test number III-9 was repeated two times.

Result. Similar results in all three tests. Test III-10 could maximum withstand 4.6 MPa before a leakage occurred around the fixing ring. There was internal piping in all three tests during the pressure ramp. This test layout is probably the limit for the bentonite ability to seal at these extreme conditions.

Test III-12. This was a pre test in order to test the idea of using a drainage tube. The advantage is that the water inflow can be controlled and also the water pressure increase rate. The bentonite blocks were centred having a slot of 10 mm to the rock. The filling time was set to 7 days. After this time a pressure ramp of 1 MPa/h was applied.

Result. The sample could withstand 1.7 MPa. A new attempt was done 12 days later and the sample could now only withstand 0.8 MPa. The applied pressure ramp was probably to fast. The retrieval of the drainage tube was also tested. In order to pull out the steel tube (D = 6mm) a force of 1.1 kN was needed. This test layout has later been repeated in the three metre long equipment, see Chapter 3.3 but in these tests the water pressure was increased in steps during a period of 2 weeks.

Test III-13. The layout of the test was: Tight distance block, t = 10/10 mm (centred blocks), pre-wetted slot, 3.5% salt in the water. The slot was filled with water. The sample did not have access to additional water.

The test simulates the case when the bentonite is installed according to the DAWE and BD design. After the pre-wetting there was no access to additional water and a re-distribution of the available water took place. Important to notice was the development of the radial swelling pressure during the water re-distribution. The test is important for the spalling issue.

Result. The test was run for three months. Before termination the bentonites tightness against the rock was tested by applying an air pressure in the supercontainer section and check if there is any leakage along the bentonite/rock interface. It was not possible to detect any leakage with this method. The same test with water was also done. A pressure ramp of 1 MPa/h was applied. After a number of internal piping the sample could withstand 5 MPa.

Test III-14. This test is under preparation. The planned test layout is: Bentonite blocks with a water ratio of 22% (Sr = 94%). Slot width 4/0 mm (blocks lying on the bottom. The filling time is planned to be 10 days simulating an inflow of 0.1 l/min and a pressure ramp of 1 MPa/h will after this time be applied. The test simulates the design alternative using tight distance blocks which are divided in three parts before installation. The surfaces are inclined which means that the parts could be pushed in position and the bentonite will be in contact with the rock. The small slot in the test simulates the roughness of the rock. This is the first test with blocks having a high initial water ratio.

K.3.2.2 Example of more detailed test results, Test III-9

Test description

The bentonite blocks in the test were centred by steel "feet" and the slot width between the blocks and the rock was 5 mm. The water used in the test had a salt content of 3.5%. The volume around the "distance blocks" was filled with water by use of two tubes passing through the fixing ring, one in the bottom and one in the top. The lower tube was used for filling and the upper for de-airing. A total amount of 3.3 litres was injected during 15 minutes. The volume around the supercontainer was filled in 24 hours and then a pressure ramp of 1 MPa/hour was applied, see Figure 3-3.

Result

In Figure 3-3 the measured water pressure and the injected water volume are shown. There was some internal piping during the ramp but after about 6 hours the applied water pressure had reached 5 MPa. Unfortunately there was a dip in pressure depending on that the pressure equipment was emptied of water.

The axial load on the fixing ring was measured during the test as well as the radial swelling pressure, Figure 3-4. These results were very evidently influenced by the applied water pressure. Figure 3-5 and 3-6 shows pictures taken during the decomposition of the tests.

This test layout was repeated in test III-10 and III-11 with similar results.
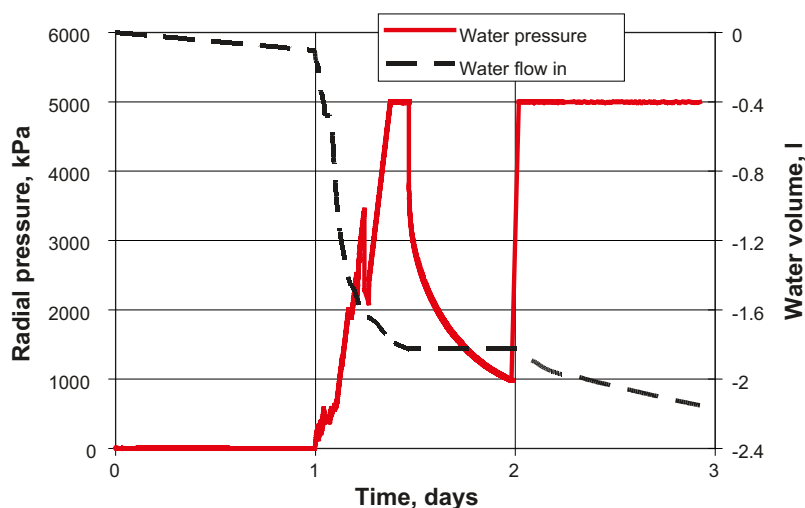
Figure 3-3. Diagram showing the water pressure build up and the water inflow. After 24 hours a pressure ramp was applied. The dip in pressure after about 36 hours depends on the pressurising device that run out of water.
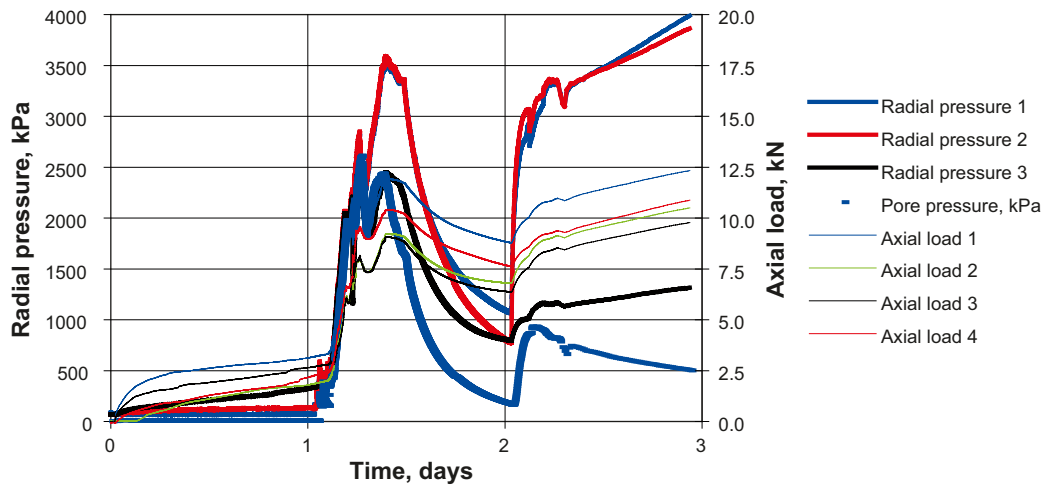
Figure 3-4. *Diagram showing the axial load built up and the radial swelling pressure that was measured in three points. The pore pressure was measured in one point.*


Figure 3-5. *Picture showing the outermost part i.e. against the load cells after removing the fixing ring.*

Figure 3-6. *Picture from the middle of the sample about 0.5m from the pressure side. The water ratio was determined in some positions with the following results: Uppermost 5 mm = 30%, next 5 mm = 29%, next 5 mm = 28%, next 5 mm = 25%, and in the centre = 17%.*

K.3.2.3   Example of more detailed test results, Test III-13

Test description

The bentonite blocks in the test were centred by steel "feet" and the slot width between the blocks and the rock was set to 10 mm. The water used in the test had a salt content of 3.5%. The volume around the "distance blocks" was filled with water by use of two tubes passing through the fixing ring, one in the bottom and one in the top. The lower tube was used for filling and the upper for de-airing. A total amount of 5.5 litres was injected during 30 minutes. When the slot between the bentonite blocks and the rock was filled, the valve was closed and the sample did not have access to additional water during the test time. This test is of importance for the spalling issue and is of interest for both DAWE and BD.

Result

The sample was left for 112 days without any access to additional water. The assumption was that the water in the slot would be drawn deeper into the buffer blocks resulting in desiccation and cracking of the bentonite in the outer parts. This phenomenon has been seen earlier in similar tests done in another project (Lasgit), see Figures 3-7 and 3-8. The results from these tests were that there were clear indications on desiccation and cracking of the surface but it was still possible to measure a swelling pressure. The radial pressure measurements in this test, Figure 3-9, also show that there still after 112 days was a swelling pressure from the clay acting on the rock. Before termination of the test it was decided to test how well the section was sealed. Two different methods were used:

1. An air pressure was applied in the supercontainer section. Any possible leakage was detected by using a flow meter on the air inlet.

2. After the air test instead a water pressure ramp of 1 MPa/h was applied, Figure 3-10.

Figure 3-7. Picture showing the distance block after removal of the fixing ring.

Figure 3-8. Picture from the middle of the sample showing a part of the outer surface. No cracks could be seen.
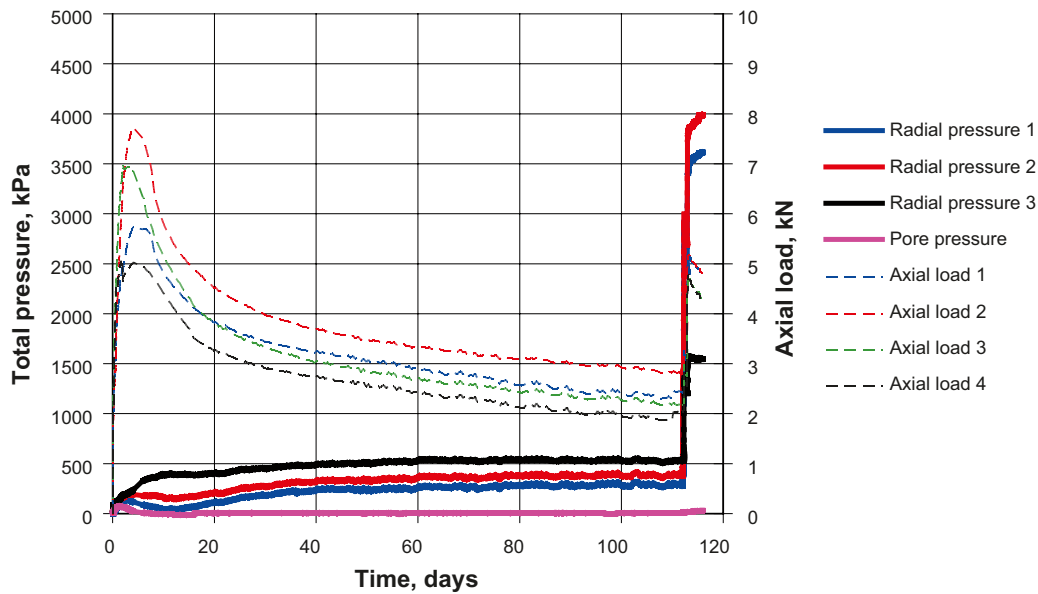
Figure 3-9. *Diagram showing the axial load and the radial swelling pressure measured in three points as a function of time. Pore pressure was measured in one point.*
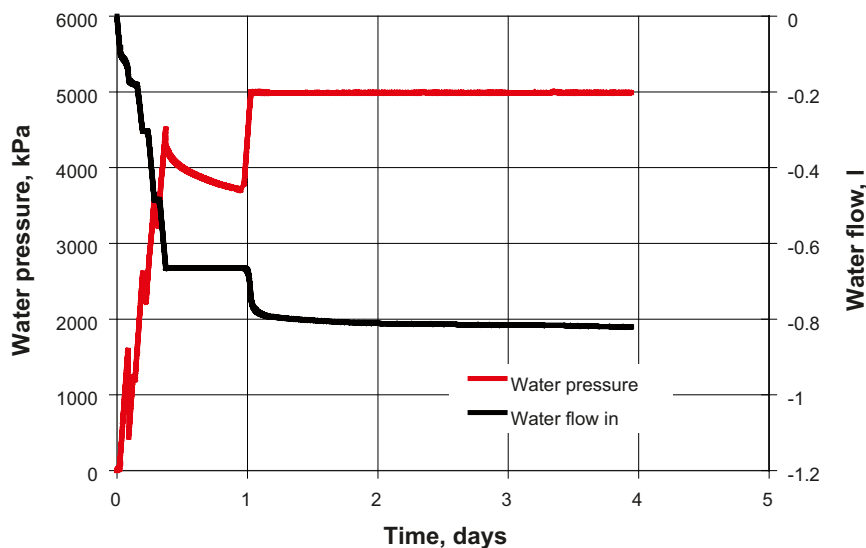
Figure 3-10. *After 112 days without access to additional water a pressure ramp was applied. The diagram shows the water pressure build up and the water inflow. During the pressure ramp internal piping occurred a number of times. The amount of water injected was quite large which meant that the pressurizing equipment had to be filled up a number of times. 24 hours after starting the pressure ramp the maximum pressure, 5 MPa, was reached. The dip in pressure after about 8 hours depends on that the pressurising device run out of water in the middle of the night.*

K.3.3   3 metre long test equipment

K.3.3.1   General

The test length was limited to about 1 metre in the 1:10 scale equipment and to 1.4 metre in the Big Bertha equipment. In order to study the influence of the test length on the piping phenomena, tests have been running parallel in a new test equipment with a length of 3 metre.

Three complete tests have been performed in this longer test equipment and test number four is under preparation. Figure 3-11 shows a picture from the laboratory showing the test setup.
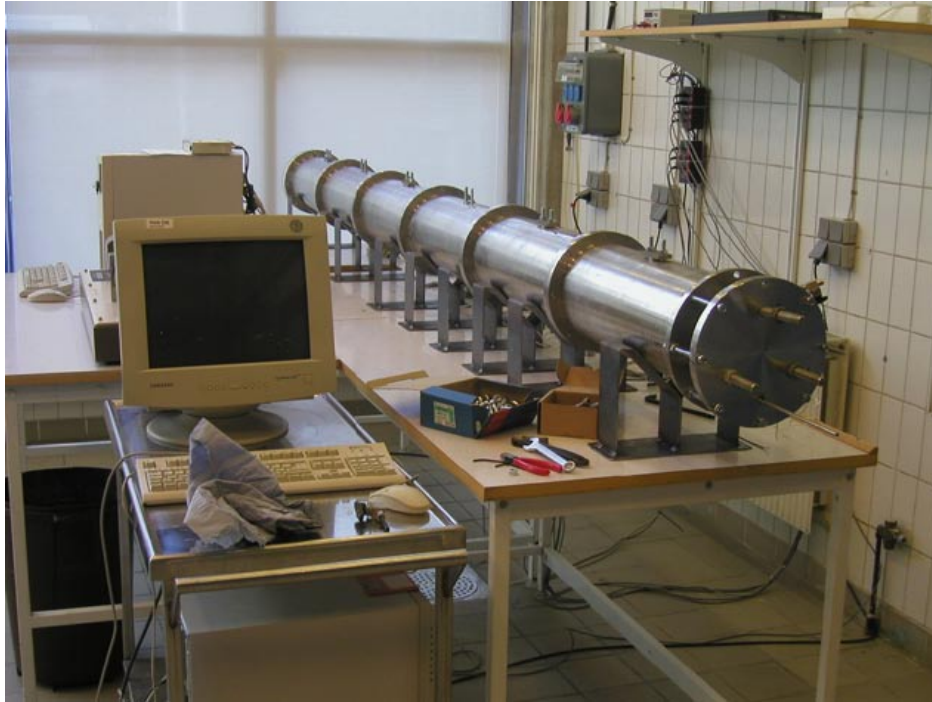
Figure 3-11. *Picture from the laboratory showing the 3 metre test equipment.*

K.3.3.2 Results

A compilation of the tests performed in the 3-meter equipment is done in Table 3-2. The three tests were done in order to verify the design solution where a drainage tube is used to control water inflow and water pressure increase rate.

K.3.3.3 Example of results, Test III-31

A schematic drawing of the test layout is shown in Figure 1. In Table 3-3 the input data of the bentonite blocks is shown.

Test description

A schematic drawing of the test layout is shown in Figure 3-12. The bentonite blocks in the test were centred by steel "feet" and the slot width between the blocks and the rock was 10 mm. The water used in the test had a salt content of 3.5%. The volume around supercontainer and distance blocks was filled with water by use of the lower filling tube, see Figure 12. The upper tube was used to de-air the volume. A total amount of 16 litres was injected during 30 minutes. The volume had access to additional water through an inlet at the container section during the maturation time.

Table 3-2. Table showing the performed tests in the 3 metre test equipment.

Test	Arrangement	Slot up/down mm	Test length m	Filling time days	Filling rate scale 1:1 l/min	Water pressure increase rate kPa/h	Maxiamal pressure kPa	Water type	Comments
III-31	Tight distance block, d bentonite 155 mm centred blocks	10/10	3.08	1	1	1000	1100	3.5% salt	The bentonite couldnt withstand the pressure. A new ramp was applied after 11 days, with the same result.
III-32	Tight distance block, d bentonite 173 mm	10/10	3.08	Controlled	Controlled	Controlled	5000	3.5% salt	The buffer samples could after 2 weeks withstand 5 MPa.
III-33	Tight distance block, d bentonite 170 mm	10/10	3.08	Controlled	Controlled	Controlled	5000	3.5% salt	The buffer samples could after 2 weeks withstand 5 MPa. Repetition of test III-32
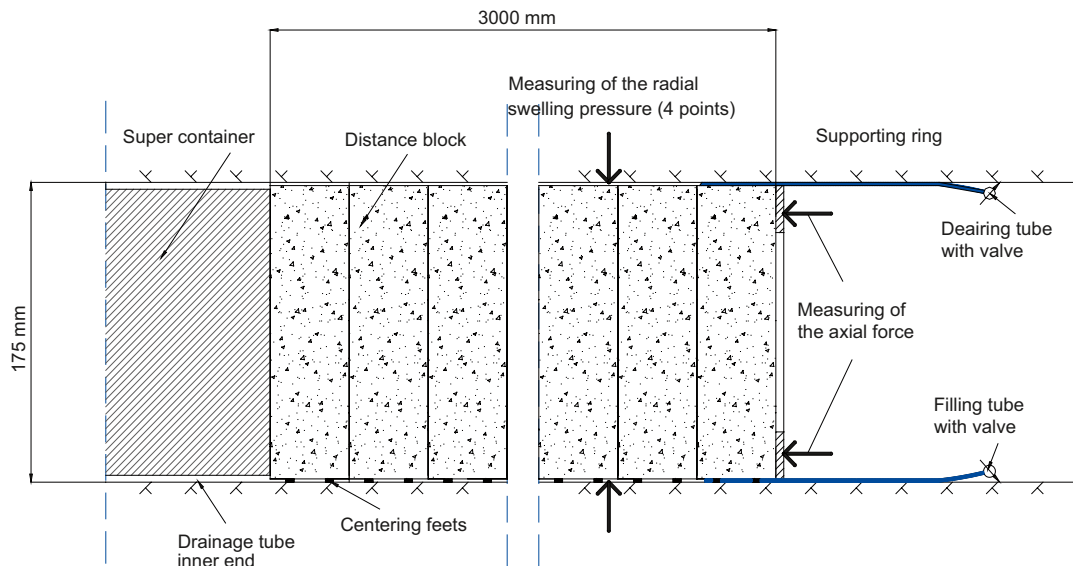
Figure 3-12. *Schematic drawing showing the test layout for test III-31.*

Table 3-3. Table showing the data for the bentonite blocks used in test number III-31.

Installed distance blocks

Raw material	MX-80, cores from full scale blocks
Water ratio, %	13.5
Bulk density, kg/m^3	1950
Dry density, kg/m^3	1720
Degree of saturation, %	60.6
Void ratio	0.617
Diameter of the blocks, mm	155
Test length, mm	3080
Total mass of blocks installed, kg	112.05

Calculated data

Final dry density, kg/m^3	1511
Void ratio	0.847
Saturated density, kg/m^3	1969

Result

24 hours after test start a pressure ramp of 1 MPa/h was applied in the supercontainer section, Figure 3-13. The distance blocks couldn't withstand this which resulted in piping at a pressure of 1,000–1,100 kPa. A new attempt was done after additional 11 days with almost the same results.

It was obvious that the bentonite had not managed to seal the slot. The measured radial swelling pressure was rather low, 50–150 kPa, Figure 3-14. As shown in Figure 3-15 and 3-16 the bentonite had swelled and filled the slot volume, but the density at the outer parts was to low. A limiting factor can be that access to additional water is limited to the rather small bentonite surface against the container section.

The water ratio was determined in some points, see Table 3-4. The water ratio in the outermost 5 mm was about 50% according to measurements afterwards. Assuming that the sample was saturated this corresponds to a density of saturation of 1,750 kg/m^3.
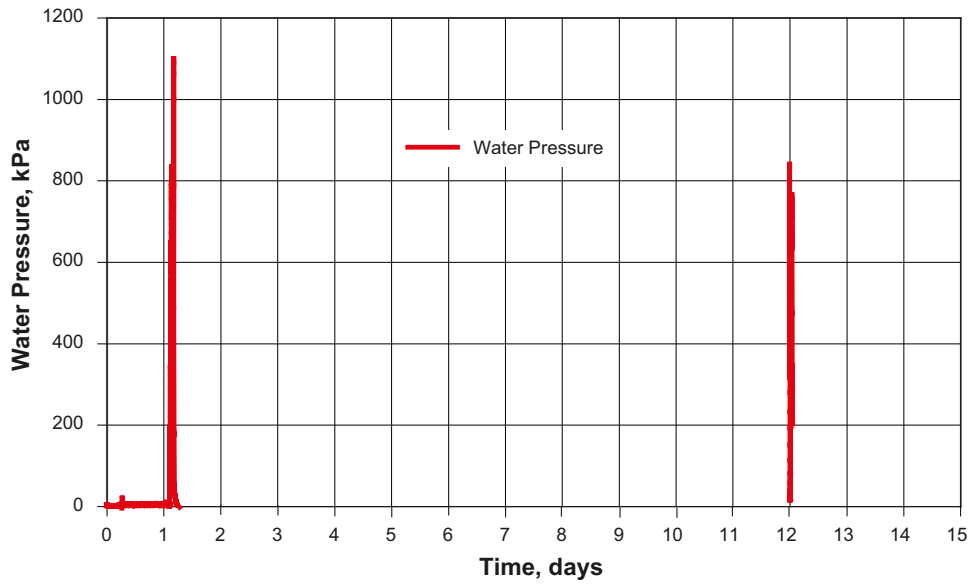
Figure 3-13. *Diagram showing the water pressure build up during the test. After 1 day a pressure ramp of 1 MPa/h was applied. The sample could withstand maximum 1,100 kPa before piping occurred. A new pressure ramp was applied after additional 11 days with similar result.*
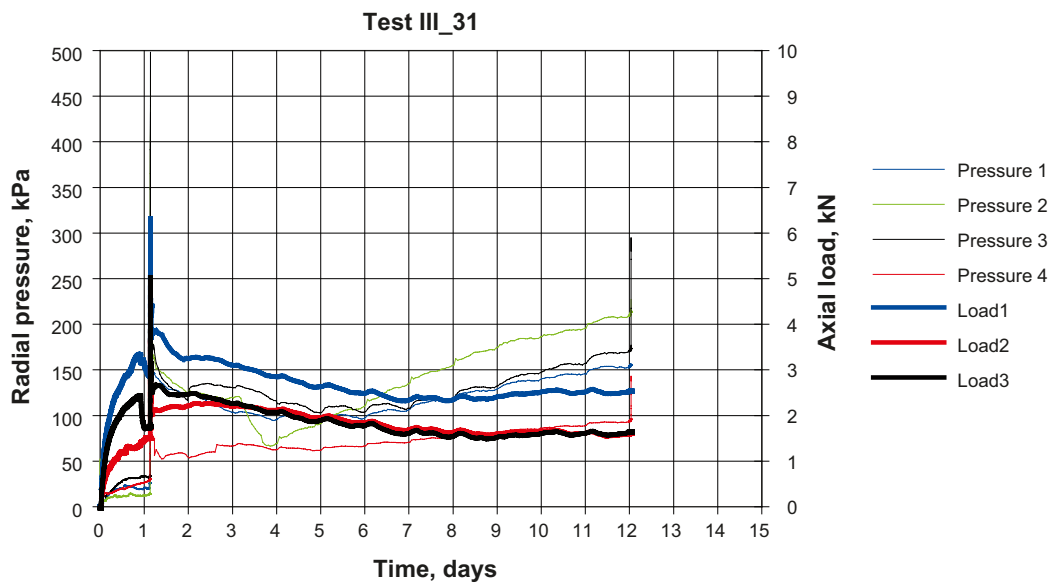
Figure 3-14. *Diagram showing the measured swelling pressure build up infour different points and axial load as a function of time.*

261

Figure 3-15. Picture showing the surface just inside the supercontainer dummy. The ring shaped "active surface" can be well distinguished.

Figure 3-16. Picture taken during decomposition of the test, about 1.5 m from the supercontainer section. The dark ring has a width of 35–40 mm. The water ratio was determined in some positions; see Table 3-4.

262

Table 3-4. Measure d water ratio of samples taken in the wat area in a section 1.5 m from the pressure side, see Figure 3-16.

Upper part	Outermost 0-5mm	**54.5%**
	5-10 mm	**49.2%**
	10-15 mm	**44.9%**
	15-30 mm	**37.6%**
Bottom part	Outermost 0-5mm	**46.5%**
	5-10 mm	**43.6%**
	10-15 mm	**38.4%**
	15-30 mm	**29.5%**

K.3.3.4 Example of results Test III-32

A schematic drawing of the test layout is shown in Figure 3-17. In Table 3-5 the input data for the bentonite blocks is shown.

Test description

The water used in the test had a salt content of 3.5%. The slot around supercontainer and distance blocks was filled with water by use of the lower drainage tube, see Figure 17. The upper tube was used to de-air the slot. A total amount of 16 litres was injected during 30 minutes. The slot had access to additional water from the supercontainer section via the drainage tube.

The bentonite blocks in the test were centred by steel "feet" and the slot width between the blocks and the rock was 10 mm. A schematic drawing of the test layout is shown in Figure 3-17 and a picture from the installation is shown in Figure 3-18. The difference from test III-31 was the drainage tube which was led the whole way through the fixing ring, under the distance blocks and into the supercontainer section. This tube could be used to control the water pressure situation in the container section and also to "feed" the bentonite with additional water during the maturation phase. This was done by increasing the water pressure in steps during a period of about two weeks. This method takes however time and can probably only be used in sections with high water inflow.

Table 3-5. Table showing the data of the bentonite blocks used in test number III-32.

Distance blocks

Installed distance blocks

Raw material	MX-80, cores from full scale blocks
Water ratio, %	17.0
Bulk density, kg/m^3	2090
Dry density, kg/m^3	1790
Degree of saturation, %	85.2
Void ratio	0.553
Diameter of the blocks, mm	155
Test length, mm	3099
Total mass of blocks installed, kg	123.6

Calculated data

Final dry density, kg/m^3	1414
Void ratio	0.973
Saturated density, kg/m^3	1907
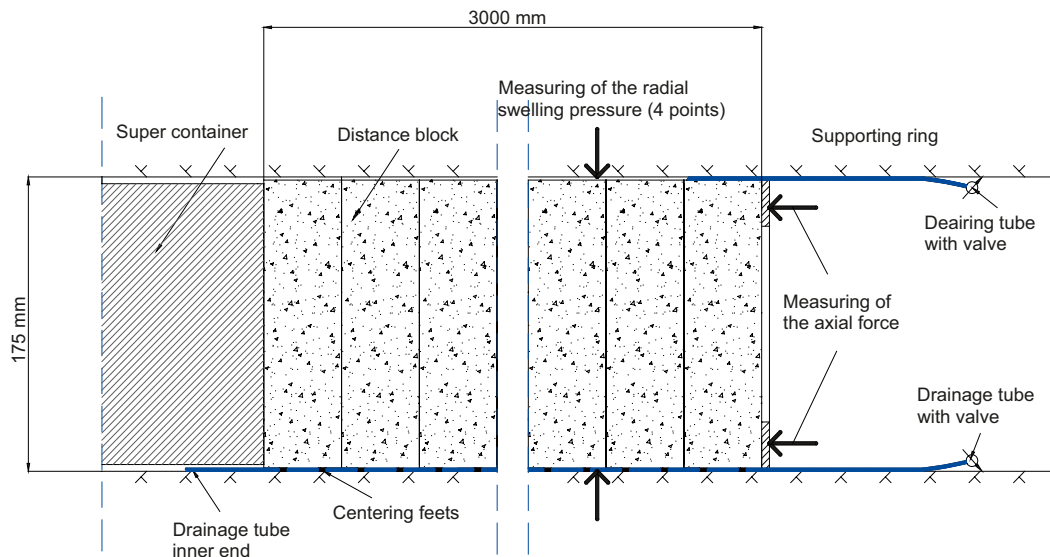
Figure 3-17. Schematic view of the test layout.
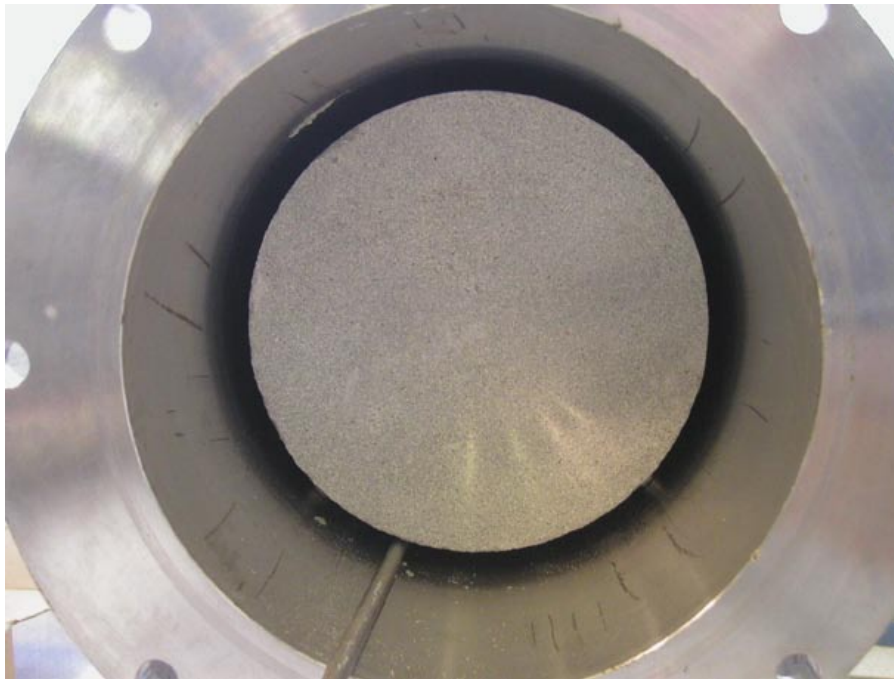
Figure 3-18. Picture from the installation showing the centred bentonite block and the drainage tube at the bottom.

Results

Very good results were obtained from this test. After 14 days the applied water pressure was 5 MPa and the system was still tight, Figure 3-19. The axial load on the fixing ring and the radial swelling pressure were also measured, Figure 3-20.

The retrieval of the steel tube was tested, Figure 3-21. This was done in 3 steps with an interval of 1 day between each step, letting the bentonite seal the remaining space. During the retrieval the water pressure through the tube was kept. Before the last pull the pressure in the tube was decreased to zero. The axial load needed for the retrieval was measured, Figure 3-22.

During the test it was observed that the outermost bentonite block i.e. closest to the fixing ring had been pressed through the fixing ring, Figure 3-23. There was a very obvious deformation of the bentonite, but there were no visible cracks in the block.

During decomposition samples were taken from the clay at different points and the water ratio and density was determined, see Table 3-6. In Figure 3-24 the water ratio distribution at the outermost parts is shown.
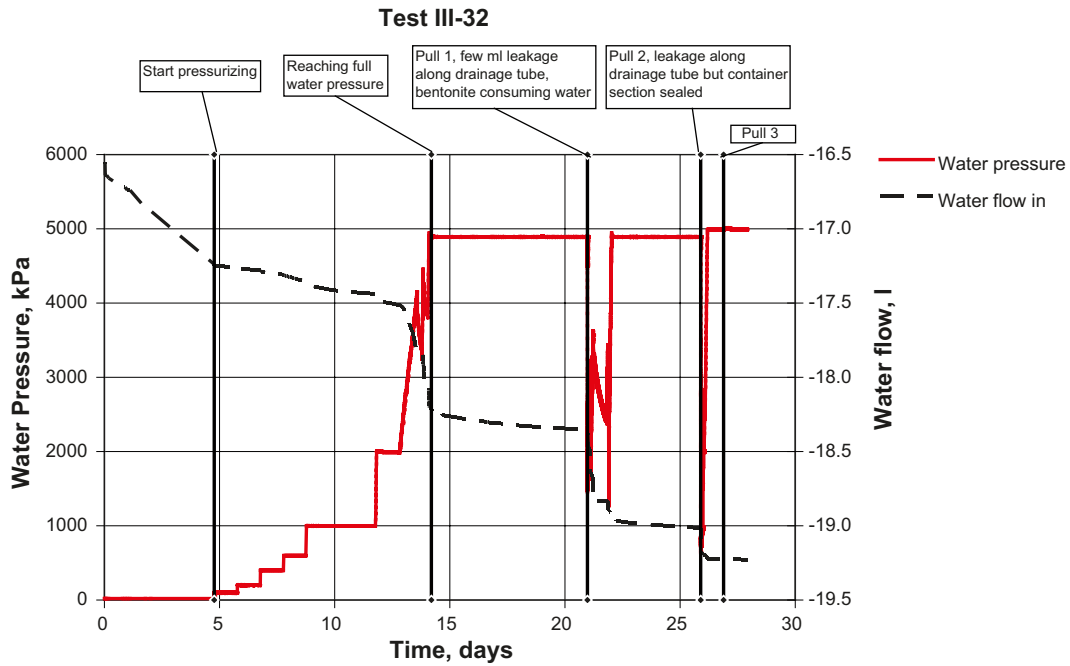
Figure 3-19. *Applied water pressure and injected water volume plotted vs. time.*
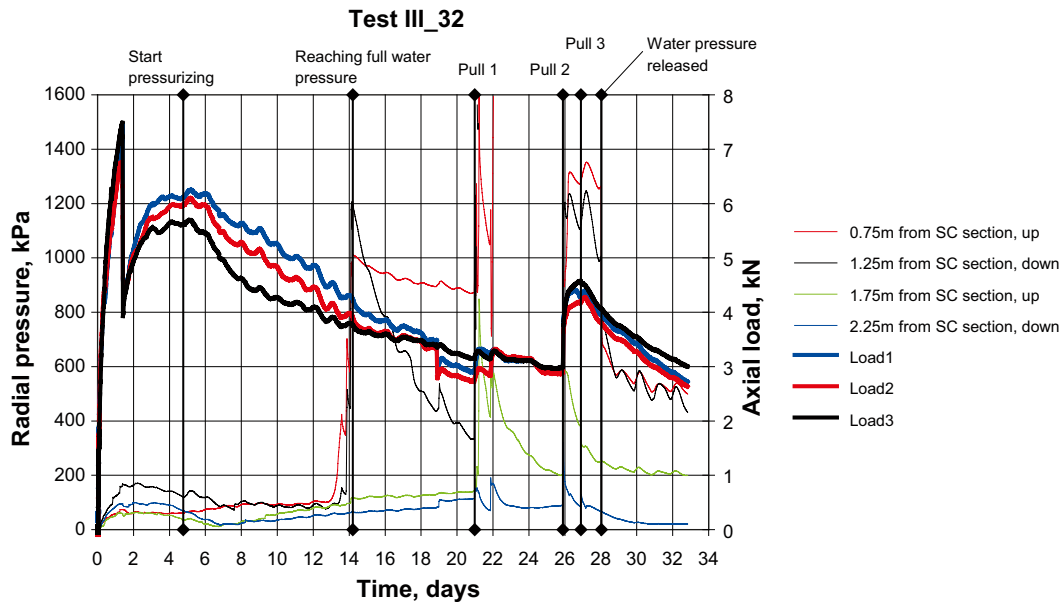
Figure 3-20. *Axial load on the fixing ring and radial swelling pressure plotted vs. time.*
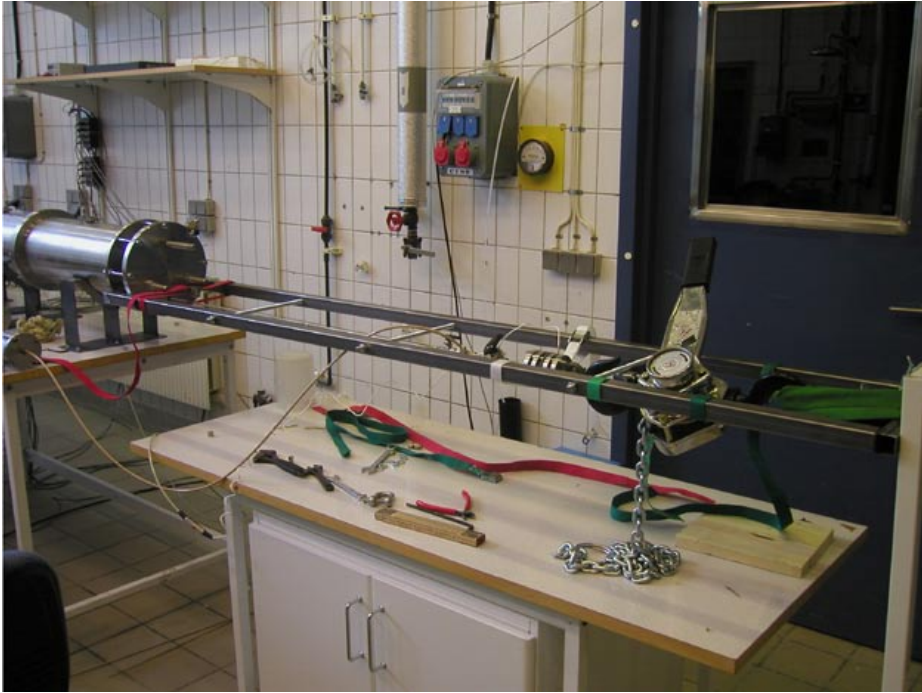
Figure 3-21. *Picture showing the equipment used for the retrieval of the drainage tube.*
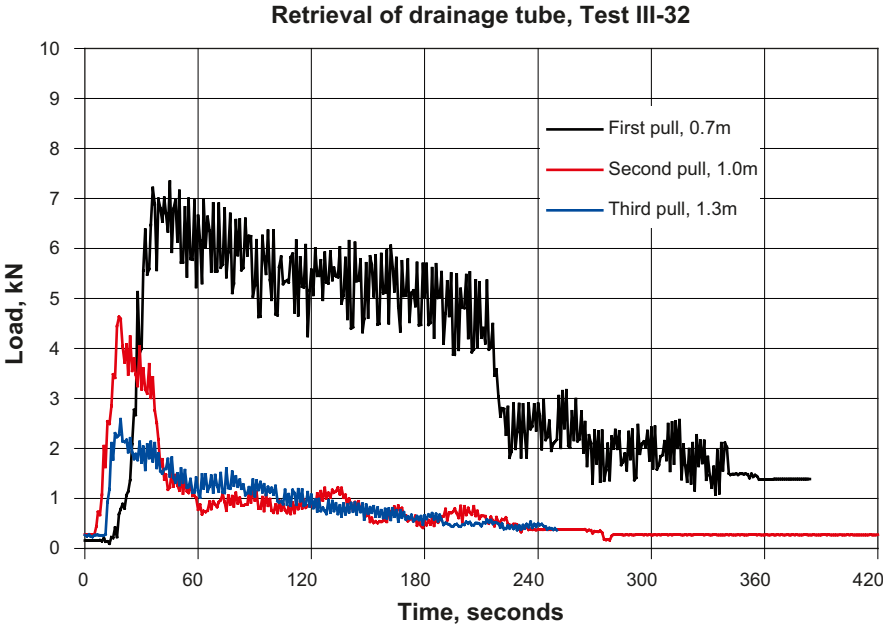
Figure 3-22. *Diagram showing the measured load needed during the retrieval of the drainage tube. The retrieval was done in three steps with 24 hours between each step.*

266

Figure 3-23. *Picture showing the fixing ring after termination of the test. The block closest to the ring has been squeezed through the central hole in the steel ring. The total displacement was estimated to 12 mm.*
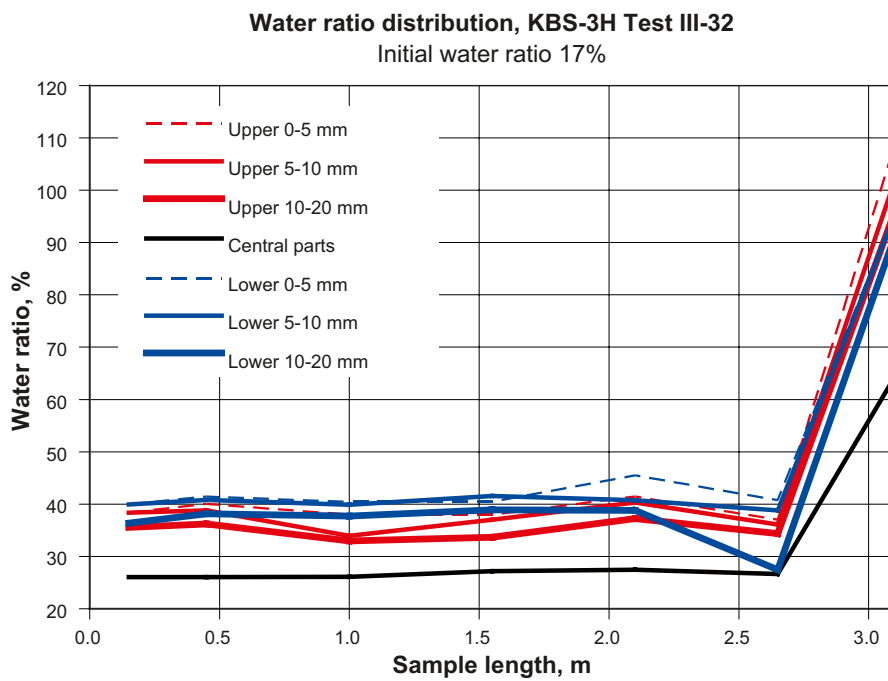
Figure 3-24. *Diagram showing the water ratio as a function of the distance to the fixing ring.*

Table 3-6. Table showing the water ratio and density of samples taken in a section 15 cm from the fixing ring.

Cut taken about 15 cm from fixing ring	w	Bulk density	Sr	e	Dry density
Examination starts at top	%	g/cm³	%		g/cm³
0-10 mm	38.38	1.84	97.5	1.094	1.33
10-20 mm	35.59	1.83	93.2	1.061	1.35
20-30 mm	31.43	1.86	90.8	0.963	1.42
30-40 mm	29.20	1.92	93.3	0.870	1.49
40-50 mm	27.90	1.94	93.3	0.832	1.52
50-60 mm	27.11	1.94	91.3	0.825	1.52
60-70 mm	26.45	1.94	90.6	0.811	1.53
70-87.5 mm	26.07	1.95	90.7	0.799	1.54
87.5-105 mm	26.18	1.95	90.6	0.803	1.54
105-115 mm	27.00	1.95	92.2	0.814	1.53
115-125 mm	27.77	1.94	92.7	0.833	1.52
125-135 mm	30.03	1.90	92.4	0.904	1.46
135-145 mm	31.05	1.89	92.6	0.932	1.44
145-155 mm	33.49	1.81	88.6	1.051	1.36
155-165 mm	36.38	1.82	93.3	1.084	1.33
165-175 mm	39.96	1.80	95.5	1.163	1.29
Starting values on bentonite core	17.00	2.09	85.2	0.553	1.79

K.3.3.5 Example of results Test III-33

This test is a repetition of III-32. The input data of the bentonite blocks is presented in Table 3-7.

Test description

The test is a repetition of Test III-32.

Result

The results are very similar to those from test III-32, see Figures 3-25 to 3-29 and Table 3-8.

Table 3-7. Table showing the input data for the bentonite blocks used in test number III-31.

Distance blocks

Installed distance blocks

Raw material	MX-80, cores from full scale blocks
Water ratio, %	17.3
Bulk density, kg/m³	2110
Dry density, kg/m³	1799
Degree of saturation, %	88.2
Void ratio	0.545
Diameter of the blocks, mm	155
Test length, mm	3080
Total mass of blocks installed, kg	122.75

Calculated data

Final dry density, kg/m³	1413
Void ratio	0.974
Saturated density, kg/m³	1907
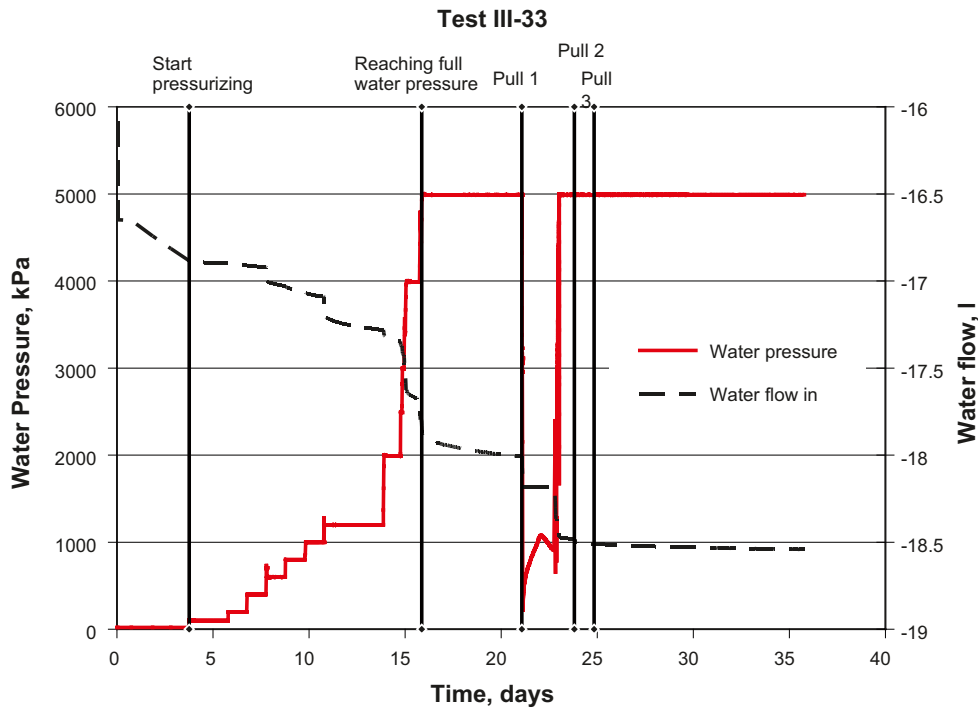
Figure 3-25. *Applied water pressure and injected water volume plotted vs. time.*
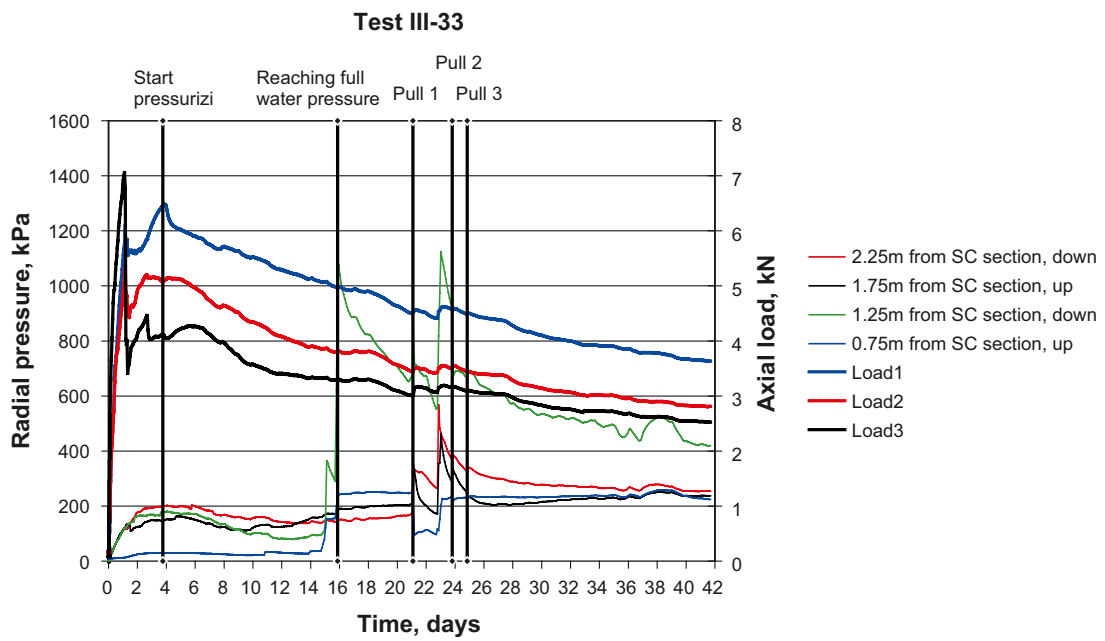

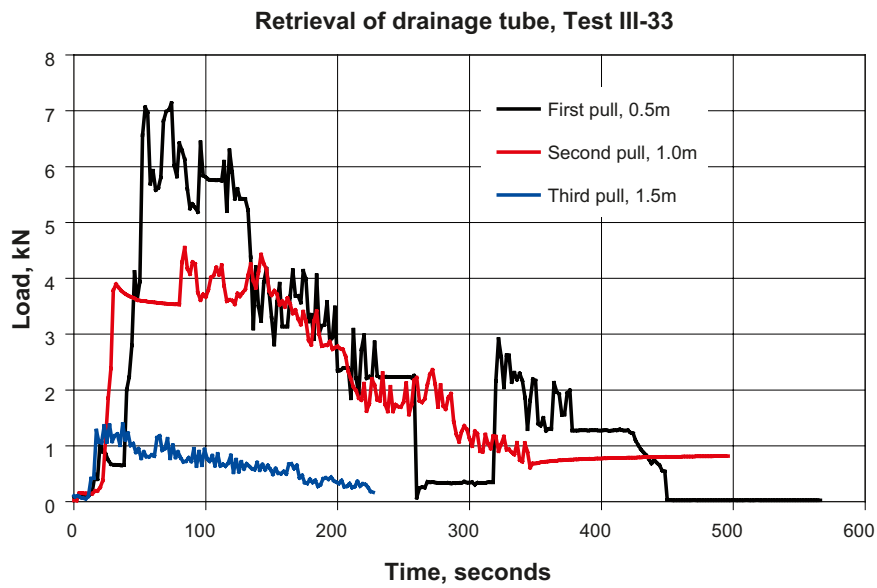**Figure 3-26.** *Axial load on the fixing ring and radial swelling pressure plotted vs. time.*

Figure 3-27. *Diagram showing the measured load needed during the retrieval of the drainage tube. The retrieval was done in three steps with 24 hours between each step.*

Figure 3-28. *Picture taken during decomposition of the test, about 1.5 m from the supercontainer section. The remaining hole from the drainage tube is still open.*

270

Water ratio distribution, KBS-3H Test III-33

Initial water ratio 17.3%
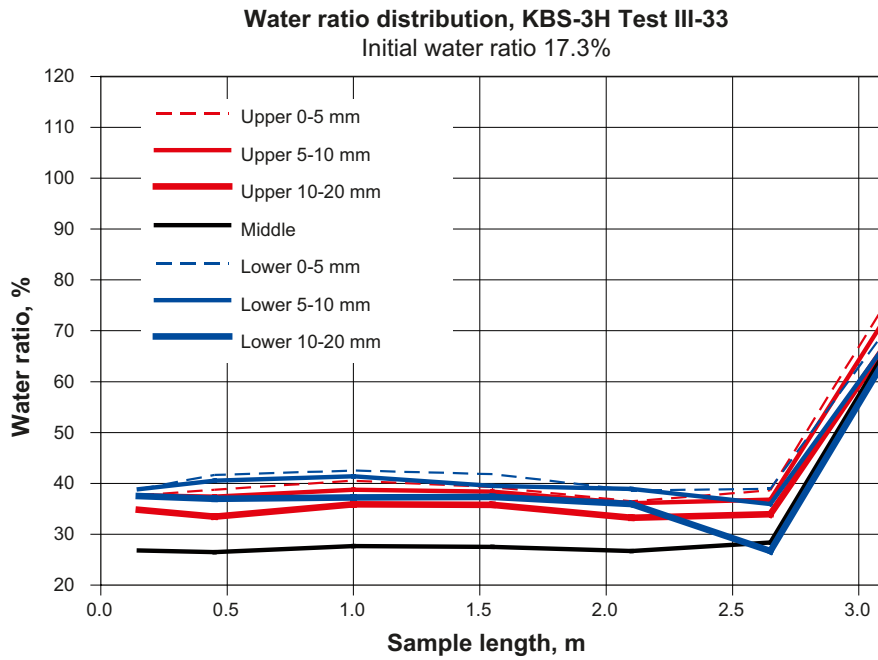
Figure 3-29. Diagram showing the water ratio as a function of the distance to the fixing ring.

Table 3-8. Table showing the water ratio and density of samples taken in a cut 15 cm from the fixing ring.

Cut taken about 15 cm from fixing ring Examination starts at top	w %	Bulk density g/cm³	Sr %	e	Dry density g/cm³
0-10 mm	37.65	1.79	92.1	1.136	1.30
10-20 mm	34.80	1.83	92.0	1.051	1.36
20-30 mm	30.92	1.90	94.4	0.911	1.45
30-40 mm	28.90	1.91	92.2	0.872	1.49
40-50 mm	27.97	1.94	93.1	0.835	1.51
50-60 mm	27.38	1.94	92.6	0.822	1.53
60-70 mm	26.96	1.93	90.3	0.830	1.52
70-87.5 mm	26.82	1.95	92.3	0.808	1.54
87.5-105 mm	26.93	1.94	91.8	0.815	1.53
105-115 mm	27.36	1.94	91.8	0.829	1.52
115-125 mm	28.00	1.93	92.0	0.846	1.51
125-135 mm	29.05	1.91	91.9	0.879	1.48
135-145 mm	30.65	1.89	92.9	0.917	1.45
145-155 mm	33.30	1.86	92.9	0.997	1.39
155-165 mm	37.51	1.82	94.3	1.106	1.32
165-175 mm	38.84	1.82	96.4	1.119	1.31
Starting values on bentonite core	17.00	2.09	85.2	0.553	1.79

K.3.4   Tests in transparent tube

K.3.4.1   General

In order to visualize the internal piping phenomena tests have been performed in transparent tubes. The tests are intended to increase the understanding of the piping phenomena by allowing flow paths to be directly observed.

The test equipment is rather similar to the one used in the scale test with a length of 1 metre. A difference is that there are no measurements of radial pressure or axial load on the fixing ring. The equipment consists of plastic tubes with an inner diameter of 100 mm made of PC (poly carbon), Figure 3-30. The wall thickness of the tube is 25 mm and the length is 1 metre. The maximum allowed inner pressure is 2 MPa. This means that the tests must be designed so that piping occurs at a level below this pressure.

Two tests have been performed so far and the preparation of test number three is going on.

K.3.4.2   Results

Test 1

The test layout was set in order to ensure piping at a rather low water pressure. The blocks were centred in the tube with a slot to the "rock" of 10 mm. The slot was pre wetted. Water with 3.5% salinity was used.

During the water filling of the slot (Figure 3-31 and 3-32) it could be observed how bentonite was loosened from the compacted blocks and then settled to the bottom. After finishing the filling, a number of air-pockets could be seen on the upper part. These air-pockets, or the tracks after them, could be seen during the whole test period, Figure 3-33, 3-34 and 3-35.

48 hours after starting the pre-wetting of the slot, a pressure ramp of 5 MPa/h was applied from the supercontainer section, Figure 3-36. When the water pressure reached about 240 kPa piping occurred i.e. the clay in the slot couldn't withstand the pressure and a channel was opened where water could flow, Figure 3-38. The channel occurred on the side of the tube where the material seemed to be very homogeneous and not as expected in the upper part where the air-pockets were situated. After additional 48 hours, a new pressure ramp was applied with almost the same result, Figure 3-37.

Figure 3-30. *Picture showing the transparent tube test equipment.*

Figure 3-31. Picture taken during the pre-wetting of the outer slot. Water is filled halfway up and bentonite has loosened from the blocks and settled down in the bottom.

Figure 3-32. Picture taken just after finishing the pre-wetting of the outer slot. Bentonite has loosened from the blocks and settled down. Half of the slot is still filled with clear water.

273

Figure 3-33. *Picture taken from above about 0.5 hour after finishing the pre-wetting of the outer slot. In spite of the inclination of the tube (about 2°) there are a number of air-pockets on the upper side.*
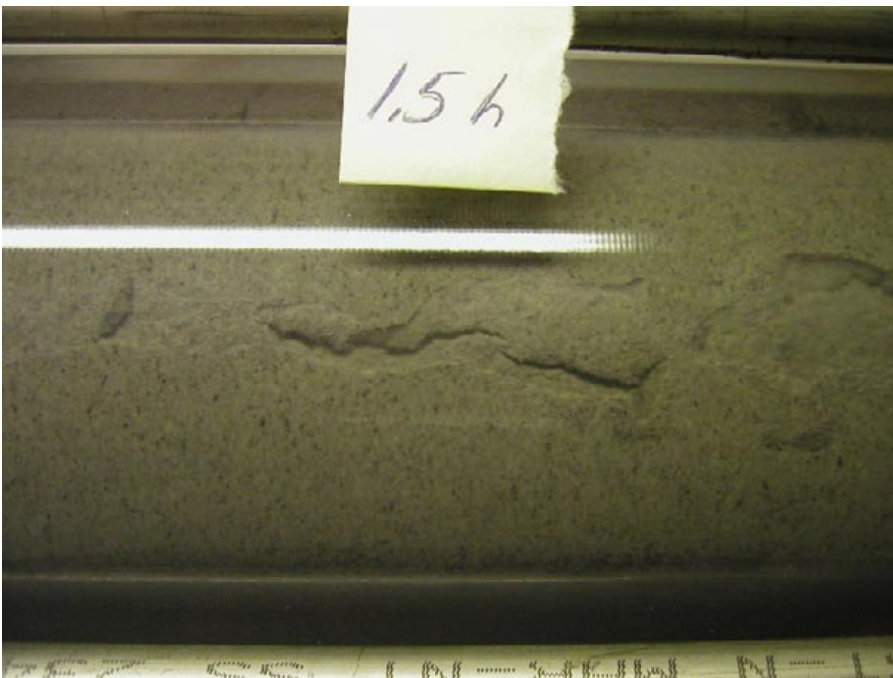
Figure 3-34. *Picture taken about 1.5 hour after finishing the pre-wetting of the outer slot. The air-pockets are still very clear.*

Figure 3-35. *Picture taken 24 hour after finishing the pre-wetting of the outer slot. The air-pockets are still very clear.*
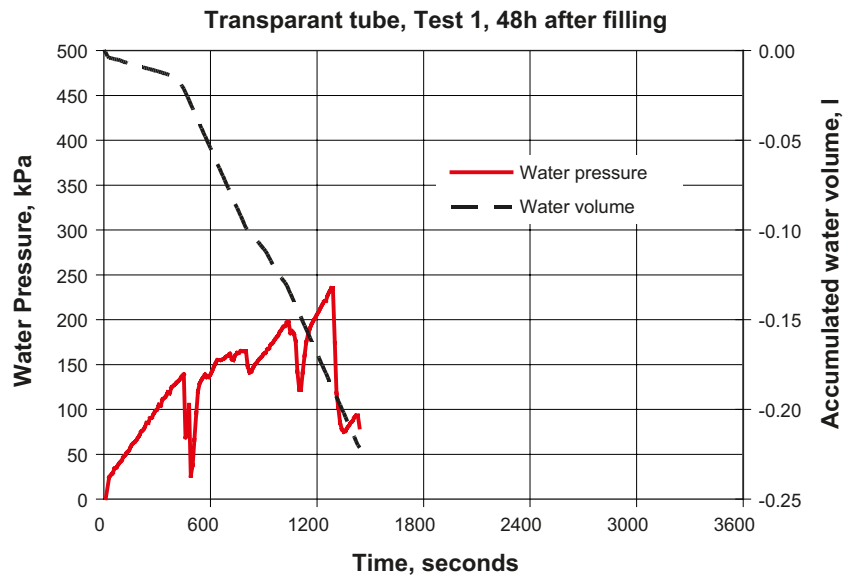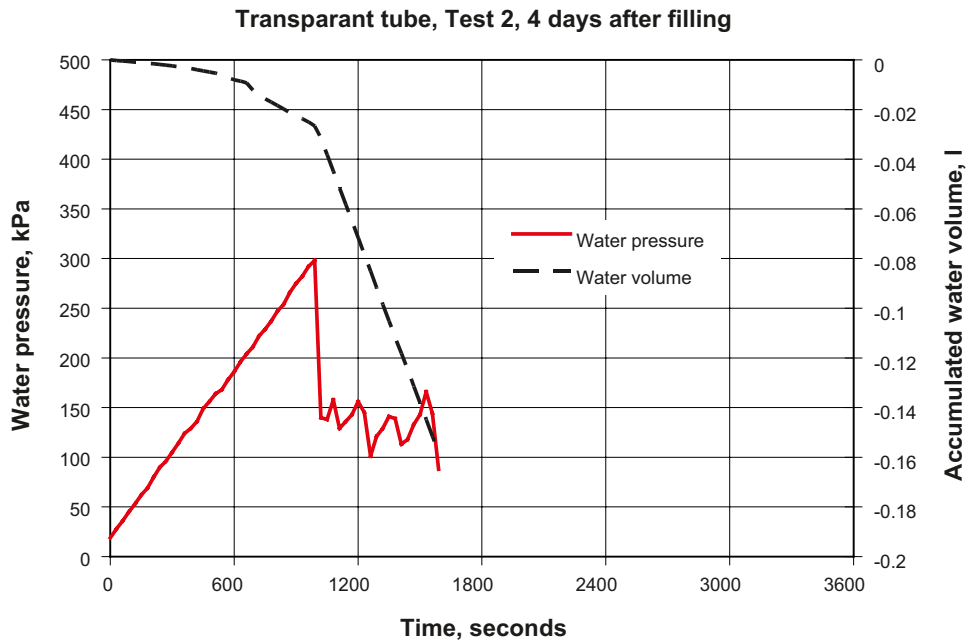

Figure 3-36. *Diagram showing the results from Test 1. 48 hours after starting the pre-wetting of the slot a pressure ramp was applied. The applied water pressure and the injected water volume are plotted vs. time.*
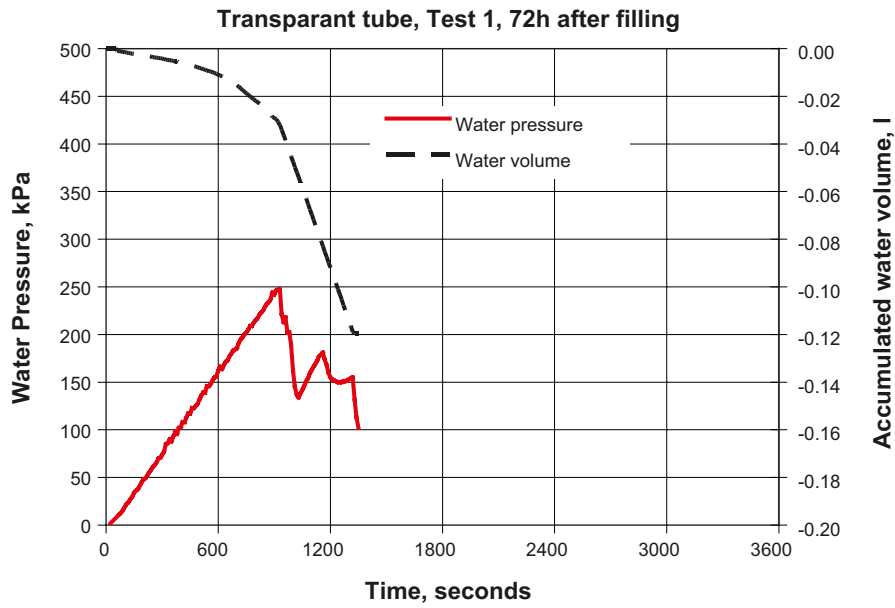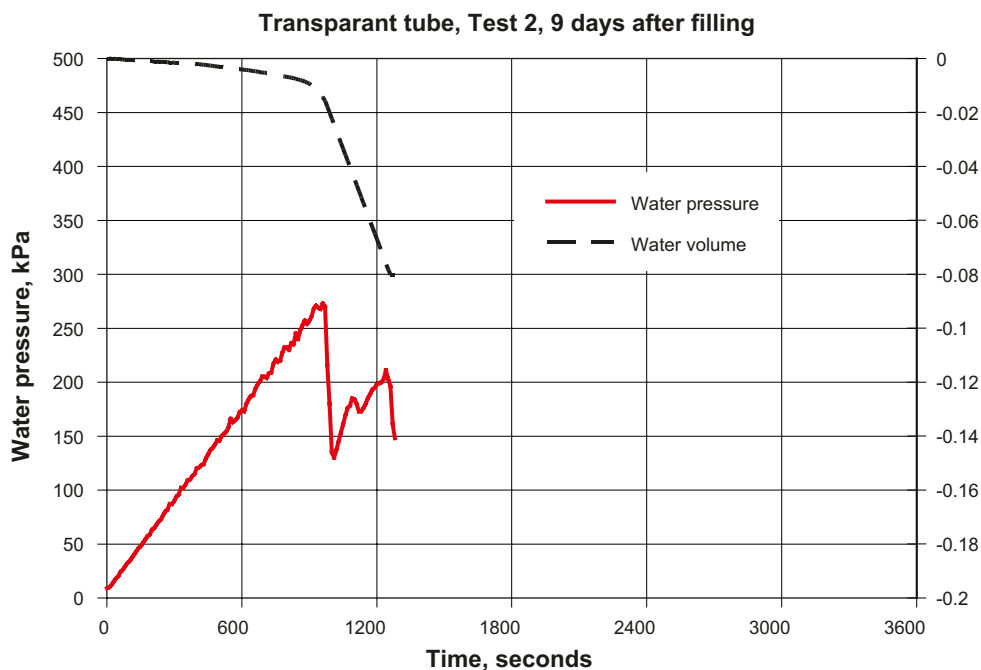
Figure 3-37. *Diagram showing the results from Test 1. A new pressure ramp was applied 72 hours after starting the pre-wetting of the slot. The applied water pressure and the injected water volume are plotted vs. time.*
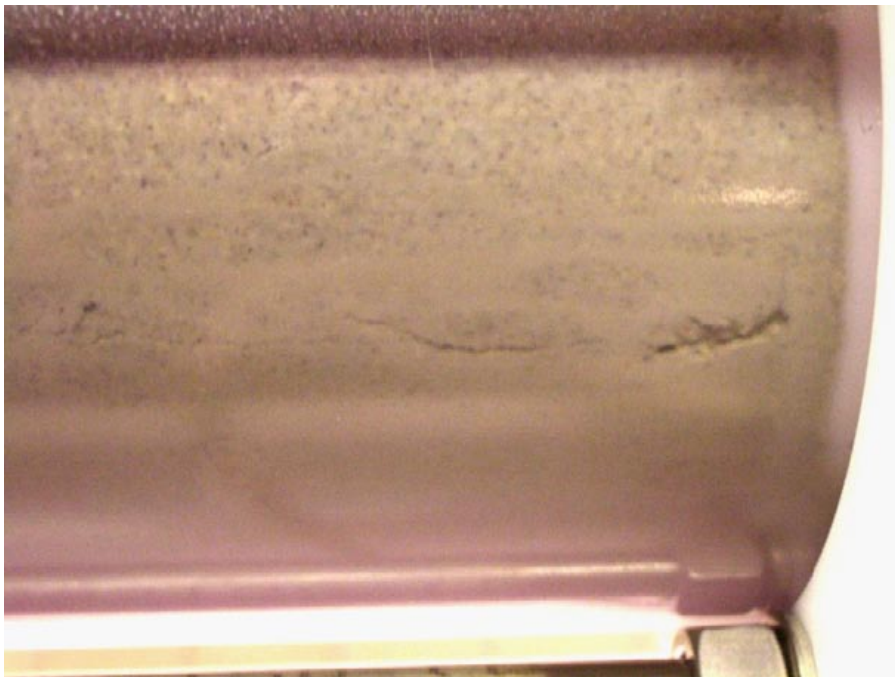
Figure 3-38. *Picture taken from beside showing the piping channel. Piping occurred for both pressure ramps on the side of the tube.*

Test 2

The layout of Test 2 was the same as in Test 1. In order to achieve piping at higher water pressure the time for homogenization was increased from 2 days to 4 days. The results from the tests were, in spite of this change, very similar. Piping was achieved at about 300 kPa (250 kPa in Test 1), Figure 3-39. A new pressure ramp was applied 9 days after test start with the same result, Figure 3-40. The piping channel occurred also in this test on the side of the tube. Photos were taken also from this test with very similar result as the one presented for Test 1.

Transparant tube, Test 2, 4 days after filling

Figure 3-39. Diagram showing the results from Test 2. 4 days after starting the pre-wetting of the slot a pressure ramp was applied. Applied water pressure and injected water volume are plotted vs. time.

Transparant tube, Test 2, 9 days after filling

Figure 3-40. Diagram showing the results from Test 2. A new pressure ramp was applied 9 days after starting the pre-wetting of the slot. Applied water pressure and injected water volume are plotted vs. time.

Test 3

The goal is to achieve piping at a higher pressure, about 1,500–2,000 kPa. This could be difficult because the bentonite is not allowed to seal "too much", because of the limited strength of the test equipment. In the two earlier tests the bentonite blocks werecentred, having a slot of 10 mm (10/10) to the "rock". Earlier tests in the 1 metre equipment has shown that with an initial slot of 5 mm (centered blocks) the bentonite will seal and withstand a water pressure of 5 MPa within 1–2 days. Therefore it was decided to have a slot somewhere between 5 and 10 mm i.e. 7.5 mm. The test is under preparation.

K.3.5 Summary of the tests regarding sealing ability

The distance blocks sealing ability are limited at these tough conditions (water inflow of 1 l/min and water pressure increase rate of 1 MPa/hour). After 13 tests in the 1 metre equipment and 3 tests in the 3 metre equipment in this test series the following conclusions can be drawn:

- A pellet filled slot wider than 1 cm does not work at these conditions. The pellets density is too low and probably needs more time to homogenize and increase the density by consolidation from the swelling of the bentonite blocks.

- When the blocks are placed on the bottom of the deposition tunnel and have a gap of 2 mm at the top, they will seal very efficiency.

- A 5 mm slot, on one side or both sides (centered block) requires a pre-wetting of the bentonite i.e. the slot needs to be filled with water in advance. During the subsequent filling of the supercontainer section the bentonite will get time to swell and seal the slot. After having repeated this test twice, it is obvious that this layout is very close to the limit of the sealing capacity.

- A 10 mm slot with centred blocks is possible with special arrangements. Two tests have been performed in the 3 metre equipment, using a drainage tube, which is led under the distance block into the supercontainer section. With this tube it is possible to control the water inflow and the water pressure in the container section. If the pressure is increased in steps it is possible to seal against a water pressure of 5 MPa within 2 weeks.

A compilation of the test results is made in Figure 3-41. The diagram shows the maximum water pressure the distance blocks can withstand within 2–3 days after test start (2 weeks for the tests performed in the 3 metre equipment).

K.3.6 Investigation of the effect and extent of hydraulic pressure on distance block end surface

There are uncertainties related to the extent of the hydraulic pressure exerted on the end surface of the distance blocks. The uncertainties are significant because they have effect on the total force on the distance blocks and the dimensioning of the fixing rings in BD. The main uncertainty is whether the pressure is exerted on a narrow rim on the end surface, which is not covered by the supercontainer end surface or whether it is possible that the pressure is exerted on the whole surface.

The extent of the pressure depends on the behaviour of joints in bentonite and the gap between distance block and supercontainer. There are indications that the pressure will be exerted on a less than 10 cm wide rim if the gap between distance block and supercontainer is 7 mm wide.

The phenomenon is investigated separately in a special equipment, see Chapter 4, but data can also be evaluated from the piping tests.

An attempt to compare the measured maximum load on the fixing ring, before applying any water pressure (swelling pressure from bentonite) and at the maximum water pressure with the calculated force which is based on the applied water pressure and the "active surface" (measured
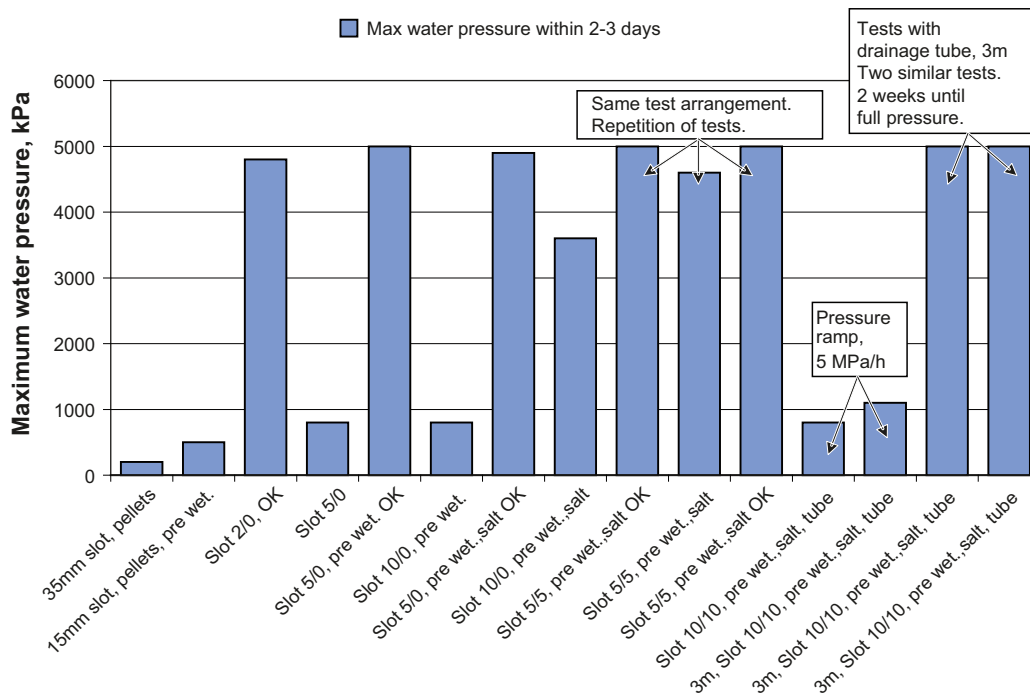
Figure 3-41. *Diagram showing the maximum water pressure the installed distance blocks could resist within 2–3 days for the different test layout. (2 weeks for the two last 3 metre tests).*

after test interruption, see example Figure 3-15) is made in Figure 3-42. The difference between the calculated load and the measured is taken up by the friction between the bentonite and the rock. The data in the diagram is very preliminary and will be revised and controlled.

The blue staples in the diagram shows the load before applying any water pressure i.e. the measured load depends on the swelling pressure from the bentonite. If the time from installation to reaching maximum water pressure is long, this load probably will be the highest, see the two latest 3-meter tests. Depending on an increasing radial swelling pressure, the load taken by friction against the rock will also increase by time and the measured load after reaching full water pressure is therefore rather low for these samples.

K.3.7   Comments to the piping tests

One basic conclusion from the tests is that uniform pellets in a wide gap do not work*.* The existing channels in the pellet filled gap will not seal in the required time due to the low average density. Another conclusion is that the initial slot between bentonite and rock has to be very small, about 2 mm, to ensure the function of the block. The gap width can be increased to 5 mm if it is pre wetted at test start (works both with tap water and even better with 3.5% salt). The artificial watering gives the bentonite more time for swelling and the salt speeds up the swelling rate of the bentonite.

In order to facilitate the installation and permit installation of blocks with a diameter of about 20 mm less than the deposition tunnel diameter, one idea was to install a drainage tube which was led in the bottom, through the fixing ring, under the distance blocks the whole way into the supercontainer section. With this tube the water pressure could be controlled during the maturation of the bentonite. After a certain time when the bentonite has swelled and sealed the tunnel, the tube could be pulled out in steps, letting the bentonite seal the volume behind. The layout has been tested in two almost identical experiments with good result.

The results from the described tests have resulted in four different design alternatives for the distance blocks presented in a draft report "Design of buffer components".
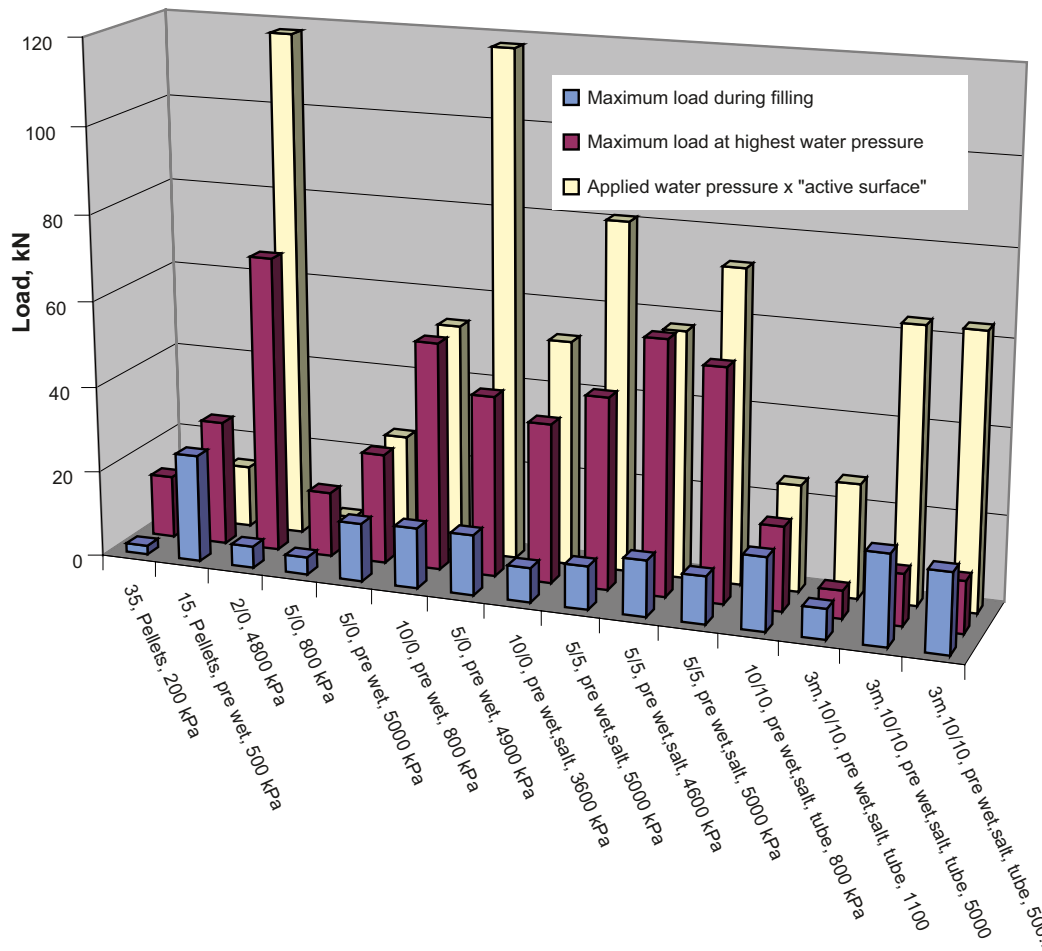
Figure 3-42. *Diagram showing the maximum load during filling before applying any water pressure, the maximum load at the highest water pressure and the calculated load (applied water pressure acting on an "active surface"(the surface between the supercontainer and the first distance block which the water pressure is acting on) which is measured after interrupting the tests. In two of the experiments the water pressure have had access to the whole area (in one case depending on weak arrangement for the load cells which allowed the distance blocks to move and in the other case depending on a planned movement of the fixing ring during the test time (gives a load of 120 kN).*

K.4 Hydraulic pressure on distance block end surface, against supercontainer

K.4.1 General

The phenomena with load transfer from pressurized water through the distance blocks to the fixing ring have been investigated earlier within the KBS-3H project and are also investigated in the issue "piping through distance block tests" (see Chapter 3) but a more systematic study was considered to be needed.

The main aim of this investigation is to measure the pressure between the supercontainer and the first distance block at different distances from the simulated rock surface and by that determine the size of the "active surface" on which the hydraulic pressure is acting.

K.4.2 Experimental setup

Earlier tests indicates that the bentonite prevents the water pressure from propagating all the way to the centreline of the distance blocks, which means that the load only seems to be developing in the outer region. The influence of the initial gap width and how the "active area" changes with time are two important parameters that are investigated.

K.4.3   Test equipment

The tests were performed in new equipment schematically described in Figure 4-1. Parts of the equipment are similar to that used in the scale tests except for the supercontainer dummy on which a number of pressure sensors are mounted.

Three tests have been performed so far. Bentonite blocks have been installed with a small radial gap width. The parameters varied in the tests are: the axial gap between distance block and supercontainer, the water filling rate and the water pressure increase rate. The radial slot is sealed quite fast when the bentonite gets access to water. The bentonite type and the radial slot are the same in all tests. The following is measured in the tests:

*   The axial load acting on the distance ring is measured with 3 load cells.

*   The radial swelling pressure is measured in two points.

*   The axial pressure between the supercontainer end surface and the first distance block is measured with six pressure cells positioned on different radius on the container, see Figure 4-1.

Test matrix

Table 4-1 shows the planned test matrix.

The parameters that will be varied in the test series are:

1. The slot width between supercontainer/bentonite will be varied in the tests from 0 up to 10 mm.

2. The water inflow rate (1 or 10 days).

3. Water pressure increase rate (100 kPa/h or 1,000 kPa/h).

4. The test time from reaching full water pressure until termination of the test may also be varied.
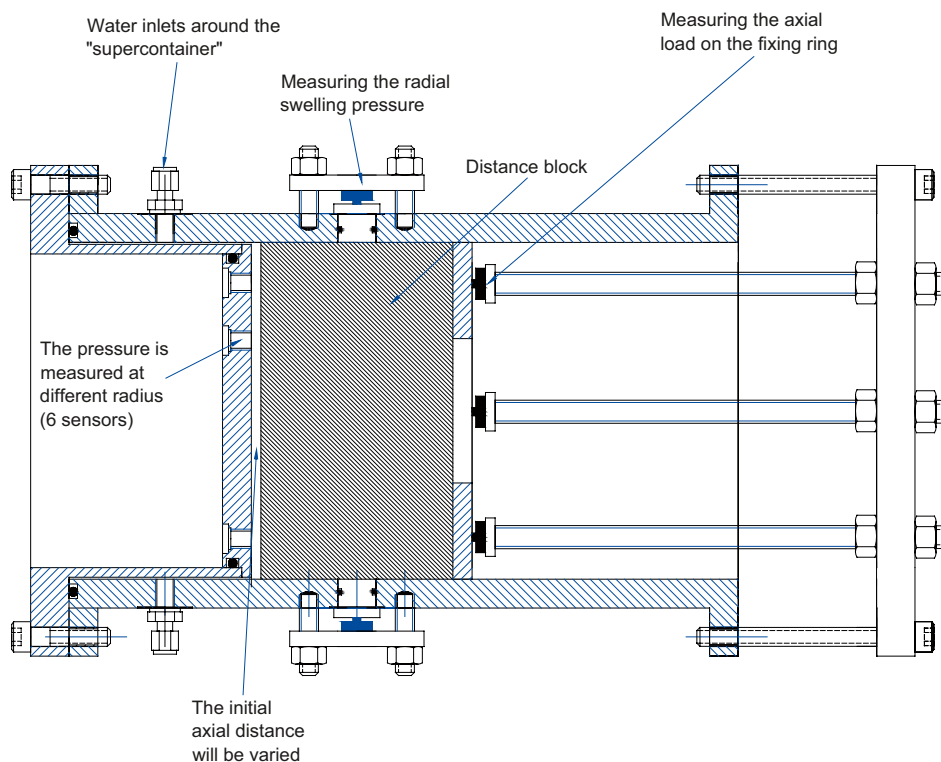

Figure 4-1. *Schematic view of the test equipment.*

Table 4-1. Table showing the test matrix for the issue Hydraulic pressure on distance block. Since the complete number of tests is rather high and the tests are quite time consuming, a selection will be done. The tests performed so far are marked with shaded boxes.

Hydraulic pressure on distance block			
Initial slot width, mm	Water inflow and pressure increase rate		
	0.1 l/min and 0.1 MPa/h	0.1 l/min and 1 MPa/h	1 l/min and 1 MPa/h
0	HP101	HP201	HP301
1	HP102	HP202	HP302
2	HP103	HP203	HP303
5	HP104	HP204	HP304
7.5	HP105	HP205	HP305
10	HP106	HP206	HP306

K.4.4   Test results

Three tests have been completed so far in the test series: HP103, HP203 and HP303. All three tests were performed with an initial slot between the supercontainer end plate and the distance block of 2 mm. The difference between the tests was the simulated water inflow (0.1 or 1 l/min) and the water pressure increase rate 0.1 or 1 MPa/h. In two of the tests, HP103 (0.1 l/min and 0.1 MPa/h) and HP203 (0.1 l/min and 1 MPa/h) the pressure measurements on the supercontainer end plate showed that the bentonite had swelled and sealed and by that prevented the applied water pressure to act on the full area of the distance block, Figure 4-2 and 4-5. These measurements were supported by the determination of the water ratio distribution on the distance block surface after finishing the tests, Figure 4-3 and 4-6, showing a strong radial water ratio gradient. Test HP303 (1 l/min and 1 MPa/h) showed however no delay in time between the applied water pressure and the pressure measured on the supercontainer end plate, Figure 4-8. This was also verified when determining the water ratio distribution on the distance block end after finishing the test, Figure 4-9. It was not possible for the bentonite to swell and seal for the fast water filling in combination with the high water pressure increase rate.
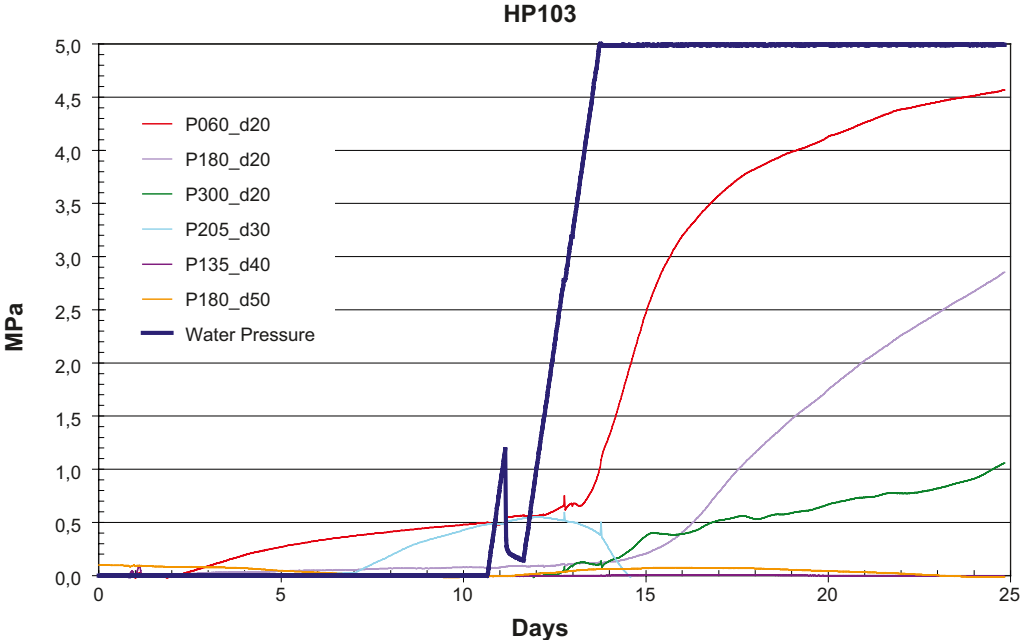

Figure 4-2. *Diagram showing the applied water pressure and the measured axial pressure on the super-container plotted vs. time for Test HP103. The label of each pressure sensor shows the position of the sensor on the supercontainer end plate (angel and distance from rock surface). The three outermost sensors, placed on a distance of 20 mm from the rock surface, starts to react slowly and with an evident delay after reaching full water pressure in the supercontainer section.*

The measurements of the radial pressure and the axial load on the fixing ring for the performed tests are presented in Figure 4-4, 4-7 and 4-10. The influence from the applied water on the measured axial load is evident for all samples.
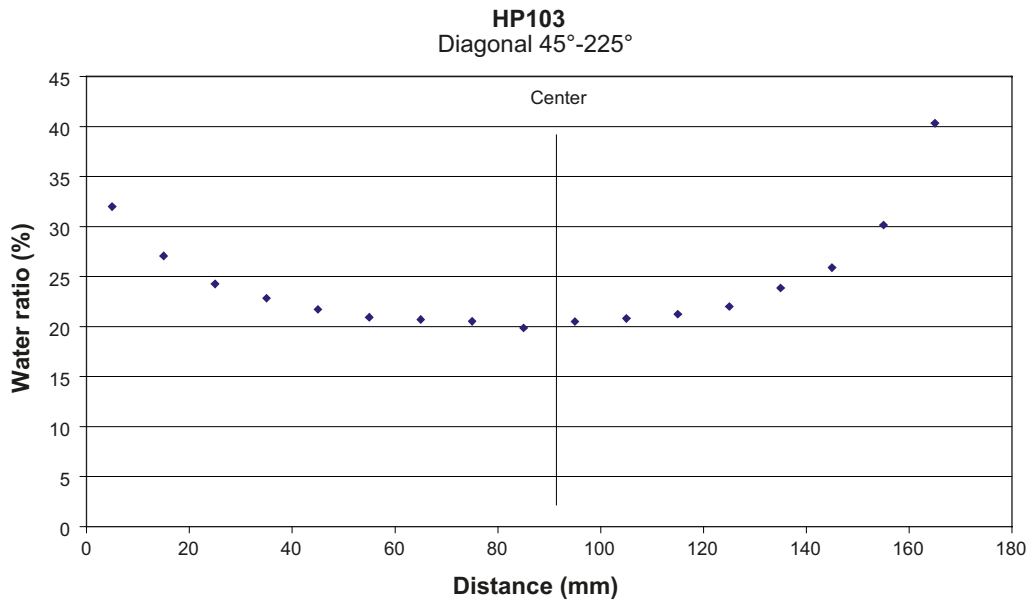

Figure 4-3. *Diagram showing the water ratio distribution on the distance block surface closest to the supercontainer end plate for Test HP103. The distribution indicates the size of the "active area" and supports the pressure measurements.*
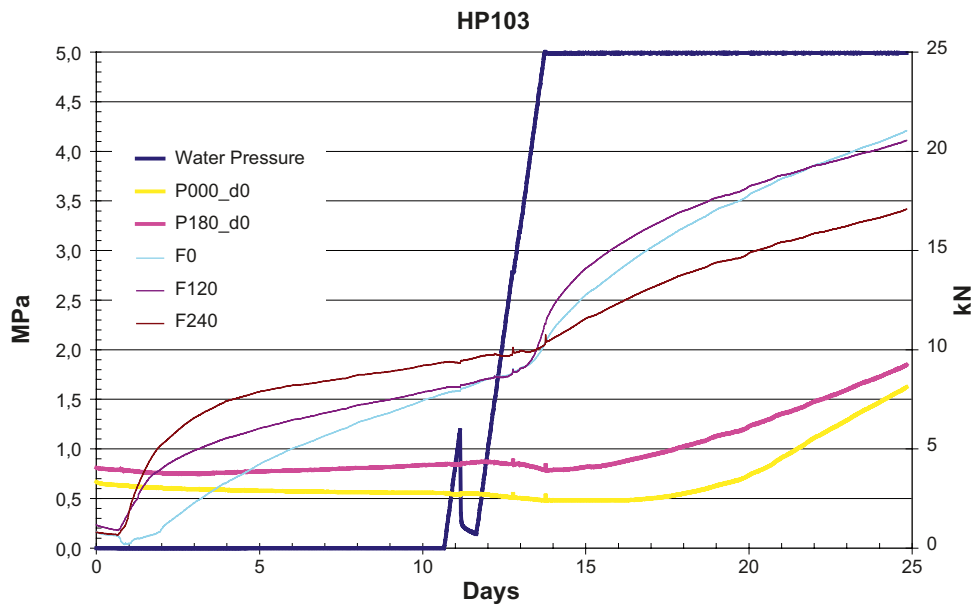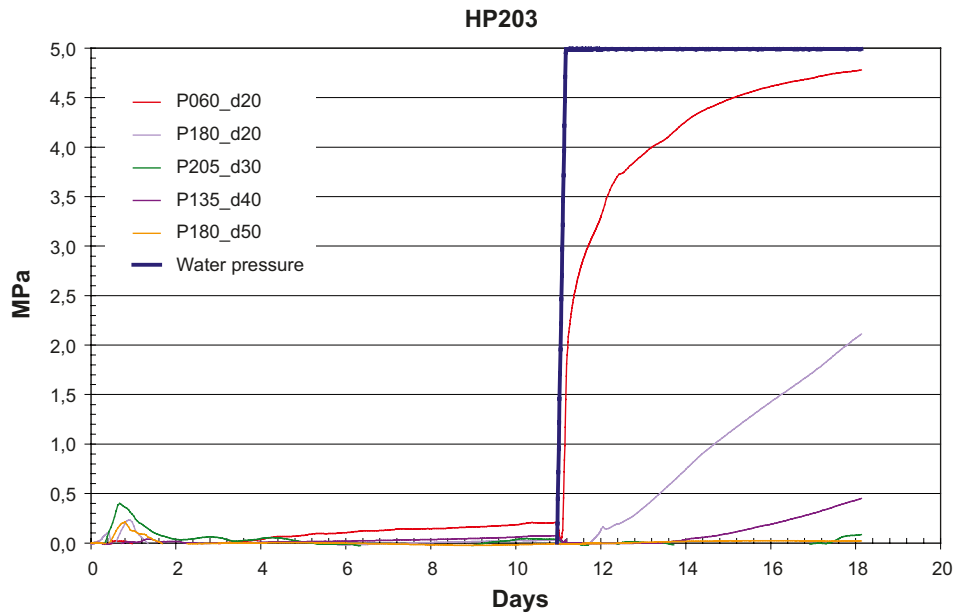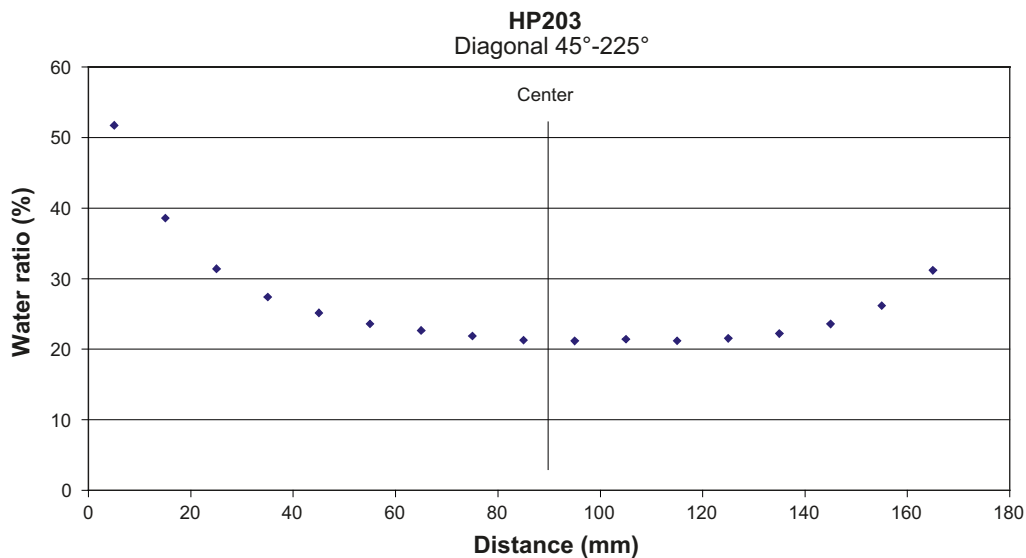

Figure 4-4. *Diagram showing the applied water pressure, the measured radial swelling pressure and the axial load as a function of time.*

Figure 4-5. *Diagram showing the applied water pressure and the measured axial pressure on the super-container plotted vs. time for Test HP203. The label of each pressure sensor shows the position of the sensor on the supercontainer end plate (angel and distance from rock surface). The two outermost sensors (one has failured), placed on a distance of 20 mm from the rock surface, starts to react slowly and with an evidently delay after reaching full water pressure in the supercontainer section.*

Figure 4-6. *Diagram showing the water ratio distribution on the distance block surface closest to the supercontainer end plate for Test HP203. The distribution indicates the size of the "active area" and supports the pressure measurements.*
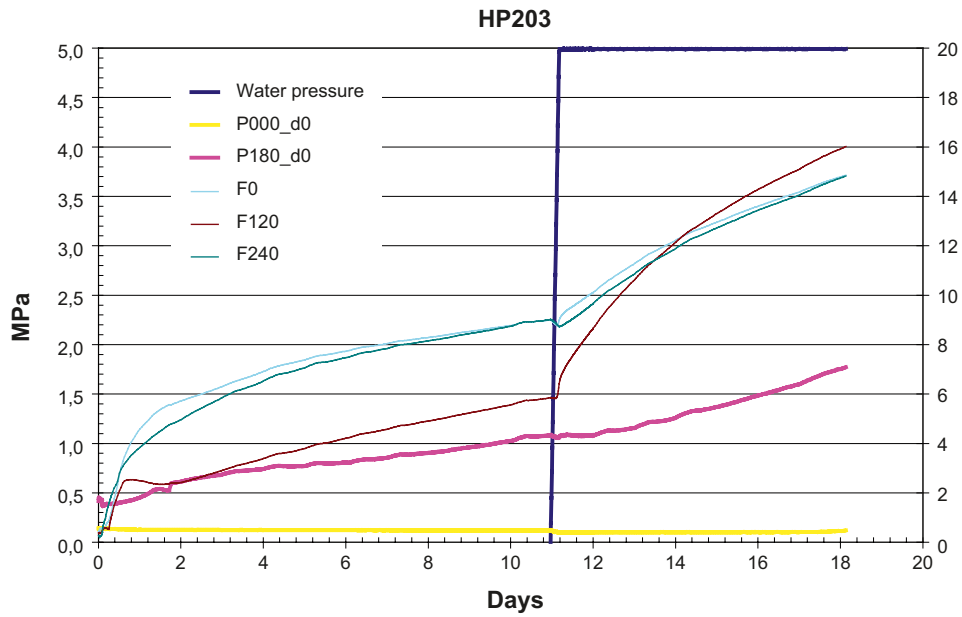
Figure 4-7. *Diagram showing the applied water pressure, the measured radial swelling pressure and the axial load as a function of time.*
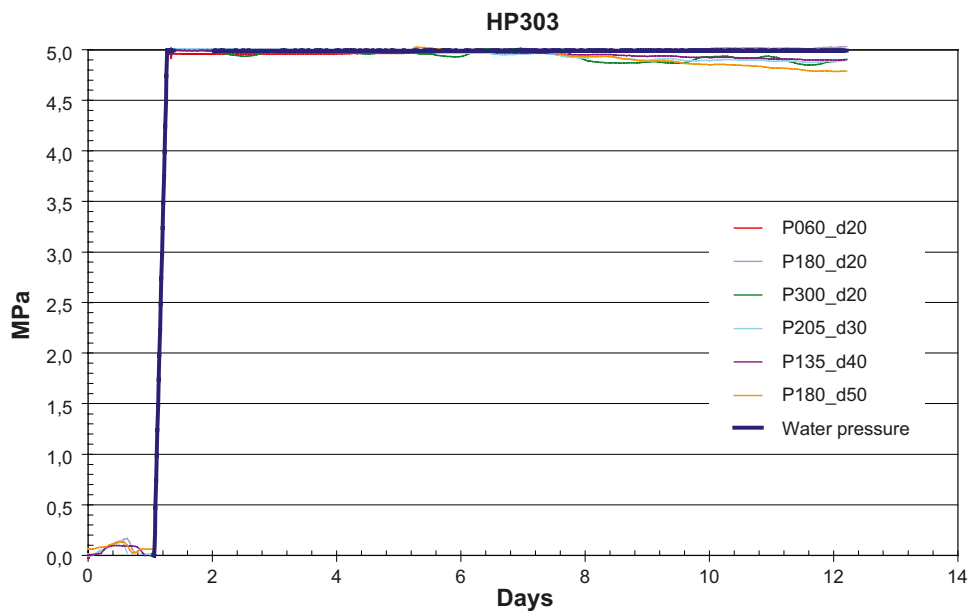

Figure 4-8. *Diagram showing the applied water pressure and the measured axial pressure on the super-container plotted vs. time for Test HP303. The label of each pressure sensor shows the position of the sensor on the supercontainer end plate (angel and distance from rock surface). All pressure sensors on the supercontainer end plate react immediately on the water pressure increase in the supercontainer section.*
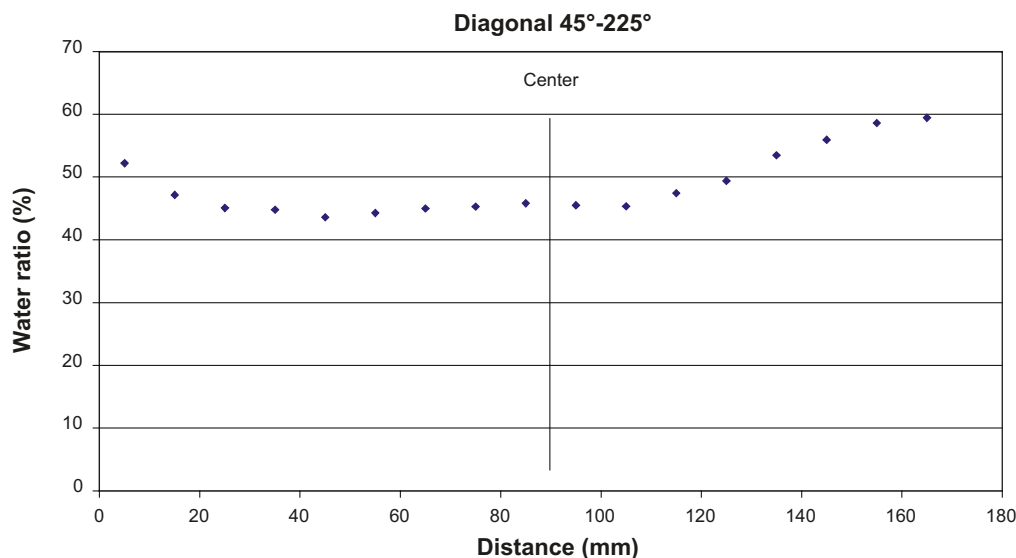
Figure 4-9. *Diagram showing the water ratio distribution on the distance block surface closest to the supercontainer end plate for Test HP303. The distribution shows that also the inner parts have had access to water. The applied water pressure has probably been working on the whole distance block area.*
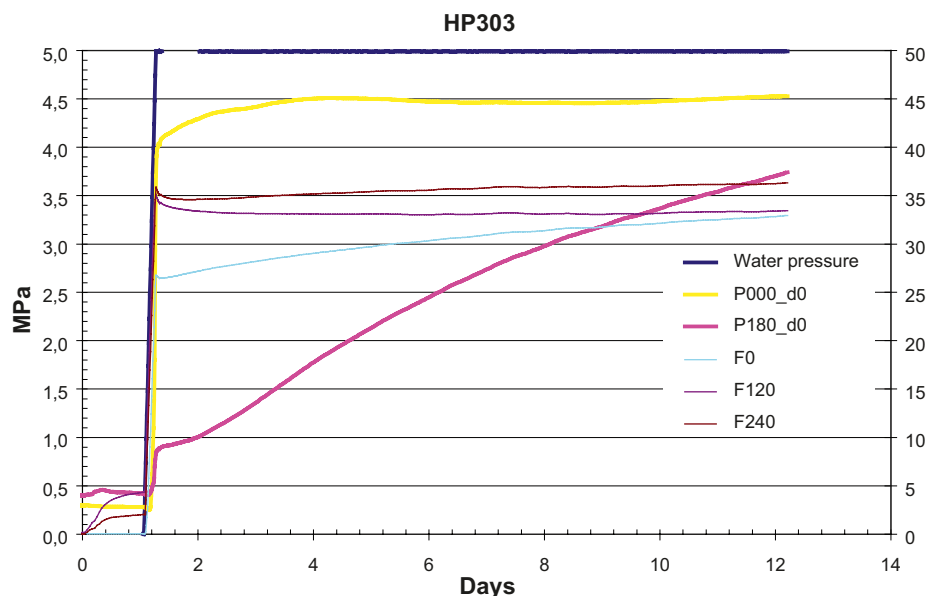

Figure 4-10. *Diagram showing the applied water pressure, the measured radial swelling pressure and the axial load as a function of time.*

K.4.5   Further tests

Test number four in this test series is running, HP204. This test has the same filling rate (0.1 l/min) and pressure increase rate (1 MPa/h) as HP203 but the distance between the supercontainer end plate and the distance block is increased to 5 mm.

References

Autio J, Börgesson L, Sandén T, 2006. KBS-3H Buffer test plan 2005-2007 to resolve critical design and early evolution issues. Memo PROJEKTI-798-15/2006, Saanio & Riekkola Oy.

Börgesson L, Sandén T, Fälth B, Åkesson M, Lindgren E, 2005. Studies of buffer behaviour in KBS-3H concept. Work during 2002-2004. Report R-05-50, Svensk Kärnbränslehantering AB, Sweden.

Sandén T, Börgesson L, 2006. KBS-3H Laboratory tests to resolve critical design and early evolution issues. Activity Plan APTDMLH3-06-036, Svensk Kärnbränslehantering AB.